

**THE EFFECT OF CALCINEURIN INHIBITION ON THE
EXPRESSION AND ACTIVATION OF RENAL
ELECTROLYTE TRANSPORTERS**

King Yan Felice Leung

A thesis submitted for the degree of Doctor of Philosophy

September 2017

Neuroscience, Physiology & Pharmacology, Division of Biosciences

University College London

Declaration

I, King Yan Felice Leung confirm that the work presented in this thesis is my own. Where information has been derived from other sources, I confirm that this has been indicated in the thesis.

King Yan Felice Leung

Abstract

Tacrolimus (FK506) is a calcineurin inhibitor (CNI), and the main immunosuppressant used in organ transplantation. It causes complications such as hypertension, hyperkalaemia, hypercalciuria and acidosis. Together with insulin resistance, dyslipidaemia and obesity, they comprise the metabolic syndrome.

CNIs induce hypertension through the activation of the WNK-NCC cascade, causing an increase in sodium chloride reabsorption, and phosphorylation is an important post-translational modification that alters the activity of the members in the WNK-NCC cascade. Using quantitative phosphoproteomics and several bioinformatic techniques, a phosphoproteome profile of the renal cortices from FK506-treated mice was generated and phosphoproteins involved in renal tubular transport were identified. In this data, AKT was phosphorylated by FK506 and was suggested to act as the intermediary protein in the calcineurin-WNK cascade. In addition, ERK1/2 was also dysregulated by FK506 and was suggested to regulate NCC through the WNK4-ERK1/2 pathway. The phosphoproteome profile also revealed several FK506-dysregulated phosphoproteins that are involved in sodium, acid-base, glucose and potassium handling.

CNIs have been suggested to cause hypercalciuria through a decrease in TRPV5 and calbindin-D28K expression, however, the effect of FK506 on other regulatory and transport proteins involved in calcium handling is unclear. In contrast to previous studies, FK506 did not dysregulate TRPV5 expression, but instead increased the expression of the basolateral calcium transporters, NCX1 and PMCA. Based on these findings, a novel mechanism explaining CNI-induced hypercalciuria, driven by the activation of NCC, is proposed and the relationship between sodium and calcium handling in the DCT is discussed.

The effects of calcineurin inhibition on renal electrolyte transporters and their potential regulators induce salt-sensitive hypertension and hypercalciuria. The findings presented in this thesis contribute to the understanding of the underlying mechanism that governs sodium and calcium handling in the DCT and full elucidation of this molecular machinery is of interest and clinical importance.

Acknowledgements

First of all, I would like to thank my supervisors, Dr. Stephen Benedict Walsh and Dr. Joanne Marks, for their unconditional support and patient guidance during my Ph.D. experience at the Centre for Nephrology in UCL. Their unlimited supply of encouragements allowed me to explore my ideas, which enabled me to achieve goals beyond my beliefs. I cannot stress the appreciation I have for both of them in providing the opportunities for me to work on several different projects and the chance to collaborate with different research groups, broadening my knowledge and sparking my interests in various fields of biology, and more importantly, for believing that I can get the job done.

The opportunity to work with Professor Jasminka Godovac-Zimmermann and her research team gave me invaluable insights into the proteomics world. The quote, "You learn something new every day." applied very literally and without the patient teachings of Dr. Benedetta Lombardi, this project would not have been as successful as it is now and on that note, I cannot emphasise on how appreciative I am of their help. I would also like to thank Dr. Anselm Zdebik for his detailed advice and ideas on the oocyte project. He inspired me to think innovatively and taught me many novel experimental techniques so that I could achieve the goals I originally set out.

Special thanks to St. Peter's Trust and UCL for my IMPACT studentship award, which funded and enabled me to complete these research projects.

Furthermore, I would also like to thank my family for their care and willingness to answer every single one of my "emergency" phone calls, despite the time difference between London and Hong Kong. I would also like to thank Dr. Adam Dyer, Anne Kesselheim and Dr. Gregory Jacquillet for their support and ability to provide last-minute accommodations whenever I needed them. Finally, thanks must also go to the colleagues and staff from the Centre for Nephrology, for being the friendliest and most approachable group I have ever worked with; never have they hesitated or failed to answer any of my questions.

Abbreviations

ACE	Angiotensin-converting enzyme
ADCY	Adenylyl cyclase
AKT	Protein kinase B
AMPK	Adenosine monophosphate-activated protein kinase
ANG	Angiotensin
AP3D1	AP-3 complex subunit delta-1
AQP2	Aquaporin-2
ASPA	Animals (Scientific Procedures) Act
ATP	Adenosine triphosphate
ATR	Angiotensin II receptor
AVPR2	Arginine vasopressin receptor 2
AWERB	Animal Welfare and the ethical review body
BCR	Broad-Complex, Tramtrack and Bric a brac-Cullin3-RING-box protein 1
BK	“big” K ⁺ channel
BSA	Bovine serum albumin
B-WNK3	Brain-WNK3
CACNA1E	Calcium voltage-gated channel subunit α 1E
CaMK-II	Calcium/calmodulin-dependent protein kinase II
CaN	Calcineurin
CANX	Calnexin
CASK	Calcium/calmodulin-dependent serine protein kinase
CaSR	Calcium-sensing receptor
CD	Collecting duct
CD8	Cluster of differentiation 8
CDK	Cyclin-dependent kinases
CDPK	Calcium-dependent protein kinase
CK-II	casein kinase II
CLCN5	Hydrogen/chloride exchange transporter 5
CLCNKB	Chloride voltage-gated channel Kb
CNI	Calcineurin inhibitor
CNT	Connecting tubule
CUL3	Cullin-3

CYP11B2	Aldosterone synthase
CyA	Cyclosporine A
DCT	Distal convoluted tubule
DGKQ	Diacylglycerol kinase theta
DNA	Deoxyribonucleic acid
DTT	Dithiothreitol
EAST syndrome	Epilepsy, ataxia, sensorineural deafness and salt-wasting renal tubulopathy
EGF	Epidermal growth factor
EMA	Epithelial membrane antigen
ENaC	Epithelial sodium channel
eNOS	Endothelial nitric oxide synthase
ER	Endoplasmic reticulum
ERK1/2	Extracellular signal-regulated kinase 1 and 2
FGF23	Fibroblast growth factor 23
FHHt	Familial hyperkalaemic hypertension
FK506	Tacrolimus
FKBP	FK506 binding protein
GSK3	Glycogen synthase kinase 3
HA	Human influenza hemagglutinin
HCD	Higher energy collision dissociation
HDL-C	High-density lipoprotein cholesterol
HEK 293H	Human embryonic kidney 293 cells
HEPES	4-(2-hydroxyethyl)-1-piperazineethanesulfonic acid
HSD	High sodium chloride diet
HSP90AB1	Heat shock protein HSP 90- β
IDH	Isolated dominant hypomagnesaemia
IGF1	insulin-like growth factor 1
IL	Interleukin
IMAC	Immobilised metal affinity chromatography
IP	Intraperitoneal
IP3R	Inositol 1,4,5-trisphosphate receptors
IRAK2	Interleukin-1 receptor-associated kinase 2
KCC	Potassium chloride cotransporter

KCNJ	Inward-rectifying potassium channel
KLHL3	Kelch-like protein 3
Klotho	β -glucuronidase klotho
KS-WNK1	Kidney specific-WNK1
Kv1.1	Shaker-related voltage-gated potassium channel
LAT4	L-type amino acid transporter 4
LB	Lysogeny Broth
LCM	Laser capture microdissection
LC-MS/MS	Liquid chromatography-mass spectrometry
LKB1	Liver kinase B1
MAPK	Mitogen-activated protein kinase
MAPK8IP4	Mitogen-activated protein kinase 8-interacting protein 4
MDCK	Madin-darby canine kidney
MO25	Mouse embryo scaffolding protein
mDCT	Mouse distal convoluted tubule
MR	Mineralocorticoid receptor
MS	Mass spectrometry
mTOR	Mechanistic/mammalian Target Of Rapamycin
Na ⁺ /K ⁺ -ATPase	Sodium-potassium adenosine triphosphatase
NaPi	Sodium phosphate cotransporter
NBCe1	sodium bicarbonate cotransporter 1
NCC	Sodium chloride cotransporter
NCX1	Sodium/calcium exchanger 1
Nedd4	E3 ubiquitin-protein ligase
NFATc	Cytoplasmic nuclear factor of activated T cells
NHE	Sodium/hydrogen exchanger
NHERF	Sodium/hydrogen exchanger regulatory factor
NKCC	Sodium chloride potassium cotransporter
NKCC2	Sodium chloride potassium cotransporter 2
NLK	Nemo-Like Kinase
NO	Nitric oxide
OSR1	Oxidative stress responsive kinase 1
PBS	Phosphate-buffered saline
PCR	Polymerase chain reaction

PCT	Proximal convoluted tubule
PI3K	Phosphatidylinositol 3-kinase
PKA/C	Protein kinase A/C
PMCA	Plasma membrane Ca ²⁺ ATPase
PNST	Post-nuclear supernatant
PPIase	Peptidylprolyl cis-trans isomerase
PsHP	Pseudohypoparathyroidism
PTH	Parathyroid hormone
PTH1R	Parathyroid hormone 1 receptor
PTK	Protein tyrosine kinase
PVDF	Polyvinylidene difluoride
RAAS	Renin-angiotensin-aldosterone system
RFx[V/I]	Arg-Phe-Xaa-Val/Ile
RLK	Receptor-like kinase
RLU/s	Relative light units per seconds
ROMK	Renal outer medullary K ⁺ channel
SLC	Solute carrier family
SLC41A1	Solute carrier family 41 member 1
RTK	Tyrosine kinase receptor
RT-qPCR	Quantitative reverse transcription polymerase chain reaction
R-WNK3	Renal-WNK3
RyR	Ryanodine receptor
SDS	Sodium dodecyl sulphate
SDS-PAGE	Sodium dodecyl sulphate-polyacrylamide electrophoresis
SERCA	Sarco endoplasmic reticulum calcium ATPase 2b
SGK1	Serum and glucocorticoid-regulated kinase 1
SGLT2	sodium glucose cotransporter 2
SGPP1	Sphingosine-1-phosphatase 1
SNP	Single nucleotide polymorphism
SPAK	STE20-like proline-alanine rich kinase
SPNA2	Spectrin α -chain
STRAD	STE20 related adapter

TAE	Tris-acetate-EDTA
TALH	Thick ascending limb of the loop of Henle
TBS	Tris-buffered saline
TEAB	Triethylammonium bicarbonate
TM	Transmembrane
TMT	Tandem mass tags
TNF- α	Tumour necrosis factor- α
TPR	Tetratricopeptide repeat
TRP	Transient receptor potential
TRPM6	Transient receptor potential cation channel subfamily M member 6
TRPP2	Transient receptor potential cation channel subfamily P member 2
TRPV5/6	Transient receptor potential cation channel subfamily V member 5/6
VDR	Vitamin D ₃ receptors
WHO	World Health Organization
WNK	With No lysine (K) kinase
1,25(OH) ₂ D ₃	1,25-Dihydroxyvitamin D ₃
11HSD2	11- β hydroxysteroid dehydrogenase 2
24,25(OH) ₂ D ₃	24,25-dihydroxyvitamin D ₃
25(OH)D ₃	25-hydroxyvitamin D ₃

Contents

Chapter 1. Introduction	24
1.1 Hypertension and the metabolic syndrome crisis	25
1.1.1 What is the metabolic syndrome?	25
1.1.2 Complications associated with the metabolic syndrome	28
1.1.3 Immunosuppressants and the metabolic syndrome	28
1.1.4 The similarities between CNIs and thiazides-associated side effects, FHt and Gitelman syndrome	29
1.2 Blood pressure homeostasis	30
1.2.1 Autonomic nervous system	30
1.2.2 Renin-angiotensin-aldosterone system	30
1.2.3 Renal system	31
1.3 The Distal Convulated Tubule	31
1.3.1 Structure of the DCT	32
1.3.2 Salt handling by the DCT	32
1.3.2.1 Sodium transport in the DCT	32
1.3.2.2 Chloride transport in the DCT	33
1.3.2.3 Potassium transport in the DCT	34
1.3.2.4 Regulation of sodium, chloride and potassium handling in the DCT	37
1.3.3 Divalent cation handling in the DCT	39
1.3.3.1 Calcium transport in the DCT	39
1.3.3.2 Regulation of calcium handling in the DCT	41
1.3.3.3 Magnesium transport in the DCT	41
1.3.3.4 Regulation of magnesium handling in the DCT	44
1.4 DCT Pathophysiology	44
1.4.1 Gitelman syndrome	44
1.4.1.1 Renal pathophysiology of Gitelman syndrome	45

1.4.2	Gitelman-like disorders.....	45
1.4.2.1	Isolated dominant hypomagnesaemia	45
1.4.2.1.1	Renal pathophysiology of isolated dominant hypomagnesaemia	45
1.4.2.2	EAST syndrome.....	46
1.4.2.2.1	Renal pathophysiology of EAST syndrome	46
1.4.3	Familial hyperkalaemic hypertension	46
1.4.3.1	Renal pathophysiology of Familial hyperkalaemic hypertension.	46
1.4.4	CNI-induced hypertension.....	47
1.4.4.1	Renal pathophysiology of CNIs.....	47
1.5	NCC.....	48
1.5.1	NCC Structure	48
1.5.2	Functional properties of NCC	48
1.5.3	Thiazide and ion affinity.....	49
1.5.3.1	Affinity controversy	49
1.5.3.2	Chloride affinity.....	49
1.5.4	Phosphorylation of NCC.....	50
1.6	WNK kinases	50
1.6.1	Structure of WNK kinases	50
1.6.2	WNK1.....	53
1.6.2.1	Influence of aldosterone, dietary potassium and sodium on WNK1	53
1.6.2.2	WNK1 and electrolyte transporters.....	54
1.6.2.3	Phosphorylation of WNK1.....	54
1.6.2.4	FHht type mutation in WNK1.....	56
1.6.3	WNK3.....	56
1.6.3.1	WNK3 and the electrolyte transporters	56
1.6.3.2	WNK3 splice variants and NCC.....	57

1.6.4	WNK4.....	57
1.6.4.1	Influence of aldosterone, dietary potassium and sodium on WNK4	57
1.6.4.2	WNK4 and electrolyte transporters	58
1.6.4.2.1	Hyperkalaemia and WNK4 regulation of ion transporters..	58
1.6.4.2.2	Hypovolemia and WNK4 regulation of ion transporters.....	59
1.6.4.3	Phosphorylation of WNK4.....	59
1.6.4.4	FHHT-type mutation in WNK4.....	61
1.6.5	SPAK/OSR1	61
1.6.5.1	Phosphorylation of SPAK and OSR1	62
1.6.5.2	Evolution of SPAK and OSR1	62
1.6.6	KLHL3 & CUL3.....	63
1.6.6.1	Phosphorylation of KLHL3 and CUL3	63
1.6.6.2	FHHT-type mutation in KLHL3 and CUL3.....	63
1.7	WNK-NCC cascade	64
1.7.1	The orthodox model of the WNK-NCC cascade	64
1.7.2	The effect of FHHT on the WNK-NCC cascade	66
1.7.3	The effect of CNIs on the WNK-NCC cascade.....	66
1.8	Calcineurin.....	69
1.8.1	Structure.....	69
1.8.2	Calmodulin	69
1.8.3	Activation of calcineurin.....	70
1.8.4	Function	70
1.8.5	The association between calcineurin and the RAAS.....	72
1.8.6	Immunophilins	72
1.8.7	Calcineurin inhibitors.....	72
1.8.7.1	Other side effects of CNIs.....	73
1.9	Calcium transport in the distal nephron	75

1.9.1	Regulators of DCT calcium transport	75
1.9.1.1	PTH	75
1.9.1.2	Vitamin D ₃	76
1.9.1.3	Klotho	76
1.9.2	TRPV5.....	80
1.9.2.1	Structure of TRPV5.....	80
1.9.2.2	Functional properties of TRPV5.....	80
1.9.2.3	TRPV5 and WNK4.....	81
1.9.2.4	Phosphorylation of TRPV5.....	81
1.9.3	NCX1.....	82
1.9.3.1	NCX1 splice variants	82
1.9.3.2	Structure of NCX1.....	82
1.9.3.3	Functional properties of NCX1	83
1.9.3.4	Phosphorylation of NCX1	83
1.9.4	PMCA.....	85
1.9.4.1	Structure of PMCA.....	85
1.9.4.2	Functional properties of PMCA	86
1.9.4.3	Phosphorylation of PMCA.....	88
1.9.5	Calbindin-D28K	88
1.10	Relationship between sodium and calcium transport at the DCT	88
1.10.1	Thiazide diuretics and calcium wasting.....	88
1.10.2	Gitelman syndrome and hypocalciuria	89
1.10.3	FHHt and hypercalciuria.....	90
1.10.4	Essential hypertension, hypercalciuria and kidney stones	90
1.10.5	CNI-induced hypercalciuria	91
1.11	Aims of thesis	91
Chapter 2.	Interaction of intermediary proteins in the calcineurin-WNK-NCC cascade	93

2.1	Introduction.....	94
2.1.1	Aims	94
2.2	Materials and Methods	95
2.2.1	The insertion of HA-epitopes in NCC	95
2.2.2	The insertion of HA-epitopes into CD8 and co-expression with NCC	95
2.2.3	Plasmid construct synthesis of CUL3, KLHL3 and SPAK.....	96
2.2.4	Molecular cloning protocol.....	96
2.2.4.1	Gel electrophoresis and gel purification.....	96
2.2.4.2	Electroporation and Cloning	99
2.2.4.3	Restriction digestion and sequencing	99
2.2.4.4	cRNA synthesis for oocyte injections.....	100
2.2.5	Animal Studies	100
2.2.5.1	Oocyte harvesting.....	101
2.2.5.2	Oocyte protein preparation	101
2.2.5.3	Western blot of oocyte proteins	101
2.2.6	Single oocyte chemiluminescence	102
2.2.7	Statistical analysis	102
2.3	Results.....	103
2.3.1	Topology of NCC.....	103
2.3.2	HA-tagged NCC construct synthesis	106
2.3.3	Single oocyte chemiluminescence assay	109
2.3.4	Co-expression of NCC and HA-tagged CD8 glycoprotein	111
2.3.5	Plasmid construct synthesis	114
2.4	Discussion	116
2.4.1	Oocyte chemiluminescence assay	116
2.4.2	Other members of the WNK-NCC cascade.....	118
2.4.3	Future experiments	118

Chapter 3. Exploring the effect of FK506 on the renal kinome	120
3.1 Introduction.....	121
3.1.1 Aims	122
3.2 Materials and methods	123
3.2.1 Animals	123
3.2.2 Electrolyte measurements in blood and urine	125
3.2.3 Kidney protein homogenisation	125
3.2.4 Western blot analysis	126
3.2.5 Statistics.....	126
3.2.6 Reduction, alkylation precipitation and tryptic digestion	126
3.2.7 TMT Labelling and Phosphopeptides enrichment	127
3.2.8 Mass Spectrometry	128
3.2.9 Proteins and Peptides Identification, Quantification and Enrichment analysis.....	128
3.3 Results.....	131
3.3.1 Validation of adverse effects caused by CNIs	131
3.3.2 Overview of the proteomics dataset	134
3.3.3 Data interpretation.....	136
3.3.3.1 FK506-dysregulated proteins.....	136
3.3.3.2 Phosphorylation motifs	143
3.3.3.3 Interactions of AKT and ERK1/2 with the calcineurin-NCC cascade	146
3.3.3.4 Effects of FK506 on ERK1/2 and AKT	148
3.3.3.5 Candidate approach: FK506-dysregulated transport and regulatory proteins	151
3.3.3.5.1 Transport proteins	151
3.3.3.5.2 Classified transport proteins identified in the membrane and cytosolic fractions	157
3.3.3.5.3 Regulatory proteins	159

3.3.3.6	Candidate approach: ACE and NHERF1	164
3.4	Discussion	166
3.4.1	Overview of quantitative phosphoproteomics	166
3.4.2	AKT and the WNK-NCC cascade	167
3.4.3	HSP90, AKT and the metabolic syndrome	168
3.4.4	ERK1/2 and the WNK-NCC cascade	168
3.4.5	Candidate approach	169
3.4.5.1	Hypertension	169
3.4.5.2	Metabolic acidosis	171
3.4.5.3	Glucose transport	172
3.4.5.4	Potassium homeostasis	173
3.4.5.5	Ubiquitous transport proteins	173
3.4.6	Future experiments	174
Chapter 4.	The effects of FK506 on distal renal calcium handling	177
4.1	Introduction	178
4.1.1	Aims	179
4.2	Materials and methods	180
4.2.1	Animals	180
4.2.2	Real-time PCR	180
4.2.3	Western blot analysis	181
4.2.1	Statistics	181
4.3	Results	183
4.3.1	Effects of FK506 on transcripts of respective calcium regulatory and transport proteins	183
4.3.2	Effects of FK506 and a high salt diet on calcium transport and buffering proteins in the DCT	185
4.3.3	Effects of FK506 and a high salt diet on DCT sodium transport proteins	192
4.3.4	Effects of FK506 and a high salt diet on PKC	196

4.3.5	Phosphoproteins in FK506-treated mice that may play a role in distal renal calcium handling	200
4.4	Discussion	206
4.4.1	The novel mechanism of CNI-induced hypercalciuria	206
4.4.2	FK506 with a HSD reversed the effect of FK506 on the calcium transport proteins.....	209
4.4.3	The effect of increased NaCl intake on calcium transport proteins....	210
4.4.4	The effects of FK506 on PKC.....	211
4.4.5	Other calcium regulatory proteins.....	212
4.4.5.1	Adenylyl cyclase 6	212
4.4.5.2	R-type calcium channel subunit α -1E	213
4.4.5.3	Calnexin.....	213
4.4.6	Future studies	214
Chapter 5.	Discussion.....	216
5.1	Summary of the thesis	217
5.2	The effect of insulin resistance on sodium retention in the metabolic syndrome.....	218
5.2.1	The effect of insulin resistance and ER stress in the metabolic syndrome	219
5.3	Fast calcium binding to calmodulin supports calcineurin activation with calcium influx into the DCT.....	222
5.4	Underlying causes of the metabolic syndrome	225
5.4.1	Vitamin D ₃ deficiency	225
5.4.2	PTH.....	226
5.4.2.1	Hyperparathyroidism.....	227
5.4.2.2	Hypoparathyroidism.....	227
5.4.2.3	Pseudohypoparathyroidism	227
5.5	Further avenues of investigation.....	228

Chapter 6.	Appendix.....	230
6.1	Topology and glycosylation of mouse NCC	231
6.2	Proteomics quality checks	233
6.3	Quantitative phosphoproteomic tables.....	236
Chapter 7.	References.....	238

Figures

Figure 1.3-1 Sodium, chloride and potassium transport at the DCT.	36
Figure 1.3-2 RAAS regulation of sodium and potassium homeostasis in the DCT	38
Figure 1.3-3 A schematic diagram of calcium transport at the DCT	40
Figure 1.3-4 A schematic diagram of magnesium transport at the DCT	43
Figure 1.6-1 Alignment of the residues encoding for substrate specificity in WNK1-4	52
Figure 1.6-2 WNK1 regulation of the distal sodium and potassium transporters	55
Figure 1.6-3 Influence of hypovolemia and hyperkalaemia on WNK4-modulated ion transporters	60
Figure 1.7-1 The orthodox model of the WNK-NCC cascade	65
Figure 1.7-2 FHHt-mutations in the WNK-NCC cascade	67
Figure 1.7-3 The effect of CNIs on the WNK-NCC cascade	68
Figure 1.8-1 Calcineurin activation.....	71
Figure 1.8-2 The immunosuppressive effects of CNIs	74
Figure 1.9-1 Regulation of calcium reabsorption in the DCT	78
Figure 1.9-2 The PTH-Vitamin D ₃ -FGF23 axis in the nephron.....	79
Figure 1.9-3 Topology prediction of NCX1.....	84
Figure 1.9-4 Activation of PMCA.....	87
Figure 2.3-1 Schematic representation pSDS_mNCC2HA	105
Figure 2.3-2 NCC2HA DNA construct synthesis	107
Figure 2.3-3 Restriction digestion analysis of pSDS_mNCC2HA.....	108
Figure 2.3-4 Western blot analysis of NCC2HA protein expression in oocytes	108
Figure 2.3-5 Single-oocyte chemiluminescence assay	110
Figure 2.3-6 Schematic representation of pSDS_mNCC_CD8HA	112
Figure 2.3-7 NCC_CD8HA DNA construct synthesis.....	113
Figure 2.3-8 CUL3 and SPAK DNA construct synthesis	115
Figure 3.2-1 Schematic representation of the experimental procedure.....	124
Figure 3.3-1 Protein expression of distal nephron transporters post-FK506 treatment.....	133

Figure 3.3-2 The number of unique phosphopeptides identified in the membrane and cytosolic fractions.....	135
Figure 3.3-3 Protein clusters identified in the network of FK506-dysregulated proteins in the membrane fraction.....	139
Figure 3.3-4 Regulatory proteins associated with kinase/phosphatase identified in the network of FK506-dysregulated proteins in the membrane fraction	140
Figure 3.3-5 Protein clusters identified in the network of FK506-dysregulated proteins in the cytosolic fraction	141
Figure 3.3-6 Regulatory proteins associated with kinase/phosphatase identified in the network of FK506-dysregulated proteins in the cytosolic fraction.....	142
Figure 3.3-7 Interactions between AKT1, ERK1/2 and WNK-NCC cascade...	147
Figure 3.3-8 Protein expression of ERK1/2 and pERK1/2 post-FK506 treatment	149
Figure 3.3-9 Protein expression of AKT1 post-FK506 treatment.....	150
Figure 4.3-1 mRNA expression of calcium regulatory and transport proteins in the kidneys post-FK506 treatment	184
Figure 4.3-2 The effects of FK506 and HSD on TRPV5 protein expression in the kidney membrane	188
Figure 4.3-3 The effects of FK506 and HSD on calbindin-D28K protein expression in the kidney.....	189
Figure 4.3-4 The effects of FK506 and HSD on NCX1 protein expression in the kidney membrane	190
Figure 4.3-5 The effects of FK506 and HSD on PMCA1/4 protein expression in the kidney membrane	191
Figure 4.3-6 The effects of FK506 and HSD on NCC protein expression in the kidney membrane	193
Figure 4.3-7 The effects of FK506 and HSD on pNCC protein expression in the kidney membrane	194
Figure 4.3-8 The effects of FK506 and HSD on Na ⁺ /K ⁺ -ATPase protein expression in the kidney membrane	195
Figure 4.3-9 The effects of FK506 and HSD on PKC β1 protein expression in the kidney	197
Figure 4.3-10 The effects of FK506 and HSD on PKC δ protein expression in the kidney	198

Figure 4.3-11 The effects of FK506 and HSD on PKC ϵ protein expression in the kidney	199
Figure 4.3-12 The effects of FK506 and HSD on ADCY6 protein expression in the kidney	204
Figure 4.3-13 The effects of FK506 and HSD on Calnexin protein expression in the kidney	205
Figure 4.4-1 Schematic model of CNi-induced hypercalciuria in the DCT	208
Figure 5.2-1 Sodium retention in the distal tubule of insulin resistant mice.....	221
Figure 5.3-1 A proposed model of a compensatory mechanism to prevent sodium reabsorption during salt overload.....	224
Figure 6.1-1 Posterior probabilities plot of mouse NCC	231
Figure 6.2-1 Purity of fractionated samples	233
Figure 6.2-2 Protein recovery after acetone precipitation	234

Tables

Table 1.1-1 The WHO diagnostic criteria of the metabolic syndrome	27
Table 2.2-1 PCR program and reagents	97
Table 2.2-2 Primers used in molecular cloning	98
Table 2.3-1 Glycosylation sites in transmembrane, intracellular and extracellular regions of NCC	104
Table 3.3-1 Serum and urine electrolytes in mice treated with vehicle or FK506	132
Table 3.3-2 Phosphorylation motifs up and downregulated in the membrane fraction.....	144
Table 3.3-3 Phosphorylation motifs up and downregulated in the cytosolic fraction.....	144
Table 3.3-4 FK506-dysregulated transport proteins identified in the membrane fraction.....	154
Table 3.3-5 FK506-dysregulated transport proteins identified in the cytosolic fraction.....	156
Table 3.3-6 FK506-dysregulated transport proteins identified in membrane and cytosolic fractions.....	158
Table 3.3-7 FK506-dysregulated kinase/phosphatase-associated proteins identified in the membrane fraction.....	161
Table 3.3-8 FK506-dysregulated kinase/phosphatase-associated proteins identified in the cytosolic fraction	162
Table 3.3-9 FK506-dysregulated kinase/phosphatase-associated proteins identified in the membrane and cytosolic fractions.....	163
Table 3.3-10 FK506-dysregulated phosphosites in NHERF1	165
Table 4.2-1 RT-qPCR programme.....	182
Table 4.3-1 Calcium creatinine ratio and serum magnesium levels of FK506 or vehicle treated mice	187
Table 4.3-2 FK506-dysregulated phosphoproteins involved in calcium handling identified in the nephron.....	203
Table 6.1-1 Predicted glycosylation sites in mouse NCC.....	232
Table 6.2-1 Labelling efficiency of the membrane and cytosolic fractions	235
Table 6.3-1 Quantified phosphopeptides identified in the membrane fraction	236
Table 6.3-2 Quantified phosphopeptides identified in the cytosolic fraction	236

Table 6.3-3 Unique phosphopeptides identified in the membrane fraction	236
Table 6.3-4 Unique phosphopeptides identified in the cytosolic fraction.....	237
Table 6.3-5 Unique phosphopeptides identified in calcium-associated proteins in the membrane fraction	237
Table 6.3-6 Unique phosphopeptides identified in calcium-associated proteins in the cytosolic fraction	237

Chapter 1. Introduction

1.1 Hypertension and the metabolic syndrome crisis

Hypertension is the single most important modifiable risk factor for premature mortality in the world. In 2000, hypertension affected 26.4 % of adults worldwide and this is estimated to increase to 29.2 % by 2025 (1). Hypertension is a major risk factor for cardiovascular diseases (2) and one of the leading risk factors for renal failure in the Western world (3), and increasingly in the developing world. Hypertension is responsible for 9.4 million deaths per year (4) and is accountable for 45 to 51 % of deaths associated with strokes and ischemic heart diseases (5). Hypertension is a public health epidemic and an estimated 10 % of healthcare expenditure is related to hypertension and its complications, therefore finding a strategy to reduce the morbidity of hypertension has become a priority in modern medicine (6).

The development of hypertension can involve both genetic and behavioural risk factors. The existence of monogenic hypertensive disorders, such as familial hyperkalaemic hypertension (FHt) (7,8), familial hyperaldosteronism type III (9) and Liddle syndrome (10), has led to the discovery of specific mutations in thirteen hypertension genes in the kidneys and the renin-angiotensin-aldosterone system (RAAS) (11). Behavioural factors which involve increased salt and fat consumption, a diet low in fruit and vegetables (low dietary potassium), excessive alcohol consumption, lack of exercise, use of tobacco and poor stress management are key determinants in the development and the progression of hypertension (12). Not only can these behavioural factors cause hypertension over time, but in combination with insulin resistance, dyslipidaemia and obesity, they comprise the metabolic syndrome (13).

1.1.1 What is the metabolic syndrome?

The metabolic syndrome was first defined by Reaven in 1988 (14) as a cluster of biochemical and physiological disorders, which include hypertension, hyperglycaemia, hypertriglyceridemia, abdominal obesity and low high-density lipoprotein cholesterol (HDL-C) levels. The metabolic syndrome is a growing epidemic and affects a reported 10 to 84 % of the population worldwide (15). This estimation of incidence has a wide variability due to several contributing factors. For example, the disparity in definitions of the metabolic syndrome and some

environmental factors, such as the region and socioeconomic status of the population studied, contribute to the variability of the estimated prevalence of the syndrome (15,16).

Several clinical definitions of the syndrome have emerged since its first characterisation, the key features that comprise the metabolic syndrome remain unchanged, and instead, the parameters for each criterion differ slightly. The World Health Organization (WHO) (17), the National Cholesterol Education Programme Adult Treatment Panel III (18), the American Association of Clinical Endocrinologists (19), the European Group for the study of Insulin Resistance (20) and the International Diabetes Federation (21) have all provided criteria for diagnosing the metabolic syndrome. As the defined diagnostic criteria differs between each of these organisations, this creates discrepancies in the assessment and intervention of the metabolic syndrome. Using the diagnostic criteria recommended by the WHO (Table 1.1-1), the metabolic syndrome was estimated to affect over 33.9 % of women and over 44.8 % of men aged between 40-65 in England (22).

Table 1.1-1 The WHO diagnostic criteria of the metabolic syndrome

Clinical measures	
Requirement	Insulin resistance or type 2 diabetes
and at least two of the criteria listed below	
Abdominal obesity	Waist/hip ratio in men: >0.9 Waist/hip ratio in women: >0.85 or BMI: >30 kg/m ²
Hypertension	Systolic blood pressure: ≥140 mmHg Diastolic blood pressure: ≥90 mmHg
Dyslipidaemia	Triglycerides level: ≥150 mg/dL HDL-C levels in men: <35 mg/dL HDL-C levels in women: <39 mg/dL
Microalbuminuria	Urinary albumin excretion: ≥20 µg/min or Albumin/creatinine ratio: ≥30 mg/g

1.1.2 Complications associated with the metabolic syndrome

The cause of the metabolic syndrome is not entirely understood, but it is known to be strongly associated with the development of cardiovascular diseases and type 2 diabetes. Individuals with the metabolic syndrome have a two-fold increased risk of developing cardiovascular diseases and a five-fold increased risk of developing diabetes over a five to ten year period (23).

Other complications are also associated with the metabolic syndrome, these include non-alcoholic fatty liver disease (24), gout (25), osteoporosis (26), and kidney stone disease (27). Both osteoporosis and kidney stone disease can result from renal tubular dysfunction caused by defective calcium and phosphate handling, which also cause hypercalciuria and hypophosphatemia (28–30). Bone demineralisation can lead to osteoporosis, which has been reported to cause over 9 million bone fractures per year (31). Kidney stone disease has become increasingly common with a rise in global incidence and prevalence (27,32–34). Kidney stone disease was estimated to affect 11.62 % of the population in the U.K., as of 2011, and the number of hospital episodes of kidney stone disease has risen by 63 % over the last decade (35). The trend shown in these studies indicates that osteoporosis and kidney stone disease are major public health issues with high morbidity and mortality, and are a great burden on the healthcare system.

1.1.3 Immunosuppressants and the metabolic syndrome

The conventional immunosuppressive protocol after kidney transplantation is the use of the triple therapy approach, consisting of a calcineurin inhibitor (CNI), a steroid and a conjugating immunosuppressant (mycophenolate mofetil or azathioprine). Of the medications used in this regimen, CNIs are the most effective for preventing allograft rejection (36,37). Cyclosporine A (CyA) was the first effective CNI, and it revolutionised transplant medicine in the 1980s (38). This was followed by tacrolimus (FK506) in the 1990s, which has a lower acute rejection rate compared to CyA (39). CNIs have become the first line pharmacological agents recommended by the Kidney Disease Improving Global Outcome and they are prescribed to at least 96 % of transplant recipients, along with mycophenolate mofetil (40).

The use of this triple immunosuppressive regimen has led to an annual graft survival rate greater than 90 % (41). However, the metabolic side effects associated with immunosuppressants (e.g. hypertension, type 2 diabetes, dyslipidaemia, obesity and renal injury) (42,43), have become risk factors for morbidity and decreased graft function (44,45). Post-transplant metabolic syndrome occurs in 63 % of kidney transplant recipients (46) and 43 to 58 % of liver transplant recipients (45,47), accounting for 30 to 49 % of cardiovascular-induced mortality in transplant recipients with functional grafts (48,49).

1.1.4 The similarities between CNIs and thiazides-associated side effects, FHHT and Gitelman syndrome

CNI-induced hypertension is a major clinical problem in transplant medicine. The prevalence of hypertension in renal transplant recipients ranges from 47 to 82 % in paediatric recipients and 50 to 80 % in adult recipients (50). CNI-induced hypertension is relatively common and is caused by abnormally avid reabsorption of sodium and chloride in the distal convoluted tubule (DCT), triggered by sodium chloride cotransporter (NCC) overactivity (51). Renal tubule dysfunction is another common adverse effect of CNI treatment. It is manifested by hyperkalaemia (52,53), metabolic acidosis (54,55), hypercalciuria (56,57), hypomagnesaemia (57,58), and hypophosphatemia (59). These side effects resemble the phenotype of FHHT, a rare autosomal dominant disorder characterised by NCC overactivity (60,61), suggesting that the pathogenesis of CNIs and FHHT may share similarities.

Gitelman syndrome is also an inherited renal disorder that is a mirror-image syndrome to FHHT. The pathogenesis of Gitelman syndrome is the loss of NCC function (62), causing blood volume depletion with a resulting hyperreninemic hyperaldosteronism which leads to a hypokalaemic metabolic alkalosis. Gitelman syndrome is also associated with hypocalciuria and hypomagnesaemia (63). The resemblance between the handling of sodium, calcium and magnesium in Gitelman patients and patients taking thiazide diuretics (a class of antihypertensive medication that inhibits NCC), reflects the genetic and pharmacologic inactivation of the same transport protein (64).

It is evident that CNIs cause electrolyte abnormalities through tubular dysfunction, however the pathogenesis remains unclear. The distal nephron is

responsible for the fine-tuning of electrolyte homeostasis, such as sodium and calcium reabsorption in the kidney, and this thesis will focus on investigating the pathogenesis of CNI-induced hypertension and hypercalciuria, salt and calcium handling in the distal renal tubules, and the pleiotropic effects of calcineurin.

1.2 Blood pressure homeostasis

Blood pressure is regulated by the cardiovascular, renal and neuroendocrine systems. These systems are interlinked through multiple feedback mechanisms and ensure both short and long-term maintenance of blood pressure and blood volume.

1.2.1 Autonomic nervous system

The cardiovascular and autonomic nervous system plays an important role in maintaining blood pressure via the baroreceptor reflex. There are two types of baroreceptors, located in different pressure receptor zones. High-pressure arterial baroreceptors are located at the aortic arch and carotid sinuses, and their activity is dependent on changes in arterial pressure. These baroreceptors are activated when blood pressure is increased and signals are sent to the rostral ventrolateral medulla, which trigger changes in heart contractions and systemic vascular resistance. Low-pressure baroreceptors are mainly situated in the venae cavae, pulmonary veins and atria, and are involved in blood volume regulation. They are activated during hypovolemia and induce activation of the RAAS. RAAS increases fluid retention in the kidneys and increases cardiac output, thereby restoring blood volume. The baroreceptor reflex provides a constant negative feedback loop to the brainstem and is the faster acting of the three systems that regulate blood pressure, the other two being the renal and endocrine system (65).

1.2.2 Renin-angiotensin-aldosterone system

The RAAS is part of the endocrine system that is involved in blood pressure regulation. It can be activated by a decrease in blood pressure, which is detected by stretch receptors in the vascular walls and by macula densa cells in the distal nephron, resulting in renin secretion by juxtaglomerular cells. Plasma renin cleaves angiotensinogen present in the plasma into angiotensin (ANG) I. Angiotensin-converting enzyme (ACE) expressed and secreted by endothelial

and renal epithelial cells, then converts ANGI to ANGI in the plasma. This causes arteriole constriction, leading to an increase in blood pressure, the stimulation of aldosterone secretion from the adrenal cortex, and the secretion of vasopressin from the posterior pituitary gland. Aldosterone binds to the mineralocorticoid receptors (MR) on the basolateral membrane of the DCT and increases sodium reabsorption. Further down the nephron, vasopressin binds to the arginine vasopressin receptor 2 (AVPR2) on the basolateral membrane of the collecting duct (CD) and causes water retention.

1.2.3 Renal system

In the kidney, salt and water reabsorption are key determinants of blood volume and therefore blood pressure regulation. Sodium reabsorption is regulated by the RAAS and is mediated by specific transporters: the sodium chloride potassium cotransporter 2 (NKCC2) in the thick ascending limb of loop of Henle (TALH), NCC in the DCT, and the epithelial sodium channel (ENaC) in the CD. More recently, sodium and chloride cotransport has been described in the CD by the paired action of pendrin and the sodium-driven chloride/bicarbonate exchanger (66). Throughout most of the nephron, water reabsorption is not regulated, instead it is reabsorbed through passive transport and coupled to solute reabsorption. In the CD, water reabsorption is regulated by vasopressin via AVPR2 and transported through aquaporin-2 (AQP2). When aldosterone binds to the MR at the DCT and vasopressin binds to AVPR2 at the CD, sodium chloride and water is reabsorbed into the bloodstream through these transport proteins (67).

1.3 The Distal Convoluted Tubule

The DCT is the shortest segment in the nephron, and lies immediately downstream of the macula densa and upstream of the CD. Even though the DCT is short in length, averaging 5 mm in humans (68), it plays an important role in electrolyte homeostasis. The DCT is responsive to hormonal stimulus and sensitive to changes in the concentration of electrolytes in the tubular fluid. The DCT is also where the fine-tuning of electrolytes occurs; this involves sodium and chloride reabsorption, potassium excretion and the handling of calcium, magnesium and acid-base.

1.3.1 Structure of the DCT

The distal tubule is composed of a short segment of TALH, the DCT, which is divided into early (DCT1) and late DCT (DCT2), and the connecting tubule (CNT). Aldosterone is a mineralocorticoid secreted in response to volume depletion and hyperkalaemia. Aldosterone has a chemical structure similar to glucocorticoids, such as cortisol. Both aldosterone and cortisol bind to the MR expressed in the DCT with equal affinity and compete for binding (69). The 11- β hydroxysteroid dehydrogenase 2 (11HSD2) allows exclusive binding of aldosterone to the MR by metabolising cortisol to cortisone, which is an inactive form of cortisol that does not bind to the MR, thereby preventing cortisol from triggering its signal transduction pathways. 11HSD2 is not expressed in the cytoplasm of DCT1 cells, but is present in DCT2, the CNT and cortical CD, which comprises the aldosterone-sensitive distal nephron (70).

Most electrolytes are reabsorbed through active transcellular transport in the DCT and require an electrochemical gradient to drive their entry via the apical membrane. The basolateral electrolyte pumps, such as the sodium-potassium adenosine triphosphatase (Na^+/K^+ -ATPase) (71) and the plasma membrane calcium ATPase (PMCA), are responsible for providing this and require adenosine triphosphate (ATP) for their activity (72). These basolateral pumps consume a high amount of ATP, therefore DCT cells are packed with mitochondria that accumulate at the basolateral infoldings to accommodate for their needs (73).

1.3.2 Salt handling by the DCT

1.3.2.1 Sodium transport in the DCT

The DCT reabsorbs 5 to 10 % of filtered sodium (74) primarily through NCC. NCC is an electroneutral cation-coupled chloride cotransporter that co-transporters Na^+ and Cl^- in a 1:1 ratio and is expressed in the apical membrane of DCT cells (75,76). In DCT1, NCC is chiefly responsible for sodium chloride reabsorption, whereas both NCC and ENaC are responsible for this process in DCT2. ENaC is an electrogenic sodium channel expressed in the apical membrane of DCT2, CNT and CD. The uptake of sodium through ENaC causes lumen negativity, thus, the transepithelial voltage progressively decreases from DCT1 to the CD (77).

This provides an electrical gradient for chloride reabsorption or the promotion of potassium secretion via the renal outer medullary potassium channel (ROMK). In addition to NCC and ENaC, the electroneutral sodium/hydrogen exchanger 2 (NHE2) is also expressed in the DCT. NHE2 transports Na⁺ into the cell and exports H⁺ into the urine. NHE2 is highly expressed in the apical membrane of TALH, DCT and CNT (78) and is activated when luminal bicarbonate levels are high, suggesting that NHE2 is primarily involved in the acidification of urine (79).

The reabsorption of sodium largely relies on the basolateral Na⁺/K⁺-ATPase which maintains the sodium gradient (80). After sodium influx through NCC and ENaC, sodium is exported via Na⁺/K⁺-ATPase into the peritubular fluid. Na⁺/K⁺-ATPase exports three Na⁺ out of the cell and imports two K⁺ into the cell, resulting in a decrease in voltage across the basolateral membrane (-60 mV to -90 mV). This is a driving force for sodium influx (71). In order for transcellular reabsorption of sodium to occur, the rate of sodium influx and efflux must reach equilibrium and basolateral potassium efflux plays an important role in this process (81) (Figure 1.3-1).

1.3.2.2 Chloride transport in the DCT

In addition to the driving force provided by Na⁺/K⁺-ATPase, the intracellular chloride concentration and basolateral extrusion of chloride also play an important role in sodium influx (82). Chloride depletion increases the activity of NCC, therefore the removal of excess intracellular chloride is crucial for maintaining a transmembrane sodium gradient (82). Chloride exits the cell through the chloride voltage-gated channel Kb (CLCNKB)-Barttin complex; the electrochemical gradient provided by Na⁺/K⁺-ATPase aids this process (83). Chloride can also exit the cell through the electroneutral potassium chloride cotransporter (KCC), which is stimulated by hypotonicity (84,85). There are four members of the KCCs and similar to NCC and NKCC2, they belong to the electroneutral cation-coupled chloride cotransporter family, *SLC12*. KCC1 is expressed ubiquitously and it is widely expressed in the DCT in humans (86), KCC2 is only expressed in the brain (87), KCC3 is expressed throughout the entire nephron (88) and KCC4 has been reported to be expressed in the rabbit DCT (84) and in α -intercalated cells of mice and rats (89)

In addition to transcellular reabsorption, 2 to 3 % of filtered chloride is reabsorbed into the peritubular fluid through paracellular transport. This process is dependent on ENaC, which provides a lumen-negative transepithelial voltage that drives this process, and claudins, which determine the paracellular permeability of ions (90). Claudins are a large family of transmembrane proteins that accumulate in the tight junctions at the apical side of the epithelium and connect adjacent epithelial cells. Different combinations of claudins define ion selectivity in different nephron segments. Claudin-1, -3, -4, -7, -8 and -14 are expressed in the DCT and claudin-3, -10, -11 and -16 at the TALH (91). Claudins can function as both a barrier and a pore at the tight junctions. *In vitro* studies of claudin-4 and claudin-8 showed that when they are overexpressed, they act as a barrier (92,93), whereas under normal conditions, claudin-4 and claudin-8 interact with each other to assemble at the tight junction, where they act as a pore for chloride ions in the distal tubule (94) (Figure 1.3-1).

1.3.2.3 Potassium transport in the DCT

Approximately 10 % of filtered potassium reaches the DCT after it is reabsorbed in the proximal tubule and the loop of Henle. Potassium is secreted throughout the entire distal nephron and the rate of secretion significantly increases as the tubular fluid travels down the DCT, which leads to an increase in transepithelial voltage (95,96). Potassium secretion in the DCT is voltage and urinary flow-dependent, and is mediated by the inward rectifying potassium channel, ROMK, and the “big” K⁺ channel (BK) (97,98). ROMK is expressed in the apical membrane of the DCT2, the CNT and the cortical CD, and potassium excretion in these segments is primarily mediated by it. ROMK-mediated potassium excretion is dependent on the activity of ENaC. An electrogenic driving force is generated through ENaC-mediated sodium uptake, which depolarises the apical membrane, acting as a stimulus for potassium excretion through ROMK. BK is expressed throughout the entire distal nephron. Under normal urinary flow, BK remains relatively inactive, however when urinary flow increases, sheer stress on DCT cells increases, resulting in BK activation and an increase in the rate of potassium efflux. The underlying mechanism for BK activation is not clear, however increased intracellular calcium concentration and nitric oxide (NO) production was suggested to stimulate BK activity (99,100).

Basolateral potassium efflux plays an important role in sodium reabsorption in the DCT (81). Whilst Na^+/K^+ -ATPase pumps potassium into the cell, in exchange for sodium, potassium is recycled back into the peritubular fluid via the inward-rectifying potassium channel (KCNJ)10 (101,102), and to some degree KCC (84). KCNJ10 and KCC are not the only potassium transport proteins expressed at the DCT, KCNJ15 and KCNJ16 are also expressed at the basolateral membrane and are members of the inward-rectifying potassium channel (103). Expression of KCNJ10/16 heterotetramers have been reported in the distal nephron and they are thought to also play a role in the recycling of potassium (102) (Figure 1.3-1).

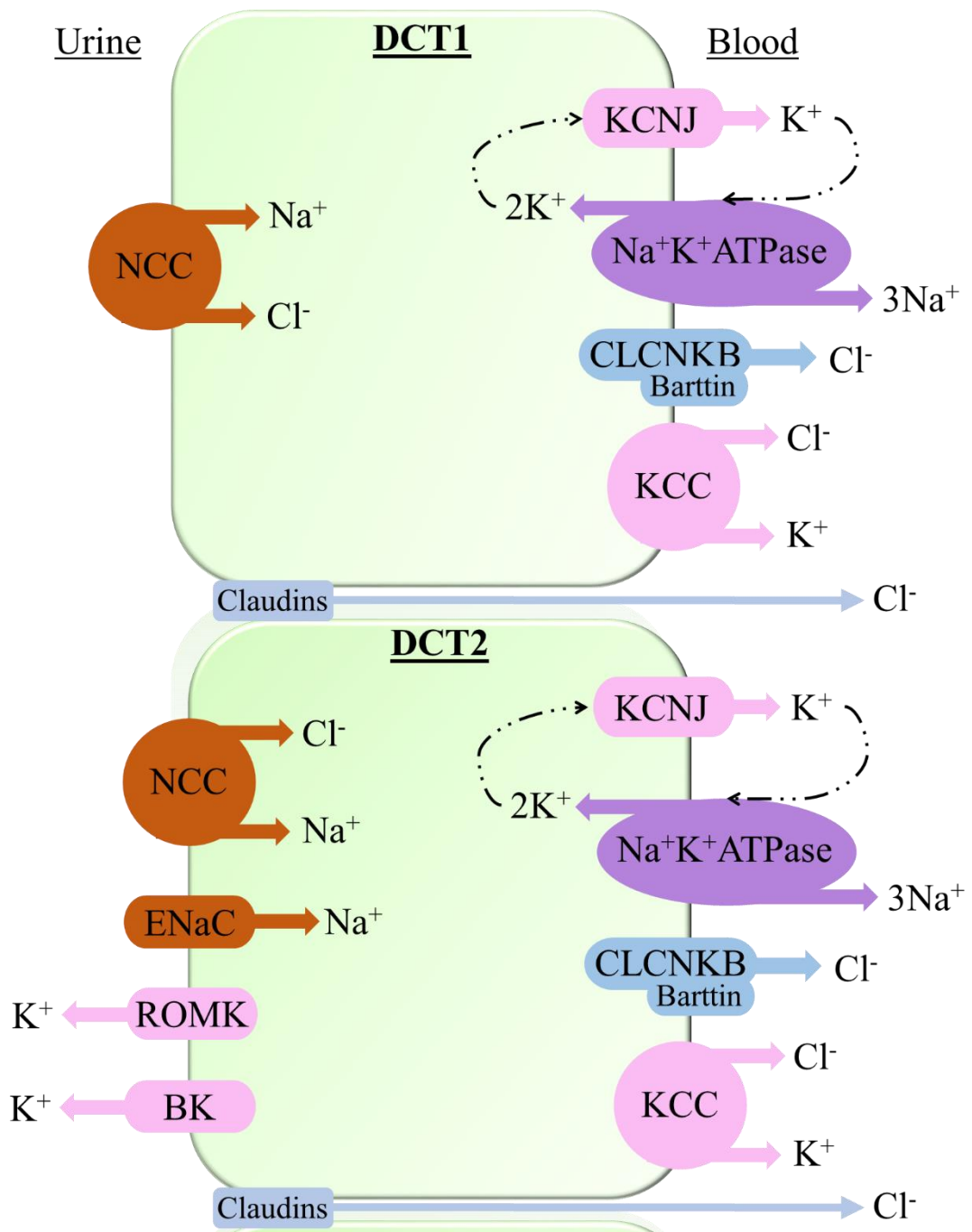


Figure 1.3-1 Sodium, chloride and potassium transport at the DCT.

Na^+/K^+ -ATPase provides the driving force for sodium influx through the apical membrane. This gradient is maintained by KCNJ10/16 , and to some degree KCC , which recycles the potassium ions inside the cell. Sodium enters the DCT through the electroneutral NCC and the electrogenic ENaC . The electrochemical gradient generated by ENaC can promote chloride reabsorption through claudins or potassium secretion through ROMK . Chloride ions that entered the cell through NCC exit through CLCNKB -Barttin complex and KCC .

1.3.2.4 Regulation of sodium, chloride and potassium handling in the DCT

Sodium and potassium handling at the DCT is regulated by dietary sodium chloride (104), dietary potassium (105,106) and hormonal stimuli, such as ANGII (107–109), aldosterone (110), vasopressin (111,112) and insulin (113,114). Distal sodium delivery is a major determinant of NaCl reabsorption in the DCT, the morphology of which changes in response to sodium delivery and adapts to the physiological needs (115). An increase in the surface area of the basolateral infoldings, mitochondrial size and activity of the Na⁺/K⁺-ATPase and NCC, enhances the capacity for sodium reabsorption in response to an increase in sodium delivery. When luminal sodium is high, NCC stored in vesicles are trafficked to the apical membrane to facilitate NaCl entry. The activity of NCC can be increased by phosphorylation to enhance NaCl influx; this process involves the STE20-like proline-alanine rich kinase (SPAK) and the oxidative stress responsive kinase 1 (OSR1) (82,116,117). Upstream regulators of SPAK and OSR1 are part of a family of serine/threonine kinases: 'With No lysine (K)' kinase (WNK) (118–120), and have been shown to regulate NCC both dependent and independent of SPAK and OSR1 (116,121).

During hypovolemia, RAAS is activated, serum aldosterone and ANGII increase and act in synergy to increase sodium reabsorption. Increased serum aldosterone causes translocation of the MR at the DCT to the nucleus, inducing serum and glucocorticoid-regulated kinase 1 (SGK1) transcription. SGK1 is a serine/threonine kinase that is expressed ubiquitously. SGK1 is a transcriptional target of aldosterone and can be rapidly induced by aldosterone secretion in the distal nephron (122), regulating NCC, ENaC and ROMK through the WNK cascade (110,123). In addition, circulating ANGII binds to the ANGII receptors (ATR) expressed on the apical and basolateral membrane of the proximal convoluted tubule (PCT), the TALH and the DCT (124). ANGII increases sodium reabsorption and decreases potassium secretion through regulatory pathways involving the WNK kinases (109,125,126) and protein tyrosine kinase (PTK) (127–129) in the DCT (Figure 1.3-2). Details of the regulatory mechanism involved in sodium handling are discussed in Section 1.6.

Renin-angiotensin-aldosterone system

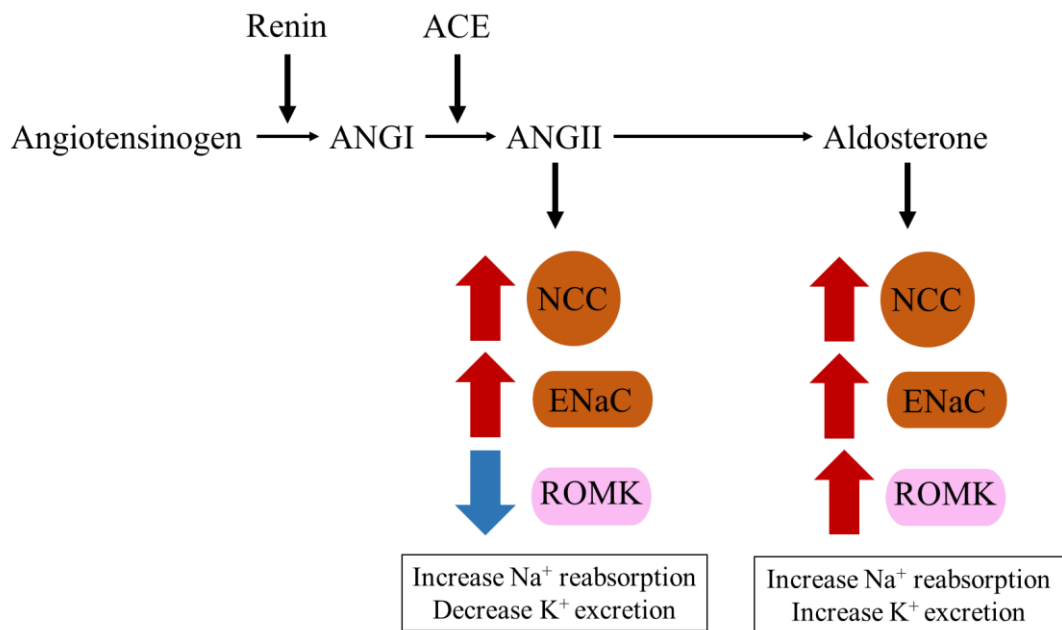


Figure 1.3-2 RAAS regulation of sodium and potassium homeostasis in the DCT

In the event of hypovolemia, the RAAS system is activated and serum ANGII and aldosterone are increased. ANGII causes sodium retention by increasing NCC and ENaC activity, and suppresses potassium excretion by decreasing ROMK membrane expression. Aldosterone causes sodium retention and potassium excretion by increasing the activity and surface abundance of NCC, ENaC and ROMK.

1.3.3 Divalent cation handling in the DCT

1.3.3.1 Calcium transport in the DCT

The DCT reabsorbs around 7 to 10 % of filtered calcium. Unlike other parts of the nephron that reabsorb calcium passively through claudins, calcium is exclusively reabsorbed through transcellular transport in the distal nephron (130). When filtered calcium arrives at the distal nephron, an electrochemical gradient drives calcium into the DCT cells through the apically expressed transient receptor potential cation channel subfamily V (TRPV) member 5 (131,132). Once calcium enters the cell, free calcium ions bind to the calcium binding protein calbindin-D28K, which acts as a buffer for maintaining low intracellular calcium levels, and shuttles calcium to the basolateral membrane for extrusion (133,134). At the basolateral membrane, PMCA1, PMCA4 and the electrogenic sodium/calcium exchanger 1 (NCX1), which exports one Ca^{2+} in exchange for three Na^{+} , are all involved in calcium efflux (135).

TRPV6 is another apical calcium channel that is expressed in the DCT2, CNT and CD (136,137), but its expression is not exclusive to the nephron and has been detected in various tissues, including the intestines, pancreas and the stomach (138). TRPV6 is best known for its role in calcium absorption in the intestine (139). However, the regulatory pathway that governs TRPV6 activity is unclear in the kidneys, therefore it is widely accepted that TRPV5 is the primary calcium channel responsible for transcellular transport of calcium in the distal nephron.

The transport mechanism of calcium differs between the early and late DCT. In the DCT, TRPV5 is absent in DCT1 (136,140) but NCX1 and PMCA are expressed at the basolateral membrane (140). This suggests that calcium may enter DCT1 through other calcium channels, possibly one similar to TRPV5 or through different subunits and isoforms of TRPV5 which have been previously identified in rats (132) and mouse DCT (mDCT) cells (141). Overall, TRPV5, calbindin-D28K, NCX1 and PMCA are most abundant at DCT2 and their expression progressively decreases down the nephron (140). This suggests that most of the calcium reabsorption occurs at DCT2 and lessens when calcium reaches the CNT, with negligible calcium transport at the cortical CD (140) (Figure 1.3-3).

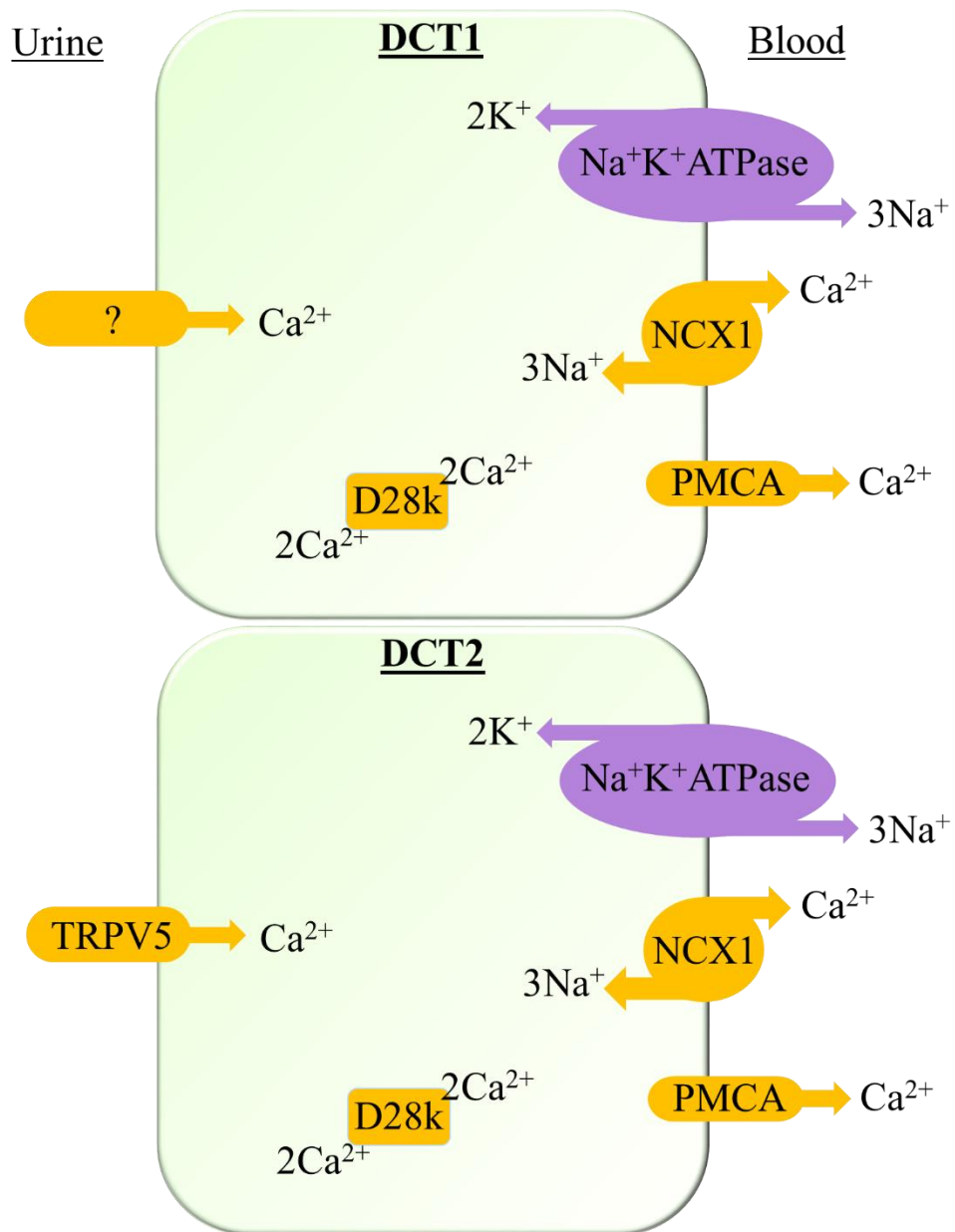


Figure 1.3-3 A schematic diagram of calcium transport at the DCT

In the DCT, calcium is driven into the cell through the apically expressed calcium channels, such as TRPV5. On entry, free calcium binds to calbindin-D28K to maintain low intracellular level of free calcium, and is shuttled across the cell to the basolateral membrane for extrusion. At the basolateral membrane, NCX1 and PMCA are involved in the efflux of calcium, providing an electrochemical gradient for calcium reabsorption.

1.3.3.2 Regulation of calcium handling in the DCT

Active transport of calcium is dependent on the activity of NCX1 and PMCA in the basolateral membrane. The electrochemical gradient generated by NCX1 accounts for 70 % of calcium uptake by TRPV5 and the remainder is provided by PMCA. Calcium reabsorption in the DCT is regulated by hormonal stimuli, such as parathyroid hormone (PTH), vitamin D₃, β -glucuronidase klotho (klotho) and oestrogen. PTH is released during hypocalcaemia from the parathyroid gland and binds to its receptor, PTH 1 receptor (PTH1R), expressed in the apical and basolateral membrane of the glomerular podocytes, the PCT, the cortical part of TALH and the DCT (142). PTH stimulates the synthesis of 1,25-dihydroxyvitamin D₃ (1,25(OH)₂D₃), the active form of vitamin D₃. 1,25(OH)₂D₃ binds to its receptors, vitamin D₃ receptors (VDR), that are abundantly expressed in the cytoplasm of the DCT and cortical CD in humans (143,144) and together with PTH increases calcium reabsorption in the DCT (131,145). Klotho is a transmembrane protein expressed abundantly at the distal nephron (146). It increases calcium uptake in the DCT by increasing the expression and activity of TRPV5 (147,148). In addition, klotho is also involved in regulating PTH secretion and 1,25(OH)₂D₃ synthesis through the fibroblast growth factor 23 (FGF23). These calcium regulatory mechanisms are interlinked and complex and involve several negative feedback loops. Details of these regulatory mechanisms are discussed in Section 1.9.

1.3.3.3 Magnesium transport in the DCT

Around 50 to 60 % of magnesium is reabsorbed via paracellular transport in the TALH (149), while, approximately 3 to 7 % of magnesium is reabsorbed through transcellular pathways in the DCT. In comparison to other electrolyte transport pathways, the mechanism for magnesium handling at the DCT is poorly understood. It is however known that the uptake of magnesium is at least in part mediated by the apically expressed TRP cation channel subfamily M member 6 (TRPM6). TRPM6 is a voltage-driven cation channel that belongs to the same family as the TRPV channels. TRPM6 is expressed throughout the entire DCT and is permeable to divalent cations, such as magnesium and calcium. TRPM6 has a 5-fold preference for magnesium ions over calcium ions, which allows it to preferentially function as a magnesium channel (150). Unlike other electrolytes,

the electrochemical gradient for magnesium influx is relatively low, therefore the activity of TRPM6 is primarily deterred by the voltage across the apical membrane.

The fate of magnesium ions upon entry into the DCT is currently unknown, and a unique magnesium binding protein has yet to be identified. However, many different proteins, such as ATP, calbindin-D28K and parvalbumin are known to bind free magnesium non-specifically (150,151). These potentially have the capacity to shuttle magnesium ions across the cell, thereby aiding the transcellular reabsorption process. Free magnesium ions can also be absorbed by subcellular organelles and function as cofactors in cellular processes that occur in the mitochondria, nucleus and the endoplasmic reticulum (ER) (151).

The mechanism for basolateral efflux of magnesium is currently unclear, but similar to the calcium extrusion system, a sodium/magnesium exchanger (152,153) and a plasma membrane magnesium ATPase (154) have been postulated as candidates involved (155). Other putative candidates, such as the ancient conserved domain-containing protein 2, cyclin M₂, is expressed at the basolateral membrane of the distal nephron and has been suggested to act as a magnesium/ion transporter with magnesium sensing properties (156,157). Another candidate is the solute carrier family 41 member 1 (SLC41A1), which is a magnesium transporter expressed at the basolateral side of the DCT (158) (Figure 1.3-4).

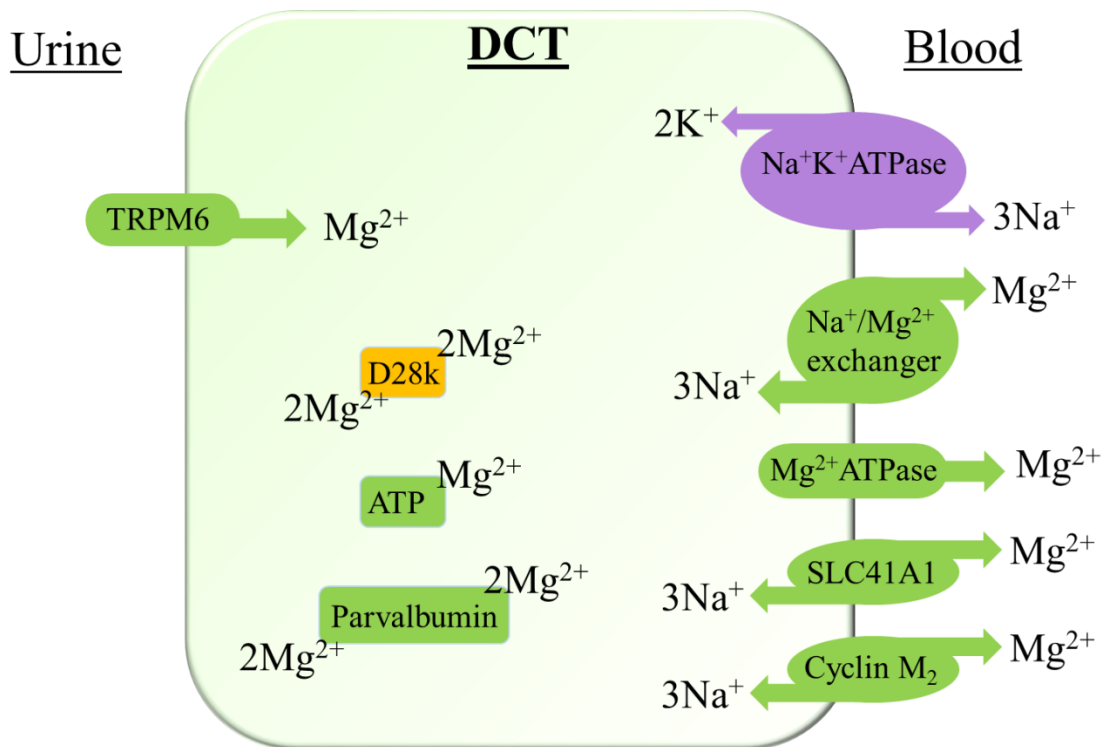


Figure 1.3-4 A schematic diagram of magnesium transport at the DCT

In the DCT, magnesium is known to be driven into the cell through TRPM6. It has been suggested that magnesium binding proteins, such as calbindin-D28K, ATP and parvalbumin, maintain intracellular magnesium levels and shuttle magnesium ions towards the basolateral membrane for extrusion. The basolateral magnesium efflux is currently unclear, but a sodium/magnesium exchanger and a plasma membrane magnesium ATPase, along with other candidates, such as cyclin M₂ and SLC41A1 are thought to be involved.

1.3.3.4 Regulation of magnesium handling in the DCT

The regulation of magnesium handling in the DCT is poorly understood. It has been suggested that the membrane voltage of the DCT plays an important role in magnesium handling, as shown in multiple disorders of renal magnesium wasting, including isolated dominant hypomagnesaemia (IDH) and the EAST syndrome (epilepsy, ataxia, sensorineural deafness and salt-wasting renal tubulopathy). The γ -subunit of Na^+/K^+ -ATPase is mutated in IDH (159–161) and *KCNJ10* is mutated in EAST syndrome (162). These mutations dysregulate the mechanism of potassium transport at the basolateral membrane of the DCT, resulting in altered basolateral membrane potential and a decrease in transcellular magnesium transport.

In addition, changes in the apical membrane potential of the DCT may also regulate magnesium reabsorption. Shaker-related voltage-gated potassium channel (*Kv1.1*) is exclusively expressed at the apical membrane of DCT1 and excretes potassium into the tubular lumen. Potassium efflux through *Kv1.1* increases lumen positivity, providing a gradient for magnesium uptake through *TRPM6*. Inactivating mutations in *Kv1.1* alter the apical membrane potential and diminish the driving force for magnesium influx, causing an autosomal dominant form of hypomagnesaemia (163,164). In addition to membrane potential, epidermal growth factor (EGF) is an important upstream regulator of magnesium homeostasis in the DCT (165). The precursor of EGF is highly expressed in the apical and basolateral membrane of the DCT and its extracellular domain can be cleaved to form EGF. EGF then binds to its receptors at the basolateral membrane and increases *TRPM6* membrane expression by activating the extracellular signal-regulated kinase 1 and 2 (*ERK1/2*) (166,167).

1.4 DCT Pathophysiology

1.4.1 Gitelman syndrome

Gitelman syndrome, also known as familial hypokalemia-hypomagnesaemia, is one of the most prevalent inherited renal tubular disorders, with a prevalence estimated at 1:40,000 (168). Gitelman patients are volume depleted with a resulting hyperreninemic hyperaldosteronism which causes a hypokalaemic metabolic alkalosis. Hypomagnesaemia and hypocalciuria are also associated

with Gitelman patients (63), causing symptoms such as muscle weakness, tetany and chondrocalcinosis. The clinical phenotype is generally quite mild and patients are often diagnosed in early adulthood, usually by incidental blood tests performed for another reason altogether (168). The clinical characteristics of Gitelman syndrome (hypokalaemic metabolic alkalosis) are very similar to Bartter syndrome. For this reason, Gitelman syndrome was initially considered as a milder subset of Bartter syndrome.

1.4.1.1 Renal pathophysiology of Gitelman syndrome

The cause of Gitelman syndrome was identified as inactivating mutations in NCC (62,169). NCC is encoded by *SLC12A3* and over 140 *SLC12A3* mutations (168) have subsequently been identified in Gitelman patients. Loss of function mutations in NCC lead to defective sodium reabsorption at the DCT and moderate intravascular volume contraction (168,169). This contraction activates the RAAS, resulting in increased sodium reabsorption in the cortical CD via ENaC and subsequent secretion of potassium and protons into the tubular lumen, causing hypokalaemia and metabolic alkalosis (168,169).

1.4.2 Gitelman-like disorders

1.4.2.1 Isolated dominant hypomagnesaemia

IDH is a rare autosomal dominant disorder that comprises of magnesium wasting, tetany and epileptiform convulsions. The phenotype of IDH closely resembles Gitelman syndrome (168) as patients with IDH have low serum magnesium levels often accompanied with secondary hypocalciuria. IDH patients also have a normal acid-base status and renin and aldosterone activity (159,170).

1.4.2.1.1 Renal pathophysiology of isolated dominant hypomagnesaemia

The γ -subunit of Na^+/K^+ -ATPase is mutated in IDH patients (159). The γ -subunit is not expressed ubiquitously like the α - and β - subunits of Na^+/K^+ -ATPase, however, it is highly expressed in the TALH, the DCT and the CNT (171). A mutation at G41 of the γ -subunit prevents the subunit from trafficking towards the cell surface membrane and therefore alters the pump function (160,161). This dysregulates the basolateral membrane potential in the distal nephron,

eliminating transcellular magnesium transport, resulting in a reduction in magnesium reabsorption.

1.4.2.2 EAST syndrome

EAST syndrome is a rare autosomal recessive disorder comprises of epilepsy, ataxia, sensorineural deafness and salt-wasting renal tubulopathy. The salt-losing tubulopathy phenotype of EAST syndrome, characterised by hypokalaemia, metabolic alkalosis, hypomagnesaemia and hypocalciuria, resembles that of Gitelman and Bartter syndromes (162,169).

1.4.2.2.1 Renal pathophysiology of EAST syndrome

The cause of EAST syndrome was identified as a loss of function mutation in KCNJ10 (162). KCNJ10 is expressed in the brain, eye, ear and at the basolateral membrane of the distal nephron and it is involved in a pump-leak coupling process that recycles potassium from the Na⁺/K⁺-ATPase back into the peritubular fluid (101). The KCNJ10 gene is located on chromosome 1q23.2 in humans and 14 pathogenic mutations have been identified (162). These mutations reduce KCNJ10 activity to less than 20 %, as reported in electrophysiological studies (172–174), reducing the efficiency of the recycling process and resulting in a reduction in Na⁺/K⁺-ATPase activity.

1.4.3 Familial hyperkalaemic hypertension

FHHt, also known as Gordon syndrome or pseudohypoaldosteronism type II, is a mirror-image syndrome to Gitelman syndrome. FHHt is a rare autosomal dominant disorder, caused by abnormally avid reabsorption of sodium and chloride in the DCT (175,176). FHHt is exquisitely sensitive to thiazide diuretics, which relieve hypertension, hyperkalaemia and the hyperchloraemic metabolic acidosis in FHHt patients (60).

1.4.3.1 Renal pathophysiology of Familial hyperkalaemic hypertension

FHHt sensitivity to thiazides prompted the hypothesis that FHHt is due to NCC overactivity (8). Increased activity of NCC increases sodium reabsorption, resulting in a lower concentration of sodium in the solute that arrives at the CD; this decreases sodium reabsorption via ENaC and consequently alters the Na⁺

and K⁺ exchange system, resulting in the decrease in potassium secretion via ROMK. A number of gene products, such as the WNK kinases, Kelch-like protein 3 (KLHL3) and Cullin-3 (CUL3), regulate NCC expression and activation. Pathogenic mutations responsible for FHt have been identified in WNK1, WNK4, CUL3 and KLHL3 (7,8,61,177), the first of which to be identified were those in the WNK kinases (details of FHt-type mutations are provided in individual sections). These mutations activate the WNK-NCC cascade increasing sodium chloride reabsorption.

Alternatively, the pathophysiological mechanism of FHt may also be caused by an increase in chloride reabsorption - a 'chloride shunt'. Rapid chloride reabsorption at the distal nephron diminishes the luminal negative driving force that drives potassium secretion under normal physiological circumstances (178,179). Alternative anions (e.g. sulphate) can act as a substitute for chloride ions in the tubular fluid when luminal potential is too high. This will ameliorate the shunt effect restoring the lumen electrical difference that was required for K⁺ secretion (178). If the luminal potential is restored, paracellular chloride reabsorption will increase and thereby increase luminal sodium influx by ENaC in the CD and thus causing hypervolaemia (178,179).

1.4.4 CNI-induced hypertension

The phenotype of CNI-induced hypertension is very similar to that seen in FHt, displaying hyperkalaemia and a variable metabolic acidosis. The prevalence of this phenotype seen in CNI-treated patients ranges from 16 to 30 % (180,181) with 33 % of FK506-treated patients exhibiting hypertension and hyperkalaemia. Hypertension may be more common in patients undergoing CyA treatment in comparison to FK506, but hyperkalaemia seems to be less common (182).

1.4.4.1 Renal pathophysiology of CNIs

CNIs cause hypertension by increasing NCC phosphorylation and the abundance of WNK3, WNK4 and SPAK (51). Calcineurin itself is a serine/threonine protein phosphatase (183). It has a number of transcriptional effects mainly due to the activation of the transcription factor NFATc (cytoplasmic nuclear factor of activated T cells), but it is the phosphatase activity that may act to inhibit the cascade of serine threonine kinases that ultimately control NCC activity.

1.5 NCC

Pharmacological agents (CNI and thiazides) and renal tubular disorders (Gitelman syndrome and FHt) have focused much attention on NCC and the molecular mechanisms of its regulation in the DCT. NCC belongs to the *SLC12* family, sharing ~50 % of its identity with NKCC1 and NKCC2 and ~25 % with KCC1 and KCC4. The *SLC12A3* gene is located on chromosome 16q13 in humans (184), chromosome 8 in mice (185) and 19p12-14 in rats (186). *SLC12A3* displays high (88.6 %) sequence conservation across humans, mice and rats. A sequence alignment of *SLC12A3* in human, mouse, rat and rabbit showed that human NCC and rabbit NCC contain an additional 17-26 amino acids in the C-terminus; these residues encode for a protein kinase A (PKA) site that is not present in mouse NCC and rat NCC (187). The precise function of this site is unknown.

1.5.1 NCC Structure

NCC is a transmembrane protein made up of 1002-1028 amino acids. The predicted topology of NCC consists of a central hydrophobic region flanked by a short cytoplasmic N-terminus and a long cytoplasmic C-terminus. The central hydrophobic region defines NCC function and consists of twelve transmembrane (TM) domains that are connected by five intracellular and six extracellular loops (188,189). The N- and C-terminus, however, have been suggested to play no role in coding for key residues (190,191).

1.5.2 Functional properties of NCC

NCC forms a functional dimer (192) and is glycosylated at multiple residues. A study by Hoover *et al.* in 2003 focused on two N-linked glycosylation sites, N404 and N424, found in extracellular loop-4 (188,189). The elimination of either glycosylation site resulted in NCC activity being reduced by over 50 %, and the removal of both sites exhibited a decrease in activity of greater than 95 % (188). Overall, elimination of these glycosylation sites in NCC has triple effects: a reduction of NCC abundance in the plasma membrane, a decrease in cotransporter activity, and an increase in chloride and thiazide affinity (188).

1.5.3 Thiazide and ion affinity

1.5.3.1 Affinity controversy

Several research groups have investigated the ion and thiazide binding affinity of NCC with contradictory results (188,190,193). Tran *et al.* (193) was the first to propose that chloride and thiazide compete for the same binding site on NCC, and that this binding site is separate from the sodium binding site. This theory was further supported by Hoover *et al.* (188) who showed that the elimination of residues N404 and N424 in extracellular loop-4 of rat NCC increased chloride and thiazide affinity, and reduced NCC activity (188). In contrast, the elimination of residues N404 and N424 in flounder NCC had no effect on thiazide affinity in the Moreno *et al.* 2006 study (190). This study also showed that chloride and thiazide binding is non-competitive as different flounder NCC TM domains are involved. This study demonstrated that the affinity-defining segment for chloride ions lies within TM domain-1 to domain-7 and the region that defines thiazide affinity lies within TM domain-8 to domain-12. Both of these regions were suggested to be involved in defining sodium affinity. As these studies presented conflicting evidence, Moreno *et al.* proposed that the effect of glycosylation site elimination on thiazide affinity is a unique feature of rat NCC, and that sodium and chloride binding may cause conformational changes in NCC, potentially resulting in reduced thiazide affinity (190).

1.5.3.2 Chloride affinity

A further study by Moreno showed that a highly conserved glycine residue (G264), located in TM domain-4, plays an important role in determining chloride affinity. A glycine to alanine single nucleotide polymorphism (SNP) caused a 50 % reduction in NCC activity and an increased affinity for chloride ions (194). Cases where patients with Gitelman syndrome were identified with the G264A mutation exhibit a greater diuretic response when furosemide is administered (195). Furosemide is a loop diuretic that inhibits NKCC2 activity in the TALH, therefore the exaggerated diuretic effect is possibly a result of increased salt delivery and impaired NCC function, causing a salt wasting phenotype.

1.5.4 Phosphorylation of NCC

The activity of NCC is increased by SPAK and OSR1-mediated phosphorylation. SPAK and OSR1 phosphorylate NCC at T46, T55 and T60 in humans, homologous to T44, T53 and T58 in mice (116).

1.6 WNK kinases

The WNK kinases comprise a family of serine/threonine kinases, four members have been identified in humans, WNK1-4. The WNK kinases play a crucial role in sodium, chloride and potassium homeostasis by regulating cation-chloride cotransporters, which includes KCC4, NKCC2, NCC, ROMK and ENaC in the kidneys (89,196–198). The WNK kinases have been localised on the following human chromosomes: *WNK1* at 12p13.33, *WNK2* at 9q22.31, *WNK3* at Xp11.22 and *WNK4* at 17q21.31. In the nephron, WNK1 and WNK3 are ubiquitously expressed in humans and mice (199,200). WNK4 is expressed in the cytoplasm and close to tight junctions of the DCT and the CD, and it is also expressed at a reduced level in the TALH (8,201). WNK2 expression has not been reported in the nephron.

1.6.1 Structure of WNK kinases

The catalytic domain of WNK kinases is located at the short N-terminus and lacks the typical lysine that is responsible for catalytic activity in other kinases (120). The four WNK kinases share 85-90 % sequence identity at the kinase domain (202). Within the C-terminus lies a highly conserved autoinhibitory domain, two coiled-coil domains and three proline-rich regions (203). The kinase domain also encodes for the substrate binding groove and two residues, V318 and A448 on WNK1 and their corresponding residues on the other WNK kinases, are suggested to play a role in defining substrate specificity (204) (Figure 1.6-1).

The autoinhibitory domain in the WNK kinases share 46 % identity (203). It binds to the catalytic domain to suppress its kinase activity and two highly conserved residues, F524 and F526 are known to play an important role in this function (203,205). The activation of the WNK kinases requires the autoinhibitory domain to dissociate from the catalytic domain and autophosphorylation of a serine residue in the activation loop (203,205). Proline-rich motifs are involved in

interactions with SH3-domains of the target proteins (203). These motifs are highly conserved and mutations within this region in WNK1 and WNK4 are pathogenic in FHHt. WNK proteins tend to form oligomers and may function as a tetramer (206). WNK kinases are also capable of inhibiting each other, as shown in several *in vitro* studies where WNK4 was phosphorylated by WNK1 and WNK3 (207), and that WNK4 can also inhibit WNK1 (205–207).

Q9H4A3	WNK1	300	VTELMTSGTLKTYLKRFK V MKIKVLRSWCRQILKGLQFLH	339
Q9Y3S1	WNK2	274	VTELMTSGTLKTYLKRFK V MKPKVLRSWCRQILKGLLFLH	313
Q9BYP7	WNK3	226	VTELMTSGTLKTYLKRFK V MKPKVLRSWCRQILKGLQFLH	265
Q96J92	WNK4	253	VTELMTSGTLKTYLRRFR E MKPRVLQRWSRQILRGLHFLH *****:***: ** :** :*.****:* **	292
Q9H4A3	WNK1	440	KPASFDK V A ^A IPEVKEIIEGCIRQNKDERYSIKDLLNHAF	479
Q9Y3S1	WNK2	414	KPASFEK V H ^H DPEIKEIIEGCICKNKEERYEIKDLLSHAF	453
Q9BYP7	WNK3	366	KPASFNK V T ^T DPEVKEIIEGCIRQNKSERLSIRDLLNHAF	405
Q96J92	WNK4	393	KPNSFHK V K ^K IPEVKEIIEGCIRTDKNERFTIQDLLAHAF ** *.** **:**** ** :*.** *:**** **	432

Figure 1.6-1 Alignment of the residues encoding for substrate specificity in WNK1-4

In humans, WNK1-V318 and WNK1-A448, and the corresponding residues on the other WNK kinases, in the substrate binding groove define substrate specificity (red). The valine residue is conserved in WNK1-3, which suggests that WNK1-3 may share the same substrate. In contrast, the second residue is not conserved, potentially suggesting different substrates for each WNK kinases.

1.6.2 WNK1

Amongst the four WNK proteins, WNK1 is the most comprehensively characterised. WNK1 is more commonly expressed in comparison to the other WNK proteins and it is most abundant in the kidneys, testis, heart and skeletal muscles (208). There are two different isoforms of WNK1, each of which has tissue-specific distributions, however both isoforms are expressed in the kidneys (208,209). L-WNK1 is the full-length WNK1 that is ubiquitously expressed and contains a catalytic kinase domain. Kidney specific-WNK1 (KS-WNK1) is a shorter transcript that lacks the kinase domain and is expressed in the DCT and CNT (201). Although KS-WNK1 is only expressed in the DCT and CNT, on a transcript level, KS-WNK1 expression is more abundant than L-WNK1 in these segments (208).

WNK1 contains 28 exons and its isoforms arise from different promoters; KS-WNK1 is generated from a promoter upstream of exon 4a, an exon that is different from exon 4 in L-WNK1 (208,209). KS-WNK1 encodes a 30 amino acid cysteine-rich region instead of the catalytic kinase domain (208,209). The remaining sequence of KS-WNK1, exon 5-28 is identical to L-WNK1 (208,209).

1.6.2.1 Influence of aldosterone, dietary potassium and sodium on WNK1

The activity of WNK1 is dependent on dietary potassium intake (210). Studies have shown that an increase in potassium loading increases the KS-WNK1 to L-WNK1 ratio (97,201,211), an effect that is also shown in chronic aldosterone excess (201). Aldosterone increases KS-WNK1 expression and has no effect on L-WNK1, analysis of the two isoforms revealed a glucocorticoid response element that is present in KS-WNK1 but absent in L-WNK1 (209). This response element allows activated MR to bind, possibly initiating transcriptional activation. Extracellular sodium concentration has not been shown to have a significant effect on the activity of L-WNK1, however, a low sodium diet significantly decreased expression of KS-WNK1 (201). This effect seems to be in contrast with the effect shown in chronic aldosterone excess and it is possible that the decrease in KS-WNK1 during low sodium intake is a response induced by hypovolemia, causing hyperaldosteronism. Recently, Piala *et al.* showed that the activity of WNK1 is sensitive to chloride. Chloride ions directly bind to WNK1 at

the catalytic domain and inhibit WNK1 autophosphorylation and activation *in vitro* (212), however the effect of chloride *in vivo* requires further investigation.

1.6.2.2 WNK1 and electrolyte transporters

Although there is no evidence of a direct interaction between the two isoforms of WNK1 and NCC, WNK1 regulation of NCC is mediated by the other WNK kinases through protein interactions, as demonstrated in the heteromeric complex that comprises WNK1 and WNK4 (213), and the phosphorylation of WNK4 by WNK1 (207). The two isoforms of WNK1 have opposing effects on WNK4-induced inhibition of NCC (214); L-WNK1 prevents WKN4-induced inhibition of NCC, whilst, KS-WNK1 exhibits a dominant-negative effect by interacting with the protein complex of L-WNK1, downregulating NCC (215).

WNK1 also regulates ENaC and ROMK. L-WNK1 increases ENaC membrane abundance through SGK1 (216). L-WNK1 induces phosphorylation of SGK1, causing it to phosphorylate and inhibit Nedd4 (E3 ubiquitin-protein ligase). Nedd4 is known to promote endocytosis of ENaC, which causes a reduction in ENaC expression in the apical membrane. Both aldosterone and insulin activate SGK1-mediated phosphorylation of L-WNK1. This promotes endocytosis of ROMK, decreasing its membrane expression and suppressing potassium secretion (217). Similar to SGK1, KS-WNK1 is also targeted by aldosterone. Aldosterone stimulates KS-WNK1, causing it to inhibit SGK1-mediated phosphorylation of L-WNK1, thereby suppressing ROMK endocytosis (97,197,211) (Figure 1.6-2). The activation of both SGK1 and KS-WNK1 may not have a net effect on the membrane abundance of ROMK, therefore it is possible that aldosterone may increase potassium excretion through ROMK by enhancing sodium reabsorption via ENaC.

1.6.2.3 Phosphorylation of WNK1

L-WNK1-T58 is a phosphorylation target of SGK1 and protein kinase B (AKT), and has been shown to reduce the membrane abundance of ROMK, decreasing potassium secretion (217).

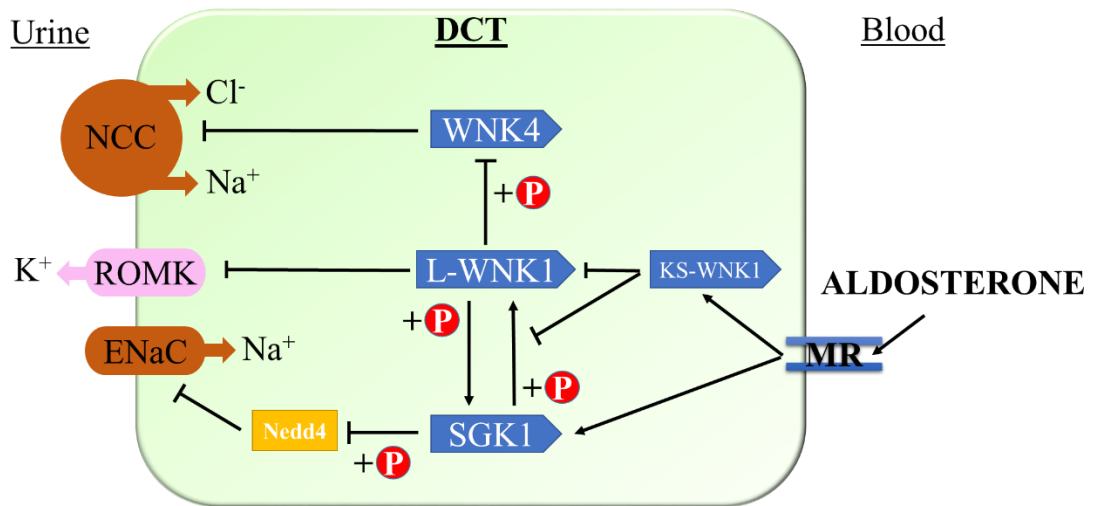


Figure 1.6-2 WNK1 regulation of the distal sodium and potassium transporters

L-WNK1 and KS-WNK1 have opposing effects on WNK4-induced inhibition of NCC. L-WNK1 prevents WNK4 from inhibiting NCC and KS-WNK1 reverses the L-WNK1-induced inhibition on WNK4. SGK1 and the L-WNK1/KS-WNK1 play an important role in the regulation of ENaC and ROMK. L-WNK1 induces phosphorylation of SGK1 and inhibits Nedd4-mediated ENaC endocytosis. Upon stimulation by aldosterone, SGK1 phosphorylates L-WNK1 and inhibits ROMK. This process is reversed by KS-WNK1, which is also a target of aldosterone.

1.6.2.4 FHHt type mutation in WNK1

WNK1 has large intronic deletions at its first intron in FHHt patients, altering the ratio of KS-WNK1 and L-WNK1 (8). *Xenopus Laevis* oocyte studies of WNK1 harbouring FHHt-mutations showed lower levels of KS-WNK1 and higher levels of L-WNK1 expression, causing an increase in NCC activity (218). Other *in vivo* studies in mouse models with a deletion of the first intron of WNK1 have also shown increased L-WNK1 expression in DCT, however an increase in KS-WNK1 was also observed (219). KS-WNK1 exerts its inhibitory effect by interacting with the protein complex of L-WNK1, therefore the deletion of the first intron may alter this interaction, suppressing the inhibitory effect of KS-WNK1.

1.6.3 WNK3

WNK3 is expressed throughout the whole nephron and also in the brain, lungs, liver and pancreas (220,221). WNK3 contains 24 exons and similar to WNK1, the distribution of WNK3 is dependent on its splice variants (221).

1.6.3.1 WNK3 and the electrolyte transporters

WNK3 has been proposed as a modulator of cell volume and intracellular chloride concentration due to its association with the cation-coupled chloride cotransporters. The net chloride movement in cells is suggested to rely on WNK3 for its activation of NKCC1, NKCC2 (222) and NCC (200), and the inhibition of KCC1-4 through WNK3-induced phosphorylation. (200,223) This activation by WNK3 is associated with the phosphorylation of two highly conserved threonines in the N-terminus of NKCC1 and NKCC2: T184 and T189 (200,223). These threonines are also highly conserved in NCC. As NCC, NKCC1 and NKCC2 are stimulated by intracellular chloride depletion and are phosphorylated at the same residues, it has been suggested that NCC may also be phosphorylated by WNK3 (82,116,119).

Oocyte studies have shown that a catalytically inactive mutation at the kinase domain of WNK3 (WNK3-D294A) had an opposing effect on the cotransporters that are normally activated by WNK3. NKCC1, NKCC2 and NCC were strongly inhibited and all four KCCs became highly activated even under isotonic conditions (85,222). Studies of oocytes injected with KCC1, KCC3 and KCC4

suggest that their expression is affected by extracellular osmolarity. KCC1, KCC3 and KCC4 activity increases in hypotonic conditions and decreases in isotonic environments (85,224). When KCC is activated it induces cell shrinkage which in turn activates NKCC1 and NKCC2 and inhibits KCC; the response is reversed during cell swelling (225). This activation of KCC can be prevented by calyculin A and cyclosporine A, suggesting that protein phosphatases 1 and 3 (i.e. calcineurin) are involved in this activation (222).

1.6.3.2 WNK3 splice variants and NCC

Splice variants of WNK3 have different cellular distributions. Two isoforms of WNK3 have been identified in the brain (B-WNK3-18a and B-WNK3-18b). Both isoforms contain exon 22, however B-WNK3-18a contains a shorter version of exon 18 compared to B-WNK3-18b, a difference of 47 amino acids. The structure of renal WNK3 (R-WNK3) differs from B-WNK3, as it lacks exon 22 and carries the shorter version of exon 18 (221,226). It has been suggested that WNK3 increases NCC activity (200), and an oocyte co-expression study (226) demonstrated that different splice variants of WNK3 had opposing effects on NCC. NCC was activated by R-WNK3 by a SPAK-independent mechanism whereas B-WNK3 inhibited NCC through a SPAK- dependent mechanism. As B-WNK3 expression has not been demonstrated in renal tissues, this interaction between WNK3 and NCC may be unique to brain cells.

1.6.4 WNK4

In comparison to the other WNK kinases, WNK4 is much smaller and only contains 19 exons. In addition to expression in the distal nephron (8,201), WNK4 has also been detected in the pancreas, bile ducts, colon, brain, epididymis and skin (227,228).

1.6.4.1 Influence of aldosterone, dietary potassium and sodium on WNK4

The activity of WNK4 is dependent on dietary potassium levels. Low dietary potassium can cause hyperpolarisation of the basolateral membrane in the DCT and decrease the intracellular chloride concentration, resulting in activated WNK4-NCC cascade and increased sodium chloride retention (229). Similar to WNK1, dietary sodium has no significant effect on the expression of WNK4 (201).

Chronic aldosterone excess has no effects on the transcription of WNK4 (201), however, two putative negative glucocorticoid response elements have been identified at -285 and -337 in the promoter of human *WNK4* gene (230). Stimulation of the glucocorticoid receptors has been shown to decrease WNK4 transcription *in vivo* and *in vitro*, which suggests that WNK4 is sensitive to mineralocorticoids and glucocorticoids, and that the mechanism underlying aldosterone regulation of WNK4 may involve other factors to allow tight regulation of WNK4 (230,231).

1.6.4.2 WNK4 and electrolyte transporters

Studies investigating the effect of WNK4 on NCC have generated conflicting results. WNK4 has been reported to both inhibit (121,232–234) and activate NCC through SPAK/OSR1 (119,120,235). *In vivo*, WNK4 was reported to activate NCC through SPAK/OSR1 (235). *In vitro*, WNK4 was shown to inhibit NCC by decreasing its surface expression and enhancing its degradation; this was demonstrated in *Xenopus laevis* oocytes (121,214) and epithelial cells (236).

WNK4 inhibits NCC, ENaC and ROMK through different mechanisms. Using oocytes co-expressing a kinase-inactive WNK4 (WNK4-D318A) and different ion transporters, several studies have shown that the inhibition of NCC is dependent on the kinase domain of WNK4 (233,237), whereas the inhibition of ENaC (238) and ROMK (237) by WNK4 is kinase independent (238). Although ENaC inhibition is independent of the kinase domain, the inhibitory effect is still alleviated by the FHHt-causing mutation in the kinase domain of WNK4 (238).

Other ion transport proteins modulated by WNK4 include claudin-4 and NKCC2 in the kidney, NKCC1 in the vasculature and the ubiquitous KCC. Claudin-4 is a mediator of paracellular Cl⁻ permeability at the distal nephron and has been shown to be phosphorylated by WNK4, resulting in the increase in paracellular Cl⁻ flux (239).

1.6.4.2.1 Hyperkalaemia and WNK4 regulation of ion transporters

Hyperkalaemia induces the release of aldosterone and inhibits the secretion of renin. Aldosterone may influence WNK4 in regulating NCC, ENaC and ROMK via SGK1. SGK1 inhibits WNK4-induced lysosomal degradation of NCC and

activates a series of phosphorylation in the WNK-NCC cascade, resulting in an increase in the surface expression and the activity of NCC (110). SGK1 increases ENaC (240) and ROMK (129,241) activity through direct phosphorylation or by alleviating WNK4 inhibition (123). An increase in the activity of ENaC generates lumen negativity, thereby providing a driving force for potassium secretion into the tubular lumen. (Figure 1.6-3).

1.6.4.2.2 Hypovolemia and WNK4 regulation of ion transporters

ANGII and aldosterone are released in response to RAAS activation during intravascular volume depletion. ANGII increases sodium retention by increasing the abundance of NCC on the apical membrane (108), WNK4-mediated NCC phosphorylation (107,242), and ENaC channel open probability (125,243). ANGII inhibits ROMK by activating PTK. PTK phosphorylates ROMK, decreasing its membrane abundance (127,128), and reverses the effect of SGK1 on WNK4-induced ROMK inhibition (129), resulting in a decrease in potassium secretion (Figure 1.6-3).

1.6.4.3 Phosphorylation of WNK4

In vivo studies revealed that increased serum aldosterone stimulates SGK1 and WNK1 to phosphorylate WNK4 at S1169 in mice, a residue that is homologous to S1190 in humans (110,123) and is responsible for reversing the inhibitory effect of WNK4 on NCC, ENaC and ROMK once phosphorylated. Phosphorylation of WNK4 by WNK3 has also been reported *in vitro* (207); at both the N and the C-terminus, however, these phosphoresidues were not mapped. WNK3 competes with WNK4 in NCC regulation, therefore it is possible that phosphorylation of these residues is responsible for WNK4 interaction and inhibition (207). Increased circulating ANGII stimulates protein kinase C (PKC) and PKA-induced phosphorylation of WNK4 at S64 and S119. Phosphorylation of these residues increases WNK4 autophosphorylation, enhancing its kinase activity, increasing SPAK phosphorylation (244).

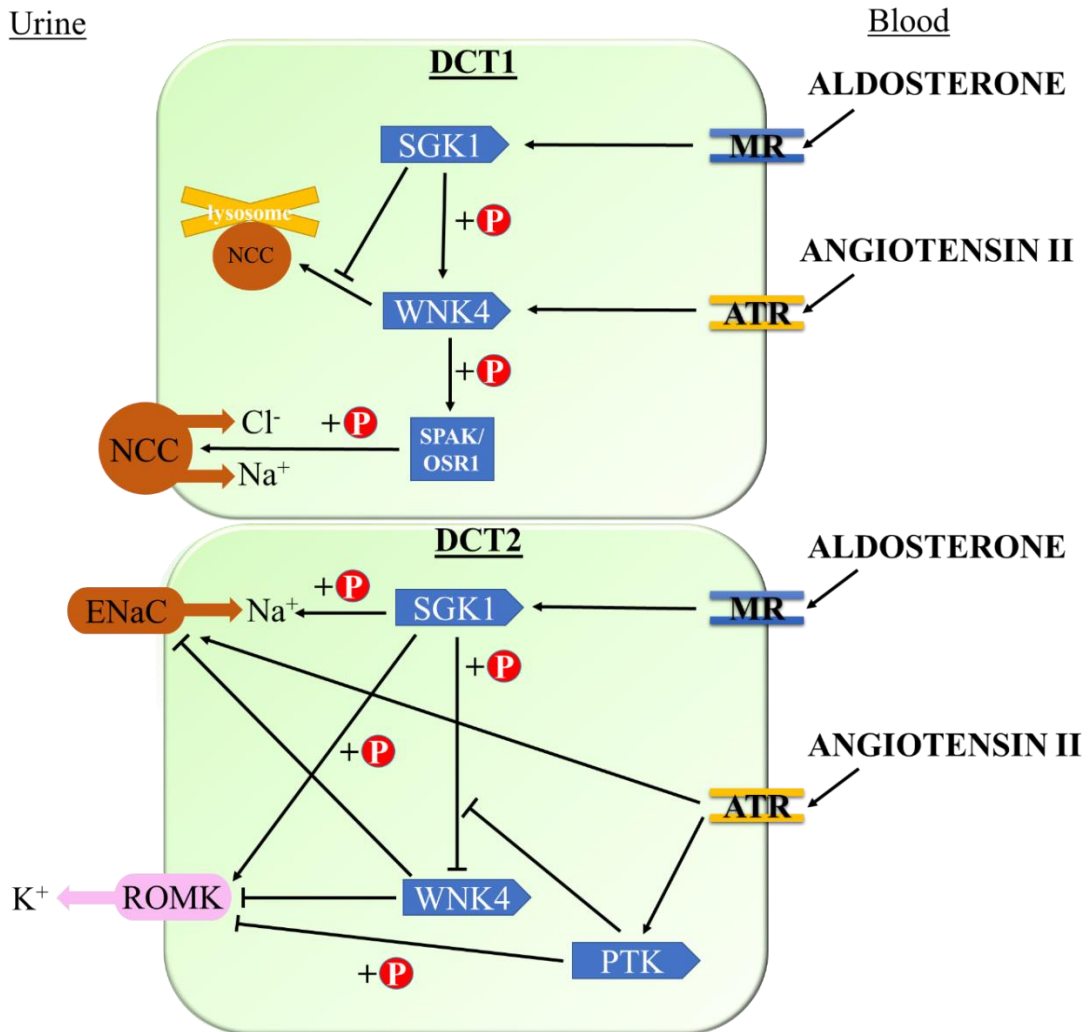


Figure 1.6-3 Influence of hypovolemia and hyperkalaemia on WNK4-modulated ion transporters

Hypovolemia activates the RAAS and increases serum ANGII and aldosterone. Hyperkalaemia induces the release of aldosterone and decreases renin secretion. Increased serum aldosterone induces SGK1-mediated phosphorylation of WNK4 and reverses its inhibitory effect on NCC, ENaC and ROMK, promoting sodium reabsorption and potassium secretion. ANGII increases WNK4 and SPAK dependent phosphorylation of NCC and increases the activity of ENaC. ANGII signals PTK to phosphorylate ROMK and reverses the inhibitory effect of SGK1 on WNK4-induced ROMK endocytosis, resulting in reduced ROMK membrane abundance.

1.6.4.4 FHht-type mutation in WNK4

It was shown that three FHht genetic pedigrees were harbouring *WNK4* mutations at E562K, D564H and Q565E (8). *In vivo* studies on transgenic mice *WNK4*^{D561A/+}, which have a FHht phenotype, were responsive to thiazide treatment, and displayed increased phosphorylation of SPAK and increased abundance of NCC-pS71 in the apical membrane of DCT (234).

FHht-type mutations also alleviate the basal inhibitory effect of WNK4 on ENaC (238) but enhances ROMK inhibition (123). Enhanced inhibition of ROMK is not dependent on the kinase activity of WNK4, instead it is dependent on clathrin-mediated endocytosis (237). Furthermore, FHht mutations at the catalytic site of WNK4 increase phosphorylation of claudin-4. This increases the Cl⁻ permeability at the tight junctions of the DCT and possibly creating a 'chloride shunt effect that drives sodium chloride into the cell via NCC (196,239).

1.6.5 SPAK/OSR1

SPAK and OSR1 both belong to the STE20 kinase subfamily and have similar structures. Key features include a catalytic domain at the N-terminus, two highly conserved serine-motifs and a conserved C-terminus (120). The C-terminus is involved in recognising the SPAK/OSR1 binding motifs, Arg-Phe-Xaa-Val/Ile (RFx[V/I]), expressed on the upstream regulators and downstream targets of SPAK/OSR1 and allows SPAK/OSR1 to interact with them (119,245,246). In addition to the core domains, an alanine and proline rich region is located at the N-terminus of SPAK, however, this region is not present in OSR1 (120).

SPAK and OSR1 participate in the regulation of NCC by the WNK cascade. SPAK/OSR1 phosphorylate and activate NCC by binding to the RFx[V/I] motifs at the cytoplasmic N-terminus of NCC; an important interaction that maximises phosphorylation (116). SPAK and OSR1 phosphorylate NCC at T46, T55 and T60 in humans (homologous to T44, T53 and T58 in mice), increasing the activity of NCC (116,117). In addition to their role in NCC regulation, SPAK/OSR1 also regulate other members of the *SLC12* family, such as NKCC1 (247,248) and NKCC2 (249). SPAK/OSR1 were also proposed to play additional roles as scaffolding proteins. A study by Piechotta *et al.* (248) showed that both SPAK/OSR1 interact with different cytoskeletal components and bring them into

proximity with cotransporters of interest in the presence of a stress stimuli. Whether this mechanism is induced by upstream regulators or sensing properties of these kinases are unclear (248).

1.6.5.1 Phosphorylation of SPAK and OSR1

WNK1 and WNK4 activate SPAK and OSR1 by phosphorylating T233 and T185 in the catalytic domain (118–120). WNK1 and WNK4 also phosphorylate SPAK at S373 and OSR1 at T325 in the conserved serine-motifs, however, the functional role of this residue is unclear (118–120). WNK3 also phosphorylates SPAK/OSR1 at the serine residue *in vitro*, however, phosphorylation of T233 and T185 has not been reported (119). The structure and functional properties of SPAK and OSR1 are similar, however, it has been reported that WNK1 and WNK4 phosphorylate OSR1 at a higher efficiency than SPAK. This is possibly due to the presence of a proline and alanine rich motif located at the N-terminus and a ~40 amino acid spanning region at the C-terminus of SPAK, both of which may affect protein conformation and its interaction with the WNK kinases (120).

1.6.5.2 Evolution of SPAK and OSR1

SPAK/OSR1 share 68 % identity in their amino acid sequences, with 89 % identity in the catalytic regions. SPAK and OSR1 (250) belong to one of the four groups of STE20 family kinases. In this family the STE20 Related Adapter (STRAD) α and STRAD β kinases (251,252) resemble SPAK and OSR1. STRAD α and STRAD β share ~30 % identity with the catalytic regions of SPAK and OSR1 (120). STRAD α and STRAD β are catalytically inactive pseudokinases that form a complex with the ubiquitously expressed tumour suppressor liver kinase B1 (LKB1) and the mouse embryo scaffolding protein (MO25) (LKB1-STRAD-MO25) (251,252). LKB1-STRAD-MO25 is involved in the phosphorylation of T172 in the α -subunit of the adenosine monophosphate-activated protein kinase (AMPK) (253,254), which is involved in regulating glucose, lipid and cholesterol homeostasis and is a major drug target for diabetes (255). A recent study by Filippi *et al.* demonstrated that MO25 is an upstream regulator of SPAK/OSR1 (256). The interaction between MO25 and SPAK/OSR1 is unclear, however, it has been suggested that MO25 may activate SPAK/OSR1 in a similar fashion to

STRAD. As a result of SPAK/OSR1 activation, MO25 is able to induce phosphorylation of NCC, NKCC1 and NKCC2 (256).

1.6.6 KLHL3 & CUL3

KLHL3 is an adaptor protein of the BCR (Broad-Complex, Tramtrack and Bric a brac-Cullin3-RING-box protein 1) E3 ligase complex that is involved in mediating the binding of substrates to the E3 ligase complex. KLHL3 has a Broad-Complex, Tramtrack and Bric a brac domain at the N-terminus, a BACK domain and six kelch motifs at the C-terminus (257). Kelch motifs are evolutionally conserved and involved in many cellular processes, such as cell morphology, gene expression and protein interactions (258). CUL3 is the core component of the BCR E3 ligase complex. Together with KLHL3, they interact and form a CUL3-KLHL3 E3 ligase complex that mediates and promotes substrate ubiquitination. This complex binds to WNK1 and WNK4, targeting them to proteasomal degradation and subsequently regulating NCC through the WNK ubiquitination (259,260). In addition, there is evidence that KLHL3 is co-expressed with NCC and that it directly downregulates NCC expression at the DCT by recruiting NCC for proteasomal degradation (177).

1.6.6.1 Phosphorylation of KLHL3 and CUL3

Increased ANGII and vasopressin induces PKA and PKC-mediated phosphorylation of KLHL3 at S433. This prevents KLHL3-WNK4 interaction and ubiquitination, resulting in an increase in WNK4 protein abundance (261,262).

1.6.6.2 FHht-type mutation in KLHL3 and CUL3

KLHL3 and *CUL3* mutations were identified in 63 % of FHht pedigrees that did not have *WNK* mutations (263). Mutations in *KLHL3* can inhibit its ability to bind to CUL3, WNK1 and WNK4, resulting in a decrease in proteasomal degradation of the WNK kinases, thereby increasing NCC activity (264–266). Multiple rare non-synonymous exonic SNPs in *KLHL3* have been shown to cause FHht; of which the most commonly found mutation in the KLHL3 protein is L387P. All of these polymorphisms lie within the evolutionarily conserved kelch-repeat domains (263). All *CUL3* mutations are intronic and cause defective splicing of exon 9. The precise pathogenesis of CUL3 mutations is unclear, but ultimately it

results in increased WNK1, WNK4 and NCC abundance (263,267). Other mutations identified in FHHt patients, such as WNK4-E562K, WNK4-Q565E and mutations in the non-catalytic region of WNK1, WNK1 Q479-N667, lead to decreased interactions with KLHL3 and the abrogation of the ubiquitination process, which results in an increase in the abundance of WNK1 and WNK4 (264).

1.7 WNK-NCC cascade

The WNK kinases control NCC membrane abundance and its activity through SPAK and OSR1. The WNK cascade is complex and involves a sequential inhibitory cascade between various WNK proteins. Several research groups have proposed models of the WNK-SPAK-NCC cascade, however, a unifying model has yet to be generated.

1.7.1 The orthodox model of the WNK-NCC cascade

The orthodox model of the WNK-SPAK-NCC cascade arose from the understanding of FHHt-type mutations in the WNK kinases. KS-WNK1 is the predominant form of WNK1 in the nephron that lacks the ability to phosphorylate proteins. KS-WNK1 inhibits L-WNK-1 and L-WNK1 inhibits WNK4, which suppresses WNK4-induced lysosomal degradation of NCC (121,214). WNK3 and WNK4 mutually inhibit one another and whilst WNK3 is stimulating the trafficking of NCC to the apical membrane, WNK4 inhibits it (207). L-WNK1 and WNK4 both phosphorylate and activate SPAK/OSR1 (118–120). An increase in SPAK/OSR1 activity increases NCC phosphorylation and its transport activity (116,117). The ratio of KS-WNK1 to L-WNK1 and WNK3 to WNK4 are tightly controlled by ubiquitination. KLHL3 binds to L-WNK1 and WNK4 and these are subject to degradation through the KLHL3-CUL3 E3 ligase complex (259) (Figure 1.7-1).

DCT

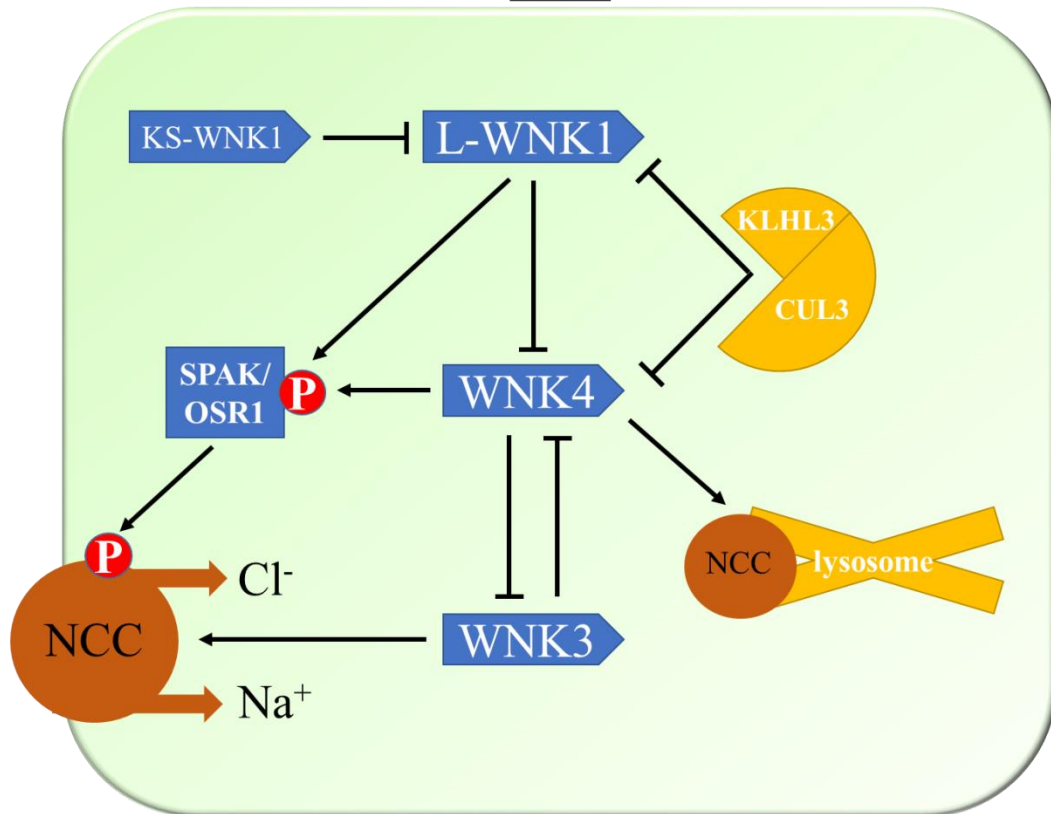


Figure 1.7-1 The orthodox model of the WNK-NCC cascade

The WNK kinases regulate the membrane expression and activity of NCC. KS-WNK1 inhibits L-WNK-1 and L-WNK1 inhibits WNK4. WNK3 and WNK4 mutually inhibit one another and whilst WNK3 is stimulating the trafficking of NCC to the apical membrane, WNK4 is inducing lysosomal degradation of NCC. L-WNK1 and WNK4 both phosphorylate and activate SPAK/OSR1. Activated SPAK/OSR1 increases NCC phosphorylation and enhances its transport activity. KLHL3 binds to L-WNK1 and WNK4 and these are subject to degradation via the KLHL3-CUL3 E3 ligase complex.

1.7.2 The effect of FHHT on the WNK-NCC cascade

FHHT is caused by the overactivity of NCC, resulting in increased sodium and chloride reabsorption in the DCT. In FHHT patients, mutations in KLHL3 and CUL3 prevent the interaction between KLHL3 and the WNK kinases, and the formation of the E3 ubiquitin ligase. This means that L-WNK1 and WNK4 are not ubiquitinated and accumulate in the cytosol, which activates SPAK/OSR1, resulting in increased NCC phosphorylation. In patients with WNK1 mutations, the ratio of L-WNK1 and KS-WNK1 is altered and L-WNK1 protein expression increases. This enhances the basal inhibitory effect of L-WNK1 on WNK4, and activates SPAK/OSR1, increasing phosphorylation of NCC. In patients with FHHT mutations in WNK4, WNK4 becomes a NCC activator and its degradation by the E3 ubiquitin ligase complex is prevented. This increases SPAK/OSR1 activity, causing an increase in NCC phosphorylation and activity, resulting in an increase in sodium chloride reabsorption (Figure 1.7-2).

1.7.3 The effect of CNIs on the WNK-NCC cascade

Similar to FHHT-induced hypertension, CNI causes hypertension by activating the WNK-NCC cascade (51). CNI increases the protein abundance of WNK3, WNK4, SPAK and phosphorylated NCC (51) and its effects on WNK1 is unclear. Increased expression of WNK3 causes an increase in the trafficking of NCC to the apical membrane. WNK4 phosphorylates and activates SPAK/OSR1, increasing NCC phosphorylation and cotransporter activity (51), causing an increase in sodium and chloride reabsorption (Figure 1.7-3).

In addition to increased sodium chloride reabsorption, CNIs also alter potassium, calcium, magnesium and acid-base homeostasis. As calcineurin is a protein phosphatase, and CNIs have been shown to alter the activity of serine/threonine kinases and dysregulate the phosphorylation status of proteins, this suggests that phosphorylation may be a key post-translational modification determining the CNI-induced activity of electrolyte transporters.

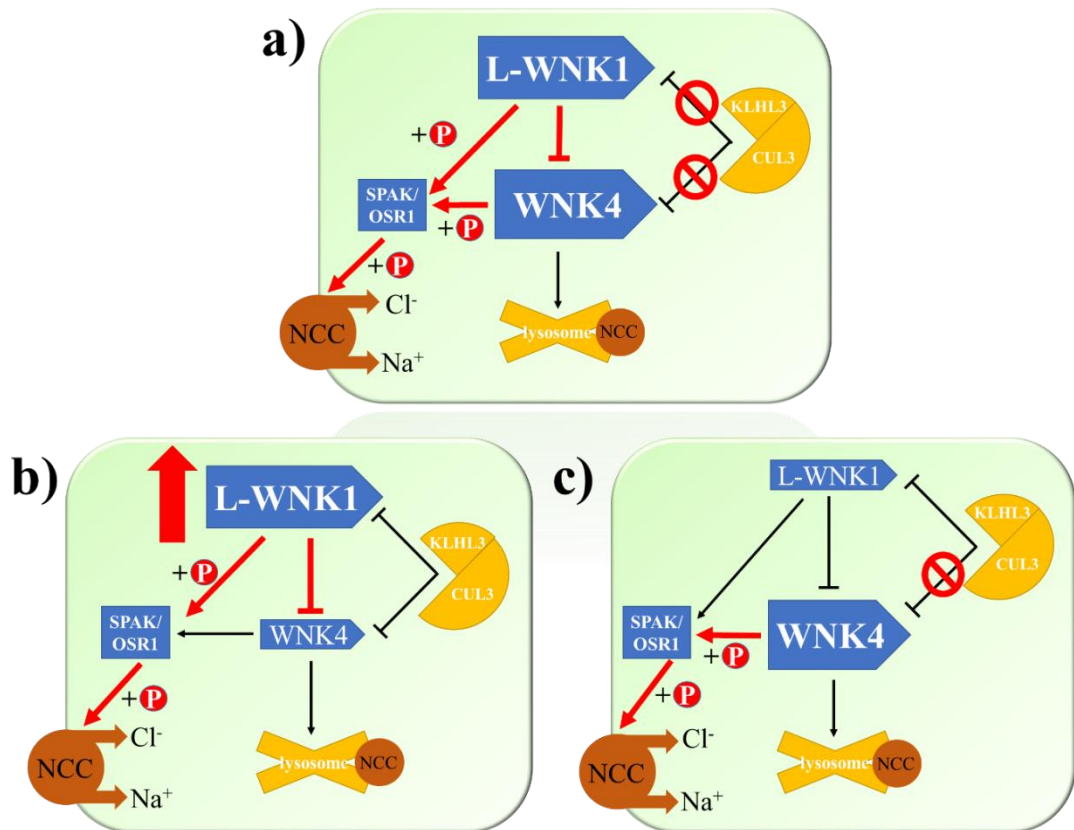


Figure 1.7-2 FHHT-mutations in the WNK-NCC cascade

Under normal conditions, L-WNK1 is a positive regulator of NCC and inhibits WNK4-induced inhibition of NCC. Both L-WNK1 and WNK4 bind to the CUL3-KLHL3 E3 ubiquitin ligase complex and are subjected to degradation. a) FHHT mutations in KLHL3 and CUL3 prevent the formation of the E3 ubiquitin ligase complex and the interaction between KLHL3 and the WNK kinases. This leads to L-WNK1 and WNK4 accumulation, activating SPAK/OSR1 and increasing NCC phosphorylation. b) FHHT mutations in WNK1 increase L-WNK1 protein expression. L-WNK1 inhibits WNK4 and activates SPAK/OSR1, increasing phosphorylation of NCC. c) FHHT mutations in WNK4 convert WNK4 to a NCC stimulator and prevent WNK4 from degradation by the E3 ubiquitin ligase complex. An increase in WNK4 phosphorylates SPAK/OSR1 and increases NCC phosphorylation.

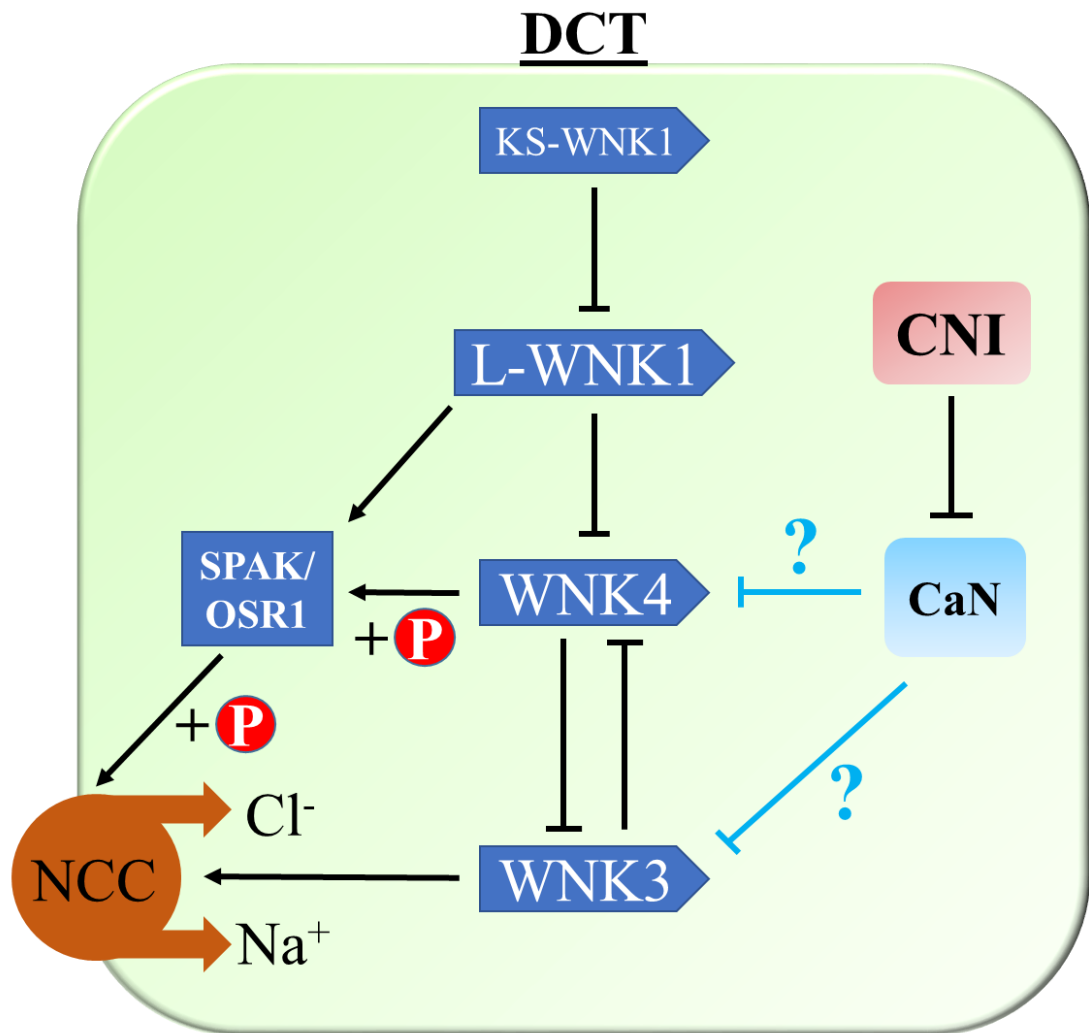


Figure 1.7-3 The effect of CNIs on the WNK-NCC cascade

CNIs activate NCC through the increase in WNK3, WNK4 and SPAK activity. The interactions between calcineurin and the WNK kinases are unclear, but since CNIs have a positive effect on WNK3 and WNK4, calcineurin may act as their negative regulator under normal conditions. An increase in WNK3 expression stimulates the trafficking of NCC to the apical membrane and the increase in WNK4 phosphorylates and activates SPAK/OSR1. An increase in SPAK/OSR1 activity increases NCC phosphorylation, and NCC transport activity is enhanced.

1.8 Calcineurin

Calcineurin is a serine/threonine protein phosphatase that is calcium and calmodulin dependent. Calcineurin is best known for its role in the immune system, stimulating the expression of cytokines involved in proliferation and differentiation of leukocytes. Calcineurin functions as a heterodimer that is composed of calcineurin A, a catalytic subunit that is ~60 kDa in size and calcineurin B, a regulatory subunit of ~19 kDa. These two calcineurin subunits are ubiquitous in mammalian tissues, highly concentrated in the brain (268) and notably present in B and T lymphocytes, kidneys (269), pancreas (270), sperm (271) and smooth muscle cells (272). The isoforms of calcineurin subunits and the abundance of these isoforms can be tissue specific (273,274).

1.8.1 Structure

Calcineurin A encodes a large catalytic domain at the N-terminus and three regulatory domains that encode for a calcineurin B binding domain, calmodulin binding domain and an autoinhibitory domain at the C-terminus (268,272) (Figure 1.8-1). Calcineurin A consists of three highly conserved isoforms: α , β and γ . All three isoforms share homology with other serine/threonine protein phosphatases with a unique C-terminus regulatory domain (275).

Calcineurin B has highly conserved isoforms: the ubiquitously expressed calcineurin B α and calcineurin B β , that is only expressed in the testes (276). Calcineurin B encodes for four EF-hand motifs and each EF-hand motif binds to one calcium ion (277). These EF-hand motifs exhibit different affinities; the two EF-hand motifs at the N-terminus have lower affinities for calcium than the two encoded at the C-terminus (278). These EF-hand motifs also play an important role in stabilising the heterodimeric structure of calcineurin, mediating the binding of calmodulin to calcineurin A and the stimulation of calcineurin when free calcium ions are bound.

1.8.2 Calmodulin

Calmodulin is a highly-conserved calcium sensor and shares 35 % homology with calcineurin B. Calmodulin is expressed in all eukaryotic cells and is involved in a range of cellular processes, such as cell proliferation, motility and apoptosis.

Similar to calcineurin B, calmodulin also has two globular domains located at the N- and C-terminus and each of these globular domains contains two EF-hand motifs. In contrast to calcineurin B, calcium ions bind to the EF-hands at the N-terminus at a higher efficiency than to the motifs at the C-terminus, giving versatility for calmodulin to adapt to different levels of intracellular calcium (279,280). The binding of calcium alters the interhelical angles in the EF-hands, exposing a hydrophobic region that allows calmodulin to interact with the canonical calcium loaded calmodulin binding sequences on the target proteins.

1.8.3 Activation of calcineurin

Calcium and calmodulin are essential for the activation of calcineurin. This process is dependent on calcineurin B, calcium and calmodulin, and involves conformational changes of calcineurin A (281). The autoinhibitory domain of calcineurin binds to the catalytic domain of calcineurin A to prevent activation (282). In the event of high intracellular calcium, free calcium binds to calcineurin B, causing it to bind to calcineurin A triggering a conformational change and exposing the calmodulin binding site (283). The subsequent binding of calmodulin disrupts the association between the autoinhibitory domain and the catalytic site on calcineurin A, stimulating phosphatase activity (281) (Figure 1.8-1).

1.8.4 Function

Calcineurin plays an important role in the activation of the immune response. This begins with the recognition of antigens by T cell antigen receptors, which causes the release of calcium from intracellular stores and triggers calcium influx, resulting in increased intracellular calcium and calcineurin activation. Calcineurin subsequently dephosphorylates and activates NFATc, resulting in NFAT translocation to the nucleus where it binds to the DNA (Deoxyribonucleic acid), causing an increase in transcriptional activation of the cytokines, including interleukin (IL) -2, IL-3, IL-4 and tumour necrosis factor- α (TNF- α) (284). Together, the expression of these cytokines stimulates the proliferation and differentiation of leukocytes, inflicting an immune response.

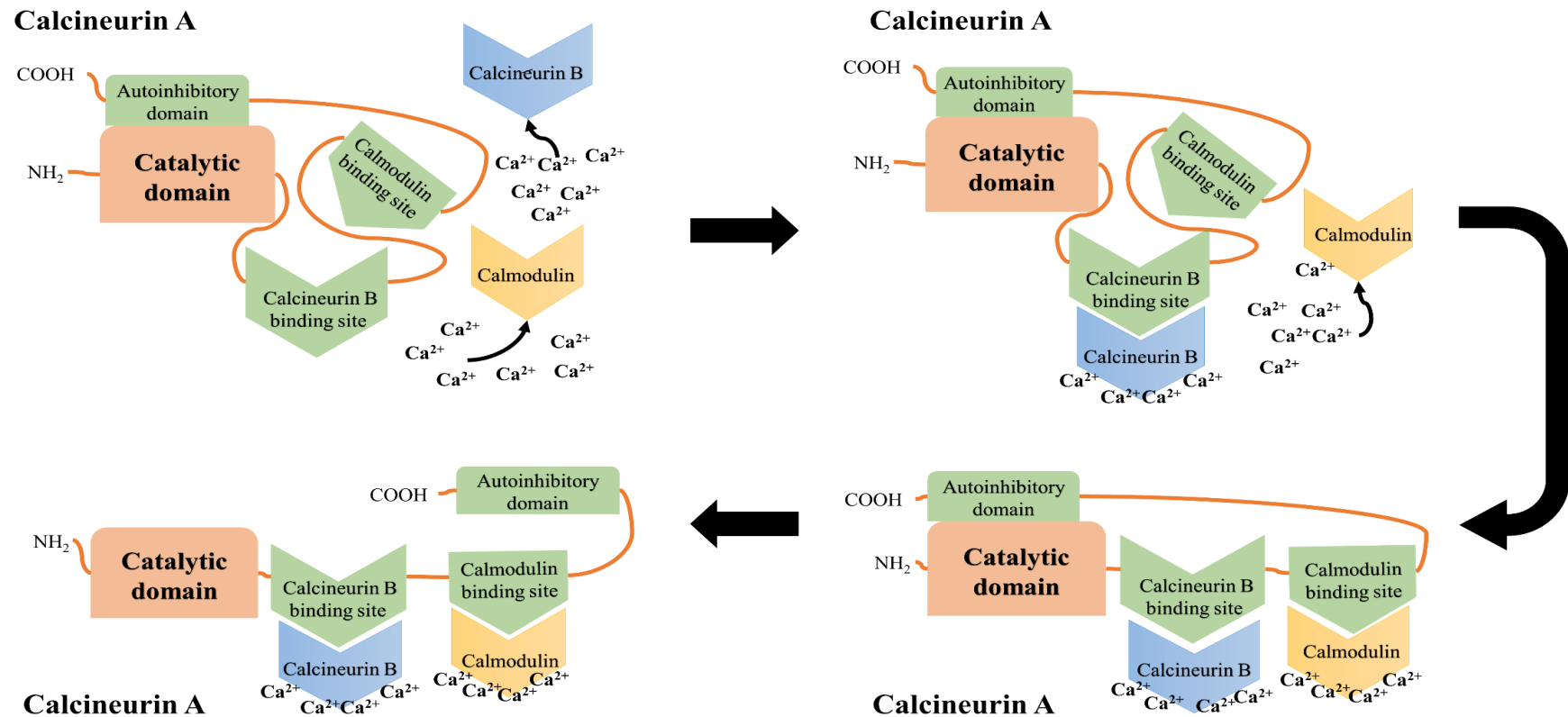


Figure 1.8-1 Calcineurin activation

Free intracellular calcium ions bind to both calmodulin and calcineurin B. Calcium-activated calcineurin B binds to calcineurin A and exposes the calmodulin binding site. Calmodulin then binds to the calcineurin A-B complex and disrupts the association between the autoinhibitory domain and the catalytic site on calcineurin A, stimulating phosphatase activity.

1.8.5 The association between calcineurin and the RAAS

Calcineurin is ubiquitous and pleiotropic. Calcineurin plays a regulatory role in the RAAS by regulating aldosterone synthase (CYP11B2) expression (285,286). ANGII-induced expression of CYP11B2 and aldosterone secretion in 3T3-L1 adipocytes are dependent on the calcineurin-NFAT signalling pathway (285,286). ANGII was able to stimulate calcineurin activity and induce NFAT translocation to the nucleus (287,288). CNIs and NFAT inhibitors were shown to suppress ANGII-induced aldosterone secretion.

1.8.6 Immunophilins

Immunophilins are sequence conserved molecular chaperones that exhibit peptidylprolyl cis-trans isomerase (PPIase) activity. PPIase catalyses the cis-trans isomerisation of peptide bonds at proline residues of proteins to facilitate protein folding and also its own folding process (289). The two main families of immunophilins are the cyclosporine-binding cyclophilins and the FK506 binding proteins (e.g. FKBP12). As their name suggests, cyclophilins bind to CyA and FKBP12 bind to FK506 (as well as rapamycin) (290). These immunosuppressants bind to their immunophilins with high affinity, form complexes with them and inhibit their PPIase activity.

1.8.7 Calcineurin inhibitors

Calcineurin inhibitors, such as CyA and FK506, are immunosuppressants widely used in transplant medicine to prevent rejection and also in treating autoimmune diseases (291). CyA and FK506 form complexes with cyclophilin A and FKBP12 respectively (290), and adopt different signalling mechanisms. CyA-cyclophilin and FK506-FKBP12 complexes bind to calcineurin, suppress its phosphatase activity and prevent the dephosphorylation of NFATc. This prevents the translocation of NFATc into the nucleus, and as a result, the signal transduction required for an immune response is suppressed.

Rapamycin is a macrolide produced by *Streptomyces hygroscopicus* that is used to prevent organ transplant rejection. Rapamycin is not a CNI, however its mode of action is similar to FK506, which involves forming a complex with FKBP12. The rapamycin-FKBP12 complex binds to and inhibits the mechanistic (or

mammalian) Target Of Rapamycin (mTOR), also known as FKBP-rapamycin-associated protein and inhibits the secretion of IL-2 (292) (Figure 1.8-2).

1.8.7.1 Other side effects of CNIs

Hyperkalaemia (52,53), hypercalciuria (56,57), hypomagnesaemia (57,58), metabolic acidosis (54,55) and hypophosphatemia (59) are also common side effects of CNIs and are risk factors for morbidity and decreased graft function (44,45).

Hyperkalaemia can be life-threatening especially in patients taking antihypertensive medications, such as ACE inhibitors and ANG receptor blockers. Hyperkalaemia occurs in 5 to 40 % of CNI-treated patients (52,53) and it is characterised by inefficient potassium excretion. CNI reduces the surface expression of ROMK and promotes paracellular chloride reabsorption through the WNK kinases (293). Increased chloride reabsorption reduces lumen negativity, thus reducing the driving force for potassium secretion. A low potassium diet, loop diuretics or thiazides and sodium bicarbonate supplements have been recommended for treating CNI-induced hyperkalaemia (294).

CNI-induced hypercalciuria is characterised by urinary calcium wasting and is associated with increased bone-turnover and osteoporosis. CNIs are thought to prevent calcium reabsorption by reducing TRPV5 and calbindin-D28K expression in the DCT (51,57). Thiazide treatment can lower urinary calcium excretion by 50 % and is the recommended treatment for CNI-induced hypercalciuria (295). CNI-induced hypomagnesaemia is caused by inefficient magnesium reabsorption in the distal tubules, possibly induced by lowered TRPM6 expression (57).

Metabolic acidosis is generally asymptomatic in CNI-treated patients. It occurs in 13 to 17 % of CNI-treated patients (54,55,296) and is characterised by bicarbonate wasting and inefficient excretion of hydrogen ions (54). Similar to metabolic acidosis, hypophosphatemia is also generally asymptomatic in CNI-treated patients. Hypophosphatemia is characterised by urinary phosphate wasting. Renal phosphate reabsorption relies on the sodium phosphate cotransporter (NaPi)-IIa expressed in the PCT (59) and CNIs, such as CyA, inhibit NaPi-IIa and suppress phosphate reabsorption (59). Patients with severe cases of CNI-induced hypophosphatemia are treated with phosphate.

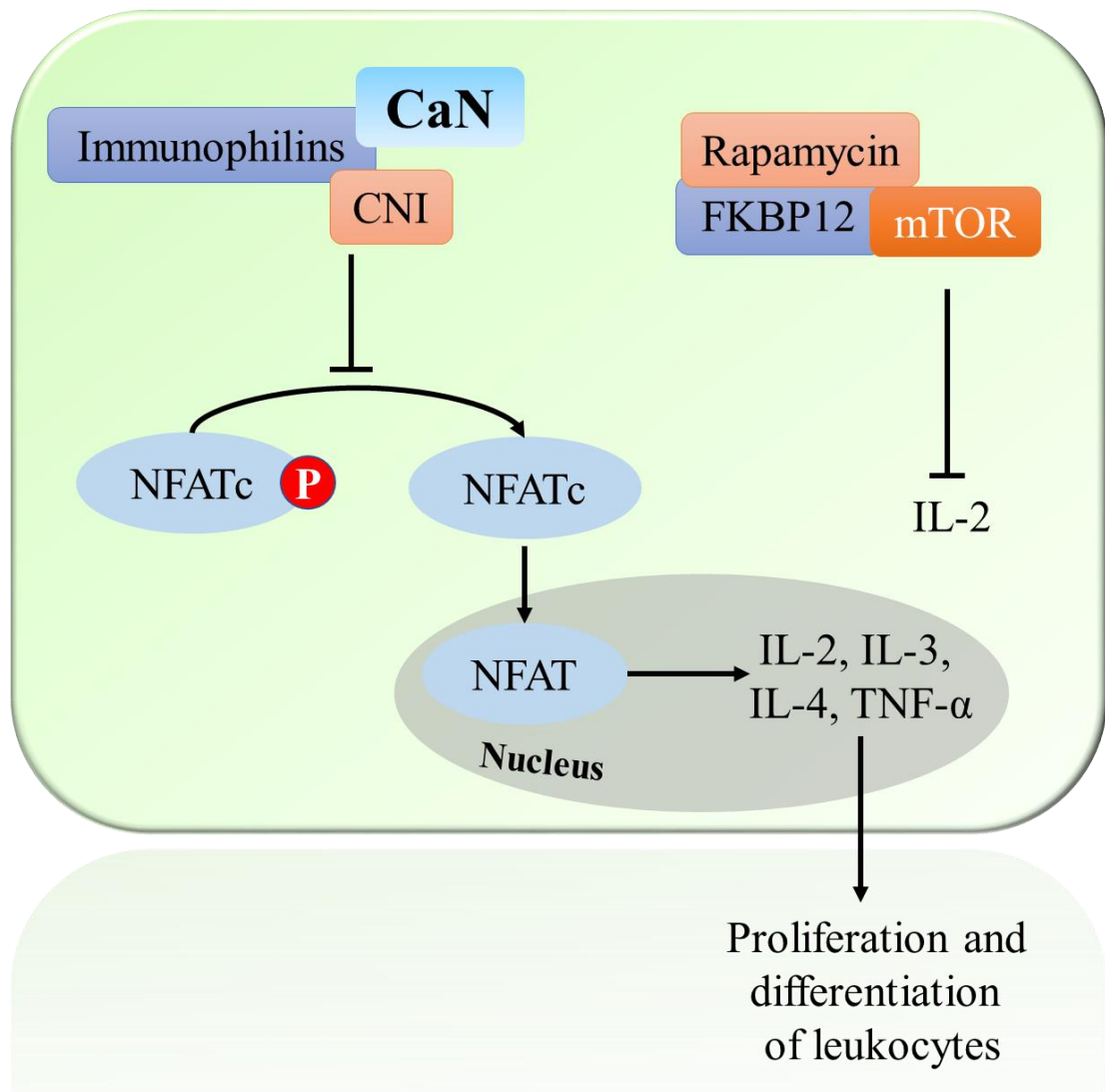


Figure 1.8-2 The immunosuppressive effects of CNIs

Calcineurin inhibitors (CyA and FK506) form complexes with immunophilins (cyclophilin A and FKBP12). CyA-cyclophilin and FK506-FKBP12 complexes bind to calcineurin, suppress its phosphatase activity and inhibit the activation of NFATc by preventing its dephosphorylation. Inactive NFATc cannot enter the nucleus and trigger cytokines transcription, preventing an immune response from being triggered. The mode of action of Rapamycin is similar to FK506. Rapamycin forms a complex with FKBP12 and inhibits mTOR, which suppresses IL-2 secretion.

1.9 Calcium transport in the distal nephron

Many studies have hypothesised that an underlying mechanism governing both sodium and calcium handling exists (297,298). Calcium reabsorption is regulated by calciotropic hormones and between 1-2 % of calcium filtered in the kidneys (10 g) is excreted per day. The rest of the filtered calcium is reabsorbed back into the serum; 60 to 70 % in the PCT, 25 % in the TALH, 10 % in the DCT, and 5 % in the CD. Calcium is reabsorbed by paracellular routes involving claudin-2, 10 and 17 in the PCT (299,300) and the remainder 20 to 30 % of the calcium flux is reabsorbed through transcellular transport with an unknown underlying mechanism (301). In the TALH, calcium is mostly reabsorbed via claudin-10, 16 and 19 through paracellular transport driven by a lumen-positive electrochemical gradient generated by NKCC2, ROMK and basolateral chloride and sodium transporter (302,303). In addition to paracellular transport, calcium is also reabsorbed through transcellular pathways in the TALH, however, since this percentage of reabsorption is relatively low, it is unlikely to have a significant effect on the overall reabsorption (304,305). Similar to sodium handling in the DCT, the fine-tuning of serum and urinary calcium concentration also occurs at the distal nephron. In the DCT, calcium is transported exclusively through transcellular pathways by TRPV5. Calcium enters the cell through TRPV5, which is highly expressed in the DCT cell (137), and binds to calbindin-D28K in the cytosol, which acts as a calcium buffering protein and shuttles calcium towards the basolateral membrane. Calcium is exported into the peritubular fluid through NCX1 and PMCA (Figure 1.9-1).

1.9.1 Regulators of DCT calcium transport

1.9.1.1 PTH

PTH is secreted from the parathyroid glands in response to hypocalcaemia, glucocorticoids and oestrogen, and it is degraded in response to hypercalcaemia by the endopeptidase in parathyroid cells (306). PTH is responsible for increasing the serum calcium concentration by inducing bone resorption, increasing dietary absorption of calcium in the intestine, and active calcium reabsorption in the nephron (Figure 1.9-2). PTH is known to upregulate NCX1 activity (307) and TRPV5 (308). The regulatory mechanism for PTH-induced NCX1 activation is

currently unknown, however it may involve PKA and PKC. The interaction between PKA/PKC and NCX1 is complex, controversial and possibly dependent on the tissue-specific splice variants of NCX1 (309–312), thus the precise interaction between PKA/PKC and NCX1 require further investigation. The regulation of TRPV5 involves two different mechanisms, the PKA and PKC signalling pathways (313,314). PTH stimulates TRPV5 through activation of the adenylyl cyclase (ADCY)-PKA pathway, upon activation of this pathway, PKA phosphorylates TRPV5, decreases calcium dependent inactivation and encourages the opening of the channel for calcium uptake (314). Alternatively, PTH has been reported to stimulate TRPV5 transcription and signals PKC to inhibit caveola-mediated endocytosis of TRPV5, resulting in the accumulation of TRPV5 at the cell membrane (313,315) (Figure 1.9-1).

1.9.1.2 Vitamin D₃

1,25(OH)₂D₃ is the active form of vitamin D₃ and it is derived from a series of hydroxylation reactions. Vitamin D₃ is a steroid that can be absorbed through the diet and can be synthesised in the skin in the presence of ultraviolet light. Vitamin D₃ is hydroxylated into 25-hydroxyvitamin D₃ (25(OH)D₃) by 25-hydroxylase secreted from the liver, and 25(OH)D₃ is hydroxylated into 1,25(OH)₂D₃ by the renal enzyme, 1 α -hydroxylase, or into the metabolically-inactive 24,25-dihydroxyvitamin D₃ (24,25(OH)₂D₃) by 24 α -hydroxylase (316). 1,25(OH)₂D₃ then binds to VDR and target gene transcription is initiated. The activity of 1 α -hydroxylase is stimulated by PTH and hypocalcaemia and it is suppressed in a negative feedback loop by 1,25(OH)₂D₃, and also by Klotho, FGF23 and hypercalcaemia, to enable the fine-tuning of serum calcium concentration (317–319) (Figure 1.9-2). 1,25(OH)₂D₃ has been shown to stimulate TRPV5, calbindin-D28K and PMCA expression, resulting in an increase in calcium reabsorption (131,145) (Figure 1.9-1). Analysis of the TRPV5 amino acid sequence revealed several vitamin D₃ response elements at the promoter region, which suggests that vitamin D₃ may directly regulate the transcription of TRPV5 (320).

1.9.1.3 Klotho

Klotho is a transmembrane protein that is expressed in the kidneys, parathyroid gland (321) and the vasculature (322). In the kidneys, klotho is most abundantly

expressed in the DCT and expressed to a lesser extent in the PCT (323). Even though klotho is a transmembrane protein, it is also abundantly expressed in the cytosol (324) and can be secreted into the serum (325), where it has the potential to be involved in various signalling pathways.

Klotho is a β -glucuronidase/sialidase that can hydrolyse D-glucuronic acid residues on mucopolysaccharides. Klotho has been shown to increase calcium entry by hydrolysing TRPV5, removing the terminal sialic acid residues from the glycan chains and exposing the galectin-1 ligands on TRPV5. The ligands then bind to the galectin-1 lattices on the plasma membrane and secures TRPV5 to the plasma membrane (147,148) (Figure 1.9-1).

Furthermore, klotho also increases calcium reabsorption by interacting with the FGF23 receptor expressed in the PCT and the DCT. FGF23 is a bone-derived hormone that is secreted in response to PTH and $1,25(\text{OH})_2\text{D}_3$. FGF23 is best known for its role in suppressing phosphate reabsorption in the PCT, PTH secretion and $1,25(\text{OH})_2\text{D}_3$ synthesis. Klotho binds to the FGF receptor, and converts it into a FGF23-specific receptor (326). When FGF23 binds to its receptor, the FGF23 signalling pathway is triggered and the activity of 1α -hydroxylase is suppressed in the nephron (318) (Figure 1.9-2). Mice with FGF23 deficiency have hypercalciuria and increased vitamin D_3 levels (327). The underlying mechanism that causes hypercalciuria in FGF23 deficient mice is unclear, but it is possible that this is due to a decrease in TRPV5 membrane abundance since FGF23 has been reported to increase TRPV5 membrane expression.

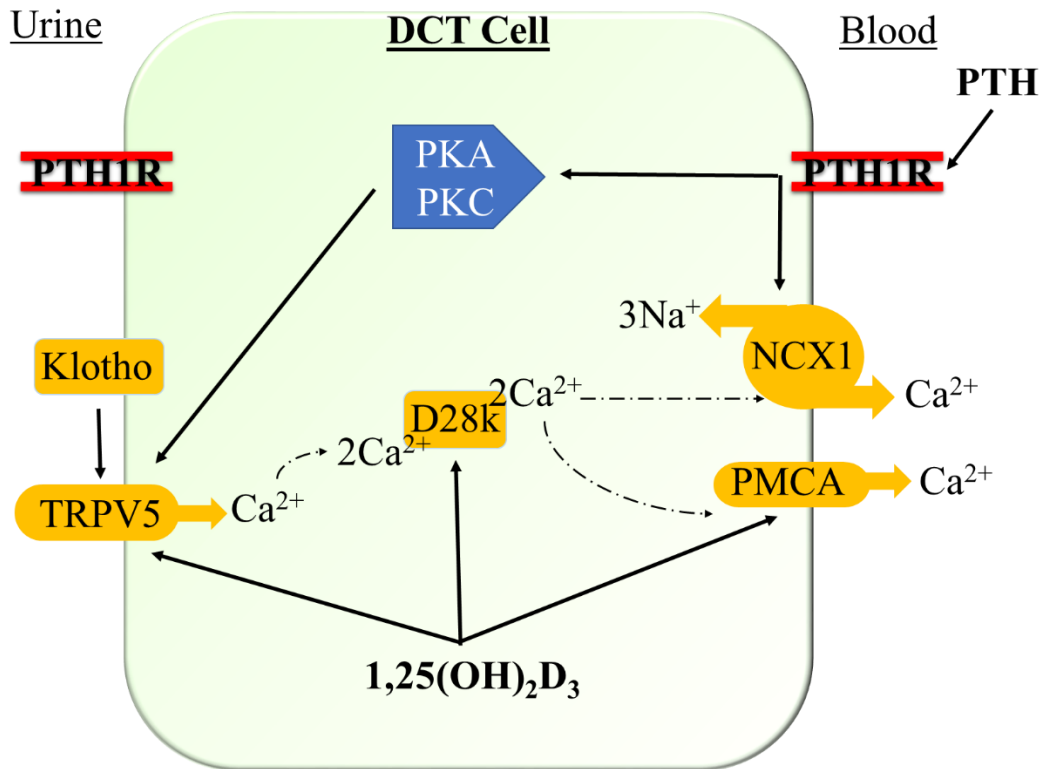


Figure 1.9-1 Regulation of calcium reabsorption in the DCT

Calcium homeostasis at the DCT is regulated by PTH, 1,25(OH)₂D₃ and klotho. Through PKA and PKC signalling, PTH stimulates an increase in apical calcium uptake through an increase in TRPV5 surface abundance and activation. PTH also increases NCX1 activity. 1,25(OH)₂D₃ stimulates TRPV5, calbindin-D28K and PMCA expression to encourage calcium reabsorption. Klotho increases TRPV5 cell surface expression by preventing TRPV5 endocytosis.

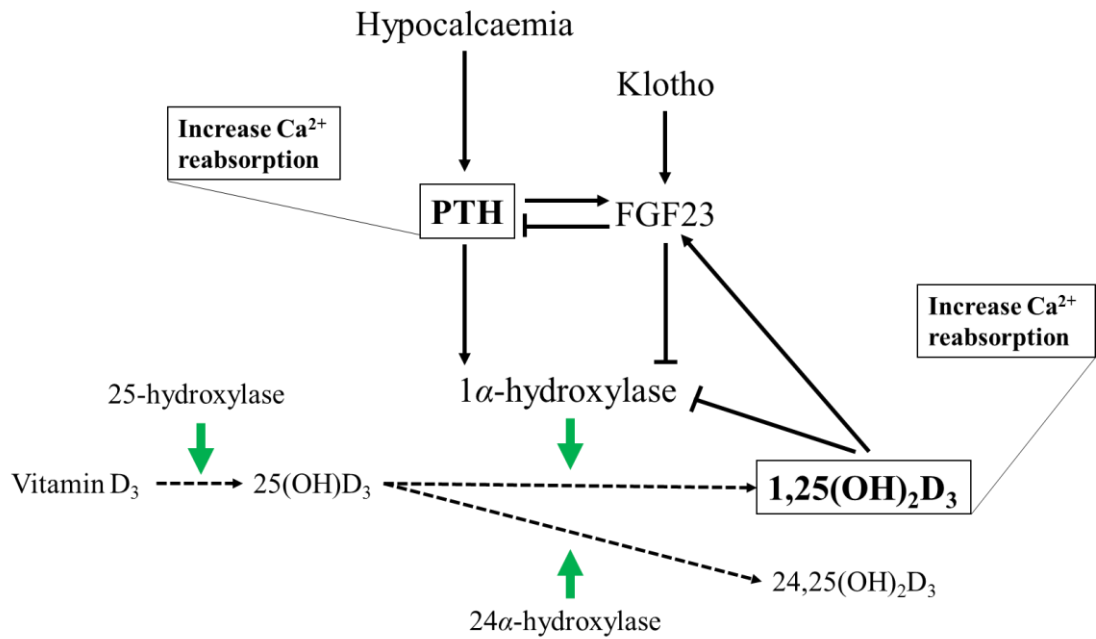


Figure 1.9-2 The PTH-Vitamin D₃-FGF23 axis in the nephron

Hypocalcaemia triggers the release of PTH from the parathyroid gland. PTH increases calcium reabsorption by stimulating TRPV5 and NCX1. In addition, PTH stimulates 1 α -hydroxylase activity, causing an increase in 1,25(OH)₂D₃ synthesis. An increase in 1,25(OH)₂D₃ stimulates TRPV5, calbindin-D28K and PMCA, which further increases calcium reabsorption. Calcium reabsorption in the DCT is governed by several negative feedback loops. 1,25(OH)₂D₃ provides negative feedback to PTH and 1 α -hydroxylase via FGF23 and PTH stimulates FGF23 to inhibit 1 α -hydroxylase.

1.9.2 TRPV5

There are six members of the TRPV channel family (TRPV1-6). Genes encoding for TRPV5 and TRPV6 have been localised on chromosome 7q34-35 in humans (328). TRPV5 and TRPV6 share the highest sequence homology amongst the TRPV members and possess unique characteristics, such as a high affinity for calcium and calcium-dependent inactivation (329). TRPV5 is expressed in the apical membrane of the DCT and the CNT and is sensitive to hormonal stimuli, diuretics, high intracellular calcium and extracellular acid-base ratio.

1.9.2.1 Structure of TRPV5

TRPV channels contain large cytoplasmic N and C-termini, flanking 3-6 ankyrin repeat motifs and six TM domains (330). An *in vitro* experiment performed on oocytes showed that TRPV5 either forms a homotetramer or forms a heterotetramer with TRPV6. The loop between TM5 and TM6 is involved in pore formation in the middle of the subunits (331). The N-terminus plays an important role in the subunit assembly of TRPV5, and the ankyrin repeat motifs have been suggested to induce a molecular zipper process that generates an intracellular anchor for the assembly of the subunits (332). Both the N and C-terminus contain a calmodulin binding region (333). W702 and R706 were identified in the C-terminus of the calmodulin binding region in rabbit TRPV5 and these were reported to play an important role in calcium-dependent inactivation of TRPV5 by enabling calmodulin binding; mutations at these residues were shown to abolish calmodulin binding, thereby reducing calcium-dependent inactivation (334).

1.9.2.2 Functional properties of TRPV5

The selectivity for calcium ions in TRPV5 is defined by D542, a residue situated in the loop between TM5 and TM6, homologous to D541 on TRPV6. Mutations at D541 in TRPV6 induce changes in the pore diameter (335). Substitution mutations replacing the negatively charged aspartic acid with residues that have a shorter side chain, alanine and glycine, increase TRPV6 permeability to larger molecules and reduce the affinity for calcium (335). In addition to calcium-dependent inactivation, uptake studies in *Xenopus* oocytes showed that extracellular protons also suppress TRPV5 activity (131). TRPV5-E522 was

reported to play an important role in acid sensitivity and this mutant, containing the non-titratable glutamine, resulted in decreased TRPV5 activity (336).

1.9.2.3 TRPV5 and WNK4

WNK4 appears to have contradictory effects on TRPV5; WNK4 was shown to stimulate caveola-mediated endocytosis of TRPV5 (337) but was also shown to increase TRPV5 surface expression, an effect that was reduced by NCC (338). Co-expression studies of WNK4-Q565E, a mutation commonly identified in FHHT patients with hypercalciuria, and TRPV5 showed that the WNK4-Q565E retained its ability to stimulate TRPV5 but this effect was reduced by NCC when NCC was co-expressed (338). This suggests that FHHT-induced hypercalciuria may result from a decrease in TRPV5 expression mediated by SPAK-NCC activation.

Furthermore, WNK4 may also play a role in the PKC-TRPV5 signalling pathway. When WNK4 was co-expressed with PKC and TRPV5, WNK4 was shown to amplify the stimulatory effect of PKC on TRPV5, despite its basal-inhibitory effect, which was reported in the same study (337). These studies examined the effects of WNK4 *in vitro*, therefore the effect of WNK4 on TRPV5 *in vivo* requires further investigation. Moreover, WNK4 has been reported to have different roles under different cellular environments (244), therefore it is conceivable that another regulatory pathway may also be involved in the WNK4-TRPV5 signalling pathway.

1.9.2.4 Phosphorylation of TRPV5

Phosphorylation of TRPV5 at S299 and S654 by PKC, and T709 by PKA are critical for TRPV5 activation (314,315). Co-expression studies of TRPV5, SGK1 and the scaffold protein that regulates the surface expression of transmembrane protein, NHE regulatory factor (NHERF) 2, demonstrate that SGK1 and NHERF2 simultaneously and directly stimulate TRPV5 activity (339). This stimulatory effect was eliminated in SGK1 knockout mice and in an oocyte model of kinase-inactive SGK1 (339,340), indicating that the stimulation of TRPV5 might be mediated by phosphorylation. Furthermore, the SGK1 knockout model caused hypocalciuria and also decreased the abundance of calbindin-D28K (340).

1.9.3 NCX1

In the distal nephron, NCX1 is expressed at high levels in the basolateral membrane and is known to contribute to transcellular calcium reabsorption (341). NCX1 is an electrogenic transporter that exchanges three Na⁺ per Ca²⁺ across the basolateral membrane.

There are three members of the NCX transporters (NCX1-3), of which NCX1 has been most comprehensively characterised. The NCX1 gene is localised on chromosome 2p22.1 in humans (342). NCX1 is ubiquitously expressed; high levels have been detected in the kidneys (135), heart (343) and brain (344). NCX2 and NCX3 are highly expressed in the brain and skeletal muscles, but their expression in the kidneys have not been reported (345).

1.9.3.1 NCX1 splice variants

Tissue specific variants of NCX1 are defined by alternative splicing. The splicing region, located on the second β repeat of NCX1, encodes for six small exons (346,347). Different combinations of the mutually exclusive exons (exon A and B) and the cassette exons (C, D, E and F) generate tissue and variant-specific distributions (345–347) (Figure 1.9-3). Over 32 variants can be generated from alternative splicing of NCX1. In general, NCX1 in excitable cells, such as cardiomyocytes and brain cells, contain exon A, and in non-excitable cells, such as those in the kidneys and astrocytes, contain exon B (344). Exon B-containing splice variants are sensitive to intracellular sodium whereas exon A-containing splice variants are insensitive (344). NCX1.2, NCX1.3 and NCX1.7 variants are reportedly expressed in the kidney but NCX1.3 is the most predominant form (312).

1.9.3.2 Structure of NCX1

Based on membrane topology predictions, NCX1 contains nine TM domains and an intracellular loop that divides the transporter into a N-terminal region, containing the first five TM domains, and a C-terminal region, containing four TM domains (348). Between TM2 and TM3 in the N-terminal region, and TM7 and TM8 in the C-terminal region, lie α repeats that are involved in ion binding and transport. The large intracellular loop is 500 amino acids in length and contains

two calcium binding domains (β repeats) that are responsible for regulating NCX1 activity (349) (Figure 1.9-3).

1.9.3.3 Functional properties of NCX1

Different splice variants of NCX1 behave differently in response to their upstream regulators. AKT has been reported to stimulate NCX1.4 transcription, a variant that is commonly expressed in the brain (350). Calcineurin was reported to downregulate cardiac NCX1 (NCX1.1) through PKC α -mediated phosphorylation and also through a process that is independent from NCX1 phosphorylation (351). These studies exclusively investigated the effects of AKT and calcineurin on exon A-containing splice variants, therefore these results may not be representative of exon B-containing variants, such as NCX1.3. PKA and PKC are also upstream regulators of NCX1, however conflicting evidence were reported by several research groups (309–312), in which they concluded that the effects of PKA and PKC may not be as simple as direct phosphorylation of NCX1 and could involve other regulatory kinases.

NCX1 has a low affinity and high transport capacity for calcium (352). NCX1 is sensitive to both intracellular calcium and sodium concentration and the polarity of NCX1 transport direction can reverse depending on the electrochemical gradient and transepithelial voltage (353,354). An increase in intracellular calcium increases NCX1 activity causing calcium efflux, whereas an increase in intracellular sodium can fully inhibit, partially inhibit or reverse the transport direction of NCX1 (344,354). In addition, depolarisation can also reverse the transport direction of NCX1, resulting in sodium efflux and calcium influx (354,355).

1.9.3.4 Phosphorylation of NCX1

Both PKA and PKC have been reported to phosphorylate NCX1 (309,310), however other studies reportedly failed to obtain similar results (311,312,356). This is possibly due to the characteristics of different NCX1 splice variants, such as that NCX1.3 is less sensitive to PKA in comparison to NCX1.1 (310). As these studies were conducted *in vitro*, any conclusion from these should bear in mind that these results may not be representative of behaviour *in vivo*.

NCX1

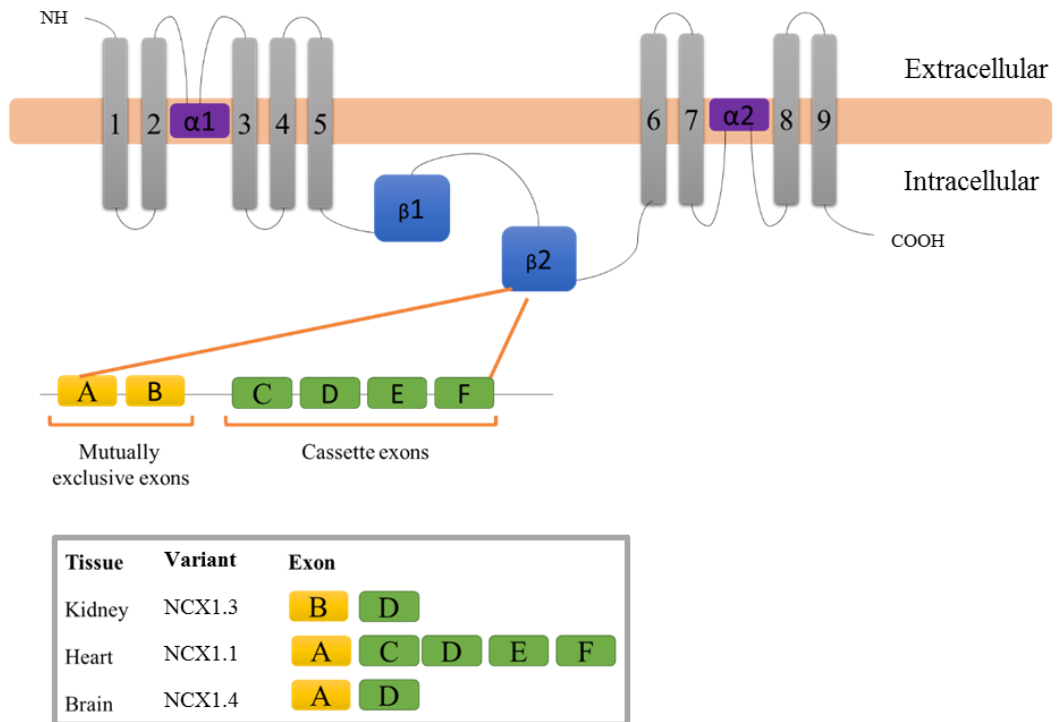


Figure 1.9-3 Topology prediction of NCX1.

Membrane topology modelling of NCX1 predicted nine TM domains (grey) and an intracellular loop that divides the transporter into an N-terminal region (TM1-5) and a C-terminal region (TM6-9). The α repeats involved in the binding and transport of ions (purple) are located between TM2 and TM3, and between TM7 and TM8. The two β repeats (blue) are located in the large intracellular loop and are responsible for regulating NCX1 activity. The splicing region is located on the second β repeat in NCX1. Different combinations of the mutually exclusive (yellow) and the cassette exons (green) generate tissue and variant-specific distributions. NCX1.3, the most predominant splice variant in the kidney, arises from exons B and D, NCX1.1 arises from exons A, C, D, E and F, and NCX1.4 is generated from exons A and D.

1.9.4 PMCA

PMCA is a plasma membrane calcium ATPase that is expressed ubiquitously in calcium transporting tissues, such as the kidney (135), intestine (357), brain (358) and the heart (359). There are four isoforms of PMCA (PMCA1-4) and over thirty splice variants (360). PMCA isoforms share 80-90 % sequence homology (361). Genes encoding PMCA have been localised on the following human chromosomes: *ATP2B1* (PMCA1) at 12q21-q23 (362), *ATP2B2* (PMCA2) at 3p25-p26 (363), *ATP2B3* (PMCA3) at Xq28 (363), and *ATP2B4* (PMCA4) at 1q25-q32 (362).

PMCA1 and PMCA4 are the ubiquitously expressed dominant isoforms (364), whereas PMCA2 and PMCA3 are tissue specific and are most abundant in neuronal tissues (365). Expression of PMCA1 and PMCA4 has been detected in mouse (135) and rat renal tissue (366), and the splice variants, PMCA1b and PMCA4b, are specifically localised to the basolateral membrane of mDCT cells (135) and Madin-Darby canine kidney (MDCK) cells (367). Out of the two PMCA, PMCA4 is the main regulated calcium pump that is dominantly expressed in the distal tubule and colocalises with TRPV5 in the DCT cell (368). This is demonstrated in TRPV5 KO mice, where the downregulation of PMCA4, NCX1 and calbindin-D28K was reported, but PMCA1 remained unchanged (368,369).

1.9.4.1 Structure of PMCA

PMCA consists of ten TM domains and two large intracellular loops that are flanked by the cytoplasmic N- and C-terminus. The N-terminus of PMCA contains a 14-3-3 protein binding site, allowing a 14-3-3 protein to inhibit the pump activity (370). The two-intracellular loops, situated between TM2 and TM3, and between TM4 and TM5, play an important autoinhibitory role by binding to the calmodulin binding domain in the regulatory region of the C-terminus. The C-terminal regulatory domain consists of the calmodulin binding domain, PKA and PKC binding sites, and high affinity calcium binding sites. The C-terminus of PMCA also contains one of the two alternative splicing sites. This determines the number of exons expressed in the variant and will affect functional differentiation, such as calcium affinity (371). When intracellular calcium is high, calmodulin is activated and will bind to the C-terminal domain in PMCA. This will dissociate the interaction between the two intracellular loops and the C-terminus, thereby

activating PMCA (Figure 1.9-4). The first intracellular loop is involved in mediating acidic phospholipids-dependent pump activation and contains the second site for alternative splicing (372). The second intracellular loop contains a catalytic domain comprising the ATP binding site.

1.9.4.2 Functional properties of PMCA

Calmodulin is a positive regulator of PMCA; acting by inhibiting PMCA oligomerisation and promoting PMCA dimerisation, thus enhancing the pump activity (373,374). The expression of PMCA isoforms and variants are also regulated by physiological stimuli, such as the changes in intracellular calcium concentration (366). An increase in intracellular calcium alters the splicing of PMCA1 and a truncated variant is generated (375). This in turn increases mRNA expression of PMCA2 and PMCA3, and inhibits PMCA4 expression in a calcineurin-mediated process (376). PMCA2 and PMCA4 have been reported to inhibit the calcineurin-NFAT signalling pathway (377,378). PMCA2 and PMCA4b recruit calcineurin from the cytoplasm to the plasma membrane, where the concentration of intracellular Ca^{2+} is kept low, and interact with calcineurin through the binding of the catalytic domains present on both the PMCA and calcineurin (377).

PMCA has a high affinity for calcium and a relatively low transport capacity. The dissociation constant of PMCA for calcium is 10 to 20 μM under resting conditions, capable of decreasing to less than 1 μM upon interaction with calmodulin (379). As PMCA is accountable for a third of calcium extrusion in the DCT cell and it has a higher affinity for calcium than NCX1, PMCA may be responsible for the fine-tuning of cytosolic calcium levels.

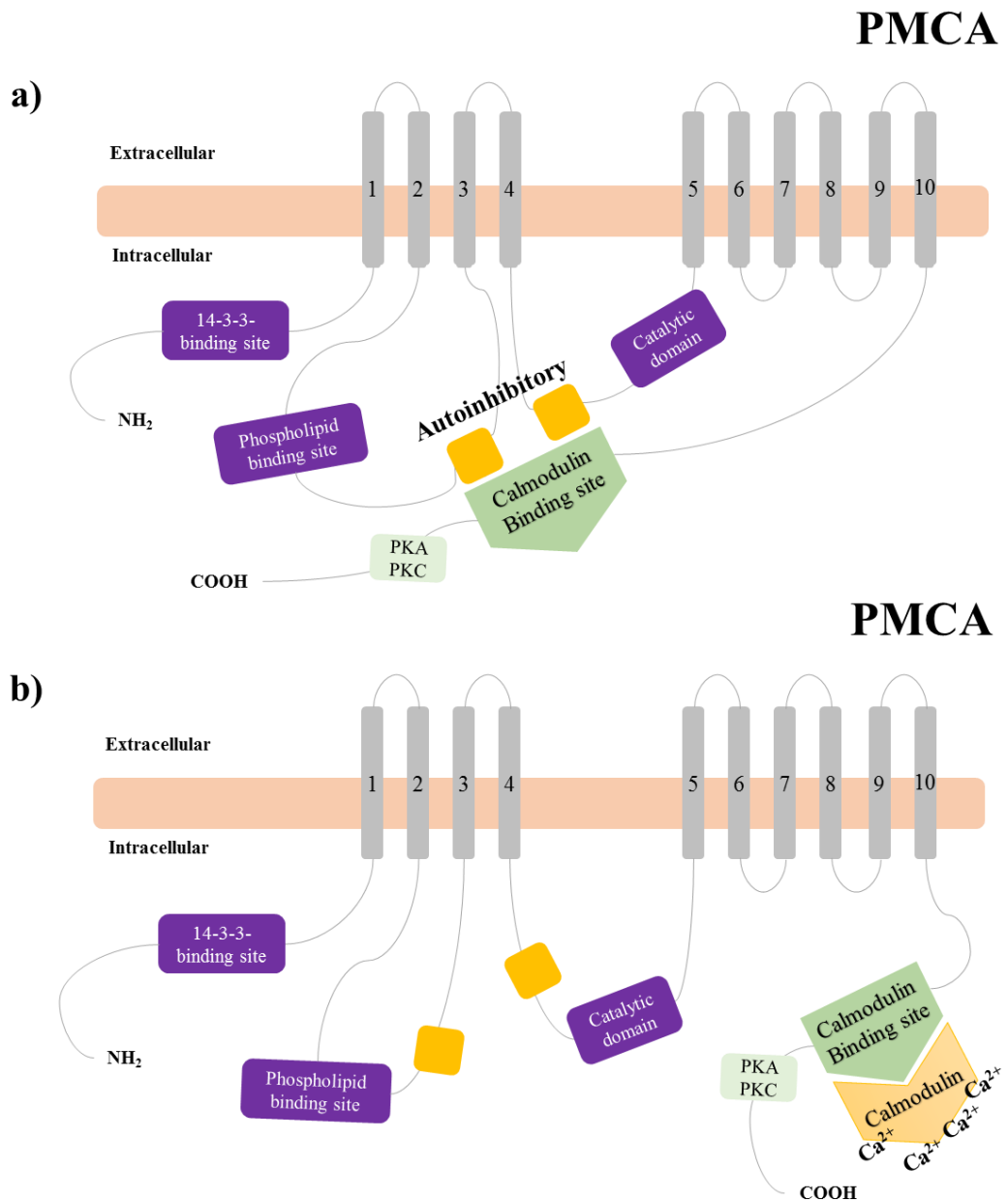


Figure 1.9-4 Activation of PMCA

a) The two-intracellular loops located between TM2 and TM3, and between TM4 and TM5 play an important role in autoinhibition by binding to the calmodulin binding domain in the regulatory region of the C-terminus. b) When intracellular calcium is high, calmodulin is activated. Calmodulin will then bind and dissociate the interaction between the intracellular loops and the C-terminus, resulting in PMCA activation.

1.9.4.3 Phosphorylation of PMCA

PKA and PKC phosphorylate PMCA by binding to their target sequences in the C-terminus. These phosphorylation sites are isoform specific and can result in activation or inactivation of the pump. PKA phosphorylates PMCA1b at S1178 and increases its calcium affinity, however, this effect alone does not lead to full activation of PMCA1b, which indicates that additional regulatory mechanisms coordinate with PKA for full activation (380). PKC phosphorylates the inhibitory region that lie downstream of the calmodulin binding site in the C-terminus of PMCA4b, and partially stimulates the pump by reversing the effect of the inhibitory domain (381,382).

1.9.5 Calbindin-D28K

Calbindin-D28K is a cytosolic calcium binding protein that is exclusively expressed in the cytosol of the DCT, the CNT and principle cells, and co-localises with TRPV5 and NCX1 in the DCT. Calbindin-D28K binds to four calcium ions and is involved in shuttling calcium ions from the apical to basolateral membrane and buffering cytosolic calcium to maintain a low intracellular calcium concentration. In addition to its role as a calcium buffering protein, calbindin-D28K also interacts with the N and C-terminus of TRPV5 under low intracellular calcium concentrations. Calbindin-D28K buffers calcium ions close to the channel's pore, preventing calcium-induced TRPV5 inactivation, and thereby promoting calcium influx (383). Similar to TRPV5, calbindin-D28K is also sensitive to hormonal stimuli, diuretics, high intracellular calcium and extracellular acid-base ratio.

1.10 Relationship between sodium and calcium transport at the DCT

1.10.1 Thiazide diuretics and calcium wasting

Diuretics, such as furosemide and thiazides, are treatments for hypertension and other electrolyte disorders, such as hyperkalaemia, hypercalciuria, hypercalcemia and metabolic acidosis (62,176). Furosemide is a diuretic that targets NKCC2 and has been used for the treatment of hypercalcemia to reduce paracellular calcium transport in the TALH. However, furosemide increases TRPV5 and calbindin-D28K expression (384), which could be a result of a compensatory adaptation to increased calcium delivery to the distal nephron.

Thiazides are diuretics that target NCC and decrease urinary calcium excretion, causing hypocalciuria and hypercalcemia (385). Several groups have studied the effects of thiazide on calcium handling in the kidney but the pathogenesis of thiazide-induced hypocalciuria remains unclear. The studies by Nijenhuis *et al.* in 2003 (386) and 2005 (64) reported that thiazide-induced hypocalciuria is a result of volume contraction, causing increased sodium and water reabsorption, thereby increasing passive paracellular calcium reabsorption in the PCT. The effects of thiazides on distal calcium transporters remain unclear due to conflicting results reported in the two studies; thiazides decreased the mRNA expression of TRPV5, calbindin-D28K and NCX1 in the 2003 study, but had no significant effect in the 2005 study. Nijenhuis *et al.* explained that the decrease in calcium transporters initially observed in the 2003 study may have been a result of apoptosis of DCT cells provoked by high-dose thiazides treatment (64), an effect that has been reported previously (387). Furthermore, Lee *et al.* (388) reported that thiazide-induced changes in the distal calcium transport proteins of mice are dependent on blood volume. Thiazides caused hypocalciuria and volume contraction but had no significant effects on TRPV5 and calbindin-D28K mRNA expression. However, when a salt supplement was administered to these mice, volume contraction was eliminated and the gene expression of TRPV5 and calbindin-D28K increased (388). These studies indicate a link between sodium and calcium handling in the DCT, however the underlying mechanisms that govern the handling of these two electrolytes are complex and require further investigation.

1.10.2 Gitelman syndrome and hypocalciuria

The pathogenesis of hypomagnesaemia and hypocalciuria in patients with Gitelman syndrome remains unclear, but the resemblance between the calcium and magnesium disturbances in Gitelman patients and thiazide-treated patients suggests that they may adopt the same or similar mechanism. In thiazide treated animals there is enhanced passive calcium reabsorption by the proximal tubule, causing a decrease in calcium delivery to the DCT (64). However, reduced NaCl influx and the continuous efflux of intracellular chloride through basolateral channels, such as CLCNKB, may influence the electrochemical gradient required for apical calcium entry. Furthermore, in patients with Gitelman syndrome and in the NCC-S707X knock-in mouse model, which corresponds to the S710X mutation found in Gitelman patients, the expression of TRPV5 is increased (389).

In addition, the mRNA expression of TRPV6, ROMK, BK and ENaC were also increased in this mouse model, which suggests that the upregulation of these channels may contribute to the hypocalciuric and hypokalaemic phenotype observed in Gitelman patients (389).

1.10.3 FHHt and hypercalciuria

Both hypercalciuria and hyperkalaemia appear at an early age in FHHt patients, before the onset of hypertension; hypertension appears 3-4 decades later and the cause of delayed onset is still unclear. Hypercalciuria in FHHt patients is generally associated with the WNK4-Q565E mutation (60,390). Co-expression studies of TRPV5 and WNK4-Q565E in oocytes showed that the WNK4-Q565E stimulated TRPV5-mediated calcium uptake, however this effect was reduced by NCC when NCC was co-expressed (338). This suggests that FHHt-patients with the WNK4-Q565E mutation may suffer hypercalciuria as a result of a decrease in TRPV5-mediated calcium transport through SPAK-NCC activation.

Hypercalciuria has not been reported in the majority of other FHHt mutations, such as those in WNK1 (391), with the exception of the recently discovered KLHL3 mutations (392). FHHt patients with Q309R and R528H mutations in KLHL3 display a less severe calcium wasting phenotype than those with the WNK4-Q565E mutation (392). The pathophysiology of FHHt-induced hypercalciuria in patients with KLHL3 mutations is unknown, however since KLHL3 mutations cause FHHt by preventing WNK4 ubiquitination, it is possible this process is a result of WNK4 accumulation (392).

1.10.4 Essential hypertension, hypercalciuria and kidney stones

The association between hypertension and abnormalities in calcium handling is evident. It has been shown in several studies that hypertension is linked to an increase in urinary calcium excretion and a decrease in serum calcium concentration (393,394). As a high sodium diet is a major determinant in the development of hypertension, studies have also shown that dietary sodium determines urinary calcium excretion; an increase in dietary sodium in normotensive individuals causes excess urinary calcium excretion (395,396) and a decrease in dietary sodium significantly reduces calciuria (397), including calciuria induced by dietary potassium depletion (398). Studies of hypertensive

individuals also showed a reduction in the severity of hypercalciuria when dietary sodium intake is decreased (399–401). However, this effect is dependent on the individual's sensitivity to dietary intervention, such that salt-resistant hypertensive individuals have a less severe form of hypercalciuria in comparison to salt-sensitive individuals (402).

Hypercalciuria is the most common risk factor for kidney stone formation (30). The risk of developing kidney stones is two-fold higher in hypertensive individuals in comparison to normotensive individuals (403). The association between hypertension and kidney stone disease was first reported back in 1761 by Giovanni Battista Morgagni (404), but the pathogenesis and the order of onset remains a mystery. A prospective study of a large cohort that consumed the Dietary Approaches to Stop Hypertension (DASH) diet, a diet low in sodium, high in fruits and vegetables, low in animal protein and consist of low fat dairy products, also showed a lower rate of kidney stone disease progression, onset and recurrence (405), further supporting the linkage between dietary sodium, hypertension, hypercalciuria and kidney stone formation.

1.10.5 CNI-induced hypercalciuria

CNI-induced hypercalciuria has been suggested to be caused by a decrease in the apical entry of calcium in the DCT. Several studies showed that CNI decreased mRNA expression and protein abundance of TRPV5 and calbindin-D28K (51,57), thereby reducing calcium reabsorption. The association between hypertension, sodium and calcium handling is strongly supported by the studies discussed previously. Therefore, it is possible that CNI-induced hypercalciuria is associated with CNI-induced hypertension and the underlying mechanism of hypercalciuria may be more complex than previously demonstrated.

1.11 Aims of thesis

The resemblance between the handling of electrolytes in Gitelman patients and thiazide-treated patients, and between FHHT patients and CNI-treated patients, suggest that NCC plays an important role in renal tubular transport of non-sodium electrolytes. The underlying mechanism that governs the WNK-NCC cascade is currently unclear but it is evident that the WNK kinases contribute to the pathogenesis of these tubular disorders. The experiments described in chapter 2

and chapter 3 were designed to identify the most important member of the WNK kinases for NCC regulation under the influence of FK506, and to identify the underlying mechanisms that regulate the WNK-NCC cascade downstream of calcineurin. Calcineurin has pleiotropic effects and CNIs cause electrolyte abnormalities through tubular dysfunction, therefore it was also the aim in chapter 3 to investigate other FK506-dysregulated transporters, such as those involved in calcium handling. Furthermore, it is evident from the literature that there is an unidentified correlation between sodium and calcium handling in the nephron, therefore experiments in the subsequent chapter were designed to investigate this in the DCT under the effects of FK506. The overall aim of this thesis was to advance the understanding of the underlying mechanisms that regulate sodium and calcium reabsorption in the DCT.

Chapter 2. Interaction of intermediary proteins in the calcineurin-WNK-NCC cascade

2.1 Introduction

CNI-induced hypertension is a significant clinical problem (180,181) that is caused by NCC overactivity (51). NCC is regulated by a complex cascade of WNK kinases. CNIs increase WNK3, WNK4, SPAK and phosphorylated NCC (51), which results in increased sodium chloride reabsorption thereby causing hypertension. Calcineurin and the WNK kinases are known to be upstream regulators of NCC but the signal transduction mechanisms upstream of the WNK kinases are unclear. Elucidation of the relationship between calcineurin, the WNK kinases and NCC may provide new drug targets for antihypertensives or therapies targeting salt losing disorders.

The WNK kinases control NCC activity through SPAK and OSR1. SPAK/OSR1 are phosphorylated by L-WNK1 and WNK4 (118–120), this increases SPAK/OSR1 activity, thereby increasing NCC activity (116,117). WNK3 and WNK4 have antagonistic effects on each other (207); WNK3 stimulates the trafficking of NCC to the apical membrane of DCT cells and this process is inhibited by WNK4. WNK1 affects NCC activity through WNK4. The two isoforms of WNK1, KS-WNK1 and L-WNK1 have opposing effects on WNK4-induced inhibition of NCC (214): L-WNK1 inhibits WNK4, which suppresses WNK4-induced lysosomal degradation of NCC, and KS-WNK1 exhibits a dominant-negative effect by interacting with L-WNK1, resulting in downregulation of NCC (215). The ratio of KS-WNK1 to L-WNK1 and WNK3 to WNK4 are tightly controlled by the ubiquitin ligases. L-WNK1 and WNK4 is subject to degradation through KLHL3 and CUL3; these are important determinants for the net effect of NCC. Using current knowledge of the calcineurin-WNK-NCC cascade and the stimulatory and inhibitory effects of WNK kinases, this study investigates the WNK-NCC cascade downstream of calcineurin.

2.1.1 Aims

- To use co-expression studies, under the influence of FK506, to determine the most important member of the WNK kinases for NCC regulation and to determine whether NCC activation requires all members of the WNK kinases.
- To use co-expression studies to determine the effect of different co-expression ratios of WNK kinases, KLHL3, CUL3 and SPAK in the regulation of NCC.

2.2 Materials and Methods

A single oocyte chemiluminescence assay was developed to detect NCC expression on the surface membrane of oocytes; an NCC construct with an extracellular human influenza hemagglutinin (HA)-epitope tag was created for sensitive and reliable detection of NCC in this assay. Utilising this approach, NCC expression was measured in co-expression studies of NCC2HA with the WNK kinases, CUL3, SPAK, and KLHL3 in FK506 pre-treated oocytes. WNK1, WNK3 and WNK4 DNA constructs were kindly gifted by Dr. J. Hadchouel and constructs of CUL3, SPAK and KLHL3 were cloned as described in Section 2.2.3.

2.2.1 The insertion of HA-epitopes in NCC

The topology of NCC from *Mus musculus* (NM_019415.2; Q543E4) was studied to determine a suitable introduction site for two HA-epitopes. The amino acid sequence of mouse NCC was submitted to Protter (406), an interactive protein visualization tool that predicts membrane topology and signal peptides through Phobius (407). Potential glycosylation sites were predicted with GlycoEP (408), an online software tool used for predicting glycosylation sites in eukaryotes. A pSDS vector (AY672108.1) containing the full-length mouse NCC (pSDS_mNCC) was a kind gift from Dr. K. O' Shaughnessy and was used as a template to generate the new NCC2HA construct (pSDS_mNCC2HA). According to the results generated by Protter and GlycoEP, HA-epitopes were inserted into the second extracellular loop of NCC, at Q245.

2.2.2 The insertion of HA-epitopes into CD8 and co-expression with NCC

The pSDS_mNCC construct was also used to create an NCC construct with the addition of a truncated single transmembrane domain glycoprotein, cluster of differentiation 8 (CD8) (NM_001145873.1; P01732), with three extracellular HA-epitopes introduced into CD8 at P21 (pSDS_mNCC_CD8HA). A pIRES-CD8 plasmid was used as a template to generate CD8HA. The stop codon of CD8HA was removed and thus fused with the N-terminus of NCC for co-expression.

2.2.3 Plasmid construct synthesis of CUL3, KLHL3 and SPAK

Constructs of pTLB_CUL3 (NM_016716.5), pTLB_KLHL3 (NM_001195075.1) and pTLB_SPAK (NM_016866.2) were created by amplifying mouse kidney cDNA. These cDNA templates were prepared by Dr. A. Zdebik.

2.2.4 Molecular cloning protocol

Amplification of DNA was performed using Phusion DNA Polymerase (New England Biolabs, USA), according to the manufacturer's protocol (Table 2.2-1). The primers used to amplify these DNA inserts introduced two restriction sites on both ends of the polymerase chain reaction (PCR) product; these restriction sites were compatible with the pTLB (409) vector. The PCR product was separated by gel electrophoresis, as explained in Section 2.2.4.1, and the DNA fragment, containing the insert, was excised and purified from the agarose gel. Insert DNA (1 µg) and vector DNA (1 µg) were digested separately with the same restriction enzyme. Vector DNA (50 ng) and insert DNA (30 ng) were combined and ligated with T4 DNA ligase (New England Biolabs, USA), according to the manufacturer's protocol. Primers used for cloning were purchased from Integrated DNA Technologies, Belgium. For details on the sequences of primers, refer to Table 2.2-2.

2.2.4.1 Gel electrophoresis and gel purification

A 1 % agarose gel containing 0.5 µg/ml ethidium bromide was made in tris-acetate-EDTA (TAE) buffer (Fisher Bioreagents, USA). Samples were loaded into the agarose gel with 0.04 % bromophenol blue, 0.04 % xylene cyanol and 5 % glycerol alongside the GeneRuler 1 kb Plus DNA ladder (Thermo Fisher Scientific, UK), for band size estimation. Agarose gels were imaged with a UV transilluminator (Peqlab, Netherlands). DNA fragments were excised from agarose gel under UV exposure and purified with an High Pure PCR Product Purification kit (Roche, UK) according to the manufacturer's protocol.

Table 2.2-1 PCR program and reagents

<u>PCR program</u>			
Initial denaturation		94 °C	2 minutes
30 cycles of	Denaturing	98 °C	20 seconds
	Annealing	55 °C	30 seconds
	Extension	72 °C	1 minute
Extension		72 °C	5 minutes
<u>PCR reagents</u>			
Template DNA	150 ng	10 µM Flanking Forward primer	1 µl
10 mM dNTPs	1 µl	10 µM Flanking Reverse Primer	1 µl
5 x Phusion HF buffer	10 µl	MilliQ Water	Up to 50 µl total volume
Phusion DNA Polymerase	0.5 µl		
1 µM Inner Forward primer *	1 µl		
1 µM Inner Reverse primer *	1 µl		
* Inner primers required for long recombinant inserts			

Table 2.2-2 Primers used in molecular cloning

Name	Function	Sequence
NCC	Forward flanking primer	TATTGTCGTTAGAACGCGGC
NCC	Reverse flanking primer	TCCCATGGTAGCTGTAGAAG
NCCexHA	Forward inner primer	ctaccAtatgacgtGccagattatgcgATCAAT GACATCCGCATCATC
NCCexHA	Reverse inner primer	cgcataatctggCacgtcataTgggtaGGGGTC TACGATGGGTGTG
CD8	Forward flanking primer	gtACCCGGGATGATAAGCTTGCCacaac c
CD8	Reverse flanking primer	gagctcgagTTAGACGTATCTCGCCGAA AG
CD8HA	Forward inner primer	gcgGTcTAGaGCAGCCAGTTCCGGGT GTCG
CD8HA	Reverse inner primer	GTGGTGGTGGTGGTGcgcataatctggCa cgcataagggtaCGGCCTGGCGGCGTGG
mKLHL3	Forward primer	CACTCGAGAtggcctactatatcatgatc
mKLHL3	Reverse primer	ggctagagtcacagggatttgaatcacagc
mCUL3	Forward primer	CGCTCGAGatgtcgaatctgagcaaaggc
mCUL3	Reverse primer	aatctagattatgctacatatgtgtatacttgc
mSPAK	Forward primer	gcctcgagATGGCGGAGCCGAGCG
mSPAK	Reverse primer	gctctagagTCAGCTCACACTCAACTG

2.2.4.2 Electroporation and Cloning

Preparation of electrocompetent *Escherichia coli* and the electroporation procedure were performed according to an established protocol (410). The experimental procedure in brief is as follows: electrocompetent cells were prepared in advance and snap frozen in liquid nitrogen. The ligation reactions that were prepared in advance were desalted by drop dialysis with 25 nm nitrocellulose membrane (Millipore, USA) at room temperature for 20 minutes. The ligation reaction was recovered and added to 30-40 μ l of thawed electrocompetent cells and electroporated by a Gene pulser (Bio-Rad) connected to a pulse controller (Bio-Rad) at 1.8 kV, 25 μ F, 200 ohm resistance. The cell suspension was recovered and resuspended in 120 μ l of Super Optimal Broth with catabolite repression, incubated at 37 °C for 1 h, and 100 μ l of bacterial culture was plated onto Lysogeny Broth (LB) agar plate containing 100 μ g/ml ampicillin and incubated at 37 °C overnight.

A number of colonies from the bacterial plates were picked and incubated in 5 ml LB medium containing 100 μ g/ml ampicillin for 16 h at 37 °C, 200 rpm. Plasmid DNA was purified from 3 ml of bacterial culture harbouring the plasmid of interest using a Nucleospin Plasmid kit (Macherey-Nagel, Camlab, UK), according to manufacturer's protocol. Concentrations of DNA were calculated from the absorbance at 280 nm measured using a NanoDrop-1000 spectrophotometer (Labtech International, UK).

2.2.4.3 Restriction digestion and sequencing

Different restriction enzymes were used to digest the DNA constructs depending on the restriction site it harbours. The standard protocol for restriction digestion involved 1 μ g of DNA and 10 U of restriction enzyme of choice along with its recommended buffer and incubated at its recommended temperature for 1 h. All restriction enzymes were purchased from New England Biolabs or Fermentas (Thermo Fisher Scientific, UK).

Restriction digestion analysis were performed on the purified DNA constructs and constructs that were successfully digested were selected for sequencing. DNA (0.5 μ g) from selected clones and 0.5 μ l of primer (10 μ M) were added to the sequencing reaction, prepared with 1 μ l of the BigDye Terminator v1.1 cycle

sequencing kit (Applied Biosystems), according to the manufacturer's protocol. The sequencing reaction was precipitated using sodium acetate and ethanol. Primers used for sequencing were purchased from Integrated DNA Technologies, Belgium. For details on the sequences of primers, refer to the Table 2.2-2.

2.2.4.4 cRNA synthesis for oocyte injections

DNA constructs (15 µg) were linearised by a chosen restriction enzyme under recommended conditions; successful linearisation was checked by gel electrophoresis. Products of linearisation were purified by High Pure PCR Product Purification kit (Roche, UK), from which cRNA was synthesised using an mMessage mMachine SP6 Transcription Kit (Ambion, Thermo Fisher Scientific, UK), according to manufacturer's protocol. The cRNA pellet was dissolved and diluted in water treated with diethylpyrocarbonate and the concentration was measured using a NanoDrop 1000 spectrophotometer (Thermo Fisher Scientific, UK). Integrity of cRNA was confirmed by gel electrophoresis on a 1 % agarose gel.

2.2.5 Animal Studies

The use of *Xenopus laevis* (African clawed frog) oocytes in these studies was approved and carried out under the UK Animals (Scientific Procedures) Act (ASPA), 1986, Amendment Regulations 2012. Protocols were approved by UCL (Royal Free Campus) Comparative biology Unit Animal Welfare and the ethical review body (AWERB) committee (PPL: 70/8064) (PIL: I3635E6BF).

X. laevis were euthanised under Schedule 1 of the ASPA act. Animals were deeply anaesthetised by immersion in 1 % MS-222 (Sigma-Aldrich, Germany) [pH 7-8, buffered with sodium bicarbonate]. Following successful anaesthesia, which was determined by the loss of righting and pain reflexes, the brain was concussed by striking the cranium, followed by decapitation. To ensure brain death, double-pithing of the frog was performed to destroy the brain and a major vessel was severed during oocyte harvesting.

2.2.5.1 Oocyte harvesting

Ovarian lobes extracted from the abdomen of *X. laevis* were washed in ND96 [96 mM NaCl, 2 mM KCL, 1.8 mM CaCl₂.2H₂O, 1 mM MgCl₂.6H₂O, 5 mM HEPES and 4.5 mM NaOH, pH 7.5] at 4 °C. The ovarian lobes were torn open and washed with ND96 until the solution was clear. Oocytes were defolliculated by incubation with 2 mg/ml collagenase type II (Fisher Scientific, UK) in ND96 for 1.5-2 h at room temperature. Oocytes at stage V-VI were selected and maintained at 17 °C in ND96 containing antibiotics [50 µg/ml penicillin, 50 µg/ml tetracycline and 0.1 mg/ml ampicillin]. cRNA (30 ng) was injected into oocytes by pipettes pulled using a DMZ-universal puller (Zeitz Augsburg, Germany). Oocytes were maintained in ND96 solution at 17 °C for three days.

2.2.5.2 Oocyte protein preparation

Oocytes were washed in cooled homogenisation buffer [1 X Tris-Buffered Saline (TBS), 300 mM sucrose and 5 mM EDTA, pH 7.5] containing protease (cOmplete tablets, Roche, Mannheim, Germany) and phosphatase inhibitors (PhosSTOP tablets, Roche, UK). Ten oocytes per treatment group were homogenised with homogenisation buffer (5 µl per oocyte) at 4 °C. The homogenate was centrifuged at 5000 g (3 x 2 minutes) at 4 °C. After each centrifugation, the interphase was collected, discarding the lipid layer and the debris pellet. Protein concentration was determined using a BCA protein assay kit (Pierce, Loughborough, UK), according to the manufacturer's protocol; absorbance was measured at 650 nm using a Multimode detector DTX 880 (Beckman Coulter, California, USA).

2.2.5.3 Western blot of oocyte proteins

Proteins were reduced by adding 10 mM dithiothreitol (DTT) and denatured at 65 °C for 10 minutes. Thirty micrograms of protein were separated by electrophoresis on a 7-10 % sodium dodecyl sulphate-polyacrylamide electrophoresis (SDS-PAGE) gel. Proteins were transferred onto polyvinylidene difluoride (PVDF) membrane (Bio-rad) with a Trans-Blot SD Semi-Dry Transfer cell (Bio-rad). PVDF membrane was blocked with 5 % skimmed milk (Marvel, UK) in TBS with 0.05 % NP-40 (Thermo Fisher Scientific, UK). Membranes were probed against NCC (1:500; MRC-PPU, Dundee) and HA (3F10) (1:1000; Roche, Mannheim, Germany). All antibodies were diluted in the blocking buffer and

incubated overnight at 4 °C. Prior to and post-secondary antibody incubations, membranes were washed in TBS for 15 minutes at room temperature. Secondary antibodies were also diluted in blocking buffer at 1:1000 and incubated for 1 h at room temperature. Equal volumes of ECL-luminol [0.25 mM 3-Aminophthalic acid hydrazide, 0.04 mM p-Coumaric acid, 100 mM Tris and 200 mM NaCl; pH adjusted to pH 8.5] and ECL-H₂O₂ [0.04 % H₂O₂] were mixed prior to imaging and densitometry was performed using the Fluor-S™ Multimager (Bio-rad).

2.2.6 Single oocyte chemiluminescence

Oocytes injected with cRNA were maintained in ND96 containing antibiotics, at 17 °C for three days to allow for protein expression. Oocytes were then removed from ND96 and blocked with 1 % bovine serum albumin (BSA) in ND96 for 30 minutes on ice. Oocytes were incubated in anti-HA antibody (3F10) (1:500; Roche, Mannheim, Germany) in blocking agent for 1 h. Oocytes were washed four times with blocking agent for 15 minutes, which was followed by secondary antibody incubation (1:400) in blocking agent for 30 minutes on ice. Finally, oocytes were washed six times in blocking agent for 5 minutes, followed by two washes with ND96 for 15 minutes on ice. Fifty microlitres of Glo substrate reagent (R and D systems, UK) were added to the oocytes immediately before measurement. Single oocyte chemiluminescence was measured using a luminometer TD-20/20 (Turner Designs, UK). This protocol was adapted from Zerangue *et al.* (411).

2.2.7 Statistical analysis

Statistical analysis was performed by one-way ANOVA followed by a Bonferroni's multiple comparison post hoc tests. The data are presented as means ± SEM.

2.3 Results

2.3.1 Topology of NCC

NCC expression on oocyte surface membrane was quantified by the single-oocyte chemiluminescence assay. To quantify NCC, extracellular HA-epitopes were inserted into the NCC construct and an anti-HA antibody was used to detect the exposed epitopes. In order to identify a suitable insertion site for the HA-tag, topology of NCC was studied to avoid regions that are required for normal function and to limit the chances of disrupting the native structure. Twelve TM domains of NCC were identified with five intracellular and six extracellular loops. The N- and C-terminus of NCC were predicted as intracellular regions and predicted glycosylation sites are shown in Table 2.3-1. The posterior probability plot of NCC (Figure 6.1-1) and the statistical score for the potential glycosylated residues (Table 6.1-1) are detailed in the appendix.

Extracellular loops -1, -5 and -6 consist of four to ten amino acids. Due to their relatively short amino acid sequences, inserting HA-epitopes into these loops may alter NCC structure, and therefore they were unsuitable candidates for the introduction of the HA-tag. Extracellular loop-4 is the largest extracellular structure and has four predicted glycosylation sites; the number of glycosylation sites it harbours implies important functional and structural roles, also making it an unsuitable candidate. Extracellular loop-3 does not harbour any predicted glycosylation site but it is situated next to the largest extracellular loop; therefore, loop-3 was considered unsuitable due to the possibility of larger extracellular structures, such as loop-4, shielding the HA-epitopes from antibody detection. The results of these topology and glycosylation site predictions suggest that extracellular loop-2 is the ideal candidate for inserting HA-epitopes. Even though a glycosylation site was predicted in loop-2 at T239, loop-2 was not shown to have any functional role in NCC (121). Moreover, loop-2 is further away from loop-4 in comparison to loop-3 therefore lowering the probability of larger extracellular structures shielding the HA-tags. Two HA-epitopes were inserted at Q245, in the middle of extracellular loop-2 (A237-I255), where an anti-HA antibody can detect the antigen presented on the surface of oocyte membrane in the oocyte chemiluminescence assay (Figure 2.3-1).

Table 2.3-1 Glycosylation sites in transmembrane, intracellular and extracellular regions of NCC

Type of domains	Amino acid	Glycosylation sites
N-terminus (intracellular)	1-134	T7, T23, S37, S38, T44, T48, T120, T122
TM domain-1	135-154	-
Extracellular loop-1	155-165	-
TM domain-2	166-191	S191
Intracellular loop-1	192-211	T192
TM domain-3	212-236	-
Extracellular loop-2	237-255	T239
TM domain-4	256-275	-
Intracellular loop-2	276-283	-
TM domain-5	284-305	-
Extracellular loop-3	306-336	-
TM domain-6	337-359	T350
Intracellular loop-3	360-370	-
TM domain-7	371-390	T373, T380, T381, T390
Extracellular loop-4	391-448	S400, T406, T408, T426
TM domain-8	449-471	T456, S466
Intracellular loop-4	472-502	-
TM domain-9	503-522	-
Extracellular loop-5	523-527	T525
TM domain-10	528-549	-
Intracellular loop-5	550-560	T551
TM domain-11	561-577	-
Extracellular loop-6	578-582	-
TM domain-12	583-602	-
C-terminus (intracellular)	603-1001	S781, T786, T801, T921

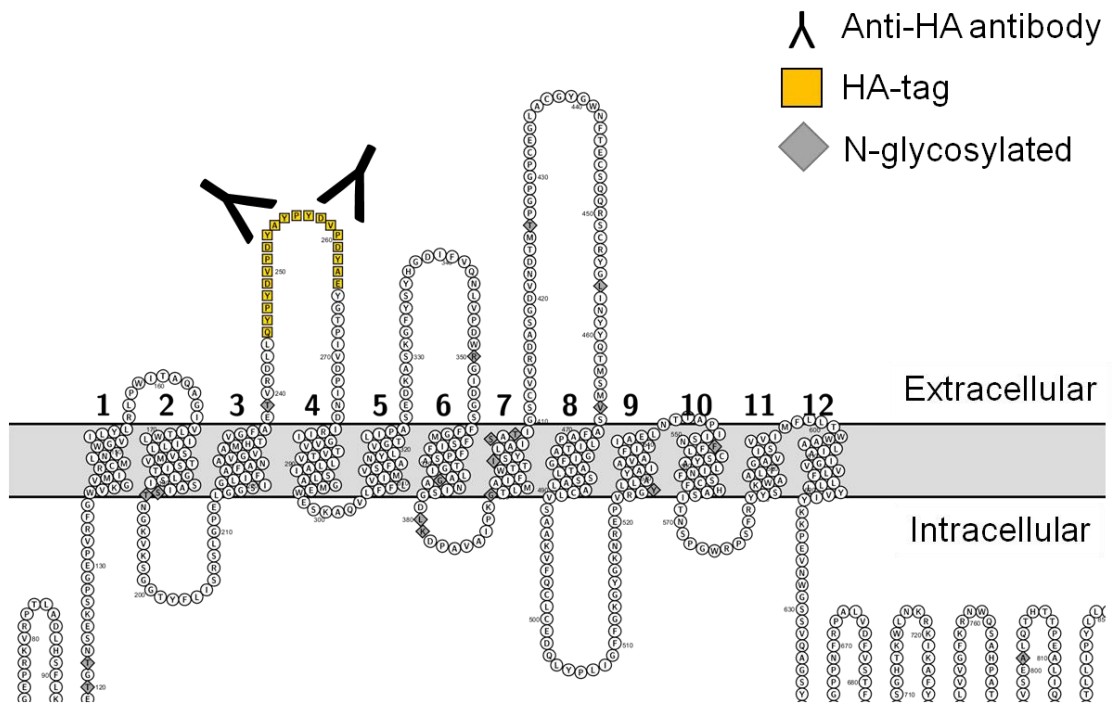


Figure 2.3-1 Schematic representation pSDS_mNCC2HA

Schematic diagram of NCC membrane topology, predicted by Phobius (407). Twelve TM domains of NCC were identified with intracellular N- and C-terminus, and five intracellular and six extracellular loops. Two HA-tags (yellow) were inserted into the second extracellular loop, where HA-epitopes are exposed to antibody detection in an oocyte chemiluminescence assay.

2.3.2 HA-tagged NCC construct synthesis

The insertion of the HA-epitopes into NCC required a two-part PCR reaction: a) the creation of two partial inserts containing the HA-epitope sequence (Figure 2.3-2a) and b) combining the partial inserts together to create the full length NCC2HA (Figure 2.3-2b); the two-part PCR reaction was successful, indicated by correct sizes of the PCR products. NCC was excised from the pSDS vector by digestion with restriction enzymes (Figure 2.3-2c) and replaced using a ligation reaction that inserted the full-length NCC2HA insert. The pSDS_mNCC2HA construct was electroporated into competent cells and selected clones were successfully digested in a restriction digestion reaction indicated by the presence of double bands (Figure 2.3-3); sequencing of the plasmid revealed correct DNA sequence.

Proteins from NCC, NCC2HA and HA-tag-injected oocytes were extracted for Western blot analysis to verify expression of the HA-epitopes. Western blot analysis revealed NCC expression in both NCC and NCC2HA-injected oocytes which was absent in the HA-tag control (Figure 2.3-4). HA-glycoprotein expression was detected in both HA-tag control and NCC2HA-injected oocytes and was absent in the NCC-injected group, indicating successful insertion and expression of HA-tag (Figure 2.3-4).

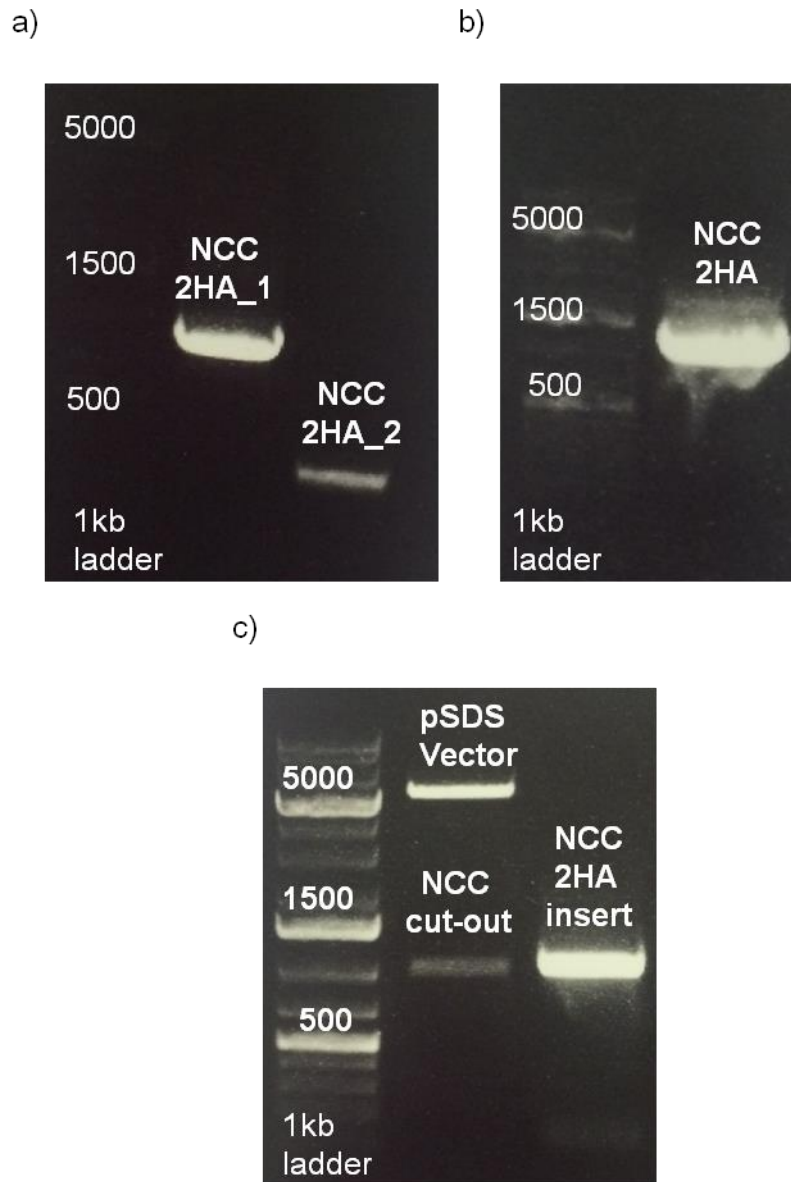


Figure 2.3-2 NCC2HA DNA construct synthesis

Agarose gel images of the two-part PCR reaction. a) The partial inserts, NCC2HA_1 (877 bp) and NCC2HA_2 (228 bp), were created using pSDS_mNCC as the template. b) The full length NCC2HA insert (1105 bp) was created from the partial inserts. c) NCC (1050 bp) was cut out of pSDS_mNCC (6111 bp) using restriction enzymes, and the same enzymes were used to produce compatible sticky ends for the ligation of NCC2HA (1105 bp) and pSDS vector.

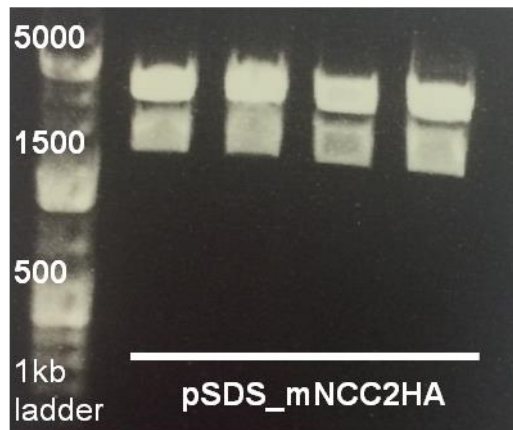


Figure 2.3-3 Restriction digestion analysis of pSDS_mNCC2HA

Plasmid DNA extracted from *E. coli* cells harbouring pSDS_mNCC2HA were digested with restriction enzymes for restriction digestion analysis. Analysis by agarose gel showed four successful pSDS_mNCC2HA clones indicated by the presence of the double bands at approximately 3876 bp and 2262 bp.

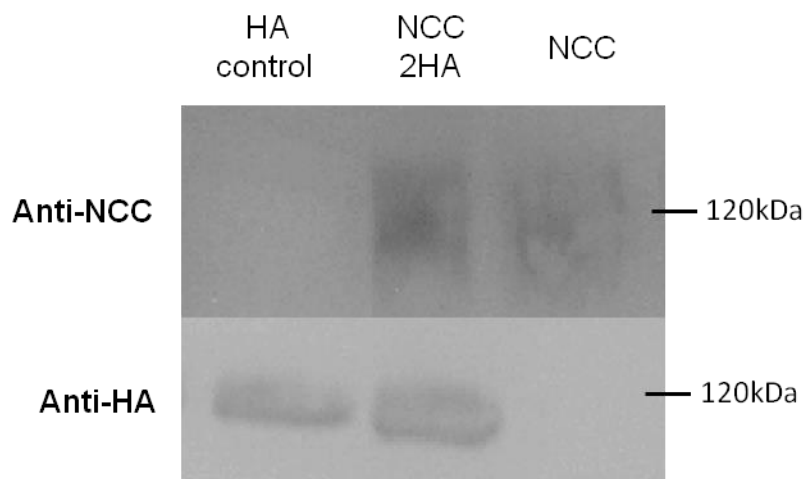


Figure 2.3-4 Western blot analysis of NCC2HA protein expression in oocytes

Western blot analysis of oocytes injected with 30 ng of HA-tag (positive control), NCC2HA and NCC cRNA. Expression of NCC was detected in NCC-injected oocytes and NCC2HA-injected oocytes. The expression of HA-glycoprotein was only detected in oocytes injected with the HA-tag positive control and NCC2HA.

2.3.3 Single oocyte chemiluminescence assay

After successful construction of NCC2HA, oocytes were injected with HA-tag positive control, NCC2HA, and uninjected, water-injected and NCC-injected negative controls to verify extracellular exposure of HA-epitopes on oocyte surface membrane. The HA-tag positive control emitted significant levels of chemiluminescence in comparison to all other groups (n= 33, $p < 0.0001$). However, NCC2HA showed no significant difference from water, NCC and uninjected-oocytes (Figure 2.3-5); this indicates that HA-epitopes in NCC2HA were not detected on surface membrane of oocytes.

Single-oocyte chemiluminescence assay

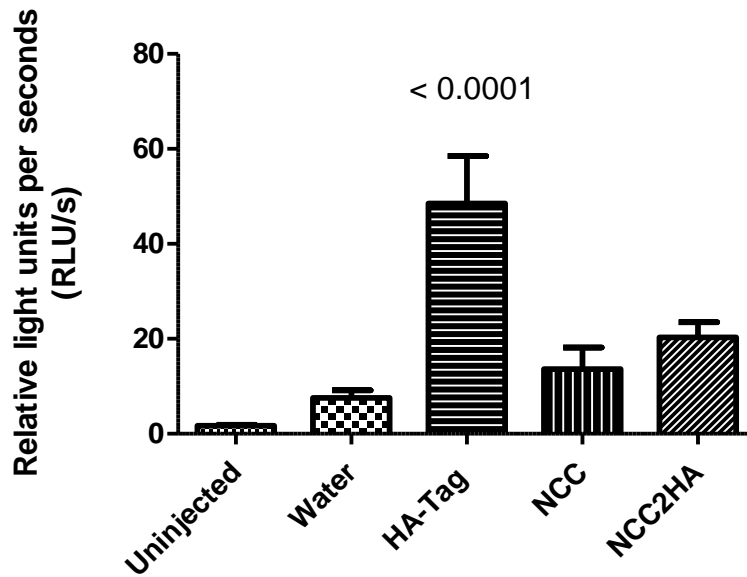


Figure 2.3-5 Single-oocyte chemiluminescence assay

Oocyte chemiluminescence assay was performed on uninjected oocytes, oocytes injected with water (30 nl) and oocytes injected with cRNA (30 ng) of HA-tag (positive control), NCC and NCC2HA. Oocytes were maintained in ND96 containing antibiotics, at 17 °C for three days, prior to the experiment. Chemiluminescence was measured using a luminometer and values are expressed in relative light units per seconds (RLU/s); data are presented as means \pm SEM, $n= 33$. Statistical values were calculated using an ANOVA followed by a Bonferroni's multiple comparison test.

2.3.4 Co-expression of NCC and HA-tagged CD8 glycoprotein

After unsuccessful construction of a working NCC construct with extracellular HA-tags at Q245, another insertion site, I251, was used but also failed to produce a working construct. Unsuccessful attempts in HA-tag insertion at extracellular loop-2 were followed by an alternative approach where a CD8 glycoprotein with three HA-epitopes attached was co-expressed with NCC. Information on the topology of CD8 (P01732) was obtained from the UniProt database (412) and three HA-epitopes were inserted at P21 between the signal peptide and the extracellular domain (Figure 2.3-6).

A two-part PCR reaction, similar to the approach used previously, was used to generate a full length CD8HA insert. The first PCR reaction generated two partial inserts required for full length CD8HA (Figure 2.3-7a) and the second part of the reaction combined the partial inserts to generate the full length CD8HA (Figure 2.3-7b); the two-part PCR reaction was successful, indicated by PCR products of approximately the correct size as analysed by agarose gel. The stop codon of CD8HA was removed and CD8HA fused with the N-terminus of NCC on pSDS_mNCC through restriction digestion and ligation. (Figure 2.3-7c). Products from the ligation reaction were electroporated into competent cells, however restriction digestion analysis of selected clones showed unsuccessful construction of pSDS_mNCC_CD8HA, indicated by the absence of double bands. This suggests failed restriction digestion and possibly the absence of restriction sites on the plasmid (Figure 2.3-7d).

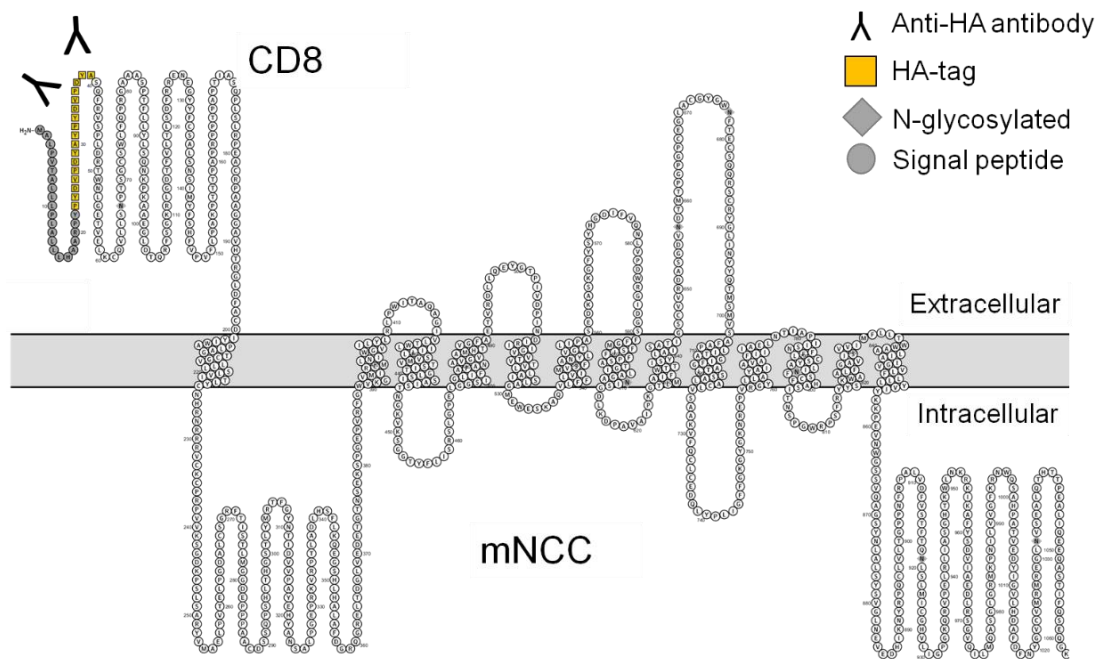


Figure 2.3-6 Schematic representation of pSDS_mNCC_CD8HA

Schematic diagram of pSDS_mNCC_CD8HA membrane topology, predicted by Phobius(407). Twelve TM domains of NCC were identified with intracellular N- and C-terminus, and five intracellular and six extracellular loops. A signal peptide was identified and located at the N-terminus of CD8 and a TM domain was identified at the C-terminus. Three extracellular HA-epitopes (yellow) are inserted into the extracellular side of CD8, where the epitopes are exposed to antibody detection in an oocyte chemiluminescence assay.

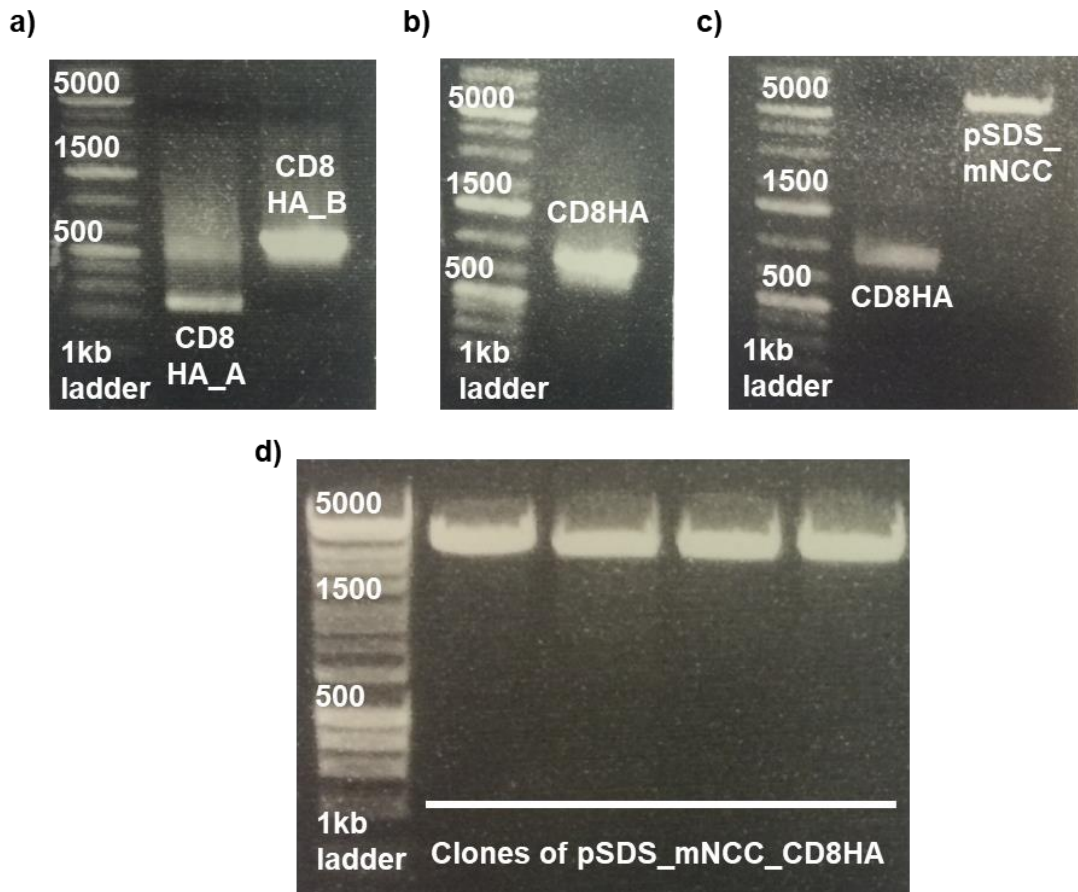


Figure 2.3-7 NCC_CD8HA DNA construct synthesis

Agarose gel images of pSDS_mNCC_CD8HA synthesis a) CD8 was used as a template to create two partial inserts: CD8HA_A (228 bp) and CD8HA_B (642 bp). b) The two partial inserts were combined together to generate a full length CD8HA (890 bp). c) pSDS_mNCC and CD8HA insert were digested with the same restriction enzymes to create sticky ends compatible for ligation. d) Plasmid DNA from colonies harbouring pSDS_mNCC_CD8HA were extracted and digested with restriction enzymes for analysis. Agarose gel image of the restriction digestion analysis shows a single band in all four clones, instead of double bands at 5245 bp and 1744 bp, which indicates uncut restriction sites and therefore unsuccessful construction of pSDS_mNCC_CD8HA.

2.3.5 Plasmid construct synthesis

KLHL3, CUL3 and SPAK, proteins also involved in the WNK-NCC cascade were cloned for co-expression studies with NCC. The amplification of KLHL3 from mouse kidney, lungs and testes cDNA were unsuccessful with no PCR product detected on agarose gel (data not shown). CUL3 was successfully amplified from mouse kidney cDNA (Figure 2.3.8a) and inserted into the pTLB vector; attempted restriction digestion of pTLB_CUL3 indicated unsuccessful insertion of CUL3 into the vector shown by the absence of double bands (Figure 2.3-8b).

SPAK was amplified successfully from mouse kidney cDNA (Figure 2.3-8c) and inserted into the pTLB vector. All clones of pTLB_SPAK presented two bands on an agarose gel when digested, indicating successful insertion of the SPAK gene (Figure 2.3-8d). The sequence of pTLB_SPAK was confirmed to be correct and in-frame by DNA sequencing.

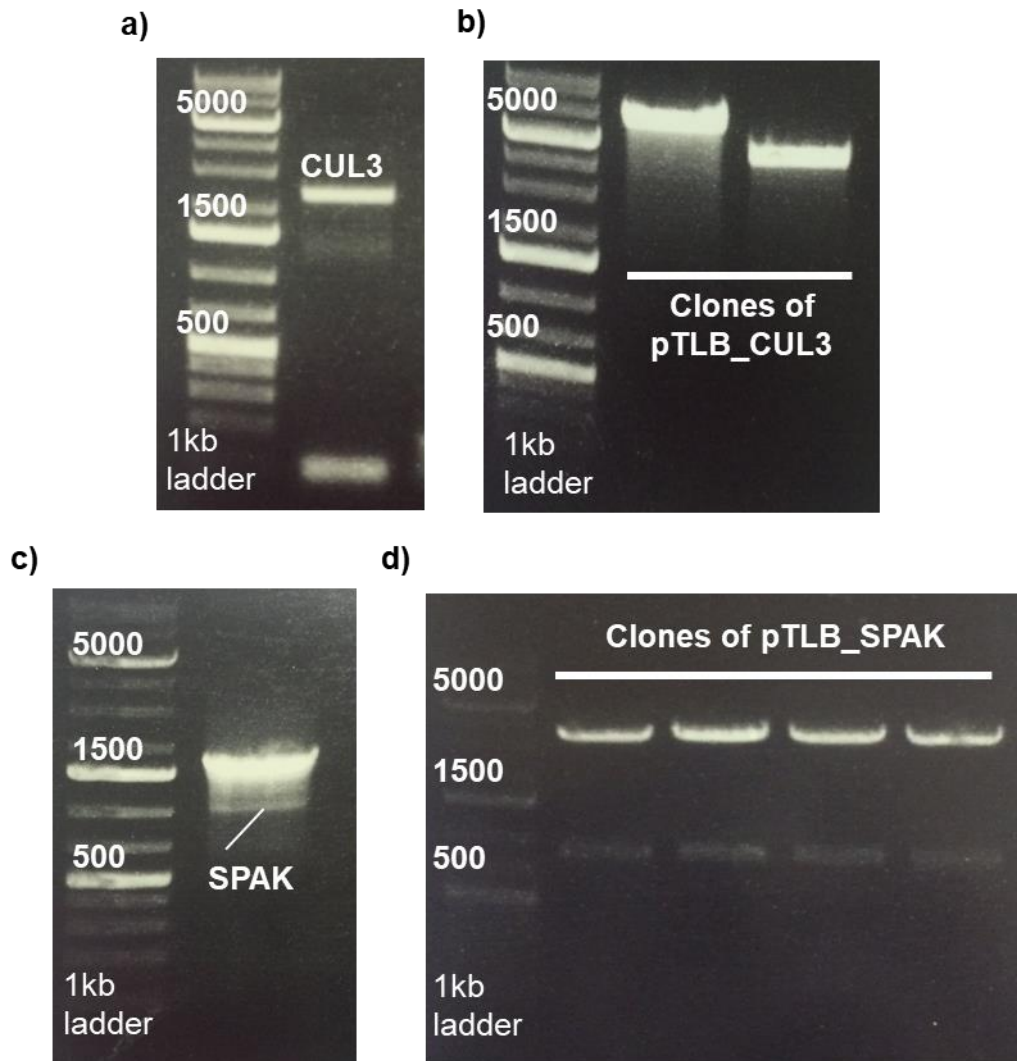


Figure 2.3-8 CUL3 and SPAK DNA construct synthesis

Agarose gel images of CUL3 and SPAK construct synthesis. a) CUL3 amplified from mouse kidney cDNA (2307 bp) and inserted into the pTLB vector. b) Restriction digestion analysis of pTLB_CUL3 (5573 bp) clones showed uncut restriction sites, indicated by the single bands shown on the gel image instead of double bands at 5185 bp and 382 bp. c) SPAK was amplified from mouse kidney cDNA (921 bp) and inserted into the pTLB vector. d) All four selected clones of pTLB_SPAK were digested with restriction enzymes and showed successful restriction digestion, indicated by correct sizes of double bands (3308 bp and 880 bp) shown on gel image.

2.4 Discussion

NCC expression is regulated by a sequential inhibitory cascade between various WNK kinases. To further elucidate the regulatory mechanism underlying the WNK-NCC cascade, different ratios of WNK kinases, CUL3, KLHL3 and SPAK were co-expressed with NCC to determine changes in NCC activity. For this study, a single-oocyte chemiluminescence assay was developed with the aim of measuring NCC expression on the surface membrane of oocytes, when expressed with WNK kinases, CUL3, KLHL3 and SPAK. Several studies have successfully expressed WNK kinases (207), CUL3 (259), KLHL3 (259), SPAK (413) and NCC (207) in oocytes, providing the capacity for investigating interactions between these proteins.

2.4.1 Oocyte chemiluminescence assay

The oocyte chemiluminescence assay was first developed in 1999 by Zerangue *et al.* (411). In the study, HA-epitopes were engineered into ATP-sensitive K⁺ channel subunits. These epitopes were recognised by an anti-HA-epitope tag antibody and chemiluminescence were then used to quantify the levels of K⁺ channels expressed on the cell surface of oocytes (411). Epitope tagging has been very well characterised and extensively used (414,415). Epitope tags such as, the HA-tag, can be genetically grafted into recombinant proteins and antibodies against these epitopes are highly specific, providing a dependable tool for protein detection in multiple quantitative techniques. Oocyte chemiluminescence assay quantifies membrane proteins that are expressed at low levels on the cell membrane by using enzyme amplification, and provides sensitivity and linearity that are comparable to other chemiluminescence technique. Since its development in 1999, this protocol has been used extensively in other studies (241,416,417).

Studies using NCC with HA-tags introduced into the extracellular loops has previously been used by Subramanya *et al.* (121). They inserted HA-epitopes into the putative second extracellular loop of NCC and expressed it on the membrane of human embryonic kidney 293 (HEK 293) cells. In this present study, two HA-epitopes were successfully inserted into the second extracellular loop of NCC, however, the oocyte chemiluminescence assay failed to detect significant

chemiluminescence from NCC2HA-injected oocytes. Since a significant level of chemiluminescence was detected from the HA-tag positive control, it is evident that the chemiluminescence assay in this experiment has been optimised. The expression of HA-glycoproteins in NCC2HA-injected oocytes was confirmed through Western blotting, therefore, the lack of chemiluminescence could be due to the fact that NCC2HA failed to express on the surface membrane of oocytes and were therefore not detected by the antibodies. To verify this, immunohistochemistry could be used to visualise the localisation of NCC2HA in oocytes (418,419). HA-epitopes were also introduced at I251 in another NCC2HA construct, the site used by Subramanya *et al.* (121), but this construct failed to express HA-epitopes.

The secondary structure of NCC is poorly understood and its crystal structure is not available in the current literature. A variety of topology prediction software packages are available for proteins with unknown structures; this is especially useful for proteins that have not yet been investigated by X-ray crystallography. Topology and glycosylation predictions are based on statistics of amino acid sequences and known topologies of membrane proteins, which means that accurate structural predictions of NCC are limited. Since chemiluminescence was not detected in the NCC2HA injected oocytes, it is possible that the HA-epitopes were inserted into a region that is not exposed extracellularly. In addition, it is also possible for other extracellular structures, such as the extracellular loop-3 and loop-4, to shield the HA-epitopes from antibody detection in oocytes. The unexposed HA-epitopes will not be detected by antibodies and therefore will not emit chemiluminescence.

Therefore, to minimise the risk of modifications interfering with normal NCC structure and function, a well characterised reporter protein (CD8) with extracellular HA-epitopes inserted, was fused with NCC. The use of reporter genes has been well documented since first introduced in 1980 (420); similar to the HA-tag, they are easily identified and measured. Several studies have used CD8 as a reporter protein and co-expressed it with other membrane proteins (421,422). In this study three extracellular HA-epitopes were inserted into CD8 and attached to the N-terminus of NCC; after multiple attempts in creating the NCC_CD8HA construct, it remained unsuccessful. One of the most common explanations for unsuccessful cloning is an incorrect DNA sequence of the

template. The DNA sequence of the pSDS_mNCC plasmid was verified prior to the initial cloning of NCC2HA; however, the CD8 DNA sequence was not verified prior to this experiment. It is possible that restriction sites present in the unverified CD8 DNA sequence were in fact, absent from the construct; without these restriction sites, sticky ends are not generated and NCC and CD8HA will not ligate. The DNA sequence of CD8 requires verification, and if the sequence is correct, perhaps a NCC construct with extracellular CD8 and the use of a CD8 antibody would solve the existing problems with HA-tag insertion.

2.4.2 Other members of the WNK-NCC cascade

In this study, SPAK was successfully cloned from mouse cDNA but CUL3 and KLHL3 were unsuccessful after multiple attempts. A potential reason for unsuccessful cloning of KLHL3 (1923 bp) and CUL3 (2307 bp) could be due to the fact that these are large genes. Sometimes long amplicons might be present in the PCR product but only at low levels, making it harder or impossible to visualise on an agarose gel, meaning it is mistaken for a failed amplification. It is possible to overcome this issue by performing a two-part PCR reaction to create partial inserts and using the partial inserts as templates for the full-length product; this is similar to the approach used for the cloning of NCC2HA in this study. Alternatively, the gene of interest might be present at low levels in the cDNA template, therefore preparing cDNA from tissues that are known to have higher expression levels of the gene of interest might aid the cloning process; in this instance using the cerebellum for CUL3 and KLHL3 amplification instead of the kidneys may have generated better results (177,423).

2.4.3 Future experiments

Once these technical issues are overcome, oocytes expressing NCC and the WNK kinases could be treated with FK506 and NCC expression can then be measured with the oocyte chemiluminescence assay. The single-oocyte chemiluminescence assay would have provided a reliable quantification method for assessing protein abundance on the plasma membrane and a tool for establishment of protein-protein interactions. One of the advantages of using an oocyte expression system is the ability to control RNA levels of different proteins injected into each oocyte; this can be used to study the effect of different protein

levels and its impact on the target protein, stoichiometry of subunits and protein complexes.

Whilst the oocyte chemiluminescence assay provides information on the membrane abundance of NCC, it does not measure the activity of NCC, therefore, oocyte chemiluminescence assay should be used in conjunction with other approaches to measure activity. Uptake studies using ^{22}Na and oocytes have previously shown successful assessment of NCC activity (121,192,214). In addition, Yang *et al.* (214) used ^{22}Na uptake assays to investigate the interaction between the WNK kinases and NCC, and showed that NCC activity was reduced by 85 % in oocytes co-expressing NCC and WNK4.

Experiments in this chapter aimed to investigate the interaction between NCC and members of the WNK cascade. However, given the technical issues encountered, a different approach was required. Phosphorylation seems to be the main determinant of protein activity in members in the WNK-NCC cascade, and CNIs are known to affect multiple phosphoproteins downstream of calcineurin. The interaction between calcineurin and the WNK kinases is poorly understood, therefore, quantitative phosphoproteomics (Chapter 3) was used to identify and measure protein phosphorylation dysregulated by CNIs and provide insights into WNK kinase regulations.

**Chapter 3. Exploring the effect of FK506 on the renal
kinome**

3.1 Introduction

Calcineurin is involved in numerous fundamental cellular pathways and plays an important role in several immune and developmental processes. Calcineurin is the target of CNIs, widely-used immunosuppressants for transplant recipients that cause many side effects. These side effects include post-transplant metabolic syndrome and electrolyte disorders caused by renal tubule dysfunction, such as hyperkalaemia, metabolic acidosis, hypercalciuria and hypomagnesaemia. The hypertensive phenotype of FK506 resembles FHHt, which is characterised by overactive NCC caused by mutations in the WNK kinases, WNK1 and WNK4, and KLHL3 and CUL3.

Phosphorylation is important in determining the activity of proteins in the calcineurin-WNK cascade, as shown through the effect of FK506 on NCC phosphorylation. WNK3 and WNK4 have opposing roles on NCC regulation and are both increased by FK506 (51). The increase in WNK4 contradicts its proposed role as an inhibitor of NCC, however WNK4 appears to have different roles under different cellular environments and its kinase activity is dependent on phosphorylation (244). Most protein phosphorylation is tightly controlled by kinase and phosphatase activity, therefore it is plausible that the activity of WNK4 is regulated and defined by an intermediary signalling pathway downstream of calcineurin. Since calcineurin is a protein phosphatase, it is likely that these intermediary proteins are inhibited and dephosphorylated by calcineurin under normal conditions. We hypothesised that CNI administration would alter the phosphorylation state of a number of proteins in the renal cortex of treated animals, importantly including the putative upstream regulators of the WNK kinase cascade. If we could identify proteins that had their phosphorylation state altered in this way, then we might be able to bring a number of analytical approaches to bear to identify likely candidates for this putative regulatory pathway.

For this study, quantitative phosphoproteomics was used to identify and measure changes in the phosphorylation of proteins in the renal cortices of mice treated with FK506. Quantitative proteomics (424) and phosphoproteomics (425–427) have been widely used in renal research for large-scale high-throughput studies

of proteins. Quantitative phosphoproteomics was first used in 2006 by Hoffert *et al.* (428), where a label-free immobilised metal affinity chromatography (IMAC) approach was used to quantify phosphopeptides in inner medullary collecting duct cells. Several label-free and label-based quantitative techniques are available and are commonly used. Label-free approaches offer a wider proteome coverage than label-based approaches (429). However, label-based approaches, such as Tandem Mass Tags (TMT), offers a greater accuracy of protein ratios and the ability to perform multiplexed analysis of multiple samples in a single experiment. This approach diminishes variations during sample preparation, chromatography and mass spectrometry (MS) acquisition (429). For these reasons, TMT was used for quantification in this study. Multiple phosphopeptide enrichment techniques are currently available, the most popular of which and typically used techniques are IMAC and metal oxide affinity chromatography (430), such as TiO₂. The two phosphopeptide enrichment strategies have comparable enrichment efficiency and number of phosphopeptides identified (431,432), however TiO₂ enrichment has been shown to be more selective than IMAC, and therefore was chosen for this study.

3.1.1 Aims

- To investigate and identify an intermediary pathway that regulates the WNK cascade and their effects on NCC regulation downstream of calcineurin.
- To generate a phosphoproteome profile of the renal cortices post-FK506 treatment, and to determine changes in the phosphorylation of other transport proteins altered by FK506.

3.2 Materials and methods

Calcineurin is a protein phosphatase and FK506 has been shown to alter the activity of serine/threonine kinases. Using quantitative phosphoproteomics, novel phosphoproteins involved in the regulation of WNK-NCC cascade were identified and the phosphorylation statuses of these proteins were measured in kidneys of FK506/vehicle-treated mice. The experimental procedure performed is illustrated in Figure 3.2-1.

3.2.1 Animals

Animal studies were carried under the UK ASPA Act, 1986, Amendment Regulations 2012. Protocols were approved by UCL (Royal Free Campus) Comparative biology Unit AWERB committee (PPL: 70/8064) (PIL: I3635E6BF). Male C57BL/6J mice of 6-8 weeks ($22.9 \text{ g} \pm 2.25$) were administered 2 mg/kg/day FK506 (LC laboratories, Boston, US) or vehicle by intraperitoneal (IP) injections for 14 days; FK506 was dissolved in vehicle solution containing 10 % ethanol, 10 % Tween-20 and 0.9 % saline. Mice were kept in metabolic cages over the treatment period and urine was collected every 24 h under mineral oil. They were fed on a standard rodent maintenance diet (Special Diet Services, UK), containing 0.25 % sodium and 0.38 % chloride.

Mice were terminally anaesthetised with 60 µg/g pentobarbitone sodium (Pentject, Animalcare Ltd, York, UK) via IP injection. Successful anaesthesia was determined by the loss of righting and pain reflexes. Two-to five hundred microlitres of blood was sampled by cardiac puncture and the mice were euthanized by cervical dislocation; death was confirmed by cessation of the heartbeat.

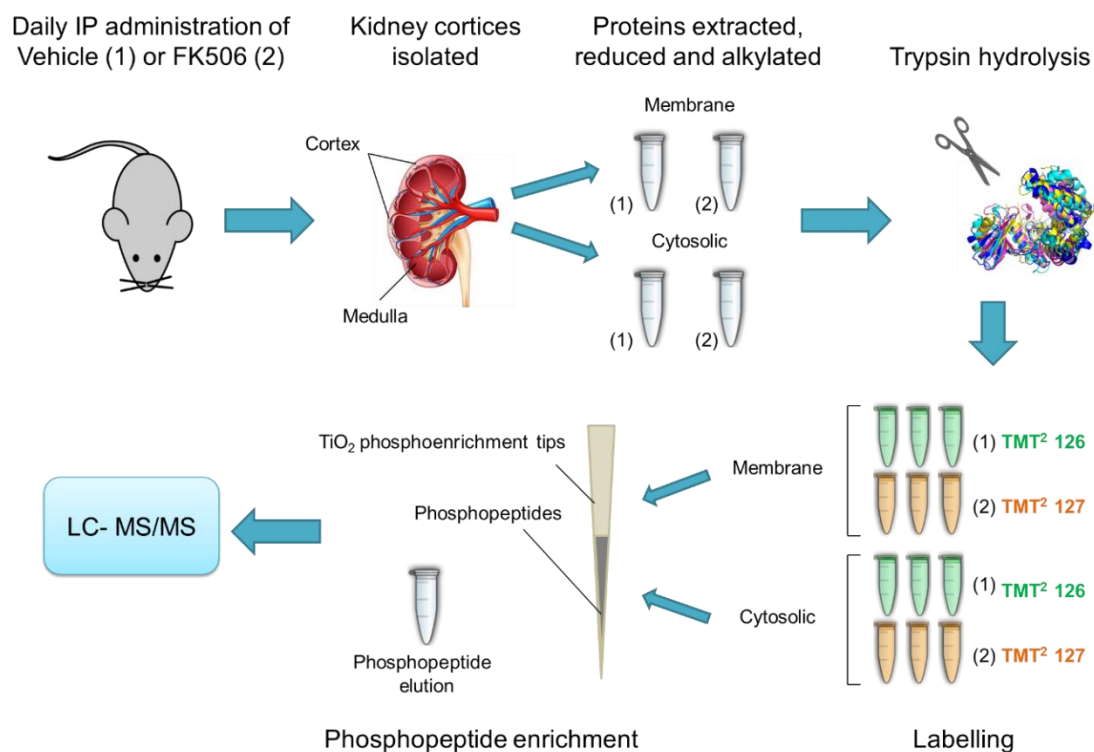


Figure 3.2-1 Schematic representation of the experimental procedure.

Mice were injected with vehicle or 2 mg/kg of FK506 daily for 14 days. Kidney cortices were isolated, homogenised and fractionated into samples containing the membrane or cytosolic fractions. Protein lysates were treated and digested into peptides by trypsin. Samples from vehicle or FK506 were chemically labelled with TMT² 126 or TMT² 127 reporter ions. TMT² 126 and TMT² 127 labelled samples were combined and phosphorylated peptides were enriched using titanium dioxide. Samples were injected into the liquid chromatography-mass spectrometry (LC-MS/MS) for quantitative phosphoproteomic analysis.

3.2.2 Electrolyte measurements in blood and urine

Immediately after blood collection, glucose concentration was measured with an Accu-Chek Aviva blood glucose meter (Roche, UK); the remaining sample was left at room temperature for 15 minutes to allow clotting. Urine and blood were centrifuged at 2,000 x g for 10 minutes at 4 °C. The resulting supernatant were collected and stored at -20 °C until use. Haemolysed serum samples were discarded. Urine and serum calcium, magnesium, bicarbonate, chloride, potassium, sodium and creatinine (using the Jaffe method) were measured using the RX Daytona plus clinical chemistry analyser (Randox, UK). Samples were processed by Department of Clinical Biochemistry (Royal Free London NHS Foundation Trust).

3.2.3 Kidney protein homogenisation

Mouse renal cortices or whole kidneys were dissected and homogenised on ice with an ultra-turrax (IKA, Staufen, Germany) in homogenisation buffer [1 x TBS, 300 mM sucrose, 5 mM EDTA, pH 7.5] containing protease (cOmplete tablets, Roche, Mannheim, Germany) and phosphatase inhibitors (PhosSTOP tablets, Roche, UK). A final concentration of 1 % Triton X-100 was added to the samples, which were then incubated at 4 °C for 10 minutes. Samples were centrifuged at 2,000 x g for 5 minutes at 4 °C to eliminate debris (pellet); the supernatant, also known as the post-nuclear supernatant (PNST), was centrifuged further at 150,000 x g for 45 minutes at 4 °C. This ultra-centrifugation step allows separation of the PNST into cytosolic (supernatant) and membrane (pellet) fraction. The membrane fraction was then ultra-sonicated on ice using an ultrasonic processor (Hielscher, Teltow, Germany) for 5 cycles at 100 % amplitude, with water containing protease and phosphatase inhibitors. Protein concentration was determined using a BCA protein assay kit (Pierce, Loughborough, UK), according to the manufacturer's protocol; absorbance was measured at 650 nm using a Multimode detector DTX 880 (Beckman Coulter, California, USA).

The purity of the enrichment was determined through Western blot analysis of a cytosolic protein, ERK1/2; details of which are in the Western blot protocol. The expression of ERK1/2 was most abundant in the cytosolic fraction and lower in the PNST and membrane fraction, indicating successful fractionation (Appendix, Figure 6.2-1).

3.2.4 Western blot analysis

Protein samples (30 µg) were separated on a 10 % SDS-PAGE gel. Proteins were transferred onto PVDF membrane (Bio-rad, UK) using a Trans-Blot Semi-Dry Transfer cell (Bio-rad, UK). Membranes were blocked with 5 % milk in phosphate-buffered saline (PBS) containing 0.1 % Tween-20 (PBS-T) for 1 h and probed with antibody against the following proteins: NCC (1-100) [1:500] and phospho-NCC (T60) [1:300] (both from MRC-PPU, Dundee, UK), phospho-NKCC2 directed at T96/T101 [1:500] (kind gift from C. Wagner), ERK1/2 (K23): sc94 [1:1000] (Santa Cruz Biotechnology, UK), phospho-ERK directed at T202/Y204 [1:500] and AKT (60203-2-Ig) [1:1000] (both from Proteintech, Manchester, UK), and phospho-AKT (S124) [1:500] and anti-β-actin (AC-15) [1:2000] (both from Abcam, Cambridge, UK). All antibodies were diluted in PBS-T and incubated overnight at 4 °C. Secondary antibodies were also diluted in PBS-T at 1:1000 and incubated for 1 h at room temperature. For details on densitometry, see Chapter 2, Section 2.2.5.3.

3.2.5 Statistics

Statistical analysis was performed by unpaired t-tests. The data are presented as means ± SEM.

3.2.6 Reduction, alkylation precipitation and tryptic digestion

Fractionated proteins (1.8-3 mg) from the renal cortices of vehicle or FK506-treated mice were reduced by adding 10 mM DTT in 0.1 M triethylammonium bicarbonate (TEAB) and incubated at 60 °C for 10 minutes. This was followed by alkylation with 25 mM iodoacetamide in 0.1 M TEAB for 30 minutes in the dark and the reaction was quenched with 25 mM DTT in 0.1 M TEAB.

Samples were precipitated overnight with 6 volumes of iced acetone at -20 °C, which were then centrifuged at 13,000 x g, at 4 °C for 15 minutes. The pellet was resuspended in 0.1 M TEAB containing 0.5 % sodium dodecyl sulphate (SDS). Protein loss after precipitation is very common; to account for this, 15 µg of protein before and after acetone precipitation was separated on a 10 % SDS-PAGE gel. The gel was silver stained with ProteoSilver™ Silver Stain kit (Sigma-Aldrich, Germany); the staining procedure was performed according to the

manufacturer's protocol. Silver staining showed minimum protein loss post-precipitation (Appendix, Figure 6.2-2).

The concentration of SDS in samples was diluted to 0.1 % prior to trypsin hydrolysis to avoid enzyme denaturation and inactivation. Proteins were cleaved by trypsin (Promega, Southampton, UK), 1 µg of trypsin was used per 100 µg of protein, overnight at 37 °C in 0.1 M TEAB.

3.2.7 TMT Labelling and Phosphopeptides enrichment

Samples were labelled using TMTduplex™ Isobaric Mass Tagging kit (Thermo Fisher Scientific, Loughborough, UK), 0.8 mg of TMT reagents were used per 400 µg of protein and labelling procedures were performed according to the manufacturer's protocol. Labelling efficiency of the samples was evaluated by LC-MS/MS to ensure that over 95 % of the peptides were labelled; refer to Figure 6.2-3 in the Appendix for the labelling efficiency. Moreover, to account for protein loss after precipitation and to ensure that the samples are mixed in equal proportions, an aliquot (1 µl) from each sample (TMT126 and TMT127) were mixed and injected into the LC-MS/MS. The total signal intensity for each of the reporter ions was calculated for sample normalisation before phosphopeptide enrichment (data not shown).

For phosphopeptide enrichment, samples were pooled together in a ratio of 1:1 after normalisation and phosphopeptides were then enriched using a Pierce™ TiO₂ Phosphopeptide Enrichment and Clean-up Kit (Thermo Fisher Scientific, Loughborough, UK), following the manufacturer's protocol. The unbound fractions (TiO₂ flow-through), containing unphosphorylated peptides, were desalted with Pierce™ C18 Spin Columns (Thermo Fisher Scientific, UK) and injected into the LC-MS/MS to obtain the ratio of TMT126/TMT127, which was then used to correct the reporter ion intensities in the datasets (data not shown). Fractions containing phosphopeptides specifically eluted from the TiO₂ columns were purified using the graphite columns provided and eluted thrice with 0.1 % formic acid in 50 % acetonitrile. All samples were dehydrated and resuspended in 0.1 % formic acid prior to LC-MS/MS analysis.

3.2.8 Mass Spectrometry

LC–MS/MS analysis was performed with an LTQ-Velos Orbitrap mass spectrometer (Thermo Fisher Scientific). Peptide samples were loaded using a nanoACQUITY UPLC (Waters, U.K.) with Symmetry C18 180 µm × 20 mm (Waters part number 186006527) trapping column for desalting and then introduced into the mass spectrometer via a Stonearch fused silica capillary column 100 µm i.d.; 360 µm o.d.; 15 cm length; 5 µm C18 particles (Nikkyo Technos CO, Tokyo, Japan part number NTCC 360/100-5-153) and a nanoelectrospray ion source at a flow rate of 0.42 µL/min. The mobile phase comprised H₂O with 0.1 % formic acid (buffer A) and 100 % acetonitrile with 0.1 % formic acid (buffer B). The gradient ranged from 1 % to 50 % buffer B in 136 minutes and a step gradient to 85 % buffer B for 10 minutes with a flow of 0.42 µL/min, finally a return to the initial conditions of 1 % buffer B for 20 minutes.

The full scan precursor survey MS spectra (400–1600 m/z) were acquired in full profile with the Velos-Orbitrap analyser with a resolution of $r = 60,000$. This was followed by data dependent MS/MS fragmentation in centroid mode of the most intense ion from the survey scan electro spray voltage 1.5 kV; capillary temperature 200 °C; and isolation width 2.00.

Firstly, using collision induced dissociation in the linear ion trap: normalized collision energy 35 %; activation Q 0.25 and activation time 10ms and the second MS/MS event, the most intense ion from the survey scan was fragmented using higher energy collision dissociation (HCD) in the HCD collision cell: normalized collision energy 50 %; resolution 7500 and activation time 0.1 ms. The two MS/MS scan events was repeated for the top 10 peaks in the MS survey scan, the targeted ions were then dynamically excluded for 30 seconds. Singly charged ions were excluded from the MS/MS analysis and Xcalibur software version 2.1.0 SP1 build 1160 (Thermo Fisher Scientific, U.K.) was used for data acquisition. Mass spectrometry procedures were performed by M. Crawford.

3.2.9 Proteins and Peptides Identification, Quantification and Enrichment analysis

Proteome Discoverer 1.3 (Thermo Fisher Scientific, UK) was used to analyse the datasets. Raw Data was searched against the UniProt *Mus musculus* database

(version 2015_10) alongside the Mascot search engine. Two trypsin missed cleavages were allowed; carbamidomethylation and TMT labels were set as static modifications whereas serine, threonine, tyrosine phosphorylation and methionine oxidation were set as dynamic modifications. Mass tolerance was set to 10 ppm for precursor ions and to 0.8 Da for fragments. False discovery rate at the peptide level was set to 0.05 and phosphosites localisation was verified through the PhosphoRS package embedded in Proteome Discoverer.

All phosphopeptide spectra were manually validated to confirm phosphosite localisations. For peptide quantification, TMT intensities were extracted from HCD scans, and corrected for isotope impurities accordingly to percentages provided by the manufacturer. Quantitative information obtained from the MS analysis of the TiO₂ flow-through samples (Appendix, Figure 6.2-3) were used to normalise the reporter ion intensities, in the case of loading imbalances.

Quantified peptides containing phosphorylation modifications with unique identifications were manually validated before being processed. In detail, quantified phosphopeptides obtained from the three replicates were grouped into unique phosphopeptide groups according to their sequences, pRS site probabilities (probability for each putatively phosphorylated site) and MH⁺ [Da] value. The average ratio, standard deviation and coefficient of variation of each unique phosphopeptide were calculated. All of the unique phosphopeptides were summarised and information on their gene name, protein name, keywords, gene ontology (biological process, molecular function, cellular component and IDs), KEGG and Reactome were obtained from UniProt Knowledgebase (412) and matched to the protein accession number of each phosphopeptide.

Phosphopeptides with >10 % change (increase or decrease) in phosphorylation were considered as FK506-dysregulated phosphopeptides. The proteins assigned to these phosphopeptides were submitted into STRING (433), a known and predicted protein-protein interactions database, and a protein interaction network was generated. These protein interaction networks were analysed through Cytoscape (434), a software platform for visualising and integrating complex interaction networks and pathways, and protein clusters were identified using the ClusterONE plugin (435), a graph clustering algorithm that identifies protein complexes in a protein-protein interaction network. Phosphorylation

motifs of the phosphopeptides were predicted with Motif-X (436,437), a software tool used for classifying phosphorylation sites with regards to overrepresented amino acid patterns in the dataset, and phosphorylation motifs with serine, threonine or tyrosine as the central residue was searched for. The sub-lists of proteins classified as 'transporters', 'channels', 'kinases', 'phosphatases' and other 'kinase/phosphatase' related phosphoproteins obtained from Panther (Protein Analysis Through Evolutionary Relationships) Classification system (438) were selected for further analysis. Verifications of phosphosites were retrieved from PhosphoSitePlus® Database (439). Sequence alignment of proteins was performed using the Clustal Omega (1.2.1) multiple sequence alignment tool (440).

3.3 Results

3.3.1 Validation of adverse effects caused by CNIs

FK506 treatment of mice was used to induce some of the known side effects of CNIs. To confirm the effectiveness of the treatment, electrolyte levels in urine and serum of mice treated with vehicle or FK506 were examined. FK506-treated mice demonstrated hypercalciuria and hypomagnesaemia (Table 3.3-1). These are well documented effects of FK506 (51,57), indicating that FK506 successfully induced dysregulation in electrolyte homeostasis in the mice used in this study.

Additionally, protein levels of NCC, activated pNCC and pNKCC2 were determined through Western blot analysis. Previous studies reported that FK506 increased pNCC levels and did not affect NCC and pNKCC2 during treatment (51). Western blot analysis revealed that FK506 significantly increased pNCC levels and confirmed that NCC and pNKCC2 levels remained unaltered (Figure 3.3-1). Blood pressure was not measured in these animals and therefore hypertension could not be confirmed.

Table 3.3-1 Serum and urine electrolytes in mice treated with vehicle or FK506

<u>Serum</u>		
	Vehicle	FK506
Ionised calcium (mmol/l) (n=5)	2.05 ± 0.136	2.31 ± 0.051
Magnesium (mmol/l) (n=5)	1.01 ± 0.068	0.80 ± 0.023 *
Bicarbonate (mmol/l) (n=6)	12.56 ± 0.756	13.90 ± 0.853
Glucose (mmol/l) (n=5)	10.42 ± 0.896	13.38 ± 1.630
Chloride (mmol/l) (n=6)	144 ± 9.462	131.20 ± 2.960
Potassium (mmol/l) (n=6)	4.80 ± 0.442	4.80 ± 0.251
Creatinine (µmol/l) (n=5)	43.74 ± 4.136	53.40 ± 11.950
<u>Urine</u>		
	Vehicle	FK506
Calcium (mmol/mmol) (n=5)	0.06 ± 0.012	0.10 ± 0.010 *
Volume (ml/day) (n=6)	0.70 - 1.20	0.50 - 1.30
Weight (g) (n=5)	22.74 ± 0.420	21.99 ± 0.264

Serum and urine electrolytes of FK506-treated mice. Mice administered 2 mg/kg/day FK506 for two weeks by daily IP injections. Statistical values were calculated using an unpaired t-test. Data are presented as means ± SEM. * P<0.05 vs. vehicle.

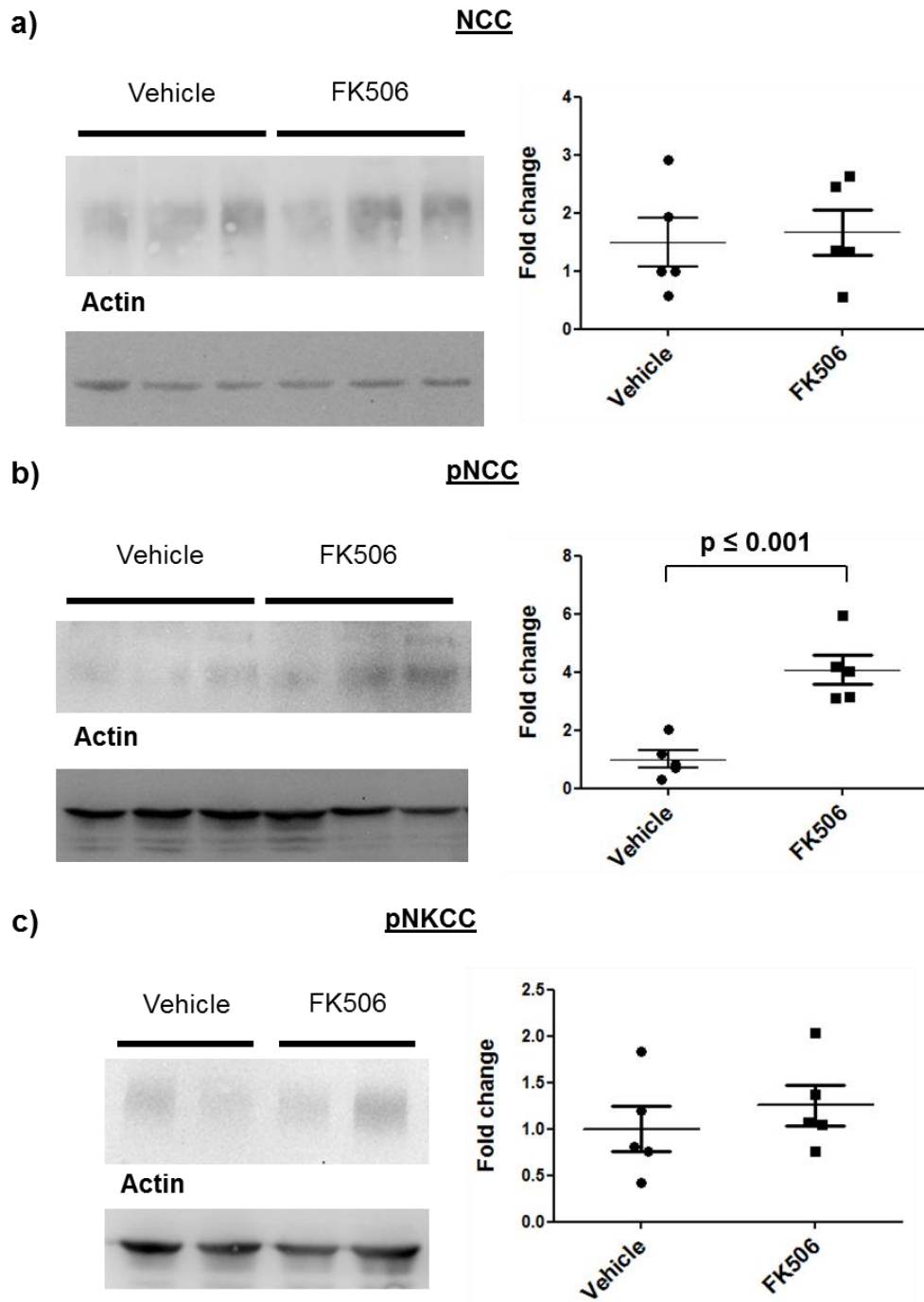


Figure 3.3-1 Protein expression of distal nephron transporters post-FK506 treatment

Western blot analysis was performed on kidney membranes of FK506 or vehicle treated mice. Representative blots of a) NCC, b) pNCC and c) pNKCC2 are shown. Band intensities of the transporters were quantified and normalised to those of β -actin and expressed as fold change of the control mean; data are presented as means \pm SEM, n=5. Statistical values were calculated using an unpaired t-test.

3.3.2 Overview of the proteomics dataset

Using quantitative phosphoproteomics, changes in the phosphorylation status of proteins in the renal cortices of FK506-treated mice were identified and quantified. Using Proteome Discoverer alongside Mascot, LC-MS/MS identified 18,971 peptides in the membrane triplicates and 5,395 in the cytosolic triplicates. Unphosphorylated, redundant and unquantified peptides without a unique identification were filtered out, resulting in a total of 3,962 phosphopeptides in the membrane fraction (Appendix, Table 6.3-1) and 1,376 in the cytosolic fraction (Appendix, Table 6.3-2).

The datasets were processed as described previously in the methods section, and as a result, 622 unique phosphopeptides were identified in the membrane fraction (Appendix, Table 6.3-3) and 415 were identified in the cytosolic fraction (Appendix, Table 6.3-4). The total number of unique phosphopeptides in the membrane fraction was 1.5-fold higher than the cytosolic fraction.

The number of unique phosphopeptides shared amongst the replicates for each fraction is shown in the Venn diagram (Figure 3.3-2). In the membrane, 64 % of unique phosphopeptides are present in two or more replicates and in the cytosol, 44 % are present in two or more replicates; these percentages represent the reproducibility of the experiment, which can vary depending on sample complexity. In each MS experiment, phosphopeptides with similar chemical properties elute from the LC column at the same time and MS detects the most abundant peptides at each time point; this reduces the chance of identifying a specific phosphopeptide that is present in every replicate, especially in a complex sample. Since the two fractions are products of a subcellular fractionation, the contents and the complexity are different. The lower percentage of unique phosphopeptides present in the replicates indicates that the cytosolic fraction is higher in complexity than the membrane fraction, therefore there is a higher chance of identifying different phosphopeptides in each replicate in the cytosolic fraction.

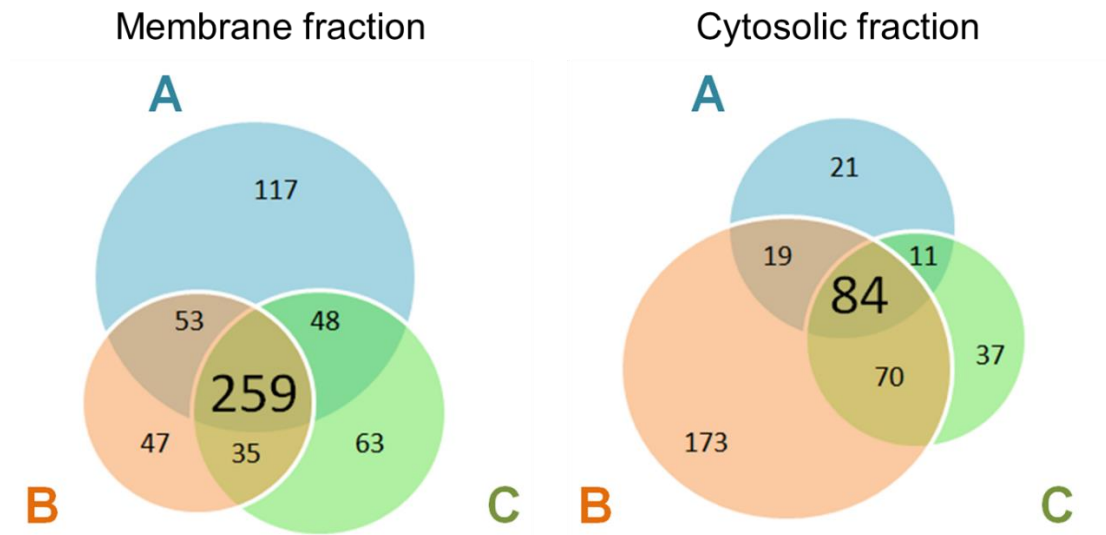


Figure 3.3-2 The number of unique phosphopeptides identified in the membrane and cytosolic fractions.

Venn diagrams showing the number of unique phosphopeptides identified in individual replicates of the membrane (left) and cytosolic fraction (right). A, B and C represents individual replicates and the number of unique phosphopeptides shared between the replicates are shown.

3.3.3 Data interpretation

Phosphopeptide ratios calculated from the reporter ion intensities (TMT127/TMT126) are presented as percentages in the data. The large proteomic datasets were analysed using several bioinformatics techniques: threshold criterion, network pathways, phosphorylation motifs and candidate approach. Using several different bioinformatic techniques to analyse large proteomic datasets is highly effective at excluding housekeeping proteins, however some proteins of interest, especially when the aim was to identify novel phosphoproteins, may be filtered out. Therefore, some proteins of interest selected from the main protein table (Appendix, Table 6.3-3 and Table 6.3-4) are also presented in Section 3.3.3.6.

3.3.3.1 FK506-dysregulated proteins

Phosphopeptides with more than a 10 % change in phosphorylation were considered up- or downregulated by FK506. FK506-dysregulated proteins were submitted into STRING (441) to search for known and predicted protein-protein interactions, and a protein interaction network for each cellular fraction was generated. The interactions between pairs of proteins were identified based on seven criteria: experimental data, curated database (such as the KEGG pathway databases) text mining in all PubMed abstracts, co-expression studies, phylogenetic distribution of orthologs of all proteins in *Mus musculus*, the presence of a hybrid gene in the respective protein and their consistency observed in the genome neighbourhood. A confidence score was calculated for each criterion and these scores were combined (combined score) to form the interaction (edge) shown in the network. These combined scores ranged from 0 to 1, the higher the combined score, the thicker the edges in the protein network, and therefore represents a higher confidence level in the established interaction. Each interaction, presented in the networks, has a combined score of over 0.4, meaning that the established interaction is true, specific and reproducible to a medium confidence level. The protein nodes in the network diagrams are colour coded, such as that FK506-upregulated proteins are coloured green and FK506-downregulated proteins are coloured yellow. Proteins without any established interactions (disconnected protein nodes) were hidden from the network and are not shown in the figures.

Using Cytoscape (434), two figures were generated from each protein interaction network. Figures 3.3-3 and Figure 3.3-5 contains information regarding protein clusters identified in the network dysregulated by FK506 in the membrane and cytosolic fractions respectively. The ClusterONE plugin (435) on Cytoscape was used to identify protein clusters present in the network. Clusters with a p-value of <0.05 were grouped according to their biological processes. In addition, Cytoscape also calculates the 'betweenness centrality' of the proteins in the networks. Betweenness centrality of an individual protein reflects its ability to exert its interactions over the interactions of other proteins in the network (442); these are directly correlated to the sizes of the protein nodes. Figures 3.3-4 and Figures 3.3-6 contain information regarding regulatory proteins associated with kinases and phosphatases dysregulated by FK506 in the membrane and cytosolic fractions respectively. These proteins were identified using the Panther Classification system (438); proteins associated with kinases are square shaped and proteins associated with phosphatases are diamond shaped.

In the membrane fraction, 260 and 151 unique phosphopeptides, represented by 225 proteins, were up- and downregulated by FK506 respectively. Of these proteins, 66 were disconnected from the network and 159 formed 465 interactions within the network. Six protein clusters involved in different biological processes were identified in the membrane protein network. These include 34 proteins involved in gene expression (blue), 13 proteins involved in ion transport (red), 6 proteins involved in endocytosis (orange), 6 proteins involved in chromatin organisation (purple), 6 proteins involved in cell division (pink) and 5 proteins involved in protein transport (cyan) (Figure 3.3-3). Six kinase-associated proteins (square) and two phosphatase-associated proteins (diamond) were identified in the network of FK506-dysregulated phosphoproteins in the membrane fraction (Figure 3.3-4). The connections and protein clusters identified in the membrane fraction are highly complex, and few phosphoproteins, such as heat shock protein HSP 90- β (HSP90AB1) and spectrin α -chain (SPNA2), appeared to act as hubs at the centre of the membrane protein network. HSP90AB1 is a chaperone protein involved in protein stabilisation and trafficking, and SPNA2 is a cytoskeletal protein involved in cell adhesion and cell cycle regulation. HSP90AB1 and SPNA2 are both ubiquitously expressed and are connected to

most of the protein clusters identified in the network, consistent with the pleiotropic effect of HSP90AB1 and SPNA2 in cellular processes.

In the cytosolic fraction, 90 and 154 unique phosphopeptides, represented by 138 proteins, were up- and downregulated by FK506 respectively. Of these proteins, 58 were disconnected from the network and 80 formed 123 interactions within the network. Three protein clusters involved in different biological processes were identified in the membrane protein network. These include 7 proteins involved in translation (blue), 6 proteins involved in ion transport (red) and 3 proteins involved in cell division (green) (Figure 3.3-5). Four kinase-associated proteins (square) were identified in the network of FK506-dysregulated phosphoproteins in the membrane fraction, but no phosphatase-associated proteins were found (Figure 3.3-6). In contrast to the membrane fraction, the connections and protein clusters identified in the cytosolic fraction are less complex. Similar to HSP90AB1, AKT1 also has pleiotropic effects in multiple cellular processes, including cell proliferation, survival and metabolism (443,444), thus AKT1 and HSP90AB1 appeared to act as the main hubs at the centre of the cytosolic protein network. In addition, AKT1 is connected to the clusters of proteins involved in sodium ion transport, suggesting that AKT1 may play a role in altered renal sodium transport downstream of calcineurin.

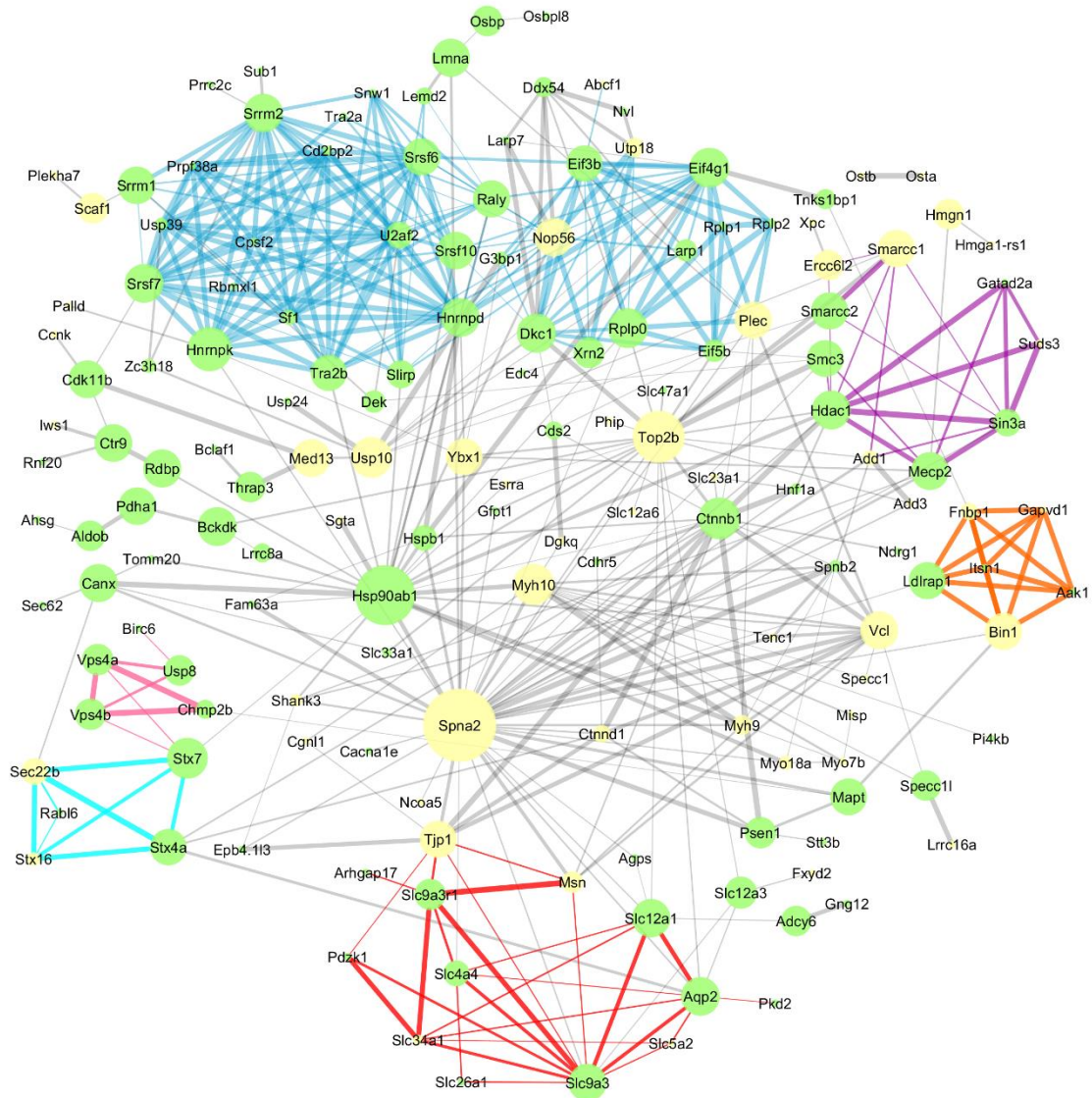


Figure 3.3-3 Protein clusters identified in the network of FK506-dysregulated proteins in the membrane fraction

In the membrane fraction, 465 interactions between 159 proteins were identified. Each interaction has a combined score of over 0.4; the edge weights are directly correlated to the score. FK506-upregulated protein nodes are coloured green and FK506-downregulated protein nodes are coloured yellow. The sizes of the protein nodes directly correlate to the betweenness centrality of the protein in the network. ClusterONE was used to identify protein clusters ($p < 0.05$) and proteins from these clusters were grouped into different biological processes: gene expression (blue), ion transport (red), endocytosis (orange), chromatin organisation (purple), cell division (pink) and protein transport (cyan).

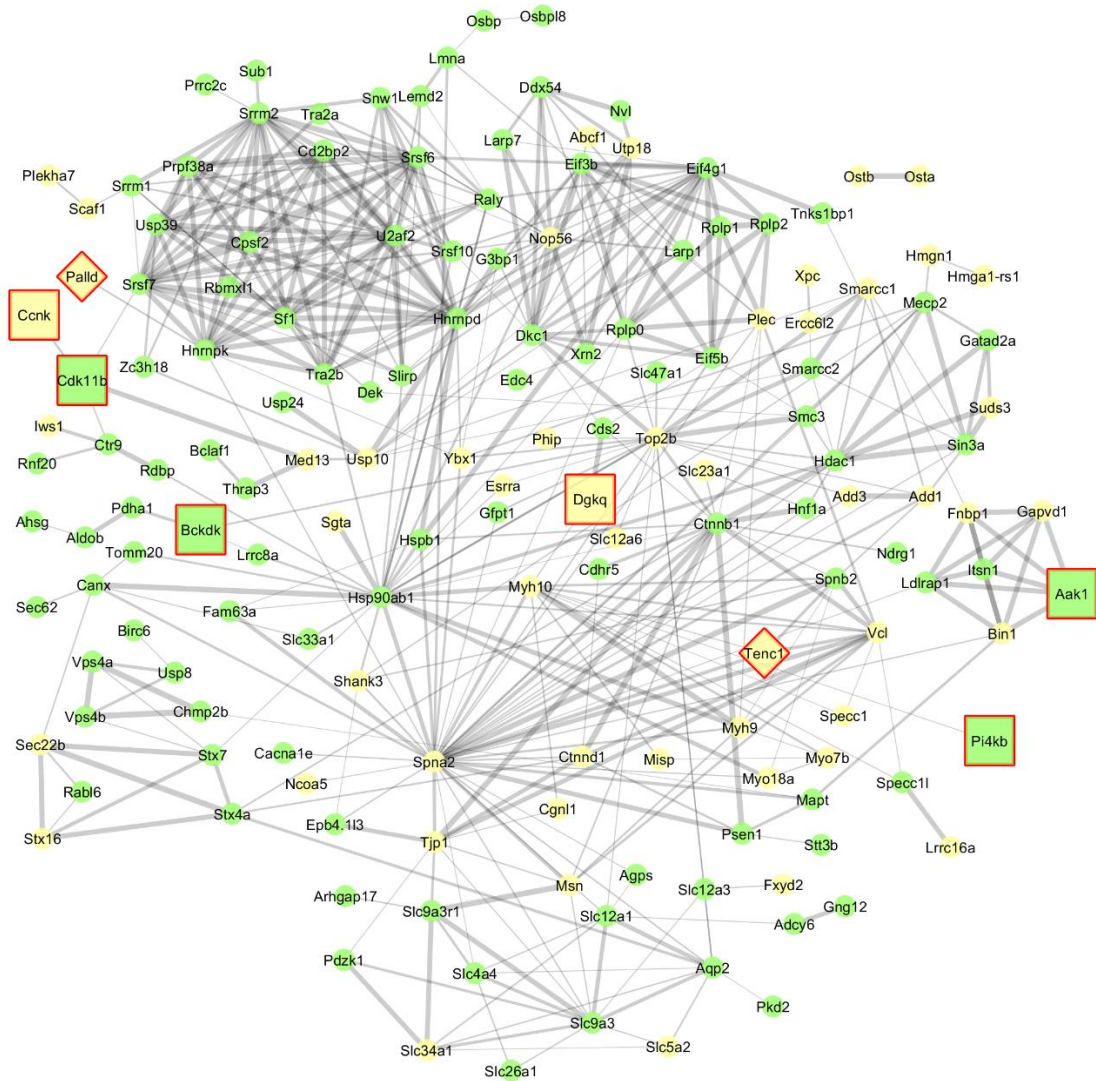


Figure 3.3-4 Regulatory proteins associated with kinase/phosphatase identified in the network of FK506-dysregulated proteins in the membrane fraction

In the membrane fraction, 465 interactions between 159 proteins were identified. Each interaction has a combined score of over 0.4; the edge weights are directly correlated to the score. FK506-upregulated protein nodes are coloured green and FK506-downregulated protein nodes are coloured yellow. Regulatory proteins associated with kinases are square shaped and those associated with phosphatases are diamond shaped.

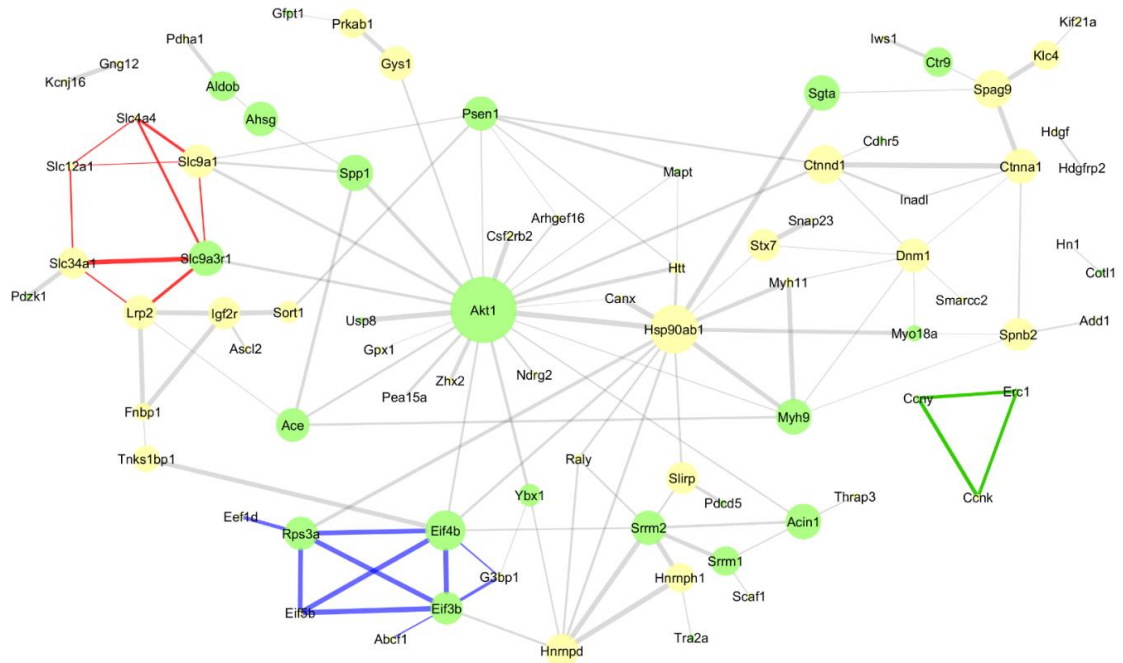


Figure 3.3-5 Protein clusters identified in the network of FK506-dysregulated proteins in the cytosolic fraction

In the cytosolic fraction, 123 interactions between 80 proteins were identified. Each interaction has a combined score of over 0.4; the edge weights are directly correlated to the score. FK506-upregulated protein nodes are coloured green and FK506-downregulated protein nodes are coloured yellow. The sizes of the protein nodes directly correlate to the betweenness centrality of the protein in the network. ClusterONE was used to identify protein clusters ($p < 0.05$) and proteins from these clusters were grouped into different biological processes: translation (blue), sodium ion transport (red) and cell division (green).

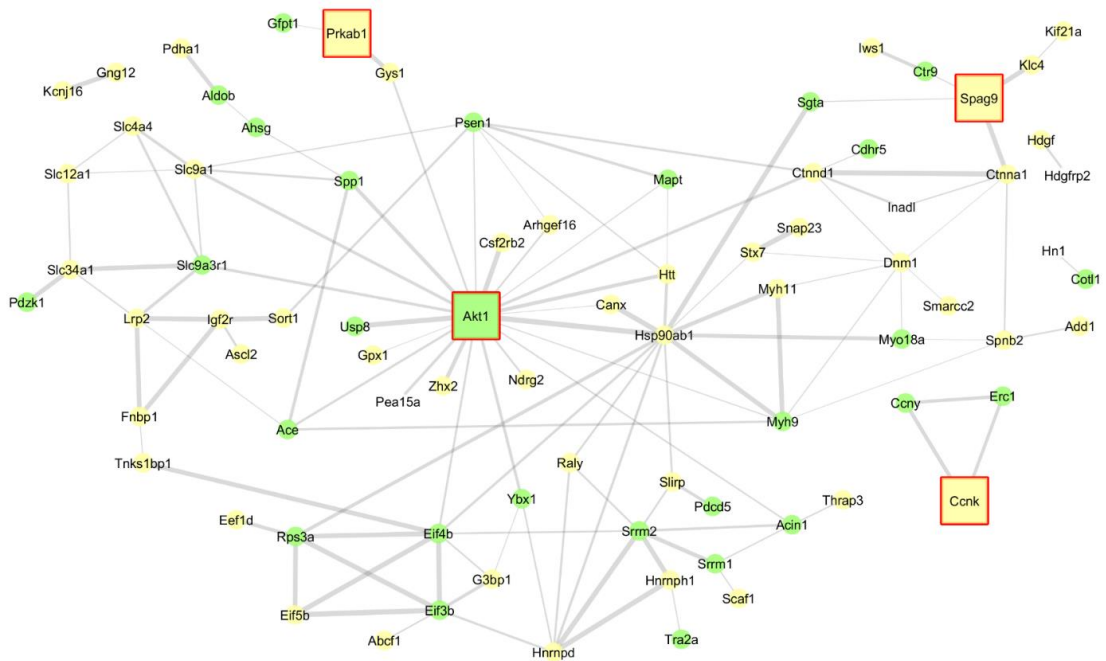


Figure 3.3-6 Regulatory proteins associated with kinase/phosphatase identified in the network of FK506-dysregulated proteins in the cytosolic fraction

In the cytosolic fraction, 123 interactions between 80 proteins were identified. Each interaction has a combined score of over 0.4; the edge weights are directly correlated to the score. FK506-upregulated protein nodes are coloured green and FK506-downregulated protein nodes are coloured yellow. Regulatory proteins associated with kinases are square shaped and those associated with phosphatases are diamond shaped.

3.3.3.2 Phosphorylation motifs

Phosphorylation motifs are specific amino acid sequences that are targeted by specific groups of kinases. Identifying these motifs in phosphopeptides can give valuable insights into their likely regulatory kinases (445). Using Motif-X (436,437), phosphorylation motifs based on repetitive sequences present in the dataset were extracted. Motif analysis of phospho-threonine and phospho-tyrosine peptides identified no phosphorylation motifs in the dataset. Motif analysis of phospho-serine peptides showed that 40.5 % of the upregulated and 36.1 % of the downregulated phosphopeptides were not assigned to any phosphorylation motifs in the membrane fraction. In the cytosolic fraction, 72.5 % of the upregulated and 36.5 % of the downregulated phosphopeptides were not assigned to any phosphorylation motifs. Table 3.3-2 and Table 3.3-3 show the amino acid sequence of the phospho-serine motifs extracted, the percentage of peptides assigned to these motifs and the group of kinases that are known to phosphorylate them.

In the membrane fraction, proline-directed motifs - 'xsPx' (446–448), were found in 18.9 % of the phosphopeptides upregulated by FK506 and 33.5 % of the phosphopeptides downregulated by FK506. In the cytosolic fraction, 'xsPx' phosphorylation motifs were found in 27.5 % and 30.1 % of the phosphopeptides up and downregulated by FK506 respectively. These are known substrates of proline-directed protein kinases which includes ERK1/2, mitogen-activated protein kinase (MAPK), cyclin-dependent kinases (CDK) and glycogen synthase kinase 3 (GSK3). In the membrane fraction, 'Rxxs' phosphorylation motifs, targeted by AKT or Ca²⁺/calmodulin-dependent protein kinase II (CaMK-II) (449–451), were found in 9.85 % and 12.9 % of FK506-upregulated and downregulated phosphopeptides respectively. In the cytosolic fraction, 'Rxxs' phosphorylation motifs were only found in 14.1 % of phosphopeptides downregulated by FK506, but were not identified in phosphopeptides upregulated by FK506. Other motifs targeted by casein kinase II (CK-II), 'sxxE' (452) and 'sDxE' (453), and receptor-like kinase (RLK) and Ca²⁺-dependent protein kinase (CDPK), 'sD' (454) were also identified. An unknown/novel phosphorylation motif - 'sxxxxE' was also identified in the dataset, however their putative regulatory kinases have not been reported in literature.

Table 3.3-2 Phosphorylation motifs up and downregulated in the membrane fraction.


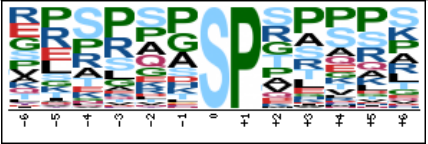
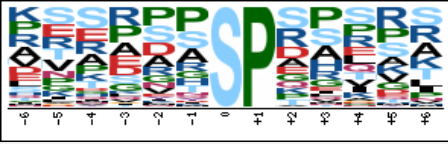


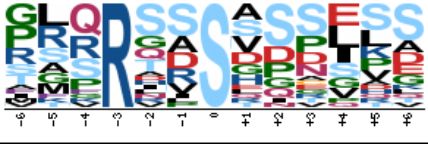
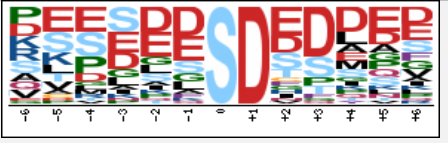

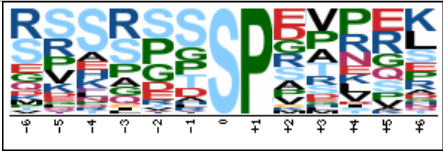
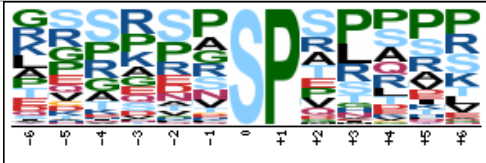
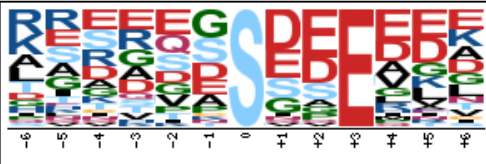

<u>Membrane</u>					
Upregulated	Percentage of peptides	Putative kinases	Downregulated	Percentage of peptides	Putative kinases
	9.47 %	CK-II		33.55 %	ERK1/2, MAPK, CDK, GSK3
	18.94 %	ERK1/2, MAPK, CDK, GSK3		17.42 %	Unknown/Novel
	12.12 %	CK-II		12.9 %	AKT, CaMK-II
	9.09 %	MAPK, RLK, CDPK			
	9.85 %	AKT, CaMK-II			

Table 3.3-3 Phosphorylation motifs up and downregulated in the cytosolic fraction.

<u>Cytosolic</u>					
Upregulated	Percentage of peptides	Putative kinases	Downregulated	Percentage of peptides	Putative kinases
	27.47 %	ERK1/2, MAPK, CDK, GSK3		30.13 %	ERK1/2, MAPK, CDK, GSK3
				19.23 %	CK-II
				14.1 %	AKT, CaMK-II

3.3.3.3 Interactions of AKT and ERK1/2 with the calcineurin-NCC cascade

Analysis of the protein-interaction network suggests that the serine/threonine protein kinases AKT1 may play a regulatory role downstream of calcineurin. Phosphorylation motif analysis further supported this hypothesis by identifying AKT/CaMK-II targeted and proline-directed phosphorylation motifs, the most common phosphorylation motifs identified in the data. These motifs are targeted by AKT1 and ERK1/2, which may play an important regulatory role in the phosphorylation of proteins downstream of calcineurin.

With the aim of identifying an intermediary pathway that regulates the calcineurin-WNK-NCC cascade, AKT1, ERK1/2 and components of the calcineurin-WNK-NCC cascade were submitted into STRING (441) to identify interactions between these proteins. The interactions between pairs of proteins were identified based on the seven criteria mentioned previously (Section 3.3.3.1). Each interaction, presented in the networks, has a combined score of over 0.4, meaning that the established interaction is true, specific and reproducible to a medium confidence level; the edge weights are directly correlated to the score. The sizes of the protein nodes directly correlate to the betweenness centrality of the protein in the network.

In this protein-interaction network, 26 interactions between 12 proteins were identified. AKT1 is connected by known or predicted protein interactions to calcineurin A α (PPP3CA), ERK1/2, WNK1 and WNK4. This suggests a close relationship between AKT1, calcineurin and the WNK kinases; AKT1 may therefore be one of the putative 'intermediate members' of the calcineurin-NCC cascade. In contrast to AKT1, ERK1/2 are only connected to calcineurin and AKT1 in the network and no predicted or known interactions between ERK1/2 and components of the WNK-NCC cascade were identified (Figure 3.3-7).

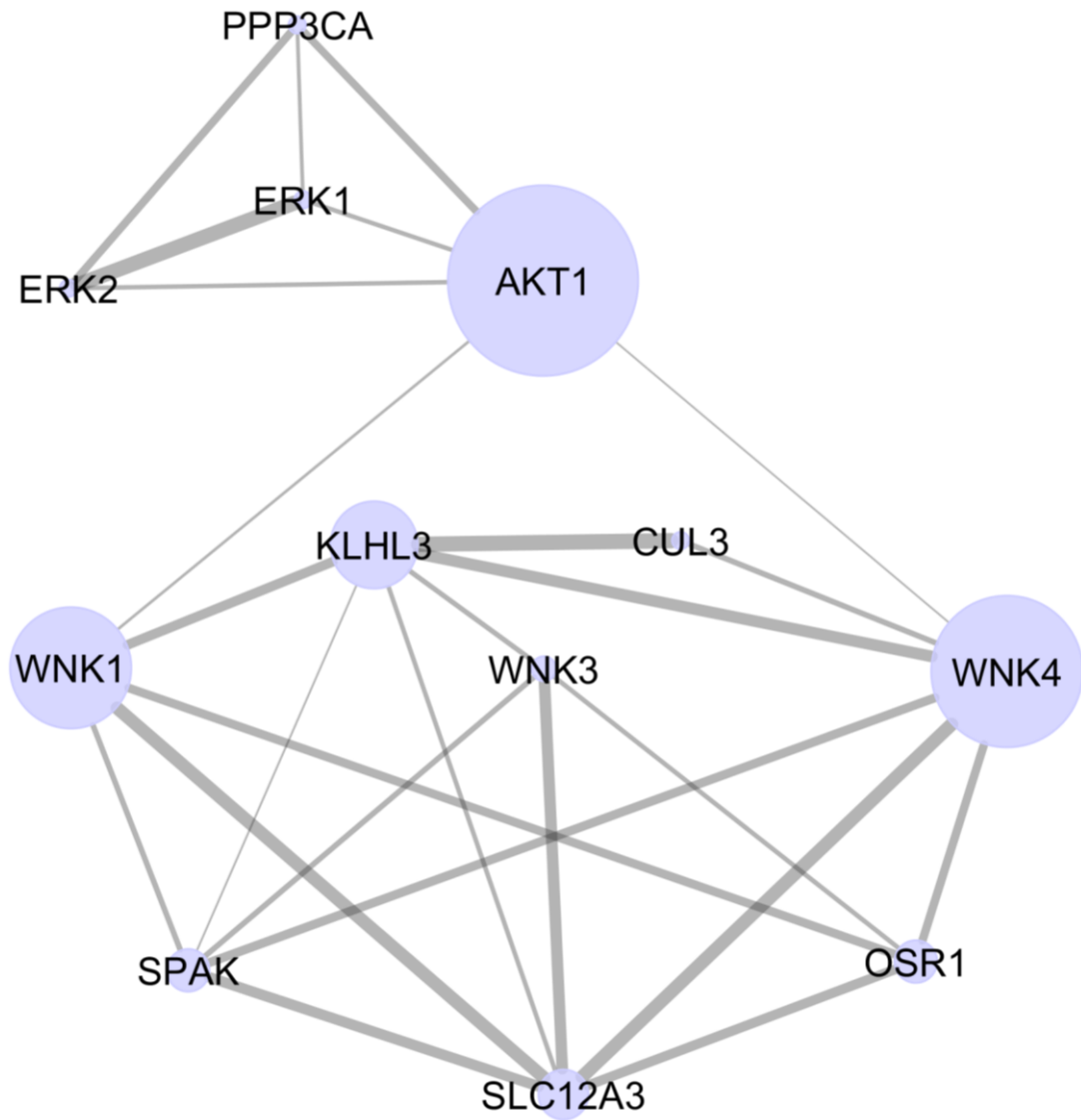


Figure 3.3-7 Interactions between AKT1, ERK1/2 and WNK-NCC cascade

Calcineurin, AKT1, ERK1/2 and components of the WNK-NCC cascade submitted into STRING to generate a protein-interaction network. In this network, 26 interactions between 12 proteins were identified. Each interaction has a combined score of over 0.4; the edge weights are directly correlated to the score. The sizes of the protein nodes directly correlate to the betweenness centrality of the protein in the network.

3.3.3.4 Effects of FK506 on ERK1/2 and AKT

Analysis of the phosphorylation motifs and protein-network analysis of AKT1, ERK1/2 and components of the calcineurin-WNK-NCC cascade, suggest an important regulatory role for AKT1 and ERK1/2 in FK506-dysregulated phosphoproteins. Therefore, the effects of FK506 on ERK1/2 and AKT1 were investigated through protein quantification. Western blot analysis revealed that FK506 significantly increased protein levels of ERK1/2 (Figure 3.3-8) and AKT1 (Figure 3.3-9) but not an activated form of ERK1/2 (pERK1/2). In addition, the effect of FK506 on phospho-AKT (pAKT)-S124 was examined, since pAKT-S124 was upregulated by FK506 in the phosphoproteomic data. Unfortunately, Western blot failed to detect signals using the anti-pAKT antibody under several conditions. This is possibly due to poor binding of the pAKT antibody to its epitopes on the Western blot, an issue commonly associated with phospho-antibodies.

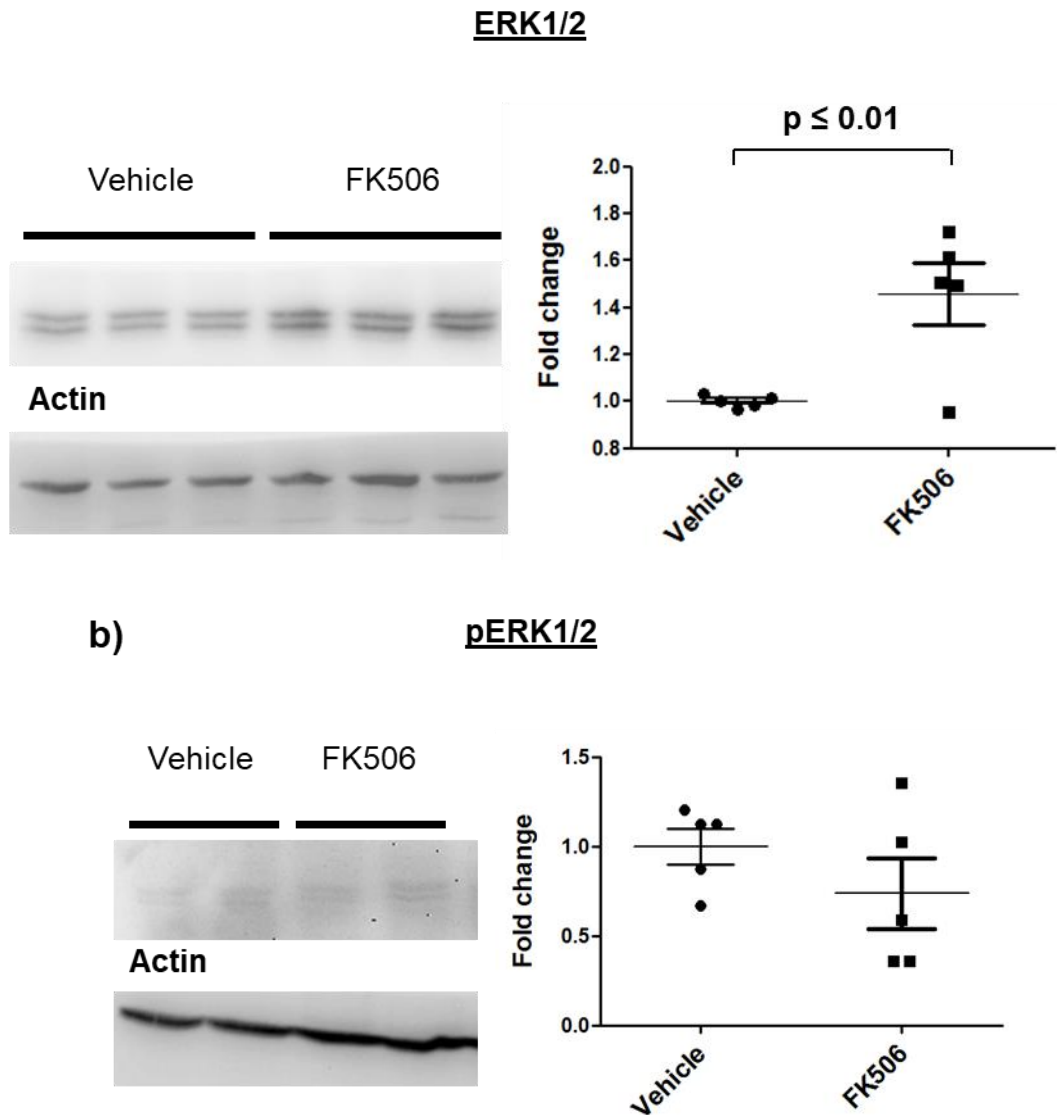


Figure 3.3-8 Protein expression of ERK1/2 and pERK1/2 post-FK506 treatment

Western blot analysis was performed on cytosolic fraction of FK506 or vehicle treated mice. Representative blots of a) ERK1/2 and b) pERK1/2 are shown. Band intensities of the transporters were quantified and normalised to those of β -actin and expressed as fold change of the control mean; data are presented as means \pm SEM, $n=5$. Statistical values were calculated using an unpaired t-test.

AKT1

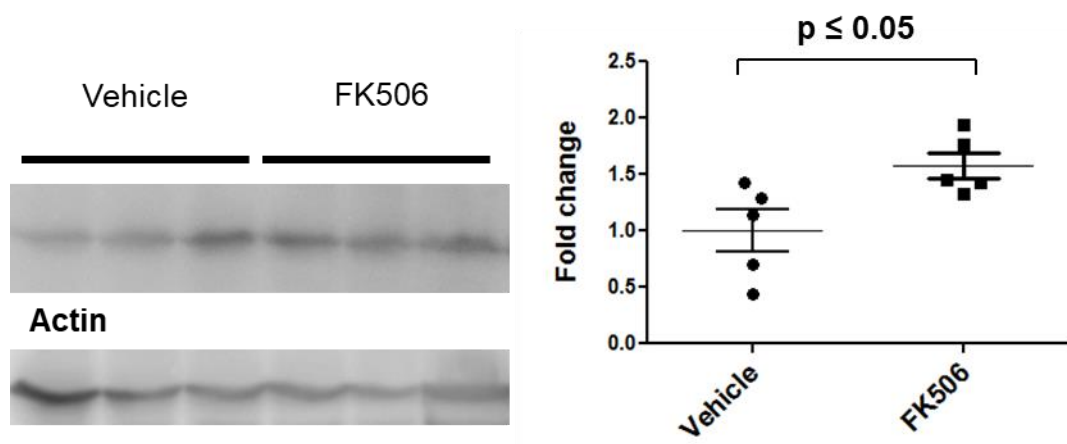


Figure 3.3-9 Protein expression of AKT1 post-FK506 treatment

Western blot analysis was performed on cytosolic fraction of FK506 or vehicle treated mice. Representative blots of AKT1 is shown on the left. Band intensities of the transporters were quantified and normalised to those of β -actin and expressed as fold change of the control mean; data are presented as means \pm SEM, n=5. Statistical values were calculated using an unpaired t-test.

3.3.3.5 Candidate approach: FK506-dysregulated transport and regulatory proteins

Calcineurin has pleiotropic effects and CNIs alter renal tubular function by dysregulating electrolyte transporters. Using the Panther classification system, (438), proteins classified as 'transporters', 'channels', 'kinase', 'phosphatase' and 'kinase/phosphatase'-related proteins were selected to narrow down the list of proteins of interest. Phosphosites identified were validated with the PhosphoSitePlus® Database and novel phosphosites are indicated by '*' in the tables. Phosphorylation motifs identified previously are also presented in the tables. Transport proteins were divided into proximal, distal and ubiquitous, depending on where these proteins are expressed in the kidney.

3.3.3.5.1 Transport proteins

In the membrane fraction, 55 % of proteins are predominantly expressed in the proximal tubule, 15 % are expressed in the distal nephron and 30 % are either expressed ubiquitously or present in both proximal and distal part of the nephron (Table 3.3-4). Many of the phosphorylation motifs present in the phosphopeptides of both membrane and cytosolic fractions are proline-directed or targeted by AKT.

In the proximal nephron, 55 % of the identified proteins are associated with sodium transport. Amongst all sodium transporters, multiple unique phosphopeptides were identified in the electrogenic sodium bicarbonate cotransporter 1 (NBCe1). Most of the NBCe1 phosphopeptides were upregulated with >20 % increase in phosphorylation; only one peptide phosphorylated at S1029 and S1044 was shown to be downregulated. A proline-directed phosphorylation motif was extracted from the peptide phosphorylated at S245 in NBCe1 and was shown to be upregulated. A novel phosphosite-S619 was identified in the sodium glucose cotransporter 2 (SGLT2) and was shown to be downregulated by FK506. Several other phosphopeptides identified in other sodium transporters, such as NaPi-IIa and NHE3, also showed FK506-induced changes in phosphorylation.

FK506-dysregulated phosphorylation of several proteins in the distal nephron that are involved in sodium and water reabsorption. S256 and S261 in AQP2 are predicted targets of AKT and proline-directed kinases, and FK506 was shown to

increase phosphorylation of these two phosphosites. Two phosphopeptides were identified in NKCC2; phosphorylation at T114 and S116 was downregulated by FK506 and the other phosphopeptide with a novel phosphosite-pY110 was upregulated. Nine unique NCC phosphopeptides were identified in the whole dataset (Appendix, Table 6.3-1). Six of these phosphopeptides showed >10 % change in phosphorylation at T122, S124 and S127; S127 is a novel phosphosite and is targeted by proline-directed kinases. FK506 upregulated 5 out of 6 of the phosphopeptides with the exception of the peptide phosphorylated at T122 and S127 which it downregulated. Since NCC is an important protein in this study, the degree of conservation in these phosphosites was investigated. A sequence alignment of *SLC12A3* in mouse, human and rat revealed that T122 and S124 are highly conserved in all three species, whereas S127 is conserved in the mouse and rat but not in humans.

The Na⁺/K⁺-ATPase subunit γ is expressed in both proximal and distal tubules. A novel phosphosite-pS15 was identified in Na⁺/K⁺-ATPase subunit γ and was downregulated by FK506. Other transport proteins involved in electrolyte transport identified in the membrane fraction are shown in Table 3.3-4.

Eleven transport proteins in the cytosolic fraction were selected from in this dataset (Table 3.3-5). In the cytosolic fraction, FK506 downregulated phosphopeptides of NBCe1 and NaPi-IIa. The only transport protein expressed in the distal nephron identified in the cytosol was NKCC2. Only one phosphopeptide was identified in NKCC2 where phosphorylation at S116 and the novel phosphosite-Y110 was downregulated. Two transport proteins involved in potassium and sodium transport, KCNJ16 and the NHE1, are both expressed in the proximal and distal nephron. Two novel phosphosites pS363 and pS366 identified in KCNJ16 were downregulated by FK506. FK506 also decreased phosphorylation of NHE1 at S810. Other transport proteins identified in the cytosolic fractions with >10 % change in phosphorylation are shown in Table 3.3-5.

Location	Gene name	Protein name	Accession No.	Peptide Sequence	Phosphosites	Motifs	Percentage Change
Proximal	<i>SLC4A4</i>	Electrogenic sodium bicarbonate cotransporter 1	O88343	GSLDsDNDDSDCPYSEKVPsIK	S1029; S1044	-	- 13.92
				MFSNPDNGsPAMTHR	S245	Proline-directed	+ 20.28
				TVsSASR	S232	-	+ 22.55
				GSLSDNDDsDCPYSEKVPSIK	S1034	-	+ 30.74
				NLtSSSLNDISDKPEK	T254	-	+ 40.15
				GSLDsDNDDsDCPYSEK	S1029; S1034	-	+ 41.47
				NLTsSLNDISDKPEK	S256	-	+ 43.57
				GSLDsDNDDSDCPYSEK	S1029	-	+ 50.32
				MFSNPDNGSPAMtHR	T249	-	+ 53.65
				GsLDsDNDDSDCPYSEK	S1026; S1029	-	+ 68.21
				KGsLSDNDDSDCPYSEK	S1026	-	+ 73.34
KGsLDsDNDDsDCPYSEK	S1026; S1029; S1034	-	+ 152.26				
Proximal	<i>SLC12A6</i>	Electroneutral potassium-chloride cotransporter 3	Q924N4	LTSIGsDEDEETETYQEK	S1032	-	- 14.07
Proximal; TALH	<i>SLC43A2</i>	L-type amino acid transporter 4	Q8CGA3	LCLsTVDLEVK	S297	-	- 10.59
				LCLsTVDLEVK	T298	-	- 24.66
Proximal	<i>SLC51A</i>	Organic solute transporter subunit alpha	Q8R000	VGYEACsLPDLDSALKA	S330	-	- 53.04
				VGYEACsLPDLDSALKA	S330; S336	-	- 33.12
Proximal	<i>SLC51B</i>	Organic solute transporter subunit beta	Q80WK2	ENNsQVFLR	S88*	-	- 51.06
				EKDSsLVFLPDPQETES	S116	-	- 58.06
				EKDsSLVFLPDPQETES	S115*	-	- 41.99
Proximal	<i>SLC6A20B</i>	Sodium- and chloride-dependent transporter XTRP3B	O88575	sTECAHPGVVEK	S35*	AKT substrate	+ 40.18
Proximal	<i>SLC5A2</i>	Sodium/glucose cotransporter 2	Q923I7	sGSGSPPTTEEVAATTR	S619*	-	- 11.04
Proximal; TALH	<i>SLC9A3</i>	Sodium/hydrogen exchanger 3	G3X939	ENVsAVCLDMQSLEQR	S588	-	+ 28.70
Proximal	<i>SLC34A1</i>	Sodium/phosphate cotransporter 2A	Q60825	VFLEELPPAtPsPR	T621; S623	Proline-directed S623	- 58.73
Proximal	<i>SLC23A1</i>	Sodium-dependent vitamin C transporter 1	Q9Z2J0	KTQNQPPVLETPDNIETGsVCtKV	S600; T603	-	- 39.39

Proximal	<i>SLC26A1</i>	Sulfate anion transporter 1	P58735	DQGPEVGVsNR	S587	-	+ 20.49
Distal	<i>AQP2</i>	Aquaporin-2	P56402	RQsVELHsPQSLPR	S256; S261	AKT substrate S256; Proline-directed S261	+ 27.21
Distal	<i>SLC12A1</i>	Kidney-specific Na-K-Cl symporter 2	P55014	IEYYRNtGsVSGPK IEyyRNTGsvSGPK	T114; S116 Y110*; Y111	-	- 23.09 + 31.43
Distal	<i>SLC12A3</i>	Thiazide-sensitive sodium-chloride cotransporter	P59158	ELTDGLVEDETGtNSEKsPGEPVR	T122; S127*	Proline-directed S127	- 23.56
				ELTDGLVEDETGtNsEKSPGEPVR	T122; S124	-	+ 13.12
				ELTDGLVEDETGTNsEKSPGEPVR	S124	-	+ 20.16
				ELTDGLVEDETGtNSEK	T122	-	+ 20.65
				ELTDGLVEDETGTNSEKsPGEPVR	S127*	Proline directed	+ 26.22
ELTDGLVEDETGTNsEKsPGEPVR	S124; S127*	Proline directed S127	+ 29.40				
Proximal; Distal	<i>FXVD2</i>	Sodium/potassium-transporting ATPase subunit gamma	Q04646	AGEISDLSANSsGGsAK	S15*	-	- 19.85
Proximal; Distal	<i>CACNA1E</i>	Voltage-dependent R-type calcium channel subunit alpha-1E	Q61290	SFStIR	T1983*	-	+ 30.99
Ubiquitous	<i>AP3D1</i>	AP-3 complex subunit delta-1	O54774	HSSLPEsDEDIAPAQR HSSLPTEsDEDIAPAQR	T758; S760 S760	-	+ 14.99 +24.66
Ubiquitous	<i>SLC33A1</i>	Acetyl-CoA transporter 1	Q99J27	RDsVGGEGDREVLLGDAGPGDLPK	S42	AKT substrate	+ 27.39
Ubiquitous	<i>TOMM20</i>	Mitochondrial import receptor subunit TOM20 homolog	Q9DCC8	IVsAQsLAEDDVE	S135; S138	AKT substrate S135	- 13.93
				IVsAQSLAEDDVE	S135	AKT substrate	+14.61
N/A	<i>SLC35A5</i>	Probable UDP-sugar transporter protein	Q921R7	LKsDDsDDDTL LKsDDsDDDTL	S432 S429; S432	-	+ 10.49 + 16.58
* Novel phosphopeptides							

Table 3.3-4 FK506-dysregulated transport proteins identified in the membrane fraction

Identification and quantification of phosphosites in transport proteins, in the membrane, after FK506 treatment. Novel phosphorylation sites were previously unidentified in PhosphoSitePlus® Database.

Location	Gene name	Protein name	Accession No.	Peptide Sequence	Phosphosites	Motifs	% Change
Proximal	<i>SLC4A4</i>	Electrogenic sodium bicarbonate cotransporter 1	O88343	TV _{ss} ASR	S232; S233	-	- 47.99
				NL _{tSs} SLNDISDKPEK	T254; S256; S257	AKT substrate S256	- 48.12
				sSTFLER	S1069	-	- 44.51
				GSLD _s DNDDSDCPYSEK	S1029	-	- 39.44
				TV _s SAsR	S232; S235	-	- 38.40
				KG _s LD _s DNDDSDCPYSEK	S1026; S1029	-	- 21.43
				NLTSS _s LNDI _s DKPEKDQLK	S257; S262	-	- 21.35
				TV _s SASR	S232	-	- 21.35
MFSNPDNG _s PAMTHR	T249	Proline-directed	- 11.90				
Proximal; TALH	<i>SLC43A2</i>	L-type amino acid transporter 4	Q8CGA3	LCL _s TVDLEVK	S297	-	- 23.87
Proximal	<i>SLC34A1</i>	Sodium/phosphate cotransporter 2A	Q60825	VFLEELPPAtPsPR	T621; S623	Proline-directed S623	- 72.21
				VFLEELPPATPsPR	S623	Proline-directed	- 47.55
				sPQLPPR	S605	Proline-directed	- 46.94
TALH; Macula densa	<i>SLC12A1</i>	Kidney-specific Na-K-Cl symporter 2	P55014	IEyYRNTGSV _s GPK	Y110*; S116	-	- 33.74
Proximal; Distal	<i>KCNJ16</i>	Inward rectifier potassium channel 16	Q9Z307	TSPARG _s CN _s DTNTR	S363*; S366*	AKT substrate S366	- 35.12
Ubiquitous	<i>AP3D1</i>	AP-3 complex subunit delta-1	O54774	HSSLPtEsDEDIAPAQR	T758; S760	-	- 24.00
				HSSLPTEsDEDIAPAQR	S760	-	- 19.19
Ubiquitous	<i>SORT1</i>	Neurotensin receptor 3	Q6PHU5	SGYHDD _s DEDLLE	S819	-	- 27.10
Ubiquitous	<i>SLC9A1</i>	Sodium/hydrogen exchanger 1	Q61165	SKEPSSPGTDDVFTPGSSDSP _s SQR	S790	-	- 19.37
Ubiquitous, highly expressed in the distal nephron	<i>TRPP2</i>	Transient receptor potential cation channel subfamily P member 2	O35245	SLDD _s EEEDDED _s SGHSSR	S810	-	+ 15.51

N/A	<i>SLC35A5</i>	Probable UDP-sugar transporter protein	Q921R7	LKSDDsDDDTL	S432	-	-10.12
-----	----------------	----------------------------------------	--------	-------------	------	---	--------

* Novel phosphosites

Table 3.3-5 FK506-dysregulated transport proteins identified in the cytosolic fraction

Identification and quantification of phosphosites in transport proteins, in the cytosol, after FK506 treatment. Novel phosphorylation sites were previously unidentified in PhosphoSitePlus® Database.

3.3.3.5.2 Classified transport proteins identified in the membrane and cytosolic fractions

A small number of unique phosphopeptides from NBCe1, L-type amino acid transporter 4 (LAT4) and NaPi-IIa were identified in both the membrane and cytosolic fractions. LAT4 and NaPi-IIa demonstrated downregulated phosphorylation of the same unique phosphopeptides in both fractions. In contrast, NBCe1 phosphopeptides were differentially regulated in the two fractions; peptides phosphorylated at S232, T249 and S1029 and at S1026 and S1029 were upregulated in the membrane fraction and downregulated in the cytosolic fraction. In addition, phosphopeptides from two other proteins, AP-3 complex subunit delta-1 (AP3D1) and probable UDP-sugar transporter protein, were also differentially regulated in the two fractions (Table 3.3-6).

Gene name	Protein name	Accession No.	Peptide Sequence	Phosphosites	Percentage change	
					<u>Memb</u>	<u>Cyto</u>
<i>SLC4A4</i>	Electrogenic sodium bicarbonate cotransporter 1	O88343	tVsSASR	S232	+ 22.55	- 21.35
			mFSNPDNGsPAMTHR	T249	+ 53.62	-11.90
			gSLDsDNDDSDcPYSEk	S1029	+ 53.62	-39.44
			kGsLDsDNDDSDcPYSEk	S1026; S1029	+ 67.00	-21.43
<i>SLC43A2</i>	L-type amino acid transporter 4	Q8CGA3	lcLsTVDLEVk	S297	- 10.59	- 23.87
<i>SLC34A1</i>	Sodium/phosphate cotransporter 2A	Q60825	vFLEELPPAtPsPR	T621; S623	- 58.73	- 72.21
<i>AP3D1</i>	AP-3 complex subunit delta-1	O54774	hSSLPtEsDEDIAPAQR	T758; S760	+ 14.99	- 24.00
			hSSLPTEsDEDIAPAQR	S760	+24.66	-19.19
<i>SLC35A5</i>	Probable UDP-sugar transporter protein	Q921R7	lkSDDsDDDTL	S432	+ 10.49	- 10.12

Table 3.3-6 FK506-dysregulated transport proteins identified in membrane and cytosolic fractions

Identification and quantification of phosphosites in transport proteins, in the membrane and cytosolic fraction, after FK506 treatment. Novel phosphorylation sites were previously unidentified in PhosphoSitePlus® Database.

3.3.3.5.3 Regulatory proteins

Fifteen proteins in the membrane fraction (Table 3.3-7) and nine in the cytosolic fraction (Table 3.3-8) were classified as 'kinase', 'phosphatase' and 'kinase/phosphatase'-related proteins. A novel phosphosite, pS1001 in Phosphatidylinositol 4,5 biphosphate 5-phosphatase, was identified in the cytosol. Five AKT-phosphorylation motifs, 4 proline-directed phosphorylation motifs and a CK-II-phosphorylated motif were identified in the membrane fraction. Four proline-directed phosphorylation motifs and an AKT-phosphorylation motif were identified in the cytosolic fraction.

CDK11b is a member of the CDK family and targets proline-directed phosphosites. CDK11b was identified in the membrane fraction and phosphorylated at S115; this phosphopeptide was upregulated and is a predicted target of AKT phosphorylation.

MAPK 8-interacting protein 4 (MAPK8IP4) is a member of the MAPK and targets proline-directed phosphosites. MAPK8IP4 was identified in the cytosol, and the phosphopeptide identified was downregulated at S732 and S733. S732 is a predicted target of AKT, indicated by the phosphorylation motif extracted from the peptide sequence, and no phosphorylation motifs were found for S733.

AKT was identified in the cytosol and targets a group of phosphopeptides identified in these datasets; it was shown to be upregulated at pS124 and pS126 where phosphorylation of S124 is proline-directed.

Phosphopeptides from cyclin-K, diacylglycerol kinase theta (DGKQ) and sphingosine-1-phosphatase 1 (SGPP1) were identified in both membrane and cytosolic fractions (Table 3.3-9). The behaviour of the phosphopeptides identified in cyclin-K and DGKQ was the same in both fractions, whereas the phosphopeptide identified in SGPP1 showed an increase in phosphorylation in the membrane fraction and a decrease in cytosolic fraction.

Gene name	Protein name	Accession No.	Peptide Sequence	Phosphosites	Motifs	Percentage Change
<i>PRKAA1</i>	AMPK subunit alpha-1	Q5EG47	SIDDEITEAKsGTAtPQR	S486; T490	-	+ 11.35
<i>AAK1</i>	AP2-associated protein kinase 1	Q3UHH0	SATTTPSGsPR VGSLtPPSsPK	S676 T618; S622	-	- 11.15 +10.69
<i>BCKDK</i>	BCKD-kinase	O55028	sTSATDTHHVELAR STSAtdTHHVELAR	S31 T35	Akt substrate -	+ 28.85 + 32.27
<i>BMP2K</i>	BMP-2-inducible protein kinase	Q91Z96	RDsQSsNEFLTISDSK	S1010; S1013	Akt substrate S1010	+ 22.94
<i>CDK11B</i>	Cyclin-dependent kinase 11B	P24788	SHsAEGGK	S115	Akt substrate	+ 38.52
<i>CCNK</i>	Cyclin-K	O88874	KPsPQsPPR	S325; S329	Proline-directed	- 16.78
<i>DGKQ</i>	Diacylglycerol kinase theta	Q6P5E8	LGsPAGsPVLGISGR	S22; S26	Proline-directed	- 17.19
<i>PRKRA</i>	Interferon-inducible double-stranded RNA-dependent protein kinase activator A	Q9WTX2	EDsGTfSLGK	S18	Akt substrate	+ 20.46
<i>NUCKS1</i>	Nuclear ubiquitous casein and cyclin-dependent kinase substrate 1	Q80XU3	SGDEGSEDEAsSGED	S230	-	- 35.36
<i>PALLD</i>	Palladin	Q9ET54	SRDsGDENEPIQER	S1146	-	- 13.15
<i>PI4KB</i>	Phosphatidylinositol 4-kinase beta	Q8BKC8	sVENLPECGITHEQR	S428	-	+ 13.09
<i>PPP1R2</i>	Protein phosphatase inhibitor 2	Q9DCL8	TREQEssGEEDNDsLSPEER	S122; S123	CK-II substrate	+ 23.55
<i>KIAA0445</i>	Rootletin	Q8CJ40	sQPPsPGLIASPAPPDLDPPEAVR	S1479; S1483	Proline-directed S1483	+ 68.99

<i>SGPPI</i>	Sphingosine-1-phosphatase 1	Q9JI99	NsLTGEEGELVK	S101	Akt substrate	+ 30.13
<i>TNS2</i>	Tensin-like C1 domain-containing phosphatase	Q8CGB6	GYPSGAHsPR	S825	Proline-directed	- 14.74
* Novel phosphosites						

Table 3.3-7 FK506-dysregulated kinase/phosphatase-associated proteins identified in the membrane fraction

Identification and quantification of phosphosites in kinases, phosphatases and other related proteins in the membrane post-FK506 treatment. Novel phosphorylation sites were previously unidentified in PhosphoSitePlus® Database.

Gene name	Protein name	Accession No.	Peptide Sequence	Phosphosites	Motif	Percentage Change
<i>PRKAB1</i>	5'-AMP-activated protein kinase subunit beta-1	Q9R078	RDsSGGAK	S24	-	- 27.41
<i>ANP32B</i>	Acidic leucine-rich nuclear phosphoprotein 32 family member B	Q9EST5	KREtDDEGEDD	T265	-	- 23.41
<i>CCNK</i>	Cyclin-K	O88874	KPsPQPpPPR	S325; S329	Proline- directed	- 14.77
<i>DGKQ</i>	Diacylglycerol kinase theta	Q6P5E8	LGsPAGsPVLGISGR	S22; S26	Proline-directed	- 21.27
<i>MAPK8IP4</i>	Mitogen-activated protein kinase 8-interacting protein 4	Q58A65	SASQssLDKLDQELKEQQK	S732; S733	Akt substrate S732	- 23.38
<i>MTMR2</i>	Phosphatidylinositol-3,5-bisphosphate 3-phosphatase	Q9Z2D1	SSsCEsLGAQLPAAR	S6; S9	-	-11.52
<i>INPP5J</i>	Phosphatidylinositol 4,5-bisphosphate 5-phosphatase A	P59644	GGsRsPsPQSR	S907; S909; S1001*	Proline directed S909; S1001	- 23.53
<i>AKT</i>	Protein kinase B	P31750	SGsPsDNSGAEEMEVS LAKPK	S124; S126	Proline-directed S124	+ 39.15
<i>SGPPI</i>	Sphingosine-1-phosphate phosphatase 1	Q9JI99	RNsLTGEEGELVK	S101	-	- 18.71

* Novel phosphosites

Table 3.3-8 FK506-dysregulated kinase/phosphatase-associated proteins identified in the cytosolic fraction

Identification and quantification of phosphosites in kinases, phosphatases and other related proteins in the cytosol post-FK506 treatment. Novel phosphorylation sites were previously unidentified in PhosphoSitePlus® Database.

Gene name	Protein name	Accession No.	Peptide Sequence	Phosphosites	Percentage change	
					<u>Memb</u>	<u>Cyto</u>
<i>CCNK</i>	Cyclin-K	O88874	kPsPQPpPPR	S325; S329	- 16.78	- 14.77
<i>DGKQ</i>	Diacylglycerol kinase theta	Q6P5E8	IGsPAGsPVLGISGR	S22; S26	- 17.19	- 21.27
<i>SGPPI</i>	Sphingosine-1-phosphatase 1	Q9JI99	nsLTGEEGELV _k	S101	+ 32.97	- 18.71

163 **Table 3.3-9 FK506-dysregulated kinase/phosphatase-associated proteins identified in the membrane and cytosolic fractions**

Identification and quantification of phosphosites in regulatory proteins, in the membrane and cytosolic fraction, after FK506 treatment. Novel phosphorylation sites were previously unidentified in PhosphoSitePlus® Database.

3.3.3.6 Candidate approach: ACE and NHERF1

The bioinformatic techniques used in this study generated a selection of proteins and phosphosites that may play a significant role in CNI-induced renal tubular dysregulation. These filters are highly effective at excluding housekeeping proteins and proteins that unlikely to play a significant role in the cascade; however, proteins that were excluded because they did not meet the criteria set in each analytical technique might still be important. Interesting candidates in the datasets that were excluded include, ACE and NHERF1.

ACE is involved in blood pressure regulation and is therefore a protein of interest. In this study, only one phosphopeptide (S1305) was identified in ACE in the cytosolic fraction, which showed >20 % upregulation by FK506 and no phosphorylation motif was found in this phosphopeptide. Regulators of S1305 in mice is currently unknown; however, in humans, the homologous site is S1299 and phosphorylation is regulated by CK-II. CK-II is a serine/threonine-selective protein kinase and has been proposed to determine plasma levels of ACE by phosphorylating ACE and preventing proteolytic cleavage of ACE from the membrane (455).

NHERF1 has pleiotropic roles and, is involved in phosphate, acid-base and sodium homeostasis (456–458). Twenty-seven unique phosphopeptides of NHERF1 in the membrane fraction and 15 phosphopeptides in the cytosolic fraction were identified; ambiguous phosphopeptides are not presented in Table 3.3-10. A total of twenty unique phosphopeptides were identified in the two fractions. A novel phosphosite S277 was identified in NHERF1 in the membrane fraction and was shown to be downregulated by FK506. Several phosphosites are regulated by leptin (459), these include S275, S285, S286 and S289 and some phosphosites are regulated by tuberous sclerosis complex 2 (460), these include S275, S283, S285 and S286. Other phosphosites were shown to be affected by rapamycin (461) and are associated with type II diabetes (462).

Gene name	Protein name	Accession No.	Phosphosites	Percentage Change	
				Memb	Cyto
<i>SLC9A3R1</i>	Sodium-hydrogen antiporter 3 regulator 1 (NHERF1)	P70441	S275	-	+ 12.18
			S277 *	- 16.59	-
			S283	0.0	-
			S285	- 1.92	- 17.26
			S286	- 18.22	+ 2.51
			T288	- 3.20	-
			S289	+ 7.76	-
			S297	- 25.86	-
			S283; S285	- 19.85	-
			S285; S286	- 0.24	-
			S285; T288	- 26.99	- 18.23
			S285; S297	- 28.80	-
			S286; T288	- 11.40	-
			S286; S289	- 13.81	- 5.51
			T288; S289	- 1.40	+ 21.63
			S294; S297	- 3.83	-
			S283; S285; S286	+ 2.31	+ 8.16
			S285, S286, T288	-	+ 22.57
S285; S286; S289	- 13.45	- 12.58			
S286; T288; S289	- 12.14	- 2.58			
* Novel phosphosite					

Table 3.3-10 FK506-dysregulated phosphosites in NHERF1

Identification and quantification of phosphosites in NHERF1, in the membrane and cytosolic fraction, after FK506 treatment. Novel phosphorylation sites were previously unidentified in PhosphoSitePlus® Database.

3.4 Discussion

3.4.1 Overview of quantitative phosphoproteomics

Proteomics was used to generate a phosphoproteome profile of the renal cortices from FK506-treated mice. To generate a complete proteome profile, it is important to fractionate the samples to reduce their complexity; not only does fractionating samples improve proteome coverage, it also allows LC-MS/MS to identify peptides of lower abundance, enhances quantitative detection of TMT reporter ions on peptides and increases efficiency of phosphopeptide enrichment (430,463). In this study, the renal cortices of FK506-treated mice were extracted and separated into membrane and cytosolic fractions through ultracentrifugation. A cytosolic protein, ERK1, was used to confirm successful fractionation (Appendix, Figure 6.2-1). Since the purpose of the fractionation was to lower sample complexity, absolute enrichment of the subcellular compartments was not deemed necessary.

Numerous bioinformatics techniques are available for proteomics data analysis. Each of these techniques have different properties and act as filters to select protein of interests from the complex mixture of proteins. Currently, there are no set guidelines on how one should interpret proteomics data; therefore, it is important to choose bioinformatic techniques that fit the purpose of the specific research. Since the aim of this study was to identify a novel regulatory pathway for the WNK cascade and to determine changes in the phosphorylation of other FK506-dysregulated transport proteins, the data was analysed utilising several bioinformatics techniques. An arbitrary cut-off point/threshold is commonly used in quantitative proteomics to filter out proteins of interest (464,465). These thresholds are often tailored to individual studies, depending on factors such as the type of samples used and the purpose of the research. Some studies that use quantitative proteomics and biomarkers for diagnostic purposes, have used higher thresholds to increase the sensitivity of the diagnostic screening (466). This approach is not necessarily beneficial for the type of research presented in this chapter as it can result in a large loss of information. Therefore, a 10 % threshold was used to prevent important proteins from being excluded at the early stages of data interpretation. Phosphopeptides with >10 % change in phosphorylation were considered to be dysregulated by FK506. These

phosphopeptides were also processed by other bioinformatics techniques, such as protein-protein interaction database and phosphorylation motif extractor software, resulting in a refined list of proteins of interests.

3.4.2 AKT and the WNK-NCC cascade

The protein network analysis revealed that a small number of phosphoproteins appeared to act as hubs at the centre of the networks of both the cytoplasmic and membrane fractions. In the cytosolic fraction, the serine/threonine kinase AKT is particularly prominent, connecting clusters of phosphoproteins involved in membrane solute transport, intracellular trafficking, transcription, translation and glucose metabolism. AKT plays an important role as part of the phosphoinositide-3-kinase (PI3K)-mediated insulin and insulin-like growth factor 1 (IGF1) signalling pathway governing glucose homeostasis (467,468).

The pathophysiology of the metabolic syndrome involves insulin resistance and the mechanisms underlying the development of insulin resistance differs in the kidney from other glucogenic tissues, such as muscle and adipose tissues (469,470). Using a mouse model of the metabolic syndrome, the activity of the PI3K and AKT in the kidneys were increased (471), whereas a decrease in AKT activity was detected in the muscles and adipose tissues of these mice (472,473).

The activity of AKT is increased by insulin through PI3K phosphorylation at T308 and S473 (474). This process is reversible by calcineurin, which directly dephosphorylates AKT in the AKT-calcineurin complex, as shown in ischemic rat retina (475) and in cardiomyocytes (476). In the current study, FK506 has been shown to increase protein levels of AKT1 and pNCC in the kidneys. This indicates that calcineurin inhibition and the use of CNIs increases AKT protein levels, prevents the dephosphorylation of AKT and increases its kinase activity. Unfortunately, AKT-pT308 and pS473 regulated by PI3K and calcineurin were not identified in phosphoproteomics. However, FK506 increased the phosphorylation of S124 and S126, and these may also play a role in AKT activity.

The PI3K/AKT signalling pathway has previously shown to phosphorylate and activate the SPAK/OSR1-NCC cascade in the kidneys in a SGK1 independent manner. This led to the development of salt-sensitive hypertension in hyperinsulinaemic mice (471) and was suggested to be one of the mechanisms

involved in the pathogenesis of essential hypertension. AKT phosphorylation motifs were previously identified in the WNK kinases (110,123,477) and together with the information obtained from this study, these suggest that AKT is the intermediary protein that phosphorylates and defines the activities of the WNK kinases downstream of calcineurin, thereby regulating NCC activity.

3.4.3 HSP90, AKT and the metabolic syndrome

The second protein hub prominently present in the protein network of both the membrane and cytosolic fraction was HSP90AB1. HSP90AB1 is a ubiquitous chaperone protein involved in protein stabilisation and trafficking, preventing misfolding during protein synthesis or denaturing stress. Although the number of known HSP90 client proteins exceeds 100, one of better characterised is AKT. HSP90 is vital to AKT function as decreased AKT-HSP90 binding results in decreased AKT function (478). Both AKT and HSP90 act synergistically to increase the activity of endothelial nitric oxide synthase (eNOS), which produces the vasodilatory NO (479).

Furthermore, in eukaryotes, cytoplasmic HSP90 complexes with other chaperone proteins, notably those containing tetratricopeptide repeat (TPR) domains such as the immunophilins, cyclophilin 40, FKBP51/FKBP52 (480). HSP90 and these immunophilins (e.g. FKBP52) are required to translocate the glucocorticoid receptor (GR) from the cytosol to the nucleus (481). This is achieved in a complex with the motor protein dynein which powers movement along the cytosolic microtubule network (481). The same mechanism applies for the MR (482). Moreover, GR polymorphism which leads to GR dysfunction is associated with hyperinsulinaemia and insulin resistance, which are components of the metabolic syndrome (483).

3.4.4 ERK1/2 and the WNK-NCC cascade

Similar to AKT, ERK is also a ubiquitous serine/threonine kinase that is essential in many biological functions, including cell growth, survival and phosphorylation of proteins in numerous signalling pathways (447). FK506 was shown to increase protein levels of ERK1/2 but not phospho-ERK1/2. The relationship between ERK1/2 and members of the WNK-NCC cascade was supported by little evidence in the protein-interaction network. However ERK1/2 have been shown to regulate

NCC expression by Zhou *et al.* (484). WNK4 was reported to increase the phosphorylation of ERK1/2 in mDCT cells in a dose-dependent manner. This effect was also increased in hypertonic conditions, and reversed in a WNK4 knock-down model and WNK4 with FHHT-type mutations in mDCT cells (484). Knock-down models of WNK4 and ERK1/2 both significantly increase total expression of NCC along with cell surface expression, which suggests that WNK4 inhibits NCC through the activation of ERK1/2 signalling pathway. It has been proposed that two signalling pathways, SPAK/OSR1 and ERK1/2, downstream of WNK4 independently regulate NCC, and are activated under different stimulants (484). This could mean that the WNK4-ERK1/2 pathway may inhibit NCC under normal conditions and the WNK4-SPAK pathway may regulate NCC in response to dietary sodium chloride intake. Together with the data obtained in this study, these results suggest that ERK1/2 are involved in regulating NCC downstream of the WNK kinases.

3.4.5 Candidate approach

3.4.5.1 Hypertension

CNI-induced hypertension is caused by an increase in NaCl reabsorption, through NCC overactivity (51), and an increase in water reabsorption. SPAK and OSR1 phosphorylate NCC at T53, T58 and S71 to activate NCC, resulting in the increase in NaCl reabsorption. NCC-pT53 and -pT58 defines NCC transport activity and do not play a role in NCC membrane trafficking (82,106,111,116). These phosphosites were not identified in this study, however, T122, S124 and a novel phosphosite-S127 were heavily phosphorylated in mice treated with FK506, therefore, might play a role in CNI-induced hypertension. Alignments of T122, S124 and S127 showed that T122 and S124 are highly conserved residues and S127 is a proline-directed phosphorylation that is only conserved in mice and rats but not in humans. Functional characterisation of pT122 and pS127 is currently unknown, but a recent study by Rosenbaek *et al* (485) showed that S124 plays a role in the transport activity of NCC and its phosphorylation is stimulated by the RAAS (485). A serine to alanine mutation at S124 reduced the transport activity of NCC but to a much lesser extent than T48A, T53A and T58A mutants (485), which indicates that the effect of pS124 alone may not define NCC activity (485). The regulation of NCC-pS124 differs from the other phosphosites.

S124 is not phosphorylated by SPAK/OSR1, instead, a protein kinase array experiment suggests that IRAK2 (IL-1 receptor-associated kinase 2), CDK6/Cyclin-D1, NLK (Nemo-Like Kinase) and mTOR may phosphorylate NCC-S124 (485). mTOR is a member of the PI3K/AKT signalling pathway and is one of the many targets of AKT. This indicates that when PI3K/AKT is stimulated, mTOR may also phosphorylate NCC alongside the WNK-SPAK pathway. In addition to T53, T58 and S71, CNIs also increased the phosphorylation of S124. The functional characterisation and regulation of NCC-S124 differs from the other phosphosites (485). NCC-S124 is phosphorylated inside the Golgi apparatus, therefore it was speculated that NCC-S124 may play a role in the maturation and trafficking of NCC, leading to increased pNCC abundance and sodium chloride reabsorption (485). The underlying mechanism of this process is unclear, however a similar maturation process has been reported in the vasopressin-regulated water channel AQP2, involving the phosphorylation of AQP2-S256 (486).

AQP2 is predominantly expressed in the apical membrane of the CD, where it is responsible for urinary concentration (487). Vasopressin induces phosphorylation of AQP2 at S256, S261, S264 and S269 (488); these serine residues are highly conserved and are located at the C-terminus of AQP2. S256 plays an important role in membrane trafficking of AQP2. Once AQP2-S256 is phosphorylated in the Golgi apparatus, AQP2 is trafficked to the plasma membrane in the vesicles, resulting in the increase of AQP2 abundance (486,489). The function of AQP2-S261 remains unclear but unlike S256, it is not involved in membrane trafficking (490). Previous studies demonstrated that FK506 has no effect on the protein and mRNA expression of AQP2 (491). However, FK506 increased phosphorylation of S256 and S261 in this study, which could increase AQP2 abundance in the plasma membrane and increase water reabsorption.

NKCC2 is responsible for reabsorbing 25 % of NaCl in the TALH and several studies have suggested that it plays a role in the pathogenesis of CNI-induced hypertension. Esteva-Font *et al.* (492) previously reported that hypertension induced by CyA was associated with increased levels of NKCC2 in the loop of Henle of rats, however the functional significance of NKCC2 was not studied. In contrast, Aker *et al.* (493) showed that CyA downregulated NKCC2 and FK506 upregulated NKCC2 activity in MDCK cells. This result was also different from the

Hoorn et al (51) study where NKCC2 and pNKCC2 (pT96, pT101 and pT114) protein levels remained unchanged in FK506-treated mice. Consistent with the Hoorn *et al.* study, FK506 had no effects on the membrane abundance of pNKCC2 in mice used in this thesis. Several NKCC2 phosphosites with unknown functional characterisation were identified in this study. FK506 increased phosphorylation of NKCC2 at Y110 and Y111 and decreased phosphorylation at Y110 and S116, and T114 and S116. These changes induced by FK506 may play a significant role in NKCC2 activity and membrane trafficking, which may provide an explanation for the differences shown in the studies mentioned above.

ACE is an essential component of the RAAS and plays a significant role in blood pressure regulation. ACE inhibitors are widely used as anti-hypertensives and for cardiovascular disease. ACE was phosphorylated by FK506 at S1305 in this study, which is homologous to human S1299 and S1270. CK2 mediates ACE S1299 phosphorylation in humans, which prevents the release of ACE into the plasma (455). Increased phosphorylation of S1305 by FK506 might thus suggest lowered plasma levels of ACE, which might be a compensatory mechanism to reduce further NaCl and water reabsorption.

NHERF1 was initially identified as an exclusive regulatory factor of NHE, but recent studies have shown pleiotropic role of NHERF1 in other solute transport process, such as sodium and phosphate reabsorption in the proximal tubule (456). Being a negative regulator of NHE3 (494), dysregulation in NHERF1 may induce changes in acid-base homeostasis (457), sodium/fluid reabsorption and blood pressure regulation (458,495). Over 20 unique phosphopeptides with different combinations of phosphosites were identified in NHERF1; these phospho-residues have various functional properties and require investigations into their role in renal electrolyte and fluid handling.

3.4.5.2 Metabolic acidosis

Metabolic acidosis is more prevalent in FK506-treated patients than those treated with CyA (54,496). FK506-induced acidosis could be caused by defective bicarbonate (HCO_3^-) reabsorption in the proximal tubule (497) and/or impaired acid (H^+) excretion in the distal tubule (498). However, acid-base homeostasis extends beyond bicarbonate reabsorption and H^+ excretion, and requires several other urinary buffers, such as NH_3 , HPO_4^{2-} , HCO_3^- and $\text{C}_6\text{H}_5\text{O}_7^{3-}$, all of which

carry free H^+ to maintain pH balance in the urine (499). FK506 has been shown to affect transport proteins involved in acid-base transport, such as, NBCe1, NHE3 and NaPi-IIa (457).

Downregulation of NBCe1 has previously been shown to induce metabolic acidosis in knockout mice where HCO_3^- reabsorption was lowered (500). This thesis showed that NBCe1 is heavily phosphorylated in the membrane fractions and phosphorylation was reduced in the cytosolic fractions of FK506-treated mice. Using Protter (406), topology studies of NBCe1 shows that these phosphosites are located in the intracellular domains of NBCe1; this provides an explanation for the difference shown in the two fractions where phosphorylation of these residues may occur after NBCe1 has been inserted into the membrane. The function of these phosphosites require further investigation and they may play an important role in the downregulation of NBCe1 activity and contribute to acidosis following FK506 treatment. In conjunction with lowered NBCe1 levels, FK506 also reduces levels of NHE3 to induce acidosis (457). Apical NHE3 reabsorbs Na^+ into the cell and excretes H^+ in the proximal tubule, and phosphorylation of NHE3-S588 was increased by FK506, suggesting that phosphorylation of S588 might reduce the activity of NHE3 and lower H^+ secretion, thereby causing acidosis.

HPO_4^{2-} is one of the H^+ buffering systems in the urine; linking phosphate transport to acid-base homeostasis. The divalent HPO_4^{2-} is reabsorbed by NaPi-IIa in the proximal tubule, but the titrated monovalent ($H_2PO_4^-$) is not. CNIs cause hyperphosphaturia through reduction in the protein and mRNA expression of NaPi-IIa (59,457) and phosphorylation of NaPi-IIa-T621, S623 and S605 were downregulated by FK506, which might contribute to the decrease in phosphate reabsorption by NaPi-IIa. Under normal conditions, hyperphosphaturia is often associated with metabolic alkalosis as a result of a compensatory mechanism that restores acid-base balance in the tubular fluid by promoting of H^+ secretion. However, since FK506 downregulates NHE3, H^+ secretion is reduced and remains in the blood.

3.4.5.3 Glucose transport

SGLT2 is involved in reabsorbing 97 % of the filtered glucose in the proximal tubule (501). It is the target of SGLT2 inhibitors which block the tubular

reabsorption of glucose, which may be an effective treatment for type 2 diabetes (502). FK506 has been reported to induce post-transplantation diabetes in up to 12 % of patients (503), however, the mechanism for FK506-induced diabetes remains unclear, and the effects of FK506 on SGLT2 have yet to be investigated. A novel phosphosite in SGLT2-S619 was identified in this study and downregulated by FK506. The function of SGLT2-S619 is unknown, however since SGLT2 is already reabsorbing glucose at almost maximal capacity under normal condition, phosphorylation at S619 may increase the membrane abundance of SGLT2, enhancing glucose reabsorption.

AMPK is another regulator with pleiotropic effects on electrolyte homeostasis that are involved in the pathogenesis of the metabolic syndrome (504). AMPK has nutrient sensing abilities and is activated in response to low cellular energy levels to regulate glucose homeostasis (504). In this study, phosphorylation of the AMPK α 1 subunit was increased by FK506 at S486 and T490, and phosphorylation of the AMPK β 1 subunit was shown to be decreased by FK506 at S24; these phosphorylation events may contribute to the dysregulation in glucose homeostasis seen with CNI treatments.

3.4.5.4 Potassium homeostasis

FK506 alters potassium transport in the kidneys and induces hyperkalaemia. KCNJ16 is expressed in both proximal and distal tubules. KCNJ16 null mice have a hypokalaemic phenotype, demonstrating the importance of KCNJ16 in potassium homeostasis (505). This current study identified two novel phosphosites S363 and S366 in KCNJ16, which were downregulated by FK506. A phosphosite, S1032 in KCC3 was also detected; decrease in the phosphorylation of which was found to be mediated by FK506. These phosphosites may have suppressive effects on the activity of these potassium transporters under normal conditions, therefore when FK506 decreases phosphorylation of these residues, potassium reabsorption increases.

3.4.5.5 Ubiquitous transport proteins

Na^+/K^+ -ATPase maintains Na^+ and K^+ across the cell membrane and provides an electrochemical gradient that drives the active transport of electrolytes. CNIs reduce basolateral Na^+/K^+ -ATPase abundance in the kidneys of rats (506) and

this reduction is likely to affect the ion transport systems that rely on Na⁺/K⁺-ATPase as a driving force. Phosphorylation of the γ subunit of Na⁺/K⁺-ATPase was reduced by FK506 at S15. Mutations in the γ -subunit reduce the binding of the γ -subunit to the pump. This results in reduced Na⁺ and K⁺ affinity, decreasing in the activity of Na⁺/K⁺-ATPase (161,507), causing hypomagnesaemia in IDH. Hypomagnesaemia is a well-known effect of FK505, and of course occurred in the animals used in this study.

3.4.6 Future experiments

The phosphoproteome profile of the FK506-dysregulated renal cortices generated in this study covered all segments of the nephron found in the cortex; for a coverage with higher specificity of the PCT or DCT, cells from these segments can be isolated through the use of cell markers and flow cytometry. For example, the co-labelling of CD10 and CD13 have been used for cell sorting of proximal tubular epithelial cells (508). A similar method has also been used to extract distal tubule and collecting duct cells from human kidneys (509). The epithelial membrane antigen (EMA) is expressed in the distal tubule and the collecting duct, and it is most abundant at the TALH. EMA expression gradually decrease along the distal tubule with the lowest expression at the collecting duct. Therefore, purification of EMA-positive cells with the strongest expression can separate distal tubule cells from collecting duct cells (509).

Alternatively, manual microdissection is a valuable tool in isolating desired tissue segments (510). However, this approach is time consuming and requires great precision, which makes this technique less reliable than newer approaches, such as, laser capture microdissection (LCM) (511,512). LCM applies a thermoplastic film, made of ethylene vinyl acetate polymers, onto tissue sections pre-stained with haematoxylin and eosin. An inverted microscope is used to produce localised heat-activation of the film, allowing targeted cells to fuse with the film, resulting in selective procurement of targeted cells in a heterogeneous tissue. LCM is becoming the method of choice in isolating specific cells in heterogeneous tissues due to its reliability, versatility and high throughput. However, LCM processed samples are subjected to processing-induced changes, for example, the dyes used to stain tissue samples can interfere with two-dimensional polyacrylamide gel electrophoresis used in proteomic analysis (513).

FK506-dysregulated proteins identified in this study require verification and investigation into the functional properties and changes in the phosphorylation of specific residues, which can be determined through Western blot analysis or immunohistochemistry using phosphosite specific antibodies. However, many phosphosite specific antibodies are not often commercially available, which means that customised antibodies are required; this can be time consuming and costly, therefore, functional characterisation of these phospho-residues can be beneficial prior to antibody production. In order to investigate the functional properties of specific phospho-residues, such as S122 found in NCC, uptake studies using ^{22}Na can be used to determine and evaluate their role. As an example, S122 is highly conserved in NCC, but the functional properties of NCC-S122 are currently unknown. An NCC-S122A mutant could be cloned and co-expressed with the WNK kinases and calcineurin in uptake studies to investigate its role in NCC activity (121,192).

The insulin/PI3K/AKT pathway has been shown to activate NCC through WNK-SPAK/OSR1 (471). To confirm that both PI3K and AKT are involved in the cascade, a PI3K inhibitor (e.g. GDC-0941) (514) and an AKT inhibitor (e.g. MK-2206) (515) could be used in conjunction with CNIs to investigate their effects on pNCC levels in mice. Since the activity of the WNK kinases is defined by phosphorylation and AKT is their upstream regulator, further studies are required to investigate the effects of AKT on the WNK kinases. Using a similar approach to previous oocyte studies, AKT, the WNK kinases, NCC and other members of the cascade can be co-expressed in oocytes and the activity of NCC can be measure using ^{22}Na , to investigate the interactions of these proteins (121,192). AKT phospho-S124 and phospho-S126 identified in this study require further investigation to determine their role in AKT activity, mutation at these residues in an AKT construct can be used to identify their function, which could then be compared to residues with established function such as, T308 and S473.

To investigate whether the FK506-dysregulated proteins identified in this study are also dysregulated in humans, biopsies from CNI-treated patients could be used for phosphoproteome profiling. Alternatively, the use of urinary exosomes and mass spectrometry have been well documented and have shown great potential for identifying diseases and evaluating disease progression (426,516). Therefore, urinary exosomes derived from CNI-treated subjects could also be

used for profiling and possibly be used for identifying biomarkers for the metabolic syndrome.

Chapter 4. The effects of FK506 on distal renal calcium handling

4.1 Introduction

Hypercalciuria can cause serious health concerns, such as kidney stones and bone demineralisation. Kidney stones affect around 1 in 10 people in the U.K. (35) and the incidence and prevalence is increasing globally (32–34). Bone demineralisation can lead to osteoporosis, which has been reported to cause over 9 million bone fractures per year (31). Kidney stone disease and osteoporosis are strongly associated with the highly prevalent metabolic syndrome (26,27), therefore it is important to understand the underlying mechanisms that govern calcium handling in the kidneys.

The side effects of CNIs resemble FHt and they both cause hypercalciuria and hypertension. CNI-induced hypercalciuria was thought to be caused by the decrease in mRNA and protein expression of TRPV5 and calbindin-D28K, resulting in a reduction in calcium reabsorption (57). CNI-induced hypertension is caused by the increase in NCC activity, resulting in an increase in sodium chloride reabsorption (51). The inhibition of calcineurin dysregulates multiple renal transport pathways, suggesting that these pathways are interlinked. Other evidence that supports the hypothesis of a close relationship between sodium and calcium handling in the DCT are demonstrated in FHt patients with mutations in WNK4 and KLHL3 (60,390,392). Both of these mutations increase WNK4 abundance and activity in the DCT, and activates SPAK and NCC. This raises the possibility that WNK4 may induce hypercalciuria through SPAK-NCC activation.

Thiazide diuretics are widely used in FHt patients and specifically target NCC to decrease water and sodium reabsorption but they can cause hypocalciuria and hypercalcemia as side effects (385). Several studies have investigated the effects of thiazides on the regulatory and transport proteins involved in calcium handling in the DCT. However, its effects remain controversial due to a number of studies showing conflicting results (64,386,388), such as that thiazides may or may not increase TRPV5 and calbindin-D28K expression, and that the distal tubules may or may not be solely responsible for thiazide-induced hypocalciuria. Similar to patients treated with thiazides, hypocalciuria is also present in Gitelman patients. In a NCC knock-in mouse model of Gitelman syndrome, mRNA expression of TRPV5, and TRPV6 were increased. Increased abundance of the calcium

channels suggests that calcium influx may increase, causing hypocalciuria in Gitelman patients. These studies provide evidence to support an underlying mechanism that governs both sodium and calcium handling in the DCT.

4.1.1 Aims

- To investigate the effects of FK506 on calcium transport and regulatory proteins in the DCT
- To identify a possible unifying mechanism for calcium and sodium reabsorption in the DCT.

4.2 Materials and methods

CNI-induced hypercalciuria is thought to be caused by altered calcium handling in the distal nephron (57). The effects of FK506 and HSD on the expression of calcium transport and regulatory proteins were investigated. In addition, sodium transport proteins were also examined to investigate the relationship between sodium and calcium handling in the DCT.

4.2.1 Animals

Male C57BL/6J mice of 6-8 weeks were divided into four treatment groups: vehicle or FK506 fed on a normal diet, and vehicle or FK506 fed on a HSD containing additional 1.5 % NaCl. For further details regarding the treatments, diets, housing conditions and the Schedule 1 protocol for euthanasia, see Chapter 3, Section 3.2.1. For details regarding electrolyte measurements in serum and urine, see Chapter 3, Section 3.2.2.

4.2.2 Real-time PCR

Mouse kidneys were homogenised with liquid nitrogen using a pestle and mortar, under RNase free conditions. Powdered kidney tissue (100 mg) was added to 1 ml of Trizol reagent (Sigma-Aldrich Co., Ltd., Poole, UK) and incubated for 5 minutes at room temperature. RNA was obtained by phenol-chloroform extraction and precipitated with isopropanol. The concentration and purity of RNA was determined using a NanoDrop-1000 spectrophotometer (Labtech International, UK), samples contaminated with impurities were discarded. RNA samples were stored at -80 °C.

RNA samples (1 µg) were treated with 2 units of DNase I (PCR Biosystems, Prague, Czech Republic) and 1 X DNaseI buffer [10 mM Tris at pH 7.5, 2.5 mM MgCl₂, 0.5 mM CaCl₂] (PCR Biosystems, Prague, Czech Republic). This mixture was incubated at room temperature for 15 minutes. DNase I was inactivated by adding 5 mM EDTA (Ethylenediaminetetraacetic acid) and incubation at 65 °C for 10 minutes. RNA samples (1 µg) were reverse transcribed into cDNA using a qPCRBIO cDNA synthesis kit (PCR Biosystems, Prague, Czech Republic) according to the manufacturer's protocol. Each transcription reaction was run in parallel with a negative control reaction lacking reverse transcriptase; samples were stored at -20 °C.

One microlitre of the resulting cDNA transcripts was amplified in a real-time quantitative PCR (RT-qPCR) reaction using primers from the RT² qPCR Primer Assays (Qiagen, Crawley, UK), a RT-qPCR master mix from the Applied Biosystems SYBR Green RT-qPCR reagents kit (Fisher Scientific, Loughborough, UK) and the Roche LightCycler 96 System (Roche, Lewes, UK); reactions were performed according to the manufacturer's protocol. RT-qPCR reaction underwent 35 cycles following the programme shown in Table 4.2-1. mRNA expression was quantified and a ratio of the relative abundance of each gene against the housekeeping gene β -actin was calculated using the LightCycler Relative Quantification software (Roche Diagnostics, Lewes, UK). The PCR products of these samples were ran on a 2 % agarose-TAE gel containing 0.5 μ g/ml ethidium bromide (Sigma-Aldrich Co., Ltd., Poole, UK) and imaged with a UV transilluminator (Peqlab, Netherlands) to check for correct size of amplicons.

4.2.3 Western blot analysis

The extraction of mouse kidney proteins and Western blotting were performed according to Chapter 3, Section 3.2.3 and Section 3.2.4. Membranes were incubated with primary antibody in PBS-T against the following proteins: TRPV5 [1:500] (kind gift from C. Wagner), NCX1 [1:1000] (Swant, Switzerland), calnexin [1:1000] (Proteintech, USA), ADCY6 (ab192652) [1:500] and β -actin (AC-15) [1:2000] (both from Abcam, Cambridge, UK), NCC (1-100) [1:500] and phospho-NCC (T60) [1:300] (both from MRC-PPU, Dundee, UK), and calbindin-D28K (c-20) [1:1000], PMCA (F-3) [1:1000], R-type Ca²⁺ CP α 1E (C-20) [1:1000], Na⁺/K⁺-ATPase (H-300) [1:1000], PKC α (sc-8393) [1:400], PKC β 1 (sc-209) [1:200], PKC δ (sc-937) [1:500], PKC ϵ (sc-214) [1:500] and phospho-PKC β 1 (T641) [1:200] (all from Santa Cruz Biotechnology, UK). For details on densitometry, see Chapter 2, Section 2.2.5.3.

4.2.1 Statistics

Statistical analysis was performed by unpaired t-tests in datasets with two treatment groups or ANOVA followed by a Bonferroni's multiple comparison test in datasets with three or more treatment groups. The data are presented as means \pm SEM.

Table 4.2-1 RT-qPCR programme

<u>RT-qPCR Programme</u>		
Pre-incubation	95 °C	10 minutes
35 cycles of Amplification	95 °C	10 seconds
	60 °C	10 seconds
	72 °C	10 seconds
High Resolution Melting	95 °C	10 seconds
	65 °C	60 seconds
	97 °C	continuous

4.3 Results

4.3.1 Effects of FK506 on transcripts of respective calcium regulatory and transport proteins

The DCT is a principal site of sodium and calcium reabsorption. FK506 and thiazide diuretics alter sodium chloride handling through NCC and dysregulate calcium homeostasis, causing hypercalciuria (57) and hypocalciuria (385) respectively. To determine the effects of FK506 on these proteins, the mRNA expression and protein expression of calcium regulatory and transport proteins expressed in the distal tubules were examined.

Renal mRNA expression of calbindin-D28K, calcineurin A α , TRPV5, NCX1 and PMCA1 and 4 were determined through RT-qPCR. Similar to previous studies, FK506 significantly decreased mRNA expression of calbindin-D28K (57). In contrast, FK506 significantly increased mRNA expression of TRPV5. The decrease in calbindin-D28K mRNA expression in FK506-treated mice indicates low intracellular calcium level, however, the increase in TRPV5 mRNA expression suggests an increase in calcium reabsorption in the distal nephron. FK506 did not significantly alter the mRNA expression of calcineurin, NCX1, PMCA1 and PMCA4 (Figure 4.3-1).

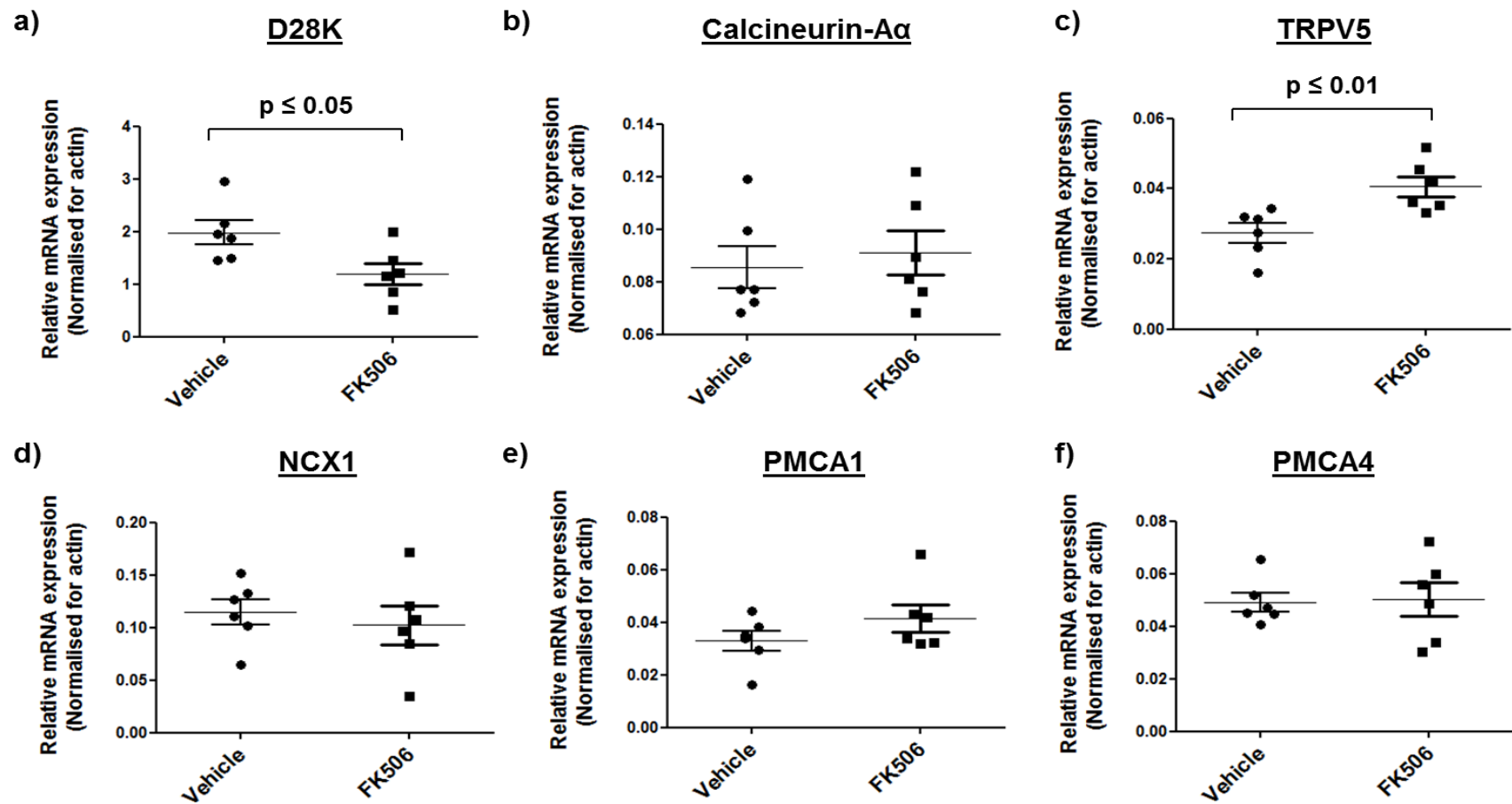


Figure 4.3-1 mRNA expression of calcium regulatory and transport proteins in the kidneys post-FK506 treatment

RT-qPCR quantification of a) calbindin-D28K, b) Calcineurin-A α , c) TRPV5, d) NCX1, e) PMCA and f) PMCA4 in kidneys of FK506 or vehicle treated mice. Data are presented as means \pm SEM, n=6. Statistical values were calculated using an unpaired t-test.

4.3.2 Effects of FK506 and a high salt diet on calcium transport and buffering proteins in the DCT

To determine whether the changes in mRNA expression would result in changes in the expression of the respective proteins, Western blot analysis was used to quantify the protein expression of TRPV5, calbindin-D28K, NCX1 and PMCA in the kidneys of FK506-treated mice. Since FK506 and thiazides both target NCC, a high NaCl diet (HSD) was fed to mice treated with vehicle or FK506 to investigate the relationship between sodium and calcium handling. In addition, the protein expression of NCC, pNCC and the Na⁺/K⁺-ATPase (493,506) of mice treated with FK506 were re-examined along with FK506-treated mice that were fed a HSD. To confirm the effectiveness of the treatment, the net urinary excretion of Ca²⁺ and serum Mg²⁺ levels of vehicle, HSD, FK506 and FK506 + HSD treated mice were determined and are depicted in Table 4.3-1. FK506-treated mice and FK506 + HSD treated mice had hypercalciuria and hypomagnesaemia. HSD alone did not significantly alter net calcium excretion or serum magnesium levels, however the effect of HSD significantly enhanced the net calcium excretion of FK506-treated mice.

The protein expression of TRPV5, calbindin-D28K, NCX1 and PMCA in mice fed a HSD or/and treated with FK506 were determined through Western blot analysis. Previously FK506 was shown to decrease mRNA expression (57) and protein expression of TRPV5 (51,57); in contrast, this study showed that the mRNA expression of TRPV5 was increased in FK506-treated mice (Figure 4.3-1) and the protein expression of TRPV5 remained unchanged (Figure 4.3-2). Similar to the FK506 treatment, TRPV5 protein expression in FK506 + HSD treated mice remained unchanged. The effect of HSD alone appears to increase TRPV5, however this effect was not statistically significant ($p=0.07$).

Similar to previously studies (57), FK506 decreased mRNA (Figure 4.3-1) and protein expression of calbindin-D28K (Figure 4.3-3) and this effect was also shown in mice treated with FK506 and fed a HSD in this chapter. The difference in calbindin-D28K protein expression between FK506 and FK506 + HSD treated mice was not statistically significant ($p=0.051$); however, there was a tendency for HSD to enhance the effect of FK506. HSD alone increased levels of calbindin-D28K. These results indicate that FK506 may only affect calbindin-D28K on a

transcriptional level, which results in a lower protein expression of calbindin-D28K in the kidney.

Next, the effect of FK506 on the basolateral calcium transport proteins were examined. Western blot analysis of NCX1 (Figure 4.3-4) and PMCA (Figure 4.3-5) revealed that FK506 significantly increased the membrane abundance of NCX1 and PMCA. Western blot analysis also revealed that the effect of FK506 on NCX1 and PMCA was not enhanced by HSD. Instead, expression of NCX1 in mice treated with FK506 and fed a HSD revealed that a HSD partially decreased the effect of FK506. In contrast, PMCA levels in FK506 + HSD treated mice were restored to baseline levels. Mice on a HSD were shown to have increased levels of NCX1 while the levels of PMCA remained unchanged.

Table 4.3-1 Calcium creatinine ratio and serum magnesium levels of FK506 or vehicle treated mice

Treatment group (n=5)	Calcium creatinine ratio (mmol/mmol)	Serum Magnesium levels (mmol/l)
Vehicle	0.057 ± 0.012	1.010 ± 0.068
HSD	0.035 ± 0.010	0.930 ± 0.023
FK506	0.101 ± 0.010 * #	0.800 ± 0.023 *
FK506 + HSD	0.172 ± 0.014 ** †	0.772 ± 0.044 *

The effect of FK506 treatment on the calcium creatinine ratio and serum magnesium level in mice. FK506-treated mice administrated 2mg/kg/day FK506 for two weeks by daily IP injections and HSD (1.5 % NaCl) were fed to 50 % of vehicle or FK506-treated mice. Statistical values were calculated using an ANOVA followed by a Bonferroni's multiple comparison test. Data are presented as means ± SEM. * P<0.05 vs. vehicle; # P<0.05 vs. HSD; ** P<0.01 vs. FK506; † P<0.001 vs. vehicle and vs. HSD.

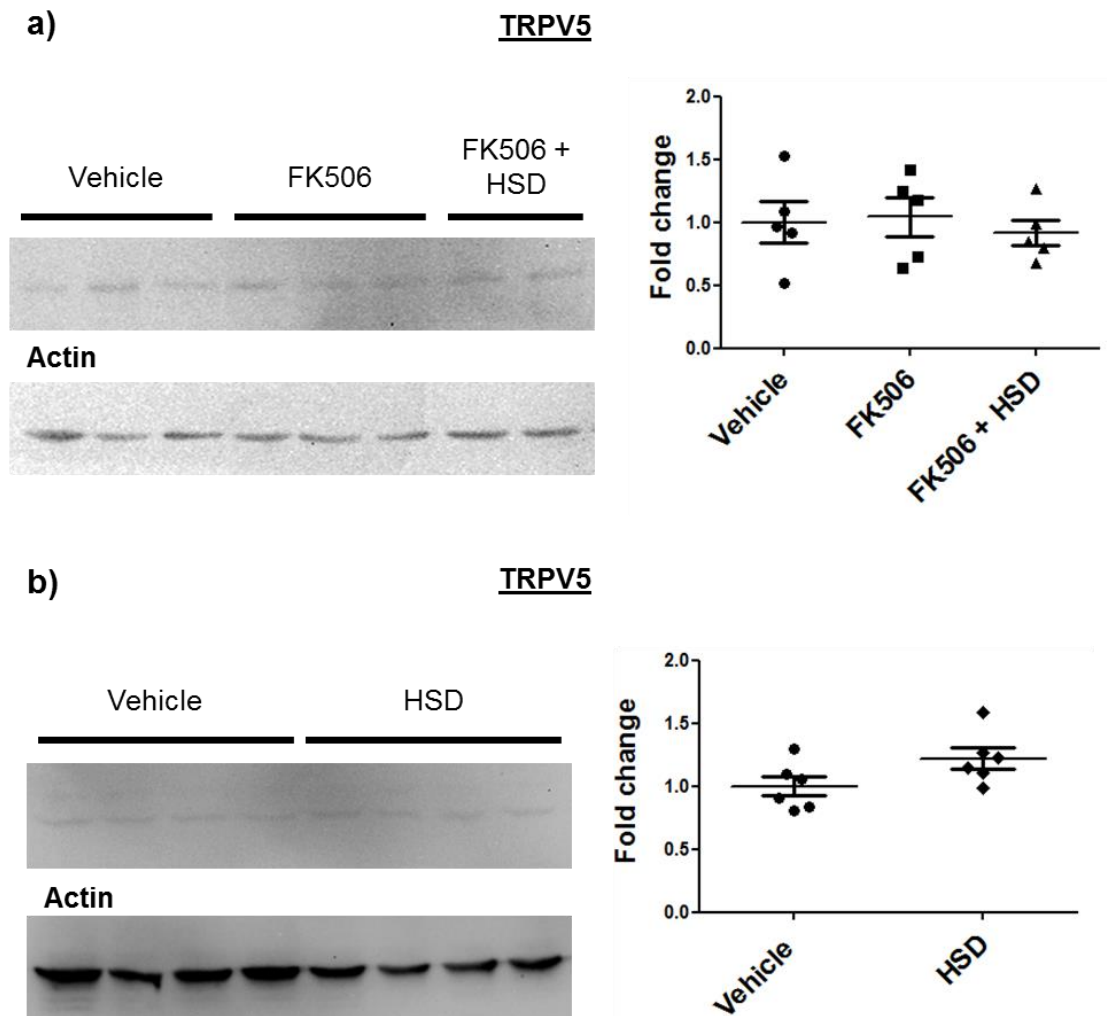


Figure 4.3-2 The effects of FK506 and HSD on TRPV5 protein expression in the kidney membrane

Western blot analysis was performed on kidney membranes of vehicle, a) FK506 or FK506 + HSD and b) HSD treated mice. Representative blots (left) and protein expression (right) of TRPV5 are shown. Band intensities of TRPV5 were quantified and normalised to those of β -actin and expressed as a fold change of the control mean; data are presented as means \pm SEM, n=5-6. Statistical values were calculated using an unpaired t-test for vehicle vs. HSD treatment and ANOVA followed by a Bonferroni's multiple comparison test for vehicle vs. FK506 vs. FK506 + HSD treatment.

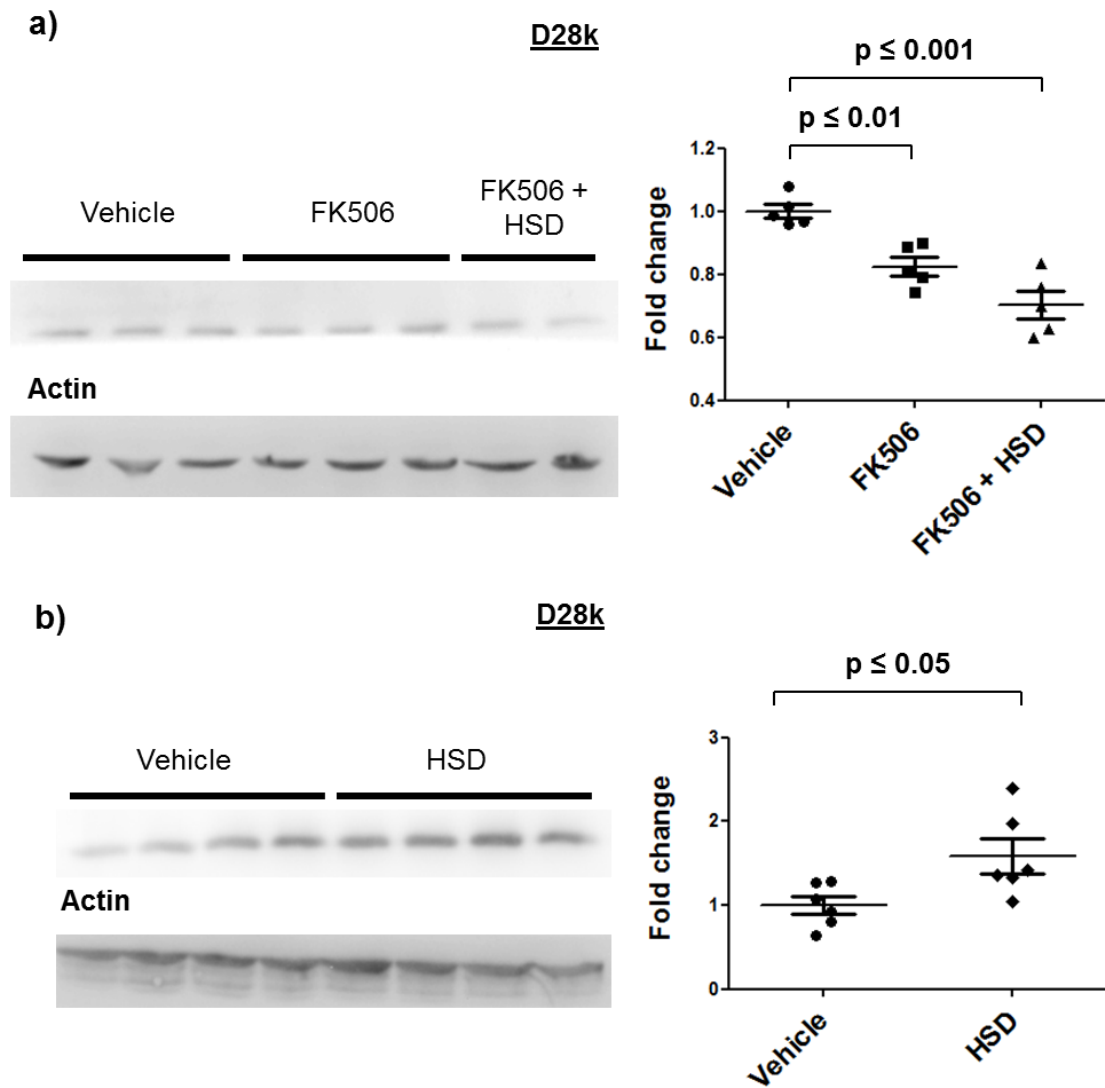


Figure 4.3-3 The effects of FK506 and HSD on calbindin-D28K protein expression in the kidney

Western blot analysis was performed on kidneys of vehicle, a) FK506 or FK506 + HSD and b) HSD treated mice. Representative blots (left) and protein expression (right) of calbindin-D28K are shown. Band intensities of calbindin-D28K were quantified and normalised to those of β -actin and expressed as a fold change of the control mean; data are presented as means \pm SEM, $n=5-6$. Statistical values were calculated using an unpaired t-test for vehicle vs. HSD treatment and ANOVA followed by a Bonferroni's multiple comparison test for vehicle vs. FK506 vs. FK506 + HSD treatment.

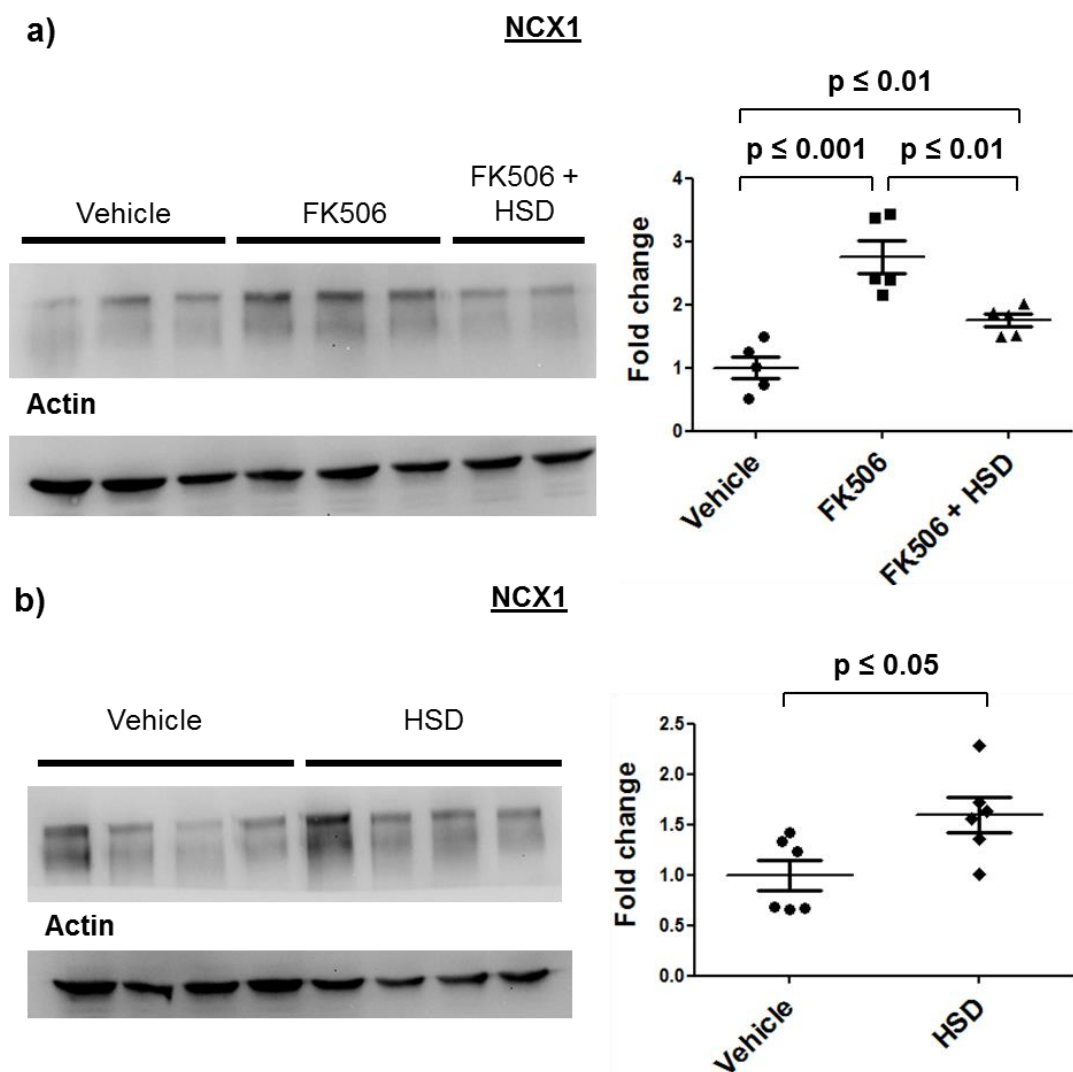


Figure 4.3-4 The effects of FK506 and HSD on NCX1 protein expression in the kidney membrane

Western blot analysis was performed on kidney membranes of vehicle, a) FK506 or FK506 + HSD and b) HSD treated mice. Representative blots (left) and protein expression (right) of NCX1 are shown. Band intensities of NCX1 were quantified and normalised to those of β -actin and expressed as a fold change of the control mean; data are presented as means \pm SEM, n=5-6. Statistical values were calculated using an unpaired t-test for vehicle vs. HSD treatment and ANOVA followed by a Bonferroni's multiple comparison test for vehicle vs. FK506 vs. FK506 + HSD treatment.

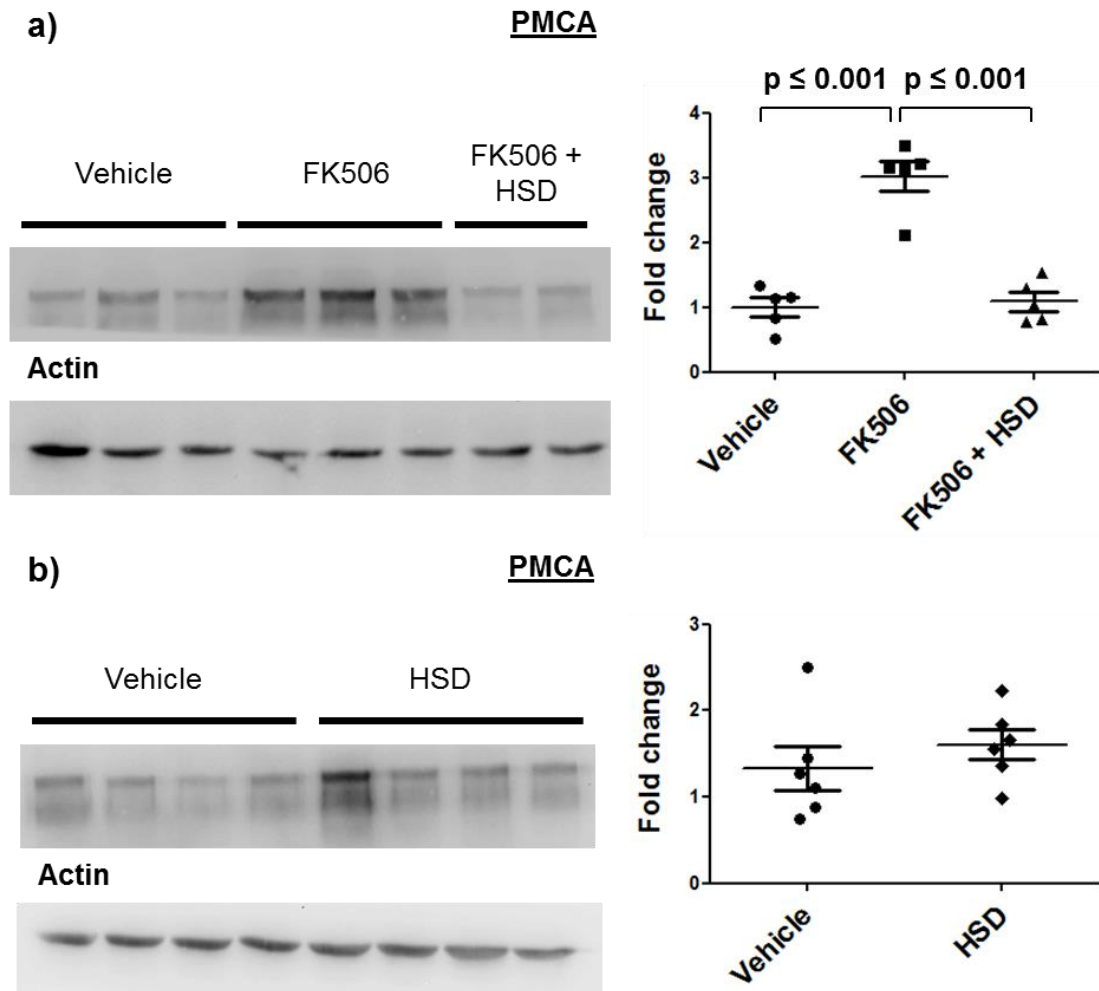


Figure 4.3-5 The effects of FK506 and HSD on PMCA1/4 protein expression in the kidney membrane

Western blot analysis was performed on kidney membranes of vehicle, a) FK506 or FK506 + HSD and b) HSD treated mice. Representative blots (left) and protein expression (right) of PMCA are shown. Band intensities of PMCA were quantified and normalised to those of β -actin and expressed as a fold change of the control mean; data are presented as means \pm SEM, n=5-6. Statistical values were calculated using an unpaired t-test for vehicle vs. HSD treatment and ANOVA followed by a Bonferroni's multiple comparison test for vehicle vs. FK506 vs. FK506 + HSD treatment.

4.3.3 Effects of FK506 and a high salt diet on DCT sodium transport proteins

Dietary NaCl affects calcium transport protein expression in the DCT, therefore, the effect of FK506 on sodium transport proteins and regulatory proteins involved in both calcium and sodium handling were investigated. The effect of FK506 on the protein expression of NCC and pNCC have previously been examined in Chapter 3, Section 3.3.1. This chapter examines the effect of a HSD on NCC, pNCC and Na⁺/K⁺-ATPase in kidneys of mice treated with vehicle and FK506.

Western blot analysis revealed that FK506, FK506 with HSD and HSD treatments have no significant effects on NCC levels (Figure 4.3-6). Next, Western blot analysis of pNCC in mice fed on a HSD and treated with FK506 showed a significant increase in pNCC expression when compared to the control. However, the difference between FK506 with HSD and FK506 alone was not significant ($p=0.13$), which indicates that HSD did not significantly enhance the effect of FK506. The abundance of pNCC in mice fed on a HSD was not significantly different than those fed on a normal diet (Figure 4.3-7).

In keeping with previous studies (493,506), protein expression of Na⁺/K⁺-ATPase decreased in FK506-treated mice. The effect of HSD on mice treated with FK506 was not significantly different from those treated with FK506 alone ($p=0.127$); however, a slight increase in Na⁺/K⁺-ATPase was observed in mice treated with FK506 + HSD. Mice fed a HSD showed a significant increase in the protein abundance of Na⁺/K⁺-ATPase (Figure 4.3-8).

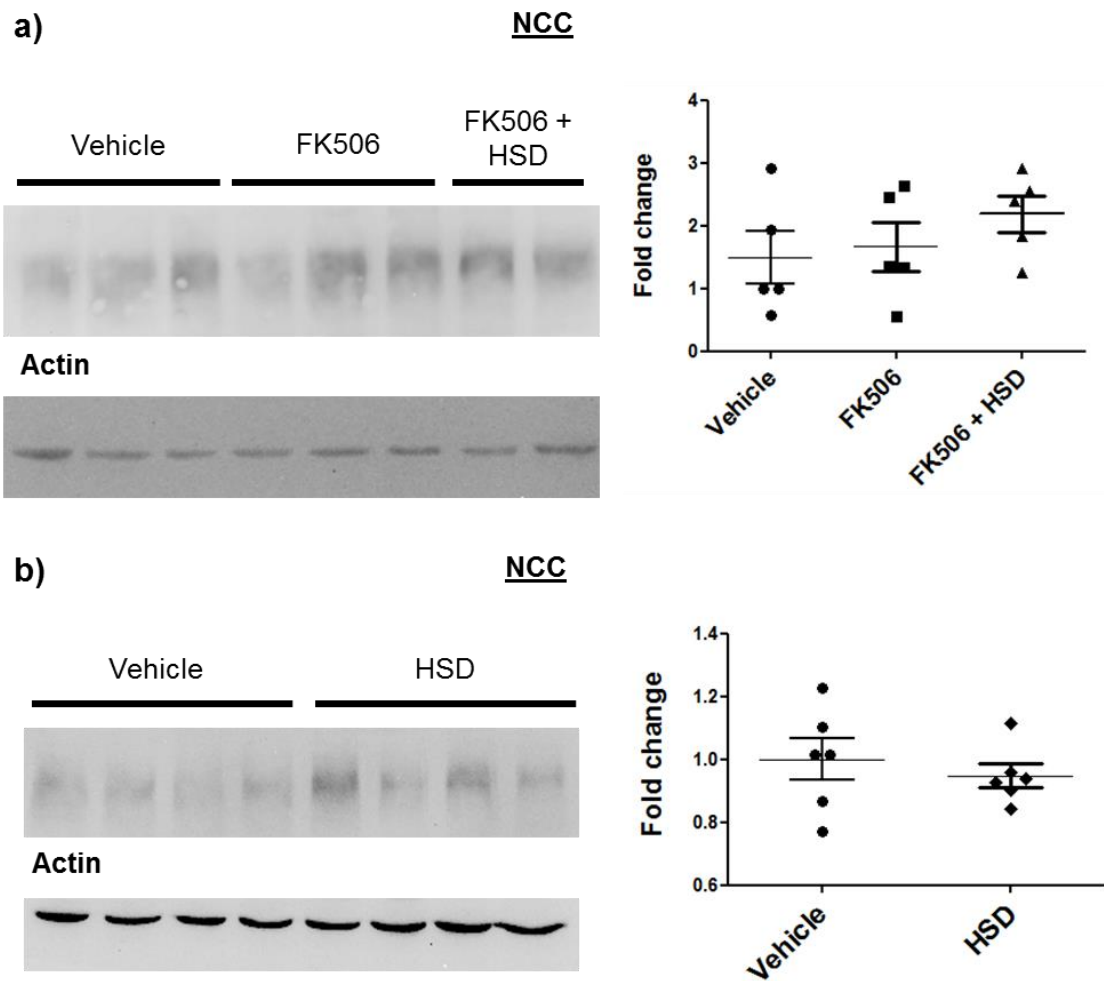


Figure 4.3-6 The effects of FK506 and HSD on NCC protein expression in the kidney membrane

Western blot analysis was performed on kidney membranes of vehicle, a) FK506 or FK506 + HSD and b) HSD treated mice. Representative blots (left) and protein expression (right) of NCC are shown. Band intensities of NCC were quantified and normalised to those of β -actin and expressed as a fold change of the control mean; data are presented as means \pm SEM, n=5-6. Statistical values were calculated using an unpaired t-test for vehicle vs. HSD treatment and ANOVA followed by a Bonferroni's multiple comparison test for vehicle vs. FK506 vs. FK506 + HSD treatment.

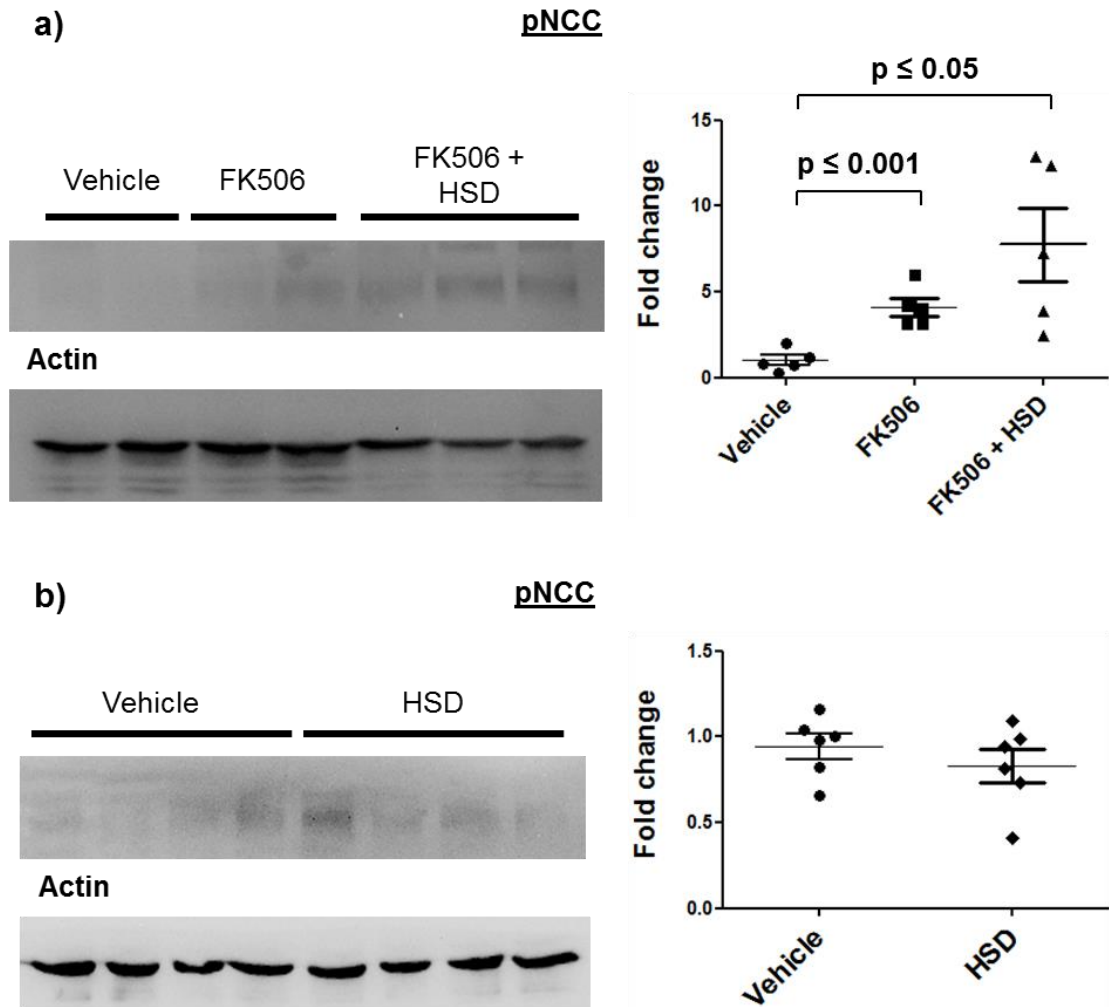


Figure 4.3-7 The effects of FK506 and HSD on pNCC protein expression in the kidney membrane

Western blot analysis was performed on kidney membranes of vehicle, a) FK506 or FK506 + HSD and b) HSD treated mice. Representative blots (left) and protein expression (right) of pNCC are shown. Band intensities of pNCC were quantified and normalised to those of β -actin and expressed as a fold change of the control mean; data are presented as means \pm SEM, n=5-6. Statistical values were calculated using an unpaired t-test for vehicle vs. HSD treatment and ANOVA followed by a Bonferroni's multiple comparison test for vehicle vs. FK506 vs. FK506 + HSD treatment.

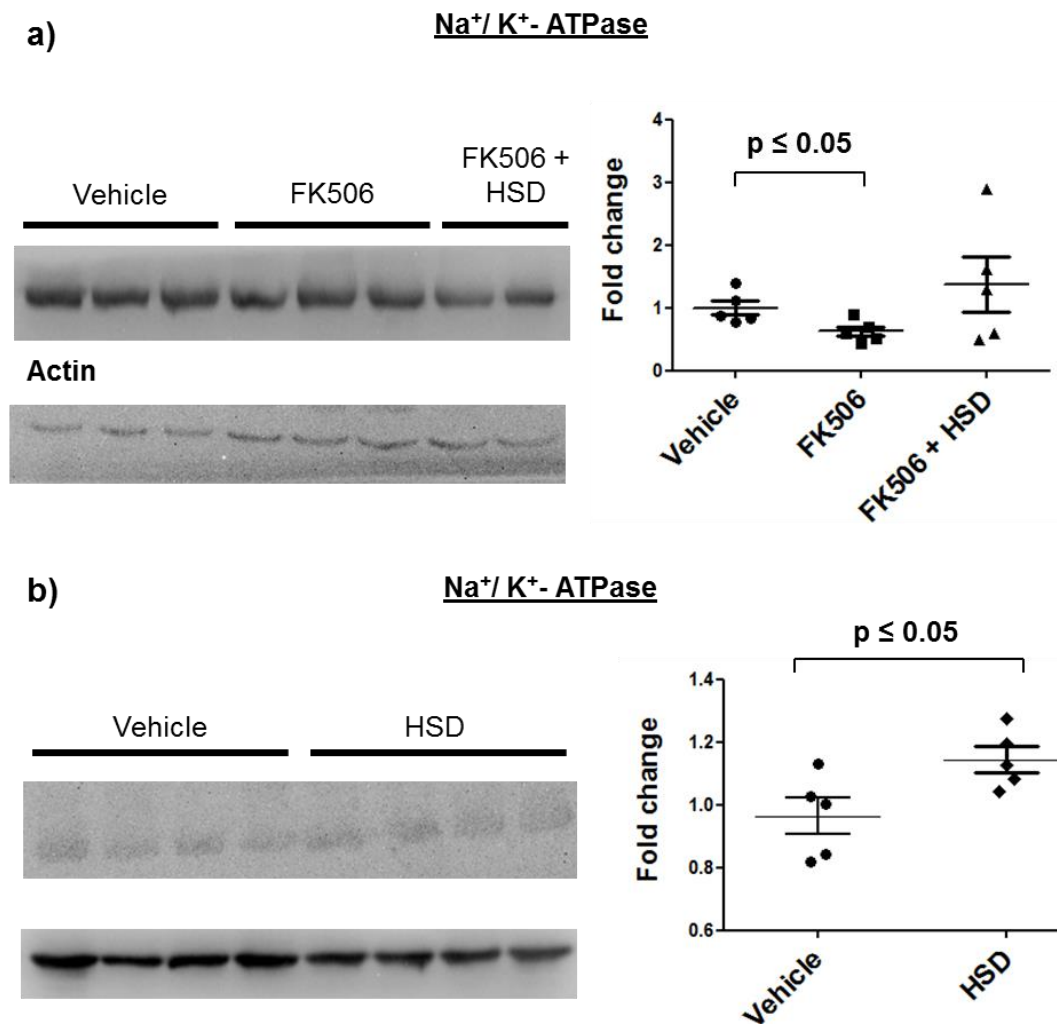


Figure 4.3-8 The effects of FK506 and HSD on Na⁺/K⁺-ATPase protein expression in the kidney membrane

Western blot analysis was performed on kidney membranes of vehicle, a) FK506 or FK506 + HSD and b) HSD treated mice. Representative blots (left) and protein expression (right) of Na⁺/K⁺-ATPase are shown. Band intensities of Na⁺/K⁺-ATPase were quantified and normalised to those of β-actin and expressed as a fold change of the control mean; data are presented as means ± SEM, n=5-6. Statistical values were calculated using an unpaired t-test for vehicle vs. HSD treatment and ANOVA followed by a Bonferroni's multiple comparison test for vehicle vs. FK506 vs. FK506 + HSD treatment.

4.3.4 Effects of FK506 and a high salt diet on PKC

PTH is a regulator of sodium and calcium handling in the DCT known to downregulate NCC and upregulate TRPV5 activity (308,517). PTH signals PKC to increase TRPV5 expression on surface membranes and WNK4 was reported to enhance this process (315,337). PKC phosphorylates KLHL3 to prevent WNK4 degradation and increases phosphorylation of WNK4, which may increase NCC activity through SPAK/OSR1 signalling pathway (244,261). The effects of FK506 on the protein expression of PKC (α , β 1, δ and ϵ) and phospho-PKC β 1 were examined and quantified using Western blot analysis.

The protein expression of PKC β 1 (Figure 4.3-9) and PKC δ (Figure 4.3-10) remained unchanged in mice treated with FK506, FK506 with HSD and HSD alone. The effect of FK506 alone did not alter the protein expression of PKC ϵ , however, the levels of PKC ϵ increased significantly in FK506-treated mice fed a HSD. The protein expression of PKC ϵ in mice fed a HSD remained unchanged (Figure 4.3-11). The levels of PKC α and phospho-PKC β 1 were also examined, however Western blot failed to detect signals using these antibodies under several conditions. The potential causes of this include low protein expression in the renal cortices and antibodies being incompatible with the Western blot technique, therefore the effects of FK506 on PKC α and phospho-PKC β 1 remain inconclusive.

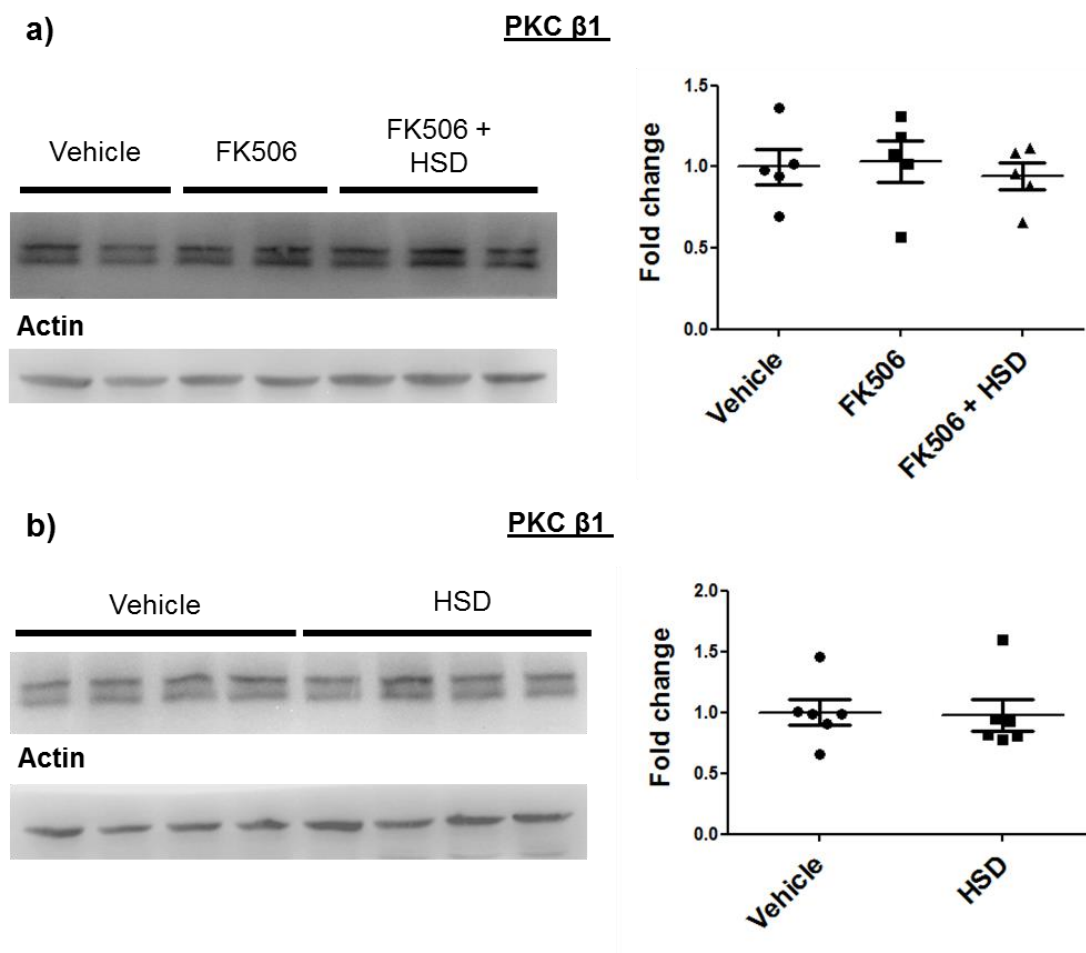


Figure 4.3-9 The effects of FK506 and HSD on PKC β 1 protein expression in the kidney

Western blot analysis was performed on kidneys of vehicle, a) FK506 or FK506 + HSD and b) HSD treated mice. Representative blots (left) and protein expression (right) of PKC β 1 are shown. Band intensities of PKC β 1 were quantified and normalised to those of β -actin and expressed as a fold change of the control mean; data are presented as means \pm SEM, n=5-6. Statistical values were calculated using an unpaired t-test for vehicle vs. HSD treatment and ANOVA followed by a Bonferroni's multiple comparison test for vehicle vs. FK506 vs. FK506 + HSD treatment.

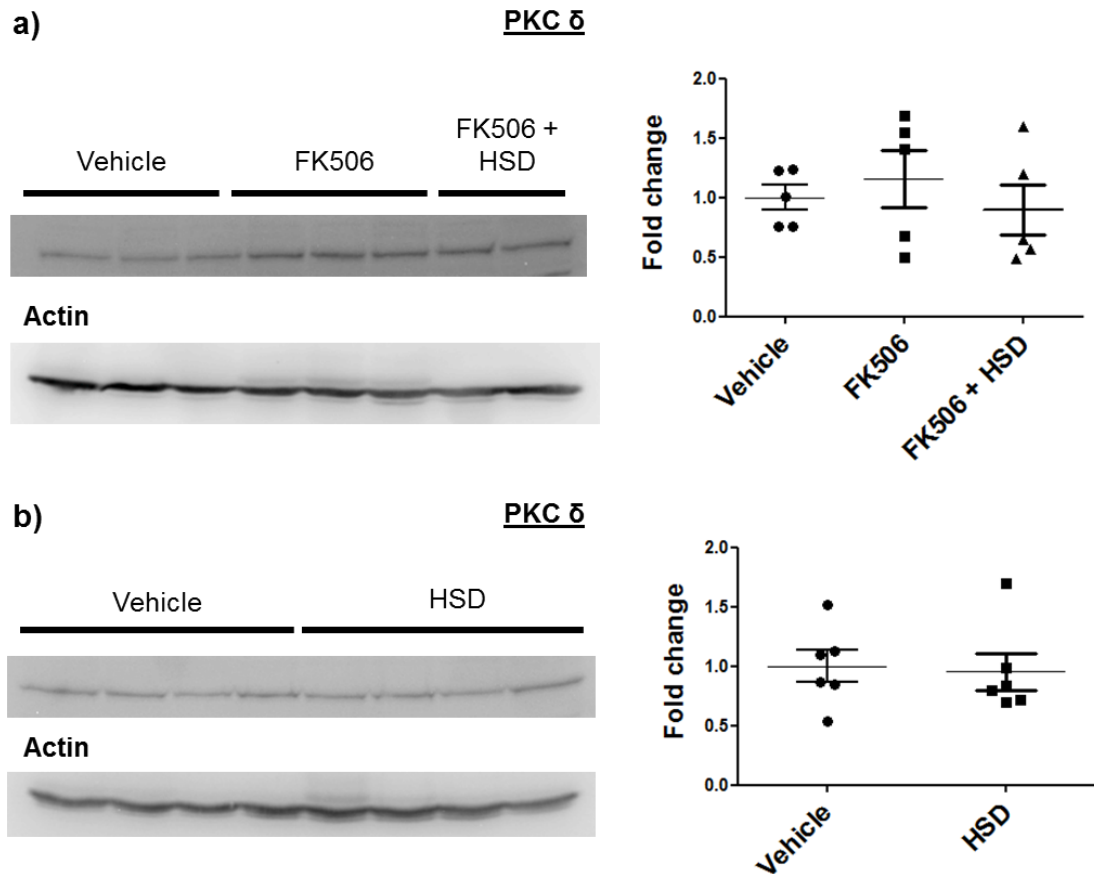


Figure 4.3-10 The effects of FK506 and HSD on PKC δ protein expression in the kidney

Western blot analysis was performed on kidneys of vehicle, a) FK506 or FK506 + HSD and b) HSD treated mice. Representative blots (left) and protein expression (right) of PKC δ are shown. Band intensities of PKC δ were quantified and normalised to those of β -actin and expressed as a fold change of the control mean; data are presented as means \pm SEM, n=5-6. Statistical values were calculated using an unpaired t-test for vehicle vs. HSD treatment and ANOVA followed by a Bonferroni's multiple comparison test for vehicle vs. FK506 vs. FK506 + HSD treatment.

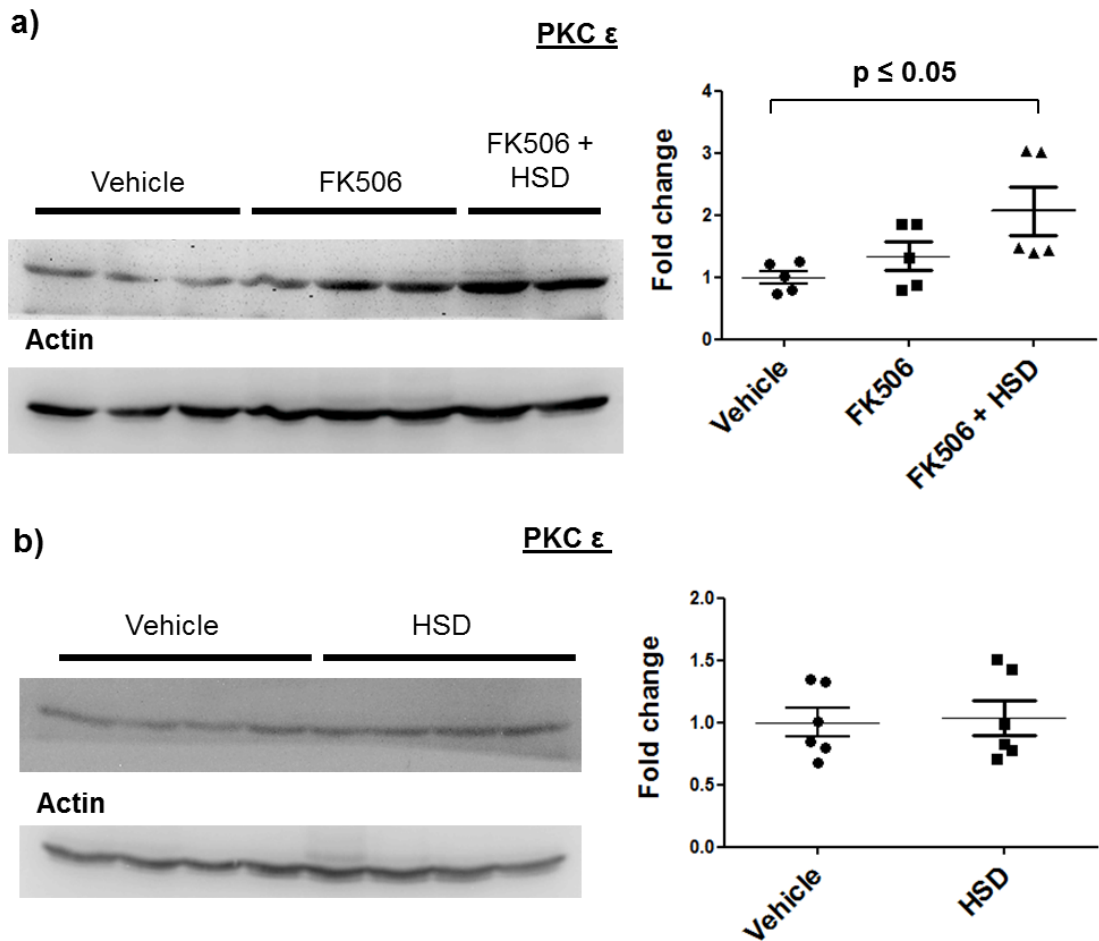


Figure 4.3-11 The effects of FK506 and HSD on PKC ϵ protein expression in the kidney

Western blot analysis was performed on kidneys of vehicle, a) FK506 or FK506 + HSD and b) HSD treated mice. Representative blots (left) and protein expression (right) of PKC ϵ are shown. Band intensities of PKC ϵ were quantified and normalised to those of β -actin and expressed as a fold change of the control mean; data are presented as means \pm SEM, n=5-6. Statistical values were calculated using an unpaired t-test for vehicle vs. HSD treatment and ANOVA followed by a Bonferroni's multiple comparison test for vehicle vs. FK506 vs. FK506 + HSD treatment.

4.3.5 Phosphoproteins in FK506-treated mice that may play a role in distal renal calcium handling

Since FK506 did not induce significant changes in PKC (β 1, δ and ϵ) protein expression in the kidney, an alternative approach was used to identify other upstream regulators involved in both renal calcium and sodium handling. The phosphoproteome profile generated from Chapter 3, was used to identify proteins that may play a role in calcium handling in the distal nephron. Phosphoproteins identified in the membrane and cytosolic fraction were filtered by GO terms from the main proteomic tables (Appendix Table 6.3-3 and Table 6.3-4), searching for the keyword “calcium”. Thirty-five phosphopeptides, which correspond to 19 proteins, were selected from the membrane fraction (Appendix, Table 6.3-5) and 19 phosphopeptides, which correspond to 12 proteins, were identified in the cytosolic fraction (Appendix, Table 3.6-6).

Phosphoproteins that are likely to be involved in FK506-dysregulated calcium homeostasis, hypertension and the metabolic syndrome were selected and presented in Table 4.3-2. ADCY6 is involved in water and electrolyte homeostasis, such as in calcium and phosphate handling (518), and FK506 was shown to increase phosphorylation of ADCY6 at S53 by 32 % in the renal cortices of FK506-treated mice. FK506 increased phosphorylation of PMCA at S1155 and T1165 by 3.43 %. Since the 10 % cut-off point was set in the previous chapter for FK506-dysregulated phosphopeptides, the effect of FK506 was unlikely to have a significant effect on PMCA.

FK506 increased the phosphorylation of the calcium voltage-gated channel subunit α 1E (CACNA1E), involved in calcium binding and transport, and glucose homeostasis (519), by 31 % at a novel phosphosite, T1983. A total of 7 phosphopeptides were dysregulated by FK506 in another calcium binding protein, calnexin (CANX). FK506 increased phosphorylation of CANX in the membrane fraction but it was shown to decrease its phosphorylation in the cytosolic fraction. This might indicate that CANX is phosphorylated after it has been inserted into the membrane. The calcium/calmodulin-dependent serine protein kinase (CASK) is co-expressed with PMCA and calbindin-D28K in the DCT (520), and it is likely to be involved in renal calcium handling. FK506

decreased the phosphorylation of CASK at S582, however, this effect is not likely to have a significant impact as CASK-pS582 was only downregulated by 4.71 %.

Megalin interacts with the H⁺/Cl⁻ exchange transporter 5 (CLCN5) and NHERF2 (521), and mutations in *CLCN5* are known to cause Dent's disease, which causes hypercalciuria (522,523). Therefore, megalin may play a role in renal calcium handling. FK506 was shown to decrease the phosphorylation of megalin at S4624 (8.19 %) and at a novel phosphosite, T4583. The effect of FK506 on T4583 is not likely to be significant, since megalin-T4583 was only downregulated by 3.17 %. TRPM7 is a divalent cation channel that is permeable to both Ca²⁺ and Mg²⁺. FK506 was shown to dysregulate the phosphorylation of TRPM7 at S1502, however, the changes may not be significant since the change in phosphorylation was only 3.44 %. Another TRP family member, the transient receptor potential cation channel subfamily P member 2 (TRPP2), was also dysregulated by FK506. TRPP2 is cation channel that is permeable to calcium ions. TRPP2 is expressed in the cilia of tubular epithelial cells and is associated with polycystic kidney disease (524). FK506 was shown to increase phosphorylation of TRPP2 at S810 in both the membrane (12.35 %) and cytosolic fraction (15.51 %), however since TRPP2 is a non-selective cation channel with diverse physiological functions including cell proliferation and apoptosis, and that its role in calcium handling in the nephron is unknown, the effects of FK506 on TRPP2 was not examined in this chapter.

The effect of FK506 on the protein expression of ADCY6, CANX and CACNA1E were investigated because they were dysregulated by FK506 (over 10 % change in phosphorylation) and could be feasibly involved in components of the metabolic syndrome. The protein expression of ADCY6 (Figure 4.3-12) remained unchanged in mice treated with FK506, FK506 with HSD and HSD alone. Western blot analysis was performed on kidneys of FK506-treated mice and revealed that FK506 did not have any effects on the protein expression of CANX. The levels of CANX increased in the kidneys of mice treated with FK506 and fed a HSD but the effect of HSD alone was not statistically significant (Figure 4.3-13). Unfortunately, there was no signal detected in the Western blot analysis of CACNA1E, possibly due to poor binding of the CACNA1E antibody to its epitopes on the Western blot. The effect of FK506 on CACNA1E remains inconclusive.

Gene name	Protein name	Accession No.	Peptide Sequence	Phosphosites	Percentage Change	
					<u>Memb</u>	<u>Cyto</u>
<i>ADCY6</i>	Adenylyl cyclase 6	Q01341	NAEPPsPTPAAHTR	S53	+ 32.32	-
<i>ATP2B1</i>	Plasma membrane calcium-transporting ATPase 1 (PMCA1)	G5E829	IEDsEPHIPLIDDtDAEDDAPTKR	S1155; T1165	+ 3.43	-
<i>CACNA1E</i>	Voltage-dependent R-type calcium channel subunit alpha-1E	Q61290	SFSIIR	T1983 *	+ 30.99	-
			QKsDAEEDGVTGSQDEEDSKPK	S553	+ 15.79	- 14.77
			SDAEEDGVTGsQDEEDSKPK	S563	+ 21.24	-
			AEDEILNRsPR	S582	+ 10.96	- 11.28
<i>CANX</i>	Calnexin	P35564	QKsDAEEDGvtGSQDEEDSKPK	S553; T561	-	- 35.99
			QKsDAEEDGVTGsQDEEDSKPK	S553; S563	+ 25.45	-
			QKSDAEEDGvtGsQDEEDSKPK	T561; S563	+ 6.08	-
			QKSDAEEDGVTGsQDEEDsKPK	S563; S569	+ 11.34	-
<i>CASK</i>	Calcium/calmodulin-dependent serine protein kinase	O70589	TQSSSCERDsPSTSR	S582	- 0.32	- 4.71
<i>LRP2</i>	Megalin	A2ARV4	SIDPSEIVPEPKPASPGADEtQGtK	T4583 *	-	- 3.17
			EAVAVAPPPsPSLPAK	S4624	- 1.11	- 8.19

<i>TRPM7</i>	Transient receptor potential cation channel subfamily M member 7	Q923J1	RA _s TEDSPEVDSK	S1502	+ 3.44	-
<i>TRPP2</i>	Transient receptor potential cation channel subfamily P member 2	O35245	SLDD _s EEEEDEDSGHSSR	S810	+ 12.35	+ 15.51
* Novel phosphosite						

Table 4.3-2 FK506-dysregulated phosphoproteins involved in calcium handling identified in the nephron

Identification and quantification of phosphosites in calcium-associated proteins after FK506 treatment. Novel phosphorylation sites were previously unidentified in PhosphoSitePlus® Database.

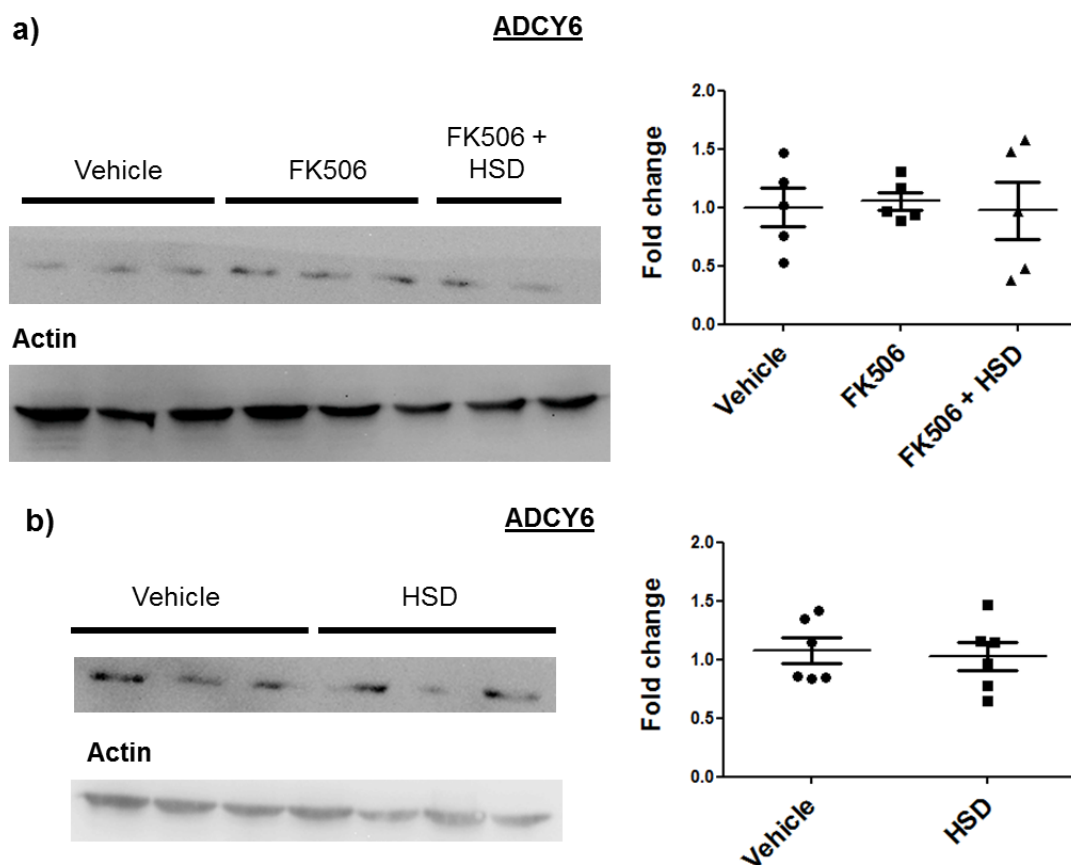


Figure 4.3-12 The effects of FK506 and HSD on ADCY6 protein expression in the kidney

Western blot analysis was performed on kidneys of vehicle, a) FK506 or FK506 + HSD and b) HSD treated mice. Representative blots (left) and protein expression (right) of ADCY6 are shown. Band intensities of ADCY6 were quantified and normalised to those of β -actin and expressed as a fold change of the control mean; data are presented as means \pm SEM, n=5-6. Statistical values were calculated using an unpaired t-test for vehicle vs. HSD treatment and ANOVA followed by a Bonferroni's multiple comparison test for vehicle vs. FK506 vs. FK506 + HSD treatment.

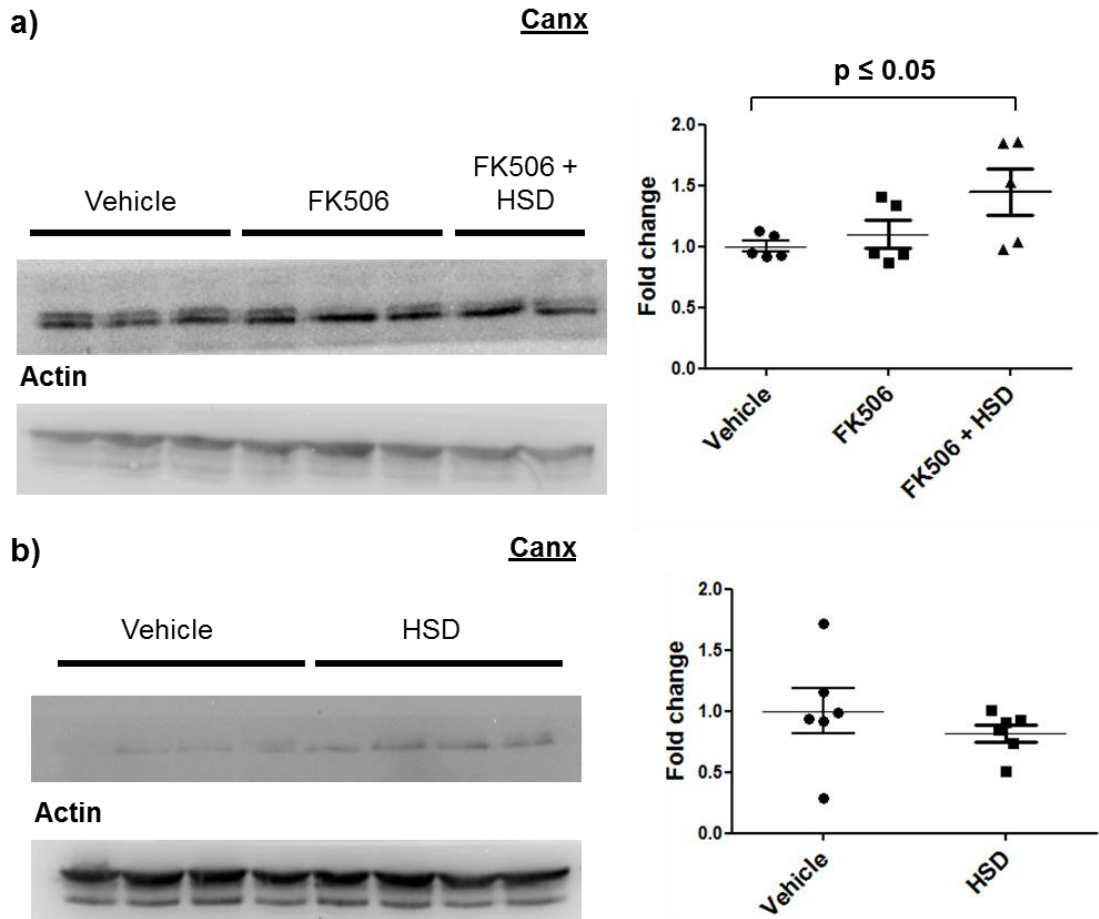


Figure 4.3-13 The effects of FK506 and HSD on Calnexin protein expression in the kidney

Western blot analysis was performed on kidneys of vehicle, a) FK506 or FK506 + HSD and b) HSD treated mice. Representative blots (left) and protein expression (right) of calnexin are shown. Band intensities of calnexin were quantified and normalised to those of β -actin and expressed as a fold change of the control mean; data are presented as means \pm SEM, n=5-6. Statistical values were calculated using an unpaired t-test for vehicle vs. HSD treatment and ANOVA followed by a Bonferroni's multiple comparison test for vehicle vs. FK506 vs. FK506 + HSD treatment.

4.4 Discussion

FK506 alters sodium and calcium transcellular transport systems in the DCT by dysregulating transporters expressed at the apical and basolateral surface of the cell membrane. The effects of FK506 on TRPV5 and calbindin-D28K have been investigated in several studies (57,51), in which it was suggested that downregulation of TRPV5 and calbindin-D28K disrupts transcellular reabsorption of calcium in the distal nephron and contributes to the pathogenesis of CNI-induced hypercalciuria. These studies focused on the changes in the transport process at the apical membrane; the effects of FK506 on the basolateral membrane transporters remain unclear. Results obtained in this chapter suggest that basolateral transport proteins in the DCT may play a role in the pathophysiology of CNI-induced hypercalciuria.

In this chapter, FK506 was found to increase urinary calcium excretion and decrease calbindin-D28K expression. In contrast to previous studies (51,57), FK506 was shown to increase mRNA expression of TRPV5 and its protein expression remained unchanged in mice in this study. Nijenhuis *et al.* (57) showed that daily administration of FK506 by oral gavage for 7 days decreased TRPV5 mRNA expression in rats. In the Hoorn *et al* study (51), TRPV5 protein expression decreased in FK506-treated mice, however, Western blot analysis of TRPV5 was performed on whole kidney lysates, which differs from the fractionated kidney samples used in this study. FK506 has no transcriptional effect on NCX1 and PMCA, however treatment with FK506 increased the abundance of these proteins in the kidney membrane fraction. Overall, these results showed low calbindin-D28K expression, which suggests low transcellular calcium movement, and an increase in the protein abundance of the basolateral calcium transport proteins, which may correlate with an increase in their activity.

4.4.1 The novel mechanism of CNI-induced hypercalciuria

The link between sodium and calcium transport at the DCT is evident; this is demonstrated by the resemblance between calcium disturbances in thiazide-treated patients and Gitelman patients, and also between CNI-treated patients and FHHt patients. In order to decipher the relationship between calcium and sodium handling, the effects of FK506 on sodium transport were also studied.

Corroborating previous studies (51,493,506), FK506 increased pNCC and decreased Na⁺/K⁺-ATPase expression. The effects of FK506 on sodium and calcium transport proteins reported in this study have led to the development of a hypothetical model of FK506-induced hypercalciuria.

Under normal conditions, the activity of Na⁺/K⁺-ATPase is the rate limiting step that exports sodium across the basolateral membrane (80) as it creates an electrochemical gradient for apical transporters such as NCC. Na⁺/K⁺-ATPase expression decreases during FK506 treatment, but the continuous influx of sodium chloride through activated NCC causes an accumulation of sodium inside the cell. This causes depolarisation of the basolateral membrane and reverses the transport direction of NCX1 (354,355,525), causing calcium influx and sodium efflux, compensating for the reduction in Na⁺/K⁺-ATPase-mediated sodium efflux.

The membrane abundance of NCX1 was increased in FK506-treated mice. This should exacerbate the increase in the intracellular calcium concentration and thus reduce the electrochemical gradient favouring calcium uptake by TRPV5. Reduction in calcium uptake increases urinary calcium excretion, and thereby causing hypercalciuria. The increase in PMCA abundance is likely a compensatory effect to prevent toxic levels of cytosolic calcium caused by NCX1-mediated calcium influx (Figure 4.4-1).

With this model of CNI-induced hypercalciuria, the magnitude of chloride and potassium efflux must be equal to their influx. In the DCT, chloride is primarily exported by CLCNKB (83) and also by KCC4 (84). The magnitude of chloride efflux by CLCNKB and KCC4 must equal to the chloride influx by NCC in this model, therefore it is predicted that FK506 would not decrease the expression or activity of these transporters. Potassium is exported by KCNJ10 and several other basolateral K⁺ channels, such as KCNJ15 and KCNJ16, in the DCT (103). KCNJ10 is known to recycle potassium from Na⁺/K⁺-ATPase (101) and reduction in KCNJ10 is associated with reduced Na⁺/K⁺-ATPase activity (162). It is therefore theorised that low levels of Na⁺/K⁺-ATPase might be accompanied by a reduction in KCNJ10. However, the exact effects of FK506 on these basolateral transport proteins are unknown and require further investigation.

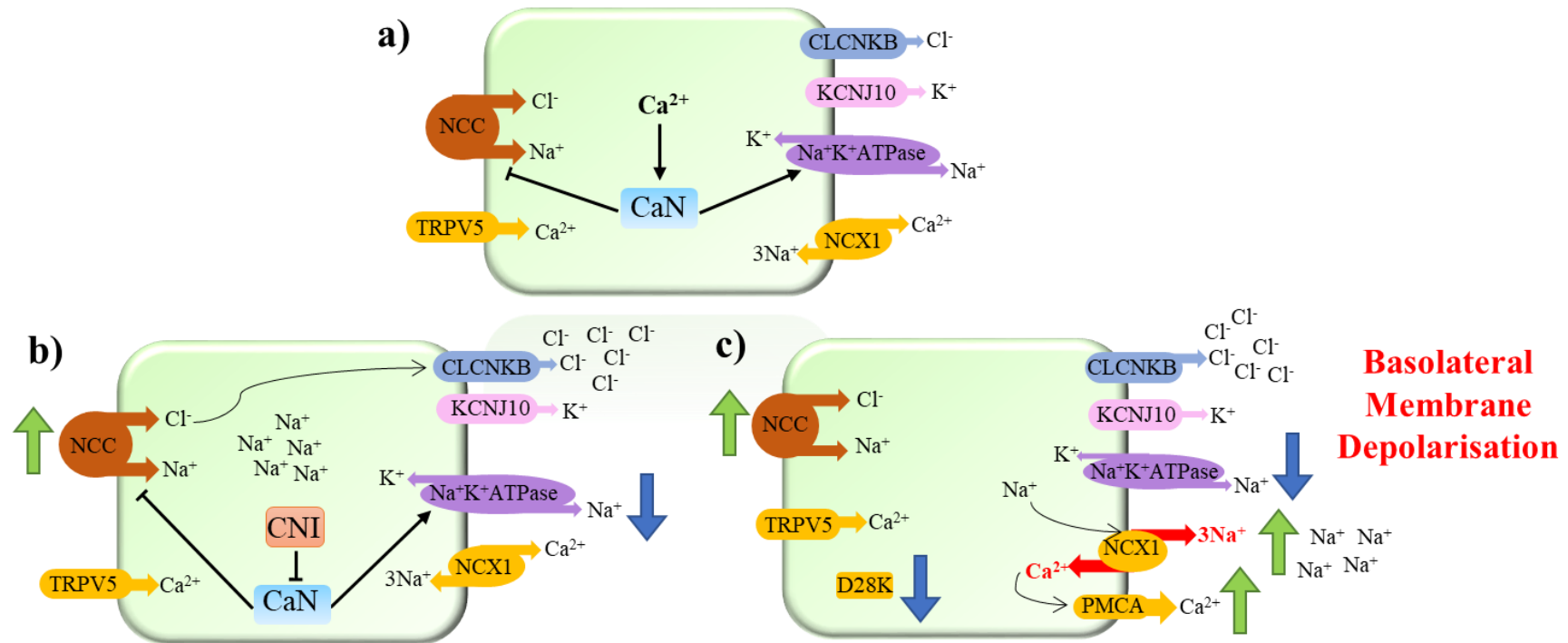


Figure 4.4-1 Schematic model of CNI-induced hypercalciuria in the DCT

A novel model of CNI-induced hypercalciuria. a) An increase in intracellular Ca^{2+} activates calcineurin, which inhibits NCC and activates Na^+/K^+ -ATPase. b) When calcineurin is inhibited by CNIs, pNCC expression increases and Na^+/K^+ -ATPase decreases, causing Na^+ accumulation in the cytosol. c) Na^+ accumulation depolarises the basolateral membrane and reverses the transport direction of NCX1, causing Na^+ efflux and Ca^{2+} influx, reducing the electrochemical gradient required for Ca^{2+} uptake through TRPV5, resulting in an increase in urinary Ca^{2+} ; this is augmented by low D28K level, which indicates low Ca^{2+} shuttling across the cell.

4.4.2 FK506 with a HSD reversed the effect of FK506 on the calcium transport proteins

High dietary salt intake and FK506 can both cause salt-sensitive hypertension (51). Previous studies used 1.5 % NaCl to enhance the disease phenotype of rodents susceptible to hypertension (526,527). Therefore, a HSD was fed to FK506-treated mice in this study to enhance the side effects of CNIs. As shown in the previous chapter, FK506 mainly dysregulated proteins at a post-translational level, therefore the effects of FK506 + HSD or HSD on mRNA expression of proteins of interests were not determined.

HSD enhanced the effect of FK506 on urinary calcium excretion and had no effects on TRPV5 protein expression in FK506-treated mice. Although not statistically significant, the protein expression of pNCC and calbindin-D28K in FK506 + HSD-treated mice showed a tendency for HSD to enhance the effect of FK506.

Vehicle-treated mice fed on a HSD showed a significant increase in the protein expression of Na⁺/K⁺-ATPase, and FK506 treatment resulted in a significant decrease in Na⁺/K⁺-ATPase. HSD and FK506 counteract each other in the expression of Na⁺/K⁺-ATPase, and HSD appeared to restore Na⁺/K⁺-ATPase expression in FK506 + HSD-treated mice. HSD reduced the effect of FK506 by decreasing the abundance of NCX1 and PMCA. Even though a HSD significantly reduced NCX1 in FK506-treated mice, NCX1 expression remained significantly higher than the control group, whereas PMCA was restored to the baseline level by a HSD during FK506 treatment.

Reduced expression of NCX1 in FK506 + HSD treated mice could be a downstream effect of Na⁺/K⁺-ATPase, since its expression level was restored; sodium can exit the cell through Na⁺/K⁺-ATPase or NCX1, reducing sodium accumulation and lessening the depolarisation of the basolateral membrane. NCX1 will continue to export sodium and import calcium into the cell as long as the cell is depolarised. However, since PMCA expression remained at baseline level in FK506 + HSD treated mice, the transport direction of NCX1 may alternate depending on intracellular sodium and calcium concentration.

4.4.3 The effect of increased NaCl intake on calcium transport proteins

Since HSD altered the effect of FK506 on some of the transport proteins in FK506 + HSD treated mice, the effect of a HSD alone was examined. The purpose of the HSD was to enhance the effect of FK506, therefore administration of this diet to vehicle-treated mice for 2 weeks might not be sufficient to cause salt-induced hypertension. Several groups have reported that a diet containing 2.8 % NaCl was considered to be a moderately-high salt diet for rats; this is comparable with a daily intake of 14 g NaCl in humans (528,529), which is above the average Western diet. Ball and Meneely (529) showed that progressive salt-induced hypertension is time and dose dependent, requiring up to 12 months on a 2.8 % NaCl diet before hypertension becomes apparent. This means that the two-week treatment period used in this study for mice fed on a 1.5 % NaCl diet may not be sufficient and may require a treatment period of over 12 months for hypertension to develop. Other studies using higher percentages of NaCl, such as 4 or 8 %, can cause hypertension in less than 7 weeks (530,531), however these studies were performed on rodents susceptible to hypertension, such as spontaneously hypertensive rats. Given the length of treatment used in this study, a diet containing >8 % of NaCl might be required to induce hypertension and changes in transporters since a 1.5 % NaCl diet had no effects on NCC and pNCC.

Although the 1.5 % NaCl diet did not induce hypertension, it was shown to alter the expression of calcium transporters in the DCT. This is possibly due to a compensatory signalling mechanism that was aimed to reduce NaCl reabsorption, which resulted in increased calcium reabsorption. The diet containing 1.5 % NaCl increased Na⁺/K⁺-ATPase and NCX1 expression. Calcium efflux through NCX1 is coupled with sodium influx, which is then recycled through Na⁺/K⁺-ATPase, providing an electrochemical gradient for cation entry through the apical membrane. Although not statistically significant, the HSD had the tendency to increase TRPV5. This together with the electrochemical gradient would drive calcium into the cell. The increased expression of calbindin-D28K indicates an increase in intracellular calcium and calcium shuttling across the cell. The increase in intracellular calcium will activate calcineurin and may act as a

homeostatic mechanism that inhibits the WNK-NCC cascade and sodium chloride influx.

4.4.4 The effects of FK506 on PKC

The DCT is a principle site for sodium and calcium handling with reabsorption occurring primarily through NCC and TRPV5, respectively. PTH is known to downregulate NCC and upregulate TRPV5 activity (308,517) and the presented hypothetical model posits that intracellular calcium may act as a homeostatic mechanism to regulate NCC. PTH regulation of TRPV5 involves PKA and PKC signalling pathways (313,314).

PTH stimulates TRPV5 through activation of the ADCY-cAMP-PKA pathway and PKA has been reported to phosphorylate TRPV5 at T709, prevent calmodulin and TRPV5 interaction, and increase the open probability of the channel for calcium uptake (314). Several PKA and calmodulin-targeted motifs have been identified on TRPV5, however amino acid sequence alignments of TRPV5 revealed that these motifs are only conserved in rabbits, mice and rats but not in humans. A recent study comparing the effects of PKA on rabbit and human TRPV5 showed that PKA stimulated rabbit TRPV5, but not human TRPV5 (532). Together, these indicate that PKA-mediated TRPV5 stimulation in rabbits might be a signalling mechanism unique to rodents, therefore these results may not be representative of the same behaviour in humans, hence the effects of FK506 on PKA were not investigated in this chapter.

PTH signals PKC to inhibit caveola-mediated endocytosis of TRPV5, which results in the accumulation of TRPV5 at the cell membrane (313,315,337). In addition, PKA and PKC also regulate the kinase activity of WNK4. PKA and PKC are known to phosphorylate KLHL3 to prevent WNK4 degradation and increases phosphorylation of WNK4 at S64 and S1196, and the autophosphorylation of WNK4 at S332; this results in the increase in WNK4 kinase activity, which promotes NCC activity (244). Since PKC is an upstream regulator of WNK4, and both PKC and WNK4 regulate TRPV5 cell surface expression, the effect of FK506 was examined on PKC. There are fifteen isoenzymes in the PKC family and these are divided into three subfamilies, the conventional, novel and atypical PKCs

(533). Conventional PKCs, such as PKC α and PKC β 1, require diacylglycerol (DAG) and calcium for activation, whereas novel PKCs, such as PKC δ and PKC ϵ , do not require calcium for activation. PKC α , β 1, δ and ϵ have been shown to be expressed at the PCT, DCT and CD of mice (534). This study shows that FK506 or a diet containing an additional 1.5 % NaCl did not alter PKC β 1, δ and ϵ protein expression. In addition, FK506 + HSD did not affect the expression of PKC β 1 and δ , but the expression of PKC ϵ was increased, which suggests that it might play a role in the pathophysiology of renal electrolyte handling. CNIs are known to dysregulate the phosphorylation state of proteins and the effect of FK506 on the phosphorylation of PKC isoenzymes are unknown, therefore further investigations into the expression of PKC α , pPKC β 1 and the expression of other phospho-PKC isoenzymes are required.

4.4.5 Other calcium regulatory proteins

The phosphoproteome profile generated from Chapter 3 identified several phosphoproteins involved in calcium homeostasis that could also be involved in the development of CNI-induced hypercalciuria or other adverse effects of CNIs.

4.4.5.1 Adenylyl cyclase 6

ADCY6 is expressed all along the nephron but it is most abundant in the distal tubules (535). ADCY6 is inhibited by extracellular calcium and plays an important role as part of the PKA-mediated PTH signalling pathway regulating TRPV5 (314,518). FK506 increased the phosphorylation of ADCY6 at S53 in the renal cortices of FK506-treated mice. ADCY6 also plays an important role in sodium handling at the DCT. ADCY6 phosphorylates and activates AKT (536), resulting in the activation of the WNK-NCC cascade (471). Quantitative analysis of ADCY6 in the kidneys of FK506-treated mice revealed that the total protein expression of ADCY6 remained unchanged, this suggests that FK506 does not interfere with the total level of ADCY6 but dysregulates phosphorylation of ADCY6, which may induce changes in the activity of PKA.

4.4.5.2 R-type calcium channel subunit α -1E

CACNA1E is a R-type calcium channel that is expressed in the brain (537), pancreas (538) and kidneys (539). It is best known for its role in synaptic plasticity in the nervous system where it mediates calcium influx into excitable cells (537). It has also been shown to play a role in sperm motility (540), pain transmission (541) and the regulation of the heart rate (542). CACNA1E also plays a role in glucose homeostasis and polymorphism in CACNA1E are associated with Type II diabetes and reduced insulin secretion (538,543,544), which are characteristics of the metabolic syndrome along with hypertension and hypercalciuria. Previous studies reported CACNA1E expression at the distal tubule, where it is predominantly expressed on the apical membrane but is also expressed at lower levels on the basolateral membrane and the cytoplasm (539). In this study, FK506 increased phosphorylation of CACNA1E at a novel phosphosite, T1983. However, the role of CACNA1E in the distal tubules is poorly understood and further investigation into pT1983 is required to determine whether it is involved in calcium and sodium homeostasis.

4.4.5.3 Calnexin

Calnexin is one of the molecular chaperones that assists protein folding in the ER. The ER plays a dynamic role in many cellular processes, which includes protein folding, lipid biosynthesis and calcium homeostasis (545). Protein folding occurs inside the ER and folded proteins are transported through the Golgi apparatus. Misfolded proteins are not exported and are retained in the ER until they are degraded in the cytoplasm. Many processes can alter ER homeostasis and cause ER stress. ER stress is caused by the accumulation of misfolded proteins in the ER, altered ER calcium homeostasis, viral infections and increased protein synthesis (545). ER stress can be alleviated under normal condition by the increase in the expression of protein folding chaperones, to accommodate the increase in protein synthesis, or the inhibition of general protein translation and increased degradation of misfolded proteins. However, if ER stress is not alleviated or it is severe, cell apoptosis will be induced (545) and this has been associated with the pathogenesis of many diseases, such as hypertension, type 2 diabetes and obesity (546,547).

Calcineurin has been shown to alleviate ER stress by inhibiting protein translation and restoring Ca^{2+} stores in the ER for optimal protein folding conditions. To restore Ca^{2+} stores, calcineurin causes intracellular Ca^{2+} oscillation by dephosphorylating calnexin at S563; this reduces the interaction between calnexin and the sarco/endoplasmic reticulum calcium ATPase 2b (SERCA) and prevents calnexin from inhibiting the SERCA (548). FK506 increased phosphorylation of calnexin at S563 in this study, which inhibits SERCA, prevents restoration of ER Ca^{2+} homeostasis and prolongs ER stress (549). Quantitative analysis of calnexin in the kidneys of FK506-treated mice revealed that the total protein expression of calnexin remained unchanged, indicating that FK506 does not interfere with total level of calnexin but dysregulates its phosphorylation. Moreover, FK506 + HSD significantly increased the total protein expression of calnexin. The causes of increased calnexin during FK506 + HSD treatment is unclear, but increased calnexin levels could accentuate SERCA inhibition, thereby increasing ER stress.

4.4.6 Future studies

The model proposed in this study is one of NCC-mediated sodium transport increasing the intracellular calcium concentration which decreases reabsorption of calcium from the urine. The model predicts that the magnitude of chloride and potassium influx must be equal to their efflux. The abundance of chloride and potassium transport proteins, such as CLCNKB and KCNJ10, can be verified through Western blot analysis and immunohistochemistry.

Intracellular calcium can be imaged in an intact kidney of a live FK506-treated mouse, using calcium sensitive dyes and multiphoton microscopy (550). Real-time imaging of Ca^{2+} signals can be used to visualise calcium influx and efflux through reversed NCX1 and PMCA, respectively, and Ca^{2+} ions localised at the basolateral membrane, in the event of sodium accumulation and membrane depolarisation. This approach may reveal alternative pathways of calcium transport in the DCT, such as that calcium may not be imported into the cell through TRPV5.

This model suggests that sodium accumulation and subsequent membrane depolarisation may reduce the electrochemical gradient required for calcium uptake through TRPV5. The net movement of ions across the cell generates a transepithelial voltage that is equal to the difference in voltage between the apical and basolateral membrane. With an Ussing chamber, the transepithelial voltage of a confluent monolayer of murine distal convoluted tubule cells from microdissected kidneys, could be measured using a current clamp method (551).

Chapter 5. Discussion

5.1 Summary of the thesis

CNIs are the main immunosuppressants used in organ transplantation. It causes complications such as hypertension, hypercalciuria, hyperkalaemia, metabolic acidosis and diabetes mellitus, which mimics the metabolic syndrome. Calcineurin is a protein phosphatase with pleiotropic effects, and the discovery of the calcineurin-WNK cascade has provided insights into the regulation of blood pressure in the kidney. The WNK cascade is extremely complex and regulates NCC through a sequential inhibitory signalling pathway, however, the underlying mechanism remains unclear due to conflicting evidence presented in literature. With the aim of elucidating the signalling pathways that govern the WNK-NCC cascade, a single-oocyte chemiluminescence assay was used. This assay uses chemiluminescence emitted from the epitope-tagged oocytes to quantify NCC expression on the surface membrane, offering a promising approach for investigating protein interactions between regulatory and transmembrane proteins. Unfortunately, technical issues were encountered in the production of DNA constructs, therefore, a different approach focusing on phosphorylation in CNI-treated animals was used to investigate the calcineurin-NCC cascade.

Phosphorylation is an important post-translational modification that defines the activity of members of the WNK-NCC cascade. Using quantitative phosphoproteomics, a phosphoproteome profile of the renal cortices from FK506-treated mice was generated, and 411 unique phosphopeptides in the membrane fraction and 244 in the cytosolic fraction were found to be dysregulated by FK506. In this data, AKT was found to be phosphorylated by FK506 and may act as the intermediary protein in the calcineurin-WNK cascade. In addition, ERK1/2 was also dysregulated by FK506 and may regulate NCC through the WNK4-ERK1/2 pathway in a WNK-SPAK pathway independent manner. Due to the pleiotropic effects of calcineurin, the phosphoproteome profile also revealed several FK506-dysregulated phosphoproteins that are involved in sodium, acid-base, glucose and potassium handling, all of which require further investigation as to their role in the adverse effects of CNIs.

Previously, CNI-induced hypercalciuria was thought to be caused by a reduction in the apically expressed TRPV5 and the cytosolic protein calcium binding

protein, calbindin-D28K. In this thesis, a novel mechanism underlying CNI-induced hypercalciuria is proposed where the decrease in calcium reabsorption in the DCT of FK506-treated mice may in fact be a result of basolateral membrane depolarisation and an increase in NCX1 expression. This eliminates the driving force for calcium influx through TRPV5. In addition, a regulatory mechanism that prevents sodium chloride overload is also proposed, in which the increase in calcium influx in the DCT will increase intracellular calcium concentration, activating calcineurin to inhibit NCC in a homeostatic negative feedback loop.

5.2 The effect of insulin resistance on sodium retention in the metabolic syndrome

CNI-induced metabolic syndrome is highly prevalent amongst transplant recipients. Since the development of the metabolic syndrome can involve both genetic and behavioural risk factors, polymorphisms in the subunits of calcineurin or genes downstream of calcineurin, such as AKT and ERK1, may increase the susceptibility of developing the metabolic syndrome in transplant recipients.

Insulin has a variety of effects on the nephron, including the regulation of sodium reabsorption, glucose uptake and the prevention of cell apoptosis. Insulin binds to a tyrosine kinase receptor (RTK) that phosphorylates and activates the PI3K/AKT and the MAP kinase signalling pathways. Activated PI3K activates the 3-phosphoinositide-dependent protein kinase 1, causing AKT phosphorylation and activation. AKT phosphorylates its substrates and activates a series of signalling pathways that results in the activation of eNOS, an increase in glucose uptake and storage, an increase in protein and lipid synthesis, and a decrease in gluconeogenesis and lipolysis. The MAP kinase pathway, which involves MAP kinase kinase and ERK1/2, acts in parallel to the PI3K/AKT pathway, is involved in cell proliferation and differentiation, is also activated.

Hyperinsulinaemia requires hyperglycaemia to induce sodium reabsorption in the PCT, TALH and DCT (552). In the distal tubule, insulin increases the expression of NCC and ENaC via two different mechanisms. When insulin binds to its receptor, PI3K/AKT and the PI3K/mTOR complex 2/SGK1 pathways are activated (553). The WNK4-NCC cascade is stimulated by AKT (471), whereas

the membrane expression of ENaC is increased by inhibiting Nedd4 through the PI3K/mTOR complex 2/SGK1 pathway, resulting in increased sodium uptake (553). Similar to the effect of aldosterone, hyperglycaemia also increases SGK1 expression and phosphorylation (554). The increase in SGK1 activity may also contribute to increased NCC activity through the WNK kinases, causing sodium retention.

Insulin resistance forms part of the metabolic syndrome and the PI3K/AKT signalling pathway is impaired in glucogenic tissues, such as muscle and adipose tissues (469,470), whilst the MAP kinase pathway remains intact. In contrast, the kidney is not affected by insulin resistance in the same manner; only the glomeruli can develop insulin resistance in which the activity of the PI3K/AKT pathway is reduced (555). In other parts of the nephron, such as the distal tubules, the insulin/PI3K/AKT pathway remains active (469). Since the distal tubules remain sensitive to insulin, hyperinsulinaemia will stimulate sodium retention through NCC and ENaC.

The thesis demonstrated that AKT was increased, phosphorylated and possibly activated in CNI-treated mice. This is consistent with previous reports in which AKT was increased in the kidneys of diabetic mice (469,471) and CNI was shown to prevent the dephosphorylation of AKT by calcineurin (475,476). The PI3K-AKT pathway has been shown to activate the WNK-NCC pathway in diabetic models, which suggests that AKT may be involved in stimulating NCC in CNI-treated animals. The activity of AKT was not determined in this study, however this may be an interesting avenue for future investigation. Since both NCC and ENaC are stimulated by the PI3K/AKT pathway, hyperinsulinaemia and the downregulation of calcineurin in the kidneys may contribute to sodium retention and the development of hypertension in the metabolic syndrome (Figure 5.2-1).

5.2.1 The effect of insulin resistance and ER stress in the metabolic syndrome

An activated PI3K/AKT cascade can cause ER stress by overproducing NO (556). If ER stress is not alleviated, accumulated ER stress can contribute to the development of hypertension, type 2 diabetes and obesity (546,547). As previously mentioned, one of the mechanisms for alleviating ER stress by

calnexin is to restore Ca^{2+} homeostasis in the ER. In the current study, FK506 prevented the dephosphorylation of calnexin, which inhibited SERCA activation, resulting in prolonged ER stress; a possible trigger for the development of the metabolic syndrome (549).

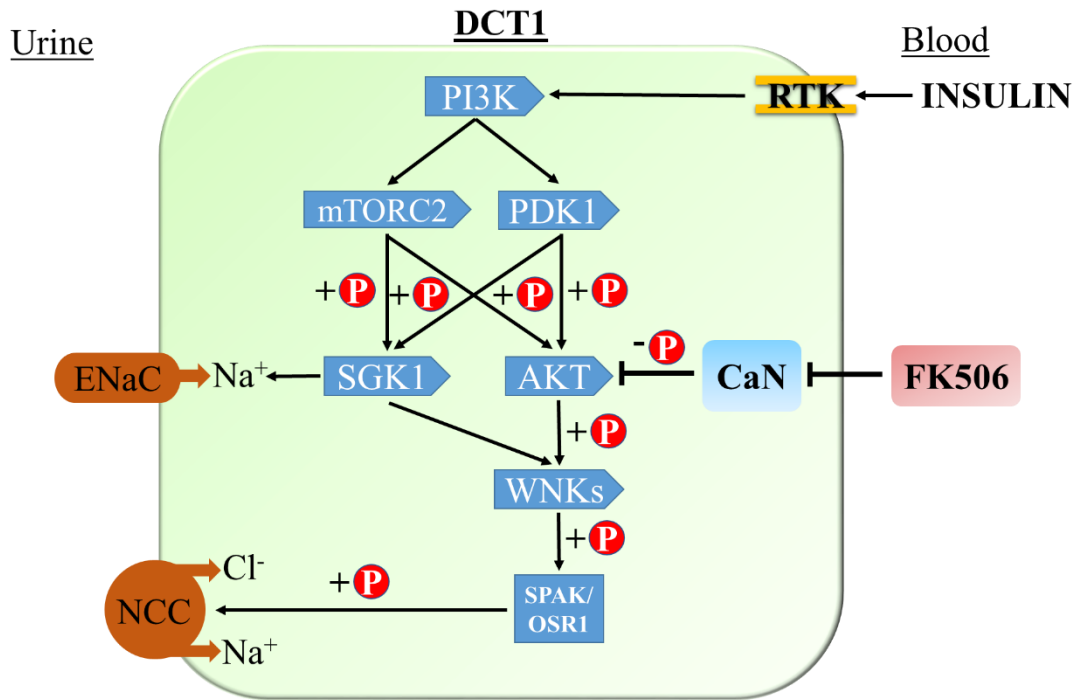


Figure 5.2-1 Sodium retention in the distal tubule of insulin resistant mice

In insulin resistant mice, the insulin signalling pathway is activated in the distal tubule, which promotes sodium retention via two interlinked pathways. PI3K stimulates the mTORC2-SGK1 signalling cascade, causing an increase in ENaC membrane expression and stimulates the AKT-WNK cascade, causing an increase in NCC activity. In addition, mTORC2 also stimulates AKT and PDK1 also stimulates SGK1, which may further increase sodium retention. CNIs prevent AKT dephosphorylation and deactivation, activating the WNK cascade and resulting in NCC activation, which leads to hypertension.

5.3 Fast calcium binding to calmodulin supports calcineurin activation with calcium influx into the DCT

Calcineurin has a basal inhibitory effect on NCC. The activation of calcineurin requires an increase in intracellular calcium and the binding of calcium ions to calmodulin and calcineurin B. Similar to calbindin-D28K, calmodulin plays a crucial role in buffering calcium ions in the cell to prevent cell toxicity, especially at high intracellular calcium concentration (557).

Recently, a study on the kinetics of calcium binding showed that calmodulin may act as a calcium ion detector, responsible for the fast buffering of incoming calcium ions in the cell (558). Calmodulin binds to free calcium ions much faster than other major calcium binding proteins, such as calbindin-D28K, and directly intercepts calcium ions before other calcium binding proteins can bind them (558). Calmodulin can bind up to four calcium ions, two at the N-terminus and two at the C-terminus globular domains. These domains have different kinetic properties (279). The initial binding of calcium is dependent on the domains in the N-terminus of calmodulin, which acts as a fast but low affinity buffer. Calcium ions are then transferred to the C-terminus globular domain of calmodulin, which has a higher affinity than the N-terminus, before finally binding to a slow but high affinity calcium binding protein, calbindin-D28K, which determines the final intracellular calcium concentration (558).

In Chapter 4, a 1.5 % NaCl diet was not sufficient to alter pNCC expression. Instead, it was proposed that the 1.5 % NaCl diet might have activated a compensatory mechanism, such as the PTH or vitamin D₃ signalling pathway (517,559) to reduce salt reabsorption during salt overload. This proposed mechanism would prevent sodium retention through increased calcium reabsorption. During salt overload, the membrane abundance of TRPV5 and NCX1 are elevated, increasing the electrochemical gradient for calcium ions and causing calcium influx. The sequential binding of incoming calcium ions allows calmodulin activation, which causes calcineurin activation and NCC inhibition. Calcium ions bound to calbindin-D28K are shuttled to the basolateral membrane and extruded through NCX1 in exchange for sodium ions, which are recycled by

Na⁺/K⁺-ATPase (Figure 5.3-1). This putative mechanism posits that calcium homeostasis indirectly modulates sodium homeostasis via calmodulin and calcineurin.

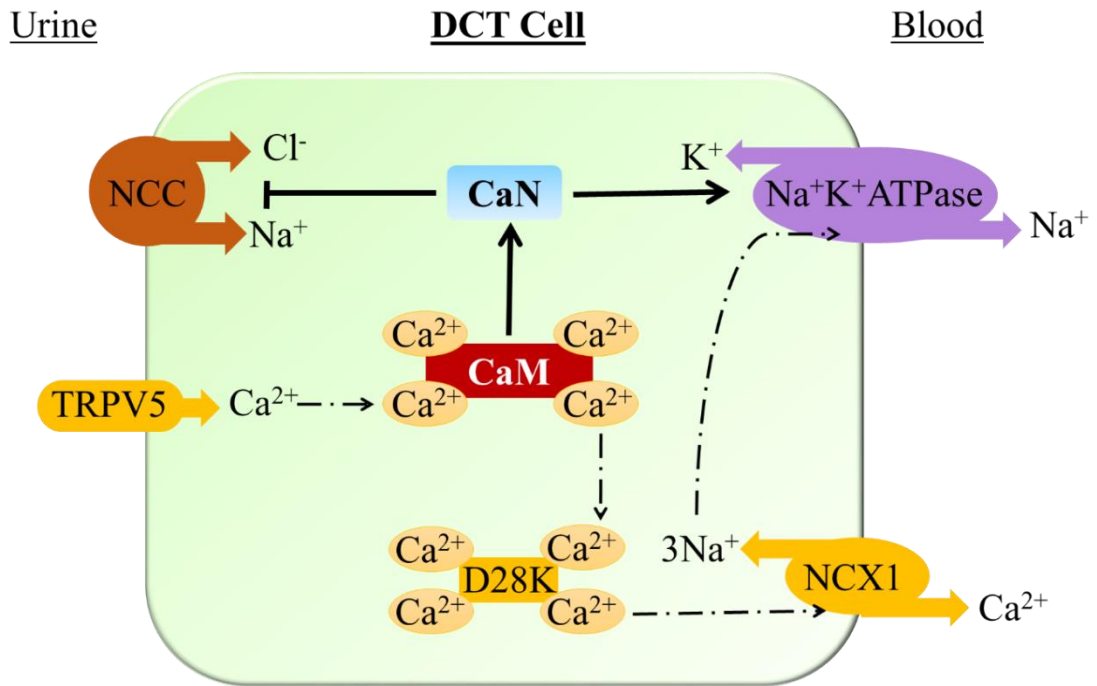


Figure 5.3-1 A proposed model of a compensatory mechanism to prevent sodium reabsorption during salt overload

The activation of calcineurin requires an increase in intracellular calcium and the binding of calmodulin. During salt overload, the expression of TRPV5, calbindin-D28K, NCX1 and Na⁺/K⁺-ATPase are increased. Calcium ions enter the DCT through TRPV5 and are immediately bound to calmodulin. Calmodulin activates calcineurin, which inhibits the WNK cascade to prevent NCC activation. Calmodulin transfers calcium ions to calbindin-D28K and calcium ions are extruded through NCX1, in exchange for sodium ions which are recycled by Na⁺/K⁺-ATPase.

5.4 Underlying causes of the metabolic syndrome

The pathogenesis of the metabolic syndrome is currently unknown, however, there is ample evidence to indicate that environmental factors play a critical role. Vitamin D₃ and PTH are regulators of calcium and phosphate homeostasis and form a feedback loop that regulate the secretion of each other. The role of Vitamin D₃ and PTH in the development of the metabolic syndrome has been examined by several epidemiological studies.

5.4.1 Vitamin D₃ deficiency

Vitamin D₃ deficiency has become a widespread epidemic with an estimate of over a billion children and adults affected worldwide (560). Vitamin D₃ deficiency is associated with many modern day diseases, including osteoporosis (561), neuro-degenerative diseases, such as Alzheimer's (562), and the metabolic syndrome (563–565). Vitamin D₃ deficiency is also prevalent in transplant recipients treated with CNIs (566,567), with 51 % to 97 % with vitamin D₃ insufficiency and 26 % to 33 % with severe vitamin D₃ deficiency (568). In addition to low serum levels of vitamin D₃, the expression of vitamin D₃ receptors in the kidney are also reduced by CNI treatment (569). These findings indicate that vitamin D₃ deficiency is associated with many diseases and the dysregulation of the 1,25(OH)₂D₃ signalling pathway may contribute to the development of the components in the metabolic syndrome.

Vitamin D₃ has many physiological roles in the body and it is best known for its role in calcium and phosphate homeostasis. Vitamin D₃ regulates calcium handling in the DCT by increasing TRPV5, calbindin-D28K, and PMCA expression, and promoting calcium reabsorption. Calcium and sodium handling are inversely regulated, therefore an increase in calcium reabsorption will activate calcineurin, causing NCC inhibition and reduced sodium chloride reabsorption. In addition, vitamin D₃ also regulates blood pressure in a process that is independent from calcium, phosphate and PTH. Vitamin D₃ interacts with the RAAS and suppresses renin expression (559,570). Low serum levels of vitamin D₃ are associated with increased renin activity and serum ANGII levels (571,572), which may contribute to increased sodium reabsorption in the distal nephron.

Lower levels of $1,25(\text{OH})_2\text{D}_3$ are also detected in individuals with essential hypertension (564), suggesting a role for vitamin D_3 in the development of hypertension.

New evidence has recently emerged indicating that vitamin D_3 may also play a role in insulin secretion and glucose homeostasis (51,64). Low serum vitamin D_3 levels are associated with dysfunctional β -pancreatic islets cells, increased resistance to insulin and decreased glucose tolerance, resulting in insulin resistance and eventually diabetes (573,574). Some studies suggest that the stimulatory effects of vitamin D_3 on calbindin-D28K may play a role in the development of diabetes by preventing apoptosis of β -pancreatic islets cells since calbindin-D28K is the only endogenous inhibitor of caspase 3 (575). Upon stimulation, calbindin-D28K inhibits caspase 3-induced cytokine secretion and the sequential activation of cell apoptosis (575) that can lead to β -pancreatic islets cell deaths.

There is also strong evidence to support the association between low serum vitamin D_3 levels and increased adipose tissue mass in obese individuals (563). However the role of vitamin D in the development of obesity remains controversial due to the fact that vitamin D_3 has been reported to act as a stimulant and an inhibitor in the differentiation of preadipocytes to mature adipocytes (576,577). Lastly, the metabolic syndrome has been described as a chronic state of low-grade inflammation (578). Interestingly, vitamin D_3 deficiency is also associated with inflammatory diseases, such as inflammatory polyarthritis (579). Vitamin D_3 has anti-inflammatory properties and inhibits the expression of pro-inflammatory cytokines and the activation of immune cells (580,581).

5.4.2 PTH

Low serum vitamin D_3 levels are often associated with increased serum PTH due to the feedback loop that governs calcium and phosphate homeostasis. In contrast to vitamin D_3 deficiency, the association between serum PTH levels and the metabolic syndrome are inconsistent (582–584). However elevated levels of PTH are detected in renal-transplant recipients (567), and are associated with the

metabolic syndrome (584) and elevated blood pressure (585), suggesting a role for PTH in the development of hypertension in the metabolic syndrome.

5.4.2.1 Hyperparathyroidism

Primary hyperparathyroidism is an endocrine disorder characterised by the overexpression of PTH. It is the predominant cause of hypercalcemia and is primarily known for its association with the development of bone diseases. It has become increasingly evident that hyperparathyroidism is also associated with an increased risk of developing hypertension, diabetes, hyperlipidaemia and cardiovascular morbidity and mortality (586–588). The underlying mechanism has been suggested to involve PTH and the RAAS, where PTH may stimulate the activity of the RAAS components, increasing blood pressure (589–591). PTH also enhances renin and aldosterone secretion through multiple pathways (591–593), and patients with primary hyperparathyroidism have also been shown to develop primary aldosteronism (594), which can be reversed by surgical parathyroidectomy (594). In contrast, other observational studies have shown no connection between RAAS and hyperparathyroidism (595), therefore further investigations are required to decipher this relationship.

5.4.2.2 Hypoparathyroidism

Hypoparathyroidism is a group of metabolic disorders characterised by hypocalcaemia and hyperphosphatemia, which is caused by low serum PTH levels or PTH resistance in the target organ, including the kidney and the skeleton (596). In patients with primary hypoparathyroidism, low levels of PTH are detected in the serum whereas PTH resistance and high levels of PTH are detected in the serum from those with pseudohypoparathyroidism (PsHP).

5.4.2.3 Pseudohypoparathyroidism

Hypertension is common in patients with PsHP and it is strongly associated with obesity (597). Although the pathophysiology of hypertension in PsHP is unclear, impairment of the PTH signalling pathway may lead to the increase in sodium chloride reabsorption and decrease in calcium reabsorption in the distal tubule, causing hypertension and calcium wasting, and possibly hypocalcaemia.

In addition to PTH resistance, PsHP may induce hypertension through hypocalcaemia. The association between serum calcium levels and renin secretion has been examined by several research groups. Serum calcium levels affect the calcium sensing receptors (CaSR) located on juxtaglomerular cells and inhibits renin secretion upon stimulation (598,599). In vivo studies showed that acute elevation of serum calcium or increased renal calcium delivery are associated with suppressed renin secretion and this effect is more prominent under renin-stimulated conditions, such as a low salt diet (598,600–602). The hypercalcaemic effect is also mimicked by pharmacologically stimulating the CaSR (603). Interestingly, chronic stimulation of the CaSR is associated with high serum renin activity. Chronic hypercalcaemia is often detected in patients with primary hyperparathyroidism, however serum renin activity is not always elevated (604,605). The underlying signal transduction pathway is not clear, however, changes in serum calcium levels may affect renin secretion through indirect interaction with the renin-signalling pathway.

5.5 Further avenues of investigation

The quantitative phosphoproteomics data generated in this thesis holds a large amount of information that can be used to decipher the tubular disturbances commonly associated with CNIs. These data may provide valuable insights into the relationship between hypertension, type II diabetes, hypomagnesaemia and many other components of the metabolic syndrome, and may provide new drug targets for these metabolic disorders.

Calcineurin is a protein phosphatase with pleiotropic effects and plays an important role in electrolyte homeostasis in the kidneys. In addition, calcineurin is also involved in regulating insulin expression in pancreatic β cells (606) and inhibiting differentiation of preadipocytes to adipocytes (607), which are all dysregulated by CNI and in the metabolic syndrome. Although the phosphoproteomic data is renal specific, these data may still provide transferable information into the signalling pathways dysregulated by CNIs.

The DCT is highly metabolically active and a critical segment of the nephron involved in electrolyte homeostasis. The existence of several inherited electrolyte

disorders has provided significant insight into the molecular machinery that governs these processes. As this segment is so important in blood pressure homeostasis, full elucidation of this machinery is of interest and clinical importance. Further work in this area is sure to follow.

Chapter 6. Appendix

6.1 Topology and glycosylation of mouse NCC

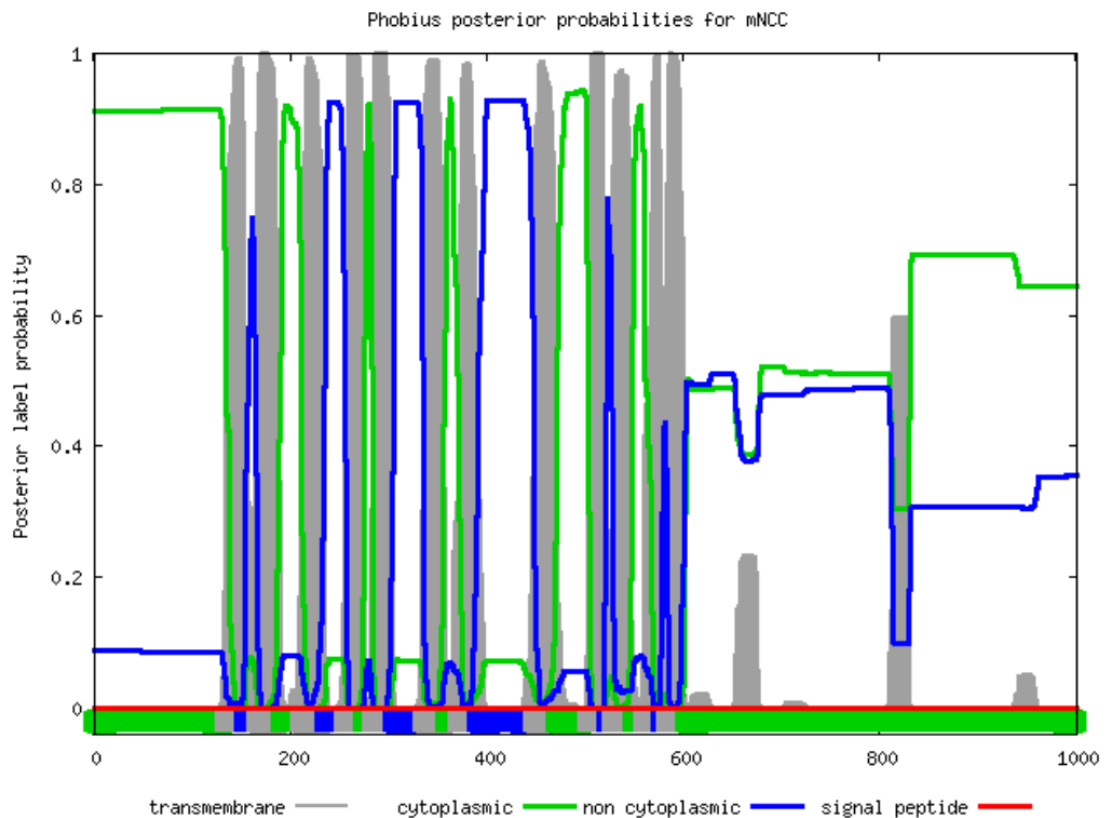


Figure 6.1-1 Posterior probabilities plot of mouse NCC

The amino acid sequence of mNCC (NM_019415.2; Q543E4) was submitted into Protter and Phobius (406,407) and the posterior probabilities plot of NCC was generated. This plot demonstrates the probabilities of individual residues belonging to the TM region (grey), intracellular/cytoplasmic (green) and extracellular/non-cytoplasmic (blue) regions, and residues that may belong to a signal peptide (red). This plot is only a complementary source of information to the membrane topology prediction (Figure 2.3-1) because it only considered probabilities of individual amino acids but did not consider the properties of the amino acid sequence.

Table 6.1-1 Predicted glycosylation sites in mouse NCC

Amino acid position	Residue	Score	Prediction
7	<u>I</u>	0.447	Potential Glycosylated
23	<u>I</u>	0.062	Potential Glycosylated
37	<u>S</u>	0.087	Potential Glycosylated
38	<u>S</u>	0.038	Potential Glycosylated
44	<u>I</u>	0.074	Potential Glycosylated
48	<u>I</u>	0.079	Potential Glycosylated
120	<u>I</u>	0.081	Potential Glycosylated
122	<u>I</u>	0.106	Potential Glycosylated
191	<u>S</u>	0.132	Potential Glycosylated
192	<u>I</u>	0.078	Potential Glycosylated
239	<u>I</u>	0.037	Potential Glycosylated
350	<u>I</u>	0.152	Potential Glycosylated
373	<u>I</u>	0.191	Potential Glycosylated
380	<u>I</u>	0.141	Potential Glycosylated
381	<u>I</u>	0.142	Potential Glycosylated
390	<u>I</u>	0.218	Potential Glycosylated
400	<u>S</u>	0.114	Potential Glycosylated
406	<u>I</u>	0.189	Potential Glycosylated
408	<u>I</u>	0.227	Potential Glycosylated
426	<u>I</u>	0.011	Potential Glycosylated
456	<u>I</u>	0.190	Potential Glycosylated
466	<u>S</u>	0.049	Potential Glycosylated
525	<u>I</u>	0.012	Potential Glycosylated
551	<u>I</u>	0.187	Potential Glycosylated
781	<u>S</u>	0.069	Potential Glycosylated
786	<u>I</u>	0.152	Potential Glycosylated
801	<u>I</u>	0.053	Potential Glycosylated
912	<u>I</u>	0.127	Potential Glycosylated

Potentially glycosylated residues in mNCC (NM_019415.2; Q543E4) were predicted with GlycoEP (408). The table shows the amino acid position, the residue and a score that shows the confidence level of each prediction. The higher the score, the higher the confidence and therefore the probability of a false positive is lower.

6.2 Proteomics quality checks

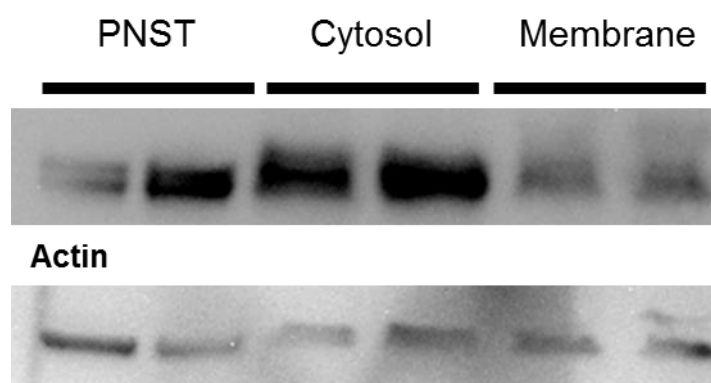


Figure 6.2-1 Purity of fractionated samples

The renal cortices of the treated animals were isolated and divided into membrane and cytosolic fractions. The purity of the enrichment was determined through Western blot analysis of a cytosolic protein, ERK1. Expression level of ERK1/2 in the three fractions obtained from the renal cortices. Lane 1, 3 and 5 are protein samples from vehicle treated animal. Lane 2, 4 and 6 are protein samples obtained from FK506 treated animal. Expression of ERK1/2 was the most abundant in the cytosolic fraction. ERK1/2 expression in PNST and membrane fraction was lower, indicating successful fractionation.



Figure 6.2-2 Protein recovery after acetone precipitation

After acetone precipitation, samples were separated on a SDS-PAGE gel and silver stained. Silver stained gel showed minimum protein loss post-precipitation. Samples were then re-suspended in the appropriate buffer and digested with trypsin. Silver stained SDS-PAGE gel of the cytosolic and membrane fraction before and after acetone precipitation. Fifteen μg of protein were loaded onto each lane. Lane 1 and 3 were samples before acetone precipitation and lane 2 and 4 were samples precipitated with acetone. The silver stained gel showed minimum loss of proteins. A positive control was included in lane 6.

Table 6.2-1 Labelling efficiency of the membrane and cytosolic fractions

Fraction	Vehicle-TMT126		FK506-TMT127	
	Protein (mg)	Labelling efficiency	Protein (mg)	Labelling efficiency
Membrane	1.86	99.92%	1.95	99.82%
Cytosolic	3.24	98.52%	3.23	98.28%

Following trypsin digestion, peptides were labelled with TMT and the labelling efficiency was determined through LC-MS/MS. All three replicates from the membrane and cytosolic fraction showed over 98 % labelling efficiency. The correction factor was also calculated from this set of data (data not shown) and TMT126 and TMT127, were combined in equal proportion before phosphopeptide enrichment.

6.3 Quantitative phosphoproteomic tables

For quantitative phosphoproteomic tables, see the attached CD. Table captions are as follows.

Table 6.3-1 Quantified phosphopeptides identified in the membrane fraction

Quantified peptides containing phosphorylation modification with a unique identification, in the membrane fraction of the renal cortices from FK506-treated mice, were manually validated before being processed. These quantified phosphopeptides obtained from the three replicates were grouped into unique phosphopeptide groups according to their sequences, pRS site probabilities (probability for each putatively phosphorylated site) and MH+ [Da] value. The average ratio, standard deviation and coefficient of variation of each unique phosphopeptide were calculated.

Table 6.3-2 Quantified phosphopeptides identified in the cytosolic fraction

Quantified peptides containing phosphorylation modification with a unique identification, in the cytosolic fraction of the renal cortices from FK506-treated mice, were manually validated before being processed. These quantified phosphopeptides obtained from the three replicates were grouped into unique phosphopeptide groups according to their sequences, pRS site probabilities (probability for each putatively phosphorylated site) and MH+ [Da] value. The average ratio, standard deviation and coefficient of variation of each unique phosphopeptide were calculated.

Table 6.3-3 Unique phosphopeptides identified in the membrane fraction

The unique phosphopeptides identified in the membrane fraction of the renal cortices from FK506-treated mice were summarised. Information on their gene name, protein name, keywords, gene ontology, KEGG and Reactome were obtained from UniProt Knowledgebase and matched to the protein accession number of each phosphopeptide.

Table 6.3-4 Unique phosphopeptides identified in the cytosolic fraction

The unique phosphopeptides identified in the cytosolic fraction of the renal cortices from FK506-treated mice were summarised. Information on their gene name, protein name, keywords, gene ontology, KEGG and Reactome were obtained from UniProt Knowledgebase and matched to the protein accession number of each phosphopeptide.

Table 6.3-5 Unique phosphopeptides identified in calcium-associated proteins in the membrane fraction

The unique phosphopeptides identified in the membrane fraction of the renal cortices from FK506-treated mice filtered by the GO term “calcium” and are presented in this table.

Table 6.3-6 Unique phosphopeptides identified in calcium-associated proteins in the cytosolic fraction

The unique phosphopeptides identified in the cytosolic fraction of the renal cortices from FK506-treated mice filtered by the GO term “calcium” and are presented in this table.

Chapter 7. References

1. Kearney PM, Whelton M, Reynolds K, Muntner P, Whelton PK, He J. Global burden of hypertension: analysis of worldwide data. *Lancet Lond Engl*. 2005 Jan 15;365(9455):217–23.
2. Levy D, Larson MG, Vasan RS, Kannel WB, Ho KK. The progression from hypertension to congestive heart failure. *JAMA*. 1996 May 22;275(20):1557–62.
3. Udani S, Lazich I, Bakris GL. Epidemiology of hypertensive kidney disease. *Nat Rev Nephrol*. 2011 Jan;7(1):11–21.
4. Lim SS, Vos T, Flaxman AD, Danaei G, Shibuya K, Adair-Rohani H, et al. A comparative risk assessment of burden of disease and injury attributable to 67 risk factors and risk factor clusters in 21 regions, 1990-2010: a systematic analysis for the Global Burden of Disease Study 2010. *Lancet Lond Engl*. 2012 Dec 15;380(9859):2224–60.
5. Causes of Death 2008 [online database]. Geneva, World Health Organization [Internet]. 2008. Available from: http://www.who.int/healthinfo/global_burden_disease/cod_2008_sources_methods.pdf.
6. Gaziano TA, Bitton A, Anand S, Weinstein MC, International Society of Hypertension. The global cost of nonoptimal blood pressure. *J Hypertens*. 2009 Jul;27(7):1472–7.
7. Boyden LM, Choi M, Choate KA, Nelson-Williams CJ, Farhi A, Toka HR, et al. Mutations in Kelch-like 3 and Cullin 3 cause hypertension and electrolyte abnormalities. *Nature*. 2012 Jan 22;482(7383):98–102.
8. Wilson FH, Disse-Nicodème S, Choate KA, Ishikawa K, Nelson-Williams C, Desitter I, et al. Human Hypertension Caused by Mutations in WNK Kinases. *Science*. 2001 Oct 8;293(5532):1107–12.
9. Choi M, Scholl UI, Yue P, Björklund P, Zhao B, Nelson-Williams C, et al. K⁺ channel mutations in adrenal aldosterone-producing adenomas and hereditary hypertension. *Science*. 2011 Feb 11;331(6018):768–72.
10. Shimkets RA, Warnock DG, Bositis CM, Nelson-Williams C, Hansson JH, Schambelan M, et al. Little's syndrome: heritable human hypertension caused by mutations in the beta subunit of the epithelial sodium channel. *Cell*. 1994 Nov 4;79(3):407–14.
11. Ehret GB, Caulfield MJ. Genes for blood pressure: an opportunity to understand hypertension. *Eur Heart J*. 2013 Apr;34(13):951–61.
12. Institute of Medicine (US) Committee on Public Health Priorities to Reduce and Control Hypertension. A Population-Based Policy and Systems Change Approach to Prevent and Control Hypertension [Internet]. Washington (DC): National Academies Press (US); 2010 [cited 2017 Apr 20]. Available from: <http://www.ncbi.nlm.nih.gov/books/NBK220087/>

13. Gami AS, Witt BJ, Howard DE, Erwin PJ, Gami LA, Somers VK, et al. Metabolic syndrome and risk of incident cardiovascular events and death: a systematic review and meta-analysis of longitudinal studies. *J Am Coll Cardiol*. 2007 Jan 30;49(4):403–14.
14. Reaven GM. Role of Insulin Resistance in Human Disease. *Diabetes*. 1988 Dec 1;37(12):1595–607.
15. Kolovou GD, Anagnostopoulou KK, Salpea KD, Mikhailidis DP. The prevalence of metabolic syndrome in various populations. *Am J Med Sci*. 2007 Jun;333(6):362–71.
16. Desroches S, Lamarche B. The evolving definitions and increasing prevalence of the metabolic syndrome. *Appl Physiol Nutr Metab Physiol Appl Nutr Metab*. 2007 Feb;32(1):23–32.
17. Alberti KG, Zimmet PZ. Definition, diagnosis and classification of diabetes mellitus and its complications. Part 1: diagnosis and classification of diabetes mellitus provisional report of a WHO consultation. *Diabet Med J Br Diabet Assoc*. 1998 Jul;15(7):539–53.
18. Expert Panel on Detection, Evaluation, and Treatment of High Blood Cholesterol in Adults. Executive Summary of The Third Report of The National Cholesterol Education Program (NCEP) Expert Panel on Detection, Evaluation, And Treatment of High Blood Cholesterol In Adults (Adult Treatment Panel III). *JAMA*. 2001 May 16;285(19):2486–97.
19. Einhorn D, Reaven GM, Cobin RH, Ford E, Ganda OP, Handelsman Y, et al. American College of Endocrinology position statement on the insulin resistance syndrome. *Endocr Pract Off J Am Coll Endocrinol Am Assoc Clin Endocrinol*. 2003 Jun;9(3):237–52.
20. Balkau B, Charles MA. Comment on the provisional report from the WHO consultation. European Group for the Study of Insulin Resistance (EGIR). *Diabet Med J Br Diabet Assoc*. 1999 May;16(5):442–3.
21. IDF Worldwide Definition of the Metabolic Syndrome [Internet]. International Diabetes Federation. [cited 2017 Apr 24]. Available from: <http://www.idf.org/metabolic-syndrome>
22. Balkau B, Charles M-A, Drivsholm T, Borch-Johnsen K, Wareham N, Yudkin JS, et al. Frequency of the WHO metabolic syndrome in European cohorts, and an alternative definition of an insulin resistance syndrome. *Diabetes Metab*. 2002 Nov;28(5):364–76.
23. Alberti KG, Eckel RH, Grundy SM, Zimmet PZ, Cleeman JI, Donato KA, et al. Harmonizing the metabolic syndrome: a joint interim statement of the International Diabetes Federation Task Force on Epidemiology and Prevention; National Heart, Lung, and Blood Institute; American Heart Association; World Heart Federation; International Atherosclerosis Society;

- and International Association for the Study of Obesity. *Circulation*. 2009 Oct 20;120(16):1640–5.
24. Hamaguchi M, Kojima T, Takeda N, Nakagawa T, Taniguchi H, Fujii K, et al. The metabolic syndrome as a predictor of nonalcoholic fatty liver disease. *Ann Intern Med*. 2005 Nov 15;143(10):722–8.
 25. Magliano M. Obesity and arthritis. *Menopause Int*. 2008 Dec;14(4):149–54.
 26. Zhou J, Zhang Q, Yuan X, Wang J, Li C, Sheng H, et al. Association between metabolic syndrome and osteoporosis: a meta-analysis. *Bone*. 2013 Nov;57(1):30–5.
 27. Romero V, Akpınar H, Assimos DG. Kidney Stones: A Global Picture of Prevalence, Incidence, and Associated Risk Factors. *Rev Urol*. 2010;12(2–3):e86–96.
 28. Prié D, Huart V, Bakouh N, Planelles G, Dellis O, Gérard B, et al. Nephrolithiasis and osteoporosis associated with hypophosphatemia caused by mutations in the type 2a sodium-phosphate cotransporter. *N Engl J Med*. 2002 Sep 26;347(13):983–91.
 29. Hodgkinson A, Pyrah LN. The urinary excretion of calcium and inorganic phosphate in 344 patients with calcium stone of renal origin. *Br J Surg*. 1958 Jul;46(195):10–8.
 30. Coe FL, Parks JH, Asplin JR. The pathogenesis and treatment of kidney stones. *N Engl J Med*. 1992 Oct 15;327(16):1141–52.
 31. Johnell O, Kanis JA. An estimate of the worldwide prevalence and disability associated with osteoporotic fractures. *Osteoporos Int J Establ Result Coop Eur Found Osteoporos Natl Osteoporos Found USA*. 2006 Dec;17(12):1726–33.
 32. Hesse A, Brändle E, Wilbert D, Köhrmann K-U, Alken P. Study on the prevalence and incidence of urolithiasis in Germany comparing the years 1979 vs. 2000. *Eur Urol*. 2003 Dec;44(6):709–13.
 33. Trinchieri A, Coppi F, Montanari E, Del Nero A, Zanetti G, Pisani E. Increase in the prevalence of symptomatic upper urinary tract stones during the last ten years. *Eur Urol*. 2000 Jan;37(1):23–5.
 34. Yasui T, Iguchi M, Suzuki S, Kohri K. Prevalence and epidemiological characteristics of urolithiasis in Japan: national trends between 1965 and 2005. *Urology*. 2008 Feb;71(2):209–13.
 35. Turney BW, Reynard JM, Noble JG, Keoghane SR. Trends in urological stone disease. *BJU Int*. 2012 Apr 1;109(7):1082–7.

36. Casey MJ, Meier-Kriesche H-U. Calcineurin inhibitors in kidney transplantation: friend or foe? *Curr Opin Nephrol Hypertens*. 2011 Nov;20(6):610–5.
37. Zsom L, Wagner L, Fülöp T. Minimization vs tailoring: Where do we stand with personalized immunosuppression during renal transplantation in 2015? *World J Transplant*. 2015 Sep 24;5(3):73–80.
38. Laupacis A, Keown PA, Ulan RA, McKenzie N, Stiller CR. Cyclosporin A: a powerful immunosuppressant. *Can Med Assoc J*. 1982 May 1;126(9):1041–6.
39. Sandrini S, Aslam N, Tardanico R, Setti G, Bossini N, Valerio F, et al. Tacrolimus versus cyclosporine for early steroid withdrawal after renal transplantation. *J Nephrol*. 2012 Feb;25(1):43–9.
40. Rush D. The impact of calcineurin inhibitors on graft survival. *Transplant Rev Orlando Fla*. 2013 Jul;27(3):93–5.
41. Lamb KE, Lodhi S, Meier-Kriesche H-U. Long-term renal allograft survival in the United States: a critical reappraisal. *Am J Transplant Off J Am Soc Transplant Am Soc Transpl Surg*. 2011 Mar;11(3):450–62.
42. Bloom RD, Reese PP. Chronic kidney disease after nonrenal solid-organ transplantation. *J Am Soc Nephrol JASN*. 2007 Dec;18(12):3031–41.
43. Bamgbola O. Metabolic consequences of modern immunosuppressive agents in solid organ transplantation. *Ther Adv Endocrinol Metab*. 2016 Jun;7(3):110–27.
44. Faenza A, Fuga G, Nardo B, Donati G, Cianciolo G, Scolari MP, et al. Metabolic syndrome after kidney transplantation. *Transplant Proc*. 2007 Aug;39(6):1843–6.
45. Laryea M, Watt KD, Molinari M, Walsh MJ, McAlister VC, Marotta PJ, et al. Metabolic syndrome in liver transplant recipients: prevalence and association with major vascular events. *Liver Transplant Off Publ Am Assoc Study Liver Dis Int Liver Transplant Soc*. 2007 Aug;13(8):1109–14.
46. De Vries APJ, Bakker SJL, Van Son WJ, Van Der Heide JJH, Ploeg RJ, The HT, et al. Metabolic Syndrome Is Associated with Impaired Long-term Renal Allograft Function; Not All Component criteria Contribute Equally. *Am J Transplant*. 2004 Oct 1;4(10):1675–83.
47. Bianchi G, Marchesini G, Marzocchi R, Pinna AD, Zoli M. Metabolic syndrome in liver transplantation: relation to etiology and immunosuppression. *Liver Transplant Off Publ Am Assoc Study Liver Dis Int Liver Transplant Soc*. 2008 Nov;14(11):1648–54.

48. Vogt DP, Henderson JM, Carey WD, Barnes D. The long-term survival and causes of death in patients who survive at least 1 year after liver transplantation. *Surgery*. 2002 Oct;132(4):775–80.
49. Marcén R. Immunosuppressive drugs in kidney transplantation: impact on patient survival, and incidence of cardiovascular disease, malignancy and infection. *Drugs*. 2009 Nov 12;69(16):2227–43.
50. Weir MR, Burgess ED, Cooper JE, Fenves AZ, Goldsmith D, McKay D, et al. Assessment and Management of Hypertension in Transplant Patients. *J Am Soc Nephrol JASN*. 2015 Jun;26(6):1248–60.
51. Hoorn EJ, Walsh SB, McCormick JA, Fürstenberg A, Yang C-L, Roeschel T, et al. The calcineurin inhibitor tacrolimus activates the renal sodium chloride cotransporter to cause hypertension. *Nat Med*. 2011 Oct;17(10):1304–9.
52. Kaplan B, Wang Z, Abecassis MM, Fryer JP, Stuart FP, Kaufman DB. Frequency of hyperkalemia in recipients of simultaneous pancreas and kidney transplants with bladder drainage. *Transplantation*. 1996 Oct 27;62(8):1174–5.
53. Kim HC, Hwang EA, Han SY, Park SB, Kim HT, Cho WH. Primary immunosuppression with tacrolimus in kidney transplantation: three-year follow-up in a single center. *Transplant Proc*. 2004 Sep;36(7):2082–3.
54. Schwarz C, Benesch T, Kodras K, Oberbauer R, Haas M. Complete renal tubular acidosis late after kidney transplantation. *Nephrol Dial Transplant*. 2006 Sep 1;21(9):2615–20.
55. Yakupoglu HY, Corsenca A, Wahl P, Wüthrich RP, Ambühl PM. Posttransplant acidosis and associated disorders of mineral metabolism in patients with a renal graft. *Transplantation*. 2007 Nov 15;84(9):1151–7.
56. Lee C-T, Huynh VM, Lai L-W, Lien Y-HH. Cyclosporine A-induced hypercalciuria in calbindin-D28k knockout and wild-type mice. *Kidney Int*. 2002 Dec;62(6):2055–61.
57. Nijenhuis T, Hoenderop JGJ, Bindels RJM. Downregulation of Ca²⁺ and Mg²⁺ Transport Proteins in the Kidney Explains Tacrolimus (FK506)-Induced Hypercalciuria and Hypomagnesemia. *J Am Soc Nephrol*. 2004 Jan 3;15(3):549–57.
58. Barton CH, Vaziri ND, Martin DC, Choi S, Alikhani S. Hypomagnesemia and renal magnesium wasting in renal transplant recipients receiving cyclosporine. *Am J Med*. 1987 Oct;83(4):693–9.
59. Moz Y, Levi R, Lavi-Moshayoff V, Cox KB, Molckentin JD, Silver J, et al. Calcineurin A β Is Central to the Expression of the Renal Type II Na/Pi Co-transporter Gene and to the Regulation of Renal Phosphate Transport. *J Am Soc Nephrol*. 2004 Jan 12;15(12):2972–80.

60. Mayan H, Vered I, Mouallem M, Tzadok-Witkon M, Pauzner R, Farfel Z. Pseudohypoaldosteronism type II: marked sensitivity to thiazides, hypercalciuria, normomagnesemia, and low bone mineral density. *J Clin Endocrinol Metab.* 2002 Jul;87(7):3248–54.
61. Vidal-Petiot E, Elvira-Matelot E, Mutig K, Soukaseum C, Baudrie V, Wu S, et al. WNK1-related Familial Hyperkalemic Hypertension results from an increased expression of L-WNK1 specifically in the distal nephron. *Proc Natl Acad Sci U S A.* 2013 Aug 27;110(35):14366–71.
62. Roser M, Eibl N, Eisenhaber B, Seringer J, Nagel M, Nagorka S, et al. Gitelman Syndrome. *Hypertension.* 2009 Jan 6;53(6):893–7.
63. Graziani G, Fedeli C, Moroni L, Cosmai L, Badalamenti S, Ponticelli C. Gitelman syndrome: pathophysiological and clinical aspects. *QJM.* 2010 Jan 10;103(10):741–8.
64. Nijenhuis T, Vallon V, van der Kemp AWCM, Loffing J, Hoenderop JGJ, Bindels RJM. Enhanced passive Ca²⁺ reabsorption and reduced Mg²⁺ channel abundance explains thiazide-induced hypocalciuria and hypomagnesemia. *J Clin Invest.* 2005 Jun 1;115(6):1651–8.
65. Levick JR. *An Introduction to Cardiovascular Physiology.* Butterworth-Heinemann; 2013. 288 p.
66. Eladari D, Chambrey R, Picard N, Hadchouel J. Electroneutral absorption of NaCl by the aldosterone-sensitive distal nephron: implication for normal electrolytes homeostasis and blood pressure regulation. *Cell Mol Life Sci.* 2014 Feb 21;71(15):2879–95.
67. Boone M, Deen PMT. Physiology and pathophysiology of the vasopressin-regulated renal water reabsorption. *Pflugers Arch.* 2008 Sep;456(6):1005–24.
68. Chabardès D, Gagnan-Brunette M, Imbert-Teboul M, Gontcharevskaja O, Montégut M, Clique A, et al. Adenylate cyclase responsiveness to hormones in various portions of the human nephron. *J Clin Invest.* 1980 Feb;65(2):439–48.
69. Arriza JL, Weinberger C, Cerelli G, Glaser TM, Handelin BL, Housman DE, et al. Cloning of human mineralocorticoid receptor complementary DNA: structural and functional kinship with the glucocorticoid receptor. *Science.* 1987 Jul 17;237(4812):268–75.
70. Bostanjoglo M, Reeves WB, Reilly RF, Velázquez H, Robertson N, Litwack G, et al. 11β-hydroxysteroid dehydrogenase, mineralocorticoid receptor, and thiazide-sensitive Na-Cl cotransporter expression by distal tubules. *J Am Soc Nephrol JASN.* 1998 Aug;9(8):1347–58.

71. Yoshitomi K, Shimizu T, Taniguchi J, Imai M. Electrophysiological characterization of rabbit distal convoluted tubule cell. *Pflüg Arch.* 1989 Aug 1;414(4):457–63.
72. Schmidt U, Dubach UC. Activity of (Na+K+)-stimulated adenosintriphosphatase in the rat nephron. *Pflugers Arch.* 1969;306(3):219–26.
73. Dørup J. Ultrastructure of distal nephron cells in rat renal cortex. *J Ultrastruct Res.* 1985 Aug;92(1–2):101–18.
74. Hierholzer K, Wiederholt M. Some aspects of distal tubular solute and water transport. *Kidney Int.* 1976 Feb;9(2):198–213.
75. Bachmann S, Velazquez H, Obermuller N, Reilly RF, Moser D, Ellison DH. Expression of the thiazide-sensitive Na-Cl cotransporter by rabbit distal convoluted tubule cells. *J Clin Invest.* 1995 Nov;96(5):2510–4.
76. Plotkin MD, Kaplan MR, Verlander JW, Lee WS, Brown D, Poch E, et al. Localization of the thiazide sensitive Na-Cl cotransporter, rTSC1 in the rat kidney. *Kidney Int.* 1996 Jul;50(1):174–83.
77. Hayslett JP, Boulpaep EL, Kashgarian M, Giebisch GH. Electrical characteristics of the mammalian distal tubule: Comparison of Ling-Gerard and macroelectrodes. *Kidney Int.* 1977 Nov;12(5):324–31.
78. Chambrey R, Warnock DG, Podevin R-A, Bruneval P, Mandet C, Bélair M-F, et al. Immunolocalization of the Na+/H+exchanger isoform NHE2 in rat kidney. *Am J Physiol - Ren Physiol.* 1998 Sep 1;275(3):F379–86.
79. Bailey MA, Giebisch G, Abbiati T, Aronson PS, Gawenis LR, Shull GE, et al. NHE2-mediated bicarbonate reabsorption in the distal tubule of NHE3 null mice. *J Physiol.* 2004 Dec 1;561(3):765–75.
80. Doucet A. Function and control of Na-K-ATPase in single nephron segments of the mammalian kidney. *Kidney Int.* 1988 Dec;34(6):749–60.
81. Hamilton KL, Devor DC. Basolateral membrane K+ channels in renal epithelial cells. *Am J Physiol - Ren Physiol.* 2012 May 1;302(9):F1069–81.
82. Pacheco-Alvarez D, Cristóbal PS, Meade P, Moreno E, Vazquez N, Muñoz E, et al. The Na+:Cl- cotransporter is activated and phosphorylated at the amino-terminal domain upon intracellular chloride depletion. *J Biol Chem.* 2006 Sep 29;281(39):28755–63.
83. Estévez R, Boettger T, Stein V, Birkenhäger R, Otto E, Hildebrandt F, et al. Barttin is a Cl- channel beta-subunit crucial for renal Cl- reabsorption and inner ear K+ secretion. *Nature.* 2001 Nov 29;414(6863):558–61.

84. Velázquez H, Silva T. Cloning and localization of KCC4 in rabbit kidney: expression in distal convoluted tubule. *Am J Physiol Renal Physiol*. 2003 Jul;285(1):F49-58.
85. Mercado A, Song L, Vázquez N, Mount DB, Gamba G. Functional Comparison of the K⁺-Cl⁻-Cotransporters KCC1 and KCC4. *J Biol Chem*. 2000 Sep 29;275(39):30326–34.
86. Liapis H, Nag M, Kaji DM. K-Cl cotransporter expression in the human kidney. *Am J Physiol*. 1998 Dec;275(6 Pt 1):C1432-1437.
87. Payne JA. Functional characterization of the neuronal-specific K-Cl cotransporter: implications for [K⁺]_o regulation. *Am J Physiol - Cell Physiol*. 1997 Nov 1;273(5):C1516–25.
88. Mount DB, Mercado A, Song L, Xu J, George AL, Delpire E, et al. Cloning and Characterization of KCC3 and KCC4, New Members of the Cation-Chloride Cotransporter Gene Family. *J Biol Chem*. 1999 Apr 6;274(23):16355–62.
89. Melo Z, Cruz-Rangel S, Bautista R, Vázquez N, Castañeda-Bueno M, Mount DB, et al. Molecular evidence for a role for K⁽⁺⁾-Cl⁽⁻⁾ cotransporters in the kidney. *Am J Physiol Renal Physiol*. 2013 Nov 15;305(10):F1402-1411.
90. Balkovetz DF. Claudins at the gate: determinants of renal epithelial tight junction paracellular permeability. *Am J Physiol - Ren Physiol*. 2006 Mar 1;290(3):F572–9.
91. Kirk A, Campbell S, Bass P, Mason J, Collins J. Differential expression of claudin tight junction proteins in the human cortical nephron. *Nephrol Dial Transplant Off Publ Eur Dial Transpl Assoc - Eur Ren Assoc*. 2010 Jul;25(7):2107–19.
92. Angelow S, Kim K-J, Yu ASL. Claudin-8 modulates paracellular permeability to acidic and basic ions in MDCK II cells. *J Physiol*. 2006 Feb 15;571(Pt 1):15–26.
93. Van Itallie C, Rahner C, Anderson JM. Regulated expression of claudin-4 decreases paracellular conductance through a selective decrease in sodium permeability. *J Clin Invest*. 2001 May;107(10):1319–27.
94. Hou J, Renigunta A, Yang J, Waldegger S. Claudin-4 forms paracellular chloride channel in the kidney and requires claudin-8 for tight junction localization. *Proc Natl Acad Sci U S A*. 2010 Oct 19;107(42):18010–5.
95. Schnermann J, Steipe B, Briggs JP. In situ studies of distal convoluted tubule in rat. II. K secretion. *Am J Physiol - Ren Physiol*. 1987 Jun 1;252(6):F970–6.

96. Wade JB, Fang L, Coleman RA, Liu J, Grimm PR, Wang T, et al. Differential regulation of ROMK (Kir1.1) in distal nephron segments by dietary potassium. *Am J Physiol - Ren Physiol*. 2011 Jun 1;300(6):F1385–93.
97. Lazrak A, Liu Z, Huang C-L. Antagonistic regulation of ROMK by long and kidney-specific WNK1 isoforms. *Proc Natl Acad Sci U S A*. 2006 Jan 31;103(5):1615–20.
98. Rieg T, Vallon V, Sausbier M, Sausbier U, Kaissling B, Ruth P, et al. The role of the BK channel in potassium homeostasis and flow-induced renal potassium excretion. *Kidney Int*. 2007 Sep;72(5):566–73.
99. Liu W, Xu S, Woda C, Kim P, Weinbaum S, Satlin LM. Effect of flow and stretch on the $[Ca^{2+}]_i$ response of principal and intercalated cells in cortical collecting duct. *Am J Physiol - Ren Physiol*. 2003 Nov 1;285(5):F998–1012.
100. Kudlacek PE, Pluznick JL, Ma R, Padanilam B, Sansom SC. Role of $h\beta 1$ in activation of human mesangial BK channels by cGMP kinase. *Am J Physiol - Ren Physiol*. 2003 Aug 1;285(2):F289–94.
101. Reichold M, Zdebik AA, Lieberer E, Rapedius M, Schmidt K, Bandulik S, et al. KCNJ10 gene mutations causing EAST syndrome (epilepsy, ataxia, sensorineural deafness, and tubulopathy) disrupt channel function. *Proc Natl Acad Sci U S A*. 2010 Aug 10;107(32):14490–5.
102. Bandulik S, Schmidt K, Bockenhauer D, Zdebik AA, Humberg E, Kleta R, et al. The salt-wasting phenotype of EAST syndrome, a disease with multifaceted symptoms linked to the KCNJ10 K^+ channel. *Pflugers Arch*. 2011 Apr;461(4):423–35.
103. Lourdel S, Paulais M, Cluzeaud F, Bens M, Tanemoto M, Kurachi Y, et al. An inward rectifier K^+ channel at the basolateral membrane of the mouse distal convoluted tubule: similarities with Kir4-Kir5.1 heteromeric channels. *J Physiol*. 2002 Jan 15;538(Pt 2):391–404.
104. Chiga M, Rai T, Yang S-S, Ohta A, Takizawa T, Sasaki S, et al. Dietary salt regulates the phosphorylation of OSR1/SPAK kinases and the sodium chloride cotransporter through aldosterone. *Kidney Int*. 2008 Dec;74(11):1403–9.
105. Castañeda-Bueno M, Cervantes-Perez LG, Rojas-Vega L, Arroyo-Garza I, Vázquez N, Moreno E, et al. Modulation of NCC activity by low and high K^+ intake: insights into the signaling pathways involved. *Am J Physiol - Ren Physiol*. 2014 Jun 15;306(12):F1507–19.
106. Vallon V, Schroth J, Lang F, Kuhl D, Uchida S. Expression and phosphorylation of the Na^+-Cl^- cotransporter NCC in vivo is regulated by dietary salt, potassium, and SGK1. *Am J Physiol - Ren Physiol*. 2009 Sep;297(3):F704–12.

107. Castañeda-Bueno M, Cervantes-Pérez LG, Vázquez N, Uribe N, Kantesaria S, Morla L, et al. Activation of the renal Na⁺:Cl⁻ cotransporter by angiotensin II is a WNK4-dependent process. *Proc Natl Acad Sci*. 2012 May 15;109(20):7929–34.
108. Sandberg MB, Riquier ADM, Pihakaski-Maunsbach K, McDonough AA, Maunsbach AB. ANG II provokes acute trafficking of distal tubule Na⁺-Cl⁻ cotransporter to apical membrane. *Am J Physiol Renal Physiol*. 2007 Sep;293(3):F662-669.
109. San-Cristobal P, Pacheco-Alvarez D, Richardson C, Ring AM, Vazquez N, Rafiqi FH, et al. Angiotensin II signaling increases activity of the renal Na-Cl cotransporter through a WNK4-SPAK-dependent pathway. *Proc Natl Acad Sci U S A*. 2009 Mar 17;106(11):4384–9.
110. Rozansky DJ, Cornwall T, Subramanya AR, Rogers S, Yang Y-F, David LL, et al. Aldosterone mediates activation of the thiazide-sensitive Na-Cl cotransporter through an SGK1 and WNK4 signaling pathway. *J Clin Invest*. 2009 Sep;119(9):2601–12.
111. Pedersen NB, Hofmeister MV, Rosenbaek LL, Nielsen J, Fenton RA. Vasopressin induces phosphorylation of the thiazide-sensitive sodium chloride cotransporter in the distal convoluted tubule. *Kidney Int*. 2010 Jul;78(2):160–9.
112. Saritas T, Borschewski A, McCormick JA, Paliege A, Dathe C, Uchida S, et al. SPAK Differentially Mediates Vasopressin Effects on Sodium Cotransporters. *J Am Soc Nephrol*. 2013 Jan 3;24(3):407–18.
113. Komers R, Rogers S, Oyama TT, Xu B, Yang C-L, McCormick J, et al. Enhanced phosphorylation of Na-Cl cotransporter in experimental metabolic syndrome – role of insulin. *Clin Sci Lond Engl* 1979. 2012 Dec;123(11):635–47.
114. Sohara E, Rai T, Yang S-S, Ohta A, Naito S, Chiga M, et al. Acute insulin stimulation induces phosphorylation of the Na-Cl cotransporter in cultured distal mpkDCT cells and mouse kidney. *PLoS One*. 2011;6(8):e24277.
115. Ellison DH, Velázquez H, Wright FS. Adaptation of the distal convoluted tubule of the rat. Structural and functional effects of dietary salt intake and chronic diuretic infusion. *J Clin Invest*. 1989 Jan;83(1):113–26.
116. Richardson C, Rafiqi FH, Karlsson HKR, Moleleki N, Vandewalle A, Campbell DG, et al. Activation of the thiazide-sensitive Na⁺-Cl⁻ cotransporter by the WNK-regulated kinases SPAK and OSR1. *J Cell Sci*. 2008 Mar 1;121(Pt 5):675–84.
117. Richardson C, Alessi DR. The regulation of salt transport and blood pressure by the WNK-SPAK/OSR1 signalling pathway. *J Cell Sci*. 2008 Oct 15;121(Pt 20):3293–304.

118. Gamba G. WNK lies upstream of kinases involved in regulation of ion transporters. *Biochem J*. 2005 Oct 1;391(Pt 1):e1-3.
119. Moriguchi T, Urushiyama S, Hisamoto N, Iemura S, Uchida S, Natsume T, et al. WNK1 regulates phosphorylation of cation-chloride-coupled cotransporters via the STE20-related kinases, SPAK and OSR1. *J Biol Chem*. 2005 Dec 30;280(52):42685–93.
120. Vitari AC, Deak M, Morrice NA, Alessi DR. The WNK1 and WNK4 protein kinases that are mutated in Gordon's hypertension syndrome phosphorylate and activate SPAK and OSR1 protein kinases. *Biochem J*. 2005 Oct 1;391(Pt 1):17–24.
121. Subramanya AR, Liu J, Ellison DH, Wade JB, Welling PA. WNK4 Diverts the Thiazide-sensitive NaCl Cotransporter to the Lysosome and Stimulates AP-3 Interaction. *J Biol Chem*. 2009 Mar 7;284(27):18471–80.
122. Chen S, Bhargava A, Mastroberardino L, Meijer OC, Wang J, Buse P, et al. Epithelial sodium channel regulated by aldosterone-induced protein sgk. *Proc Natl Acad Sci U S A*. 1999 Mar 2;96(5):2514–9.
123. Ring AM, Leng Q, Rinehart J, Wilson FH, Kahle KT, Hebert SC, et al. An SGK1 site in WNK4 regulates Na⁺ channel and K⁺ channel activity and has implications for aldosterone signaling and K⁺ homeostasis. *Proc Natl Acad Sci U S A*. 2007 Mar 6;104(10):4025–9.
124. Mujais SK, Kauffman S, Katz AI. Angiotensin II binding sites in individual segments of the rat nephron. *J Clin Invest*. 1986 Jan;77(1):315–8.
125. Sun P, Yue P, Wang W-H. Angiotensin II stimulates epithelial sodium channels in the cortical collecting duct of the rat kidney. *Am J Physiol Renal Physiol*. 2012 Mar 15;302(6):F679-687.
126. Yue P, Sun P, Lin D-H, Pan C, Xing W, Wang W. Angiotensin II diminishes the effect of SGK1 on the WNK4-mediated inhibition of ROMK1 channels. *Kidney Int*. 2011 Feb;79(4):423–31.
127. Lin D-H, Sterling H, Lerea KM, Welling P, Jin L, Giebisch G, et al. K depletion increases protein tyrosine kinase-mediated phosphorylation of ROMK. *Am J Physiol - Ren Physiol*. 2002 Oct 1;283(4):F671–7.
128. Sterling H, Lin D-H, Gu R-M, Dong K, Hebert SC, Wang W-H. Inhibition of Protein-tyrosine Phosphatase Stimulates the Dynamin-dependent Endocytosis of ROMK1. *J Biol Chem*. 2002 Aug 2;277(6):4317–23.
129. Yue P, Lin D-H, Pan C-Y, Leng Q, Giebisch G, Lifton RP, et al. Src family protein tyrosine kinase (PTK) modulates the effect of SGK1 and WNK4 on ROMK channels. *Proc Natl Acad Sci*. 2009 Jan 9;106(35):15061–6.
130. Greger R, Lang F, Oberleithner H. Distal site of calcium reabsorption in the rat nephron. *Pflüg Arch Eur J Physiol*. 1978 May 18;374(2):153–7.

131. Hoenderop JGJ, Kemp AWCM van der, Hartog A, Graaf SFJ van de, Os CH van, Willems PHGM, et al. Molecular Identification of the Apical Ca²⁺Channel in 1,25-Dihydroxyvitamin D₃-responsive Epithelia. *J Biol Chem*. 1999 Mar 26;274(13):8375–8.
132. Yu ASL. Identification and localization of calcium channel α 1 and β subunit isoforms in the kidney. *Kidney Int - KIDNEY INT*. 1995;48(4):1097–101.
133. Gross M, Kumar R. Physiology and biochemistry of vitamin D-dependent calcium binding proteins. *Am J Physiol - Ren Physiol*. 1990 Aug 1;259(2):F195–209.
134. Hemmingsen C. Regulation of renal calbindin-D28K. *Pharmacol Toxicol*. 2000;87 Suppl 3:5–30.
135. Magyar CE, White KE, Rojas R, Apodaca G, Friedman PA. Plasma membrane Ca²⁺-ATPase and NCX1 Na⁺/Ca²⁺ exchanger expression in distal convoluted tubule cells. *Am J Physiol - Ren Physiol*. 2002 Jul 1;283(1):F29–40.
136. Nijenhuis T, Hoenderop JGJ, Kemp AWCM van der, Bindels RJM. Localization and Regulation of the Epithelial Ca²⁺ Channel TRPV6 in the Kidney. *J Am Soc Nephrol*. 2003 Jan 11;14(11):2731–40.
137. Hoenderop JGJ, Hartog A, Stuiver M, Doucet A, Willems PHGM, Bindels RJM. Localization of the Epithelial Ca²⁺ Channel in Rabbit Kidney and Intestine. *J Am Soc Nephrol*. 2000 Jan 7;11(7):1171–8.
138. Peng J-B. TRPV5 and TRPV6 in transcellular Ca(2+) transport: regulation, gene duplication, and polymorphisms in African populations. *Adv Exp Med Biol*. 2011;704:239–75.
139. Christakos S, Dhawan P, Porta A, Mady LJ, Seth T. Vitamin D and Intestinal Calcium Absorption. *Mol Cell Endocrinol*. 2011 Dec 5;347(1–2):25–9.
140. Loffing J, Loffing-Cueni D, Valderrabano V, Kläusli L, Hebert SC, Rossier BC, et al. Distribution of transcellular calcium and sodium transport pathways along mouse distal nephron. *Am J Physiol - Ren Physiol*. 2001 Dec 1;281(6):F1021–7.
141. Barry EL, Gesek FA, Yu AS, Lytton J, Friedman PA. Distinct calcium channel isoforms mediate parathyroid hormone and chlorothiazide-stimulated calcium entry in transporting epithelial cells. *J Membr Biol*. 1998 Jan 1;161(1):55–64.
142. Lee K, Brown D, Urena P, Ardaillou N, Ardaillou R, Deeds J, et al. Localization of parathyroid hormone/parathyroid hormone-related peptide receptor mRNA in kidney. *Am J Physiol - Ren Physiol*. 1996 Jan 1;270(1):F186–91.

143. Kumar R, Schaefer J, Grande JP, Roche PC. Immunolocalization of calcitriol receptor, 24-hydroxylase cytochrome P-450, and calbindin D28k in human kidney. *Am J Physiol*. 1994 Mar;266(3 Pt 2):F477-485.
144. Wang Y, Borchert ML, DeLuca HF. Identification of the vitamin D receptor in various cells of the mouse kidney. *Kidney Int*. 2012 May;81(10):993–1001.
145. Xi Q, Wang S, Ye Z, Liu J, Yu X, Zhu Z, et al. Adenovirus-delivered microRNA targeting the vitamin D receptor reduces intracellular Ca²⁺ concentrations by regulating the expression of Ca²⁺-transport proteins in renal epithelial cells. *BJU Int*. 2011 Apr 1;107(8):1314–9.
146. Kuro-o M, Matsumura Y, Aizawa H, Kawaguchi H, Suga T, Utsugi T, et al. Mutation of the mouse *klotho* gene leads to a syndrome resembling ageing. *Nature*. 1997 Nov 6;390(6655):45–51.
147. Chang Q, Hoefs S, van der Kemp AW, Topala CN, Bindels RJ, Hoenderop JG. The beta-glucuronidase *klotho* hydrolyzes and activates the TRPV5 channel. *Science*. 2005 Oct 21;310(5747):490–3.
148. Cha S-K, Ortega B, Kurosu H, Rosenblatt KP, Kuro-o M, Huang C-L. Removal of sialic acid involving *Klotho* causes cell-surface retention of TRPV5 channel via binding to galectin-1. *Proc Natl Acad Sci*. 2008 Jul 15;105(28):9805–10.
149. Morel F, Roinel N, Le Grimellec C. Electron probe analysis of tubular fluid composition. *Nephron*. 1969;6(3):350–64.
150. Voets T, Nilius B, Hoefs S, van der Kemp AWCM, Droogmans G, Bindels RJM, et al. TRPM6 forms the Mg²⁺ influx channel involved in intestinal and renal Mg²⁺ absorption. *J Biol Chem*. 2004 Jan 2;279(1):19–25.
151. Günther T. Total and free Mg²⁺ contents in erythrocytes: a simple but still undisclosed cell model. *Magnes Res*. 2007 Sep;20(3):161–7.
152. Schweigel M, Park H-S, Etschmann B, Martens H. Characterization of the Na⁺-dependent Mg²⁺ transport in sheep ruminal epithelial cells. *Am J Physiol - Gastrointest Liver Physiol*. 2006 Jan 1;290(1):G56–65.
153. Günther T. Na⁺/Mg²⁺ antiport in non-erythrocyte vertebrate cells. *Magnes Res*. 2007 Jun;20(2):89–99.
154. Schweigel M, Martens H. Magnesium transport in the gastrointestinal tract. *Front Biosci J Virtual Libr*. 2000 Aug 1;5:D666-677.
155. Dai LJ, Ritchie G, Kerstan D, Kang HS, Cole DE, Quamme GA. Magnesium transport in the renal distal convoluted tubule. *Physiol Rev*. 2001 Jan;81(1):51–84.

156. Stuiver M, Lainez S, Will C, Terryn S, Günzel D, Debaix H, et al. CNNM2, encoding a basolateral protein required for renal Mg²⁺ handling, is mutated in dominant hypomagnesemia. *Am J Hum Genet.* 2011 Mar 11;88(3):333–43.
157. Baaij JHF de, Stuiver M, Meij IC, Lainez S, Kopplin K, Venselaar H, et al. Membrane Topology and Intracellular Processing of Cyclin M2 (CNNM2). *J Biol Chem.* 2012 Apr 20;287(17):13644–55.
158. Hurd TW, Otto EA, Mishima E, Gee HY, Inoue H, Inazu M, et al. Mutation of the Mg²⁺ transporter SLC41A1 results in a nephronophthisis-like phenotype. *J Am Soc Nephrol JASN.* 2013 May;24(6):967–77.
159. Kantorovich V, Adams JS, Gaines JE, Guo X, Pandian MR, Cohn DH, et al. Genetic heterogeneity in familial renal magnesium wasting. *J Clin Endocrinol Metab.* 2002 Feb;87(2):612–7.
160. Cairo ER, Friedrich T, Swarts HGP, Knoers NV, Bindels RJM, Monnens LA, et al. Impaired routing of wild type FXVD2 after oligomerisation with FXVD2-G41R might explain the dominant nature of renal hypomagnesemia. *Biochim Biophys Acta.* 2008 Feb;1778(2):398–404.
161. Meij IC, Koenderink JB, van Bokhoven H, Assink KF, Groenestege WT, de Pont JJ, et al. Dominant isolated renal magnesium loss is caused by misrouting of the Na(+),K(+)-ATPase gamma-subunit. *Nat Genet.* 2000 Nov;26(3):265–6.
162. Bockenbauer D, Feather S, Stanescu HC, Bandulik S, Zdebik AA, Reichold M, et al. Epilepsy, Ataxia, Sensorineural Deafness, Tubulopathy, and KCNJ10 Mutations. *N Engl J Med.* 2009 May 7;360(19):1960–70.
163. Glaudemans B, van der Wijst J, Scola RH, Lorenzoni PJ, Heister A, van der Kemp AW, et al. A missense mutation in the Kv1.1 voltage-gated potassium channel-encoding gene KCNA1 is linked to human autosomal dominant hypomagnesemia. *J Clin Invest.* 2009 Apr;119(4):936–42.
164. Wijst J van der, Glaudemans B, Venselaar H, Nair AV, Forst A-L, Hoenderop JGJ, et al. Functional Analysis of the Kv1.1 N255D Mutation Associated with Autosomal Dominant Hypomagnesemia. *J Biol Chem.* 2010 Jan 1;285(1):171–8.
165. Groenestege WMT, Thébault S, van der Wijst J, van den Berg D, Janssen R, Tejpar S, et al. Impaired basolateral sorting of pro-EGF causes isolated recessive renal hypomagnesemia. *J Clin Invest.* 2007 Aug 1;117(8):2260–7.
166. Ikari A, Okude C, Sawada H, Yamazaki Y, Sugatani J, Miwa M. TRPM6 expression and cell proliferation are up-regulated by phosphorylation of ERK1/2 in renal epithelial cells. *Biochem Biophys Res Commun.* 2008 May 16;369(4):1129–33.

167. Thebault S, Alexander RT, Tiel Groenestege WM, Hoenderop JG, Bindels RJ. EGF Increases TRPM6 Activity and Surface Expression. *J Am Soc Nephrol JASN*. 2009 Jan;20(1):78–85.
168. Knoers NV, Levtchenko EN. Gitelman syndrome. *Orphanet J Rare Dis*. 2008 Jul 30;3:22.
169. Scheinman SJ, Guay-Woodford LM, Thakker RV, Warnock DG. Genetic Disorders of Renal Electrolyte Transport. *N Engl J Med*. 1999;340(15):1177–87.
170. Geven WB, Monnens LA, Willems HL, Buijs WC, ter Haar BG. Renal magnesium wasting in two families with autosomal dominant inheritance. *Kidney Int*. 1987 May 1;31(5):1140–4.
171. Arystarkhova E, Wetzell RK, Sweadner KJ. Distribution and oligomeric association of splice forms of Na⁺-K⁺-ATPase regulatory γ -subunit in rat kidney. *Am J Physiol - Ren Physiol*. 2002 Mar 1;282(3):F393–407.
172. Parrock S, Hussain S, Issler N, Differ A-M, Lench N, Guarino S, et al. KCNJ10 mutations display differential sensitivity to heteromerisation with KCNJ16. *Nephron Physiol*. 2013;123(3–4):7–14.
173. Freudenthal B, Kulaveerasingam D, Lingappa L, Shah MA, Brueton L, Wassmer E, et al. KCNJ10 mutations disrupt function in patients with EAST syndrome. *Nephron Physiol*. 2011;119(3):p40-48.
174. Williams DM, Lopes CMB, Rosenhouse-Dantsker A, Connelly HL, Matavel A, O-Uchi J, et al. Molecular Basis of Decreased Kir4.1 Function in SeSAME/EAST Syndrome. *J Am Soc Nephrol JASN*. 2010 Dec;21(12):2117–29.
175. Gordon RD. Syndrome of hypertension and hyperkalemia with normal glomerular filtration rate. *Hypertension*. 1986 Feb;8(2):93–102.
176. Hadchouel J, Delaloy C, Fauré S, Achard J-M, Jeunemaitre X. Familial Hyperkalemic Hypertension. *J Am Soc Nephrol*. 2006 Jan 1;17(1):208–17.
177. Louis-Dit-Picard H, Barc J, Trujillano D, Miserey-Lenkei S, Bouatia-Naji N, Pylypenko O, et al. KLHL3 mutations cause familial hyperkalemic hypertension by impairing ion transport in the distal nephron. *Nat Genet*. 2012 Apr;44(4):456–60, S1-3.
178. Gamba G. Role of WNK kinases in regulating tubular salt and potassium transport and in the development of hypertension. *Am J Physiol Renal Physiol*. 2005 Feb;288(2):F245-252.
179. Schambelan M, Sebastian A, Rector FC Jr. Mineralocorticoid-resistant renal hyperkalemia without salt wasting (type II pseudohypoaldosteronism): role of increased renal chloride reabsorption. *Kidney Int*. 1981 May;19(5):716–27.

180. Adu D, Turney J, Michael J, McMaster P. Hyperkalaemia in cyclosporin-treated renal allograft recipients. *Lancet Lond Engl.* 1983 Aug 13;2(8346):370–2.
181. Heering PJ, Kurschat C, Vo DT, Klein-Vehne N, Fehsel K, Ivens K. Aldosterone resistance in kidney transplantation is in part induced by a down-regulation of mineralocorticoid receptor expression. *Clin Transplant.* 2004 Apr;18(2):186–92.
182. Higgins R, Ramaiyan K, Dasgupta T, Kanji H, Fletcher S, Lam F, et al. Hyponatraemia and hyperkalaemia are more frequent in renal transplant recipients treated with tacrolimus than with cyclosporin. Further evidence for differences between cyclosporin and tacrolimus nephrotoxicities. *Nephrol Dial Transplant Off Publ Eur Dial Transpl Assoc - Eur Ren Assoc.* 2004 Feb;19(2):444–50.
183. Ingebritsen T, Cohen P. Protein phosphatases: properties and role in cellular regulation. *Science.* 1983;(221):331–8.
184. Mastroianni N, De Fusco M, Zollo M, Arrigo G, Zuffardi O, Bettinelli A, et al. Molecular cloning, expression pattern, and chromosomal localization of the human Na-Cl thiazide-sensitive cotransporter (SLC12A3). *Genomics.* 1996 Aug 1;35(3):486–93.
185. Pathak BG, Shaughnessy JD, Meneton P, Greeb J, Shull GE, Jenkins NA, et al. Mouse chromosomal location of three epithelial sodium channel subunit genes and an apical sodium chloride cotransporter gene. *Genomics.* 1996 Apr 1;33(1):124–7.
186. Taniyama Y, Sato K, Sugawara A, Uruno A, Ikeda Y, Kudo M, et al. Renal tubule-specific transcription and chromosomal localization of rat thiazide-sensitive Na-Cl cotransporter gene. *J Biol Chem.* 2001 Jul 13;276(28):26260–8.
187. Gamba G. The thiazide-sensitive Na⁺-Cl⁻ cotransporter: molecular biology, functional properties, and regulation by WNKs. *Am J Physiol - Ren Physiol.* 2009 Oct;297(4):F838–48.
188. Hoover RS, Poch E, Monroy A, Vázquez N, Nishio T, Gamba G, et al. N-Glycosylation at Two Sites Critically Alters Thiazide Binding and Activity of the Rat Thiazide-sensitive Na⁺:Cl⁻ Cotransporter. *J Am Soc Nephrol.* 2003 Jan 2;14(2):271–82.
189. Castañeda-Bueno M, Vázquez N, Bustos-Jaimes I, Hernández D, Rodríguez-Lobato E, Pacheco-Alvarez D, et al. A single residue in transmembrane domain 11 defines the different affinity for thiazides between the mammalian and flounder NaCl transporters. *Am J Physiol - Ren Physiol.* 2010 Jan 11;299(5):F1111–9.
190. Moreno E, Cristóbal PS, Rivera M, Vázquez N, Bobadilla NA, Gamba G. Affinity-defining Domains in the Na-Cl Cotransporter A DIFFERENT

LOCATION FOR Cl⁻ AND THIAZIDE BINDING. *J Biol Chem*. 2006 Jun 23;281(25):17266–75.

191. Stokes JB. Sodium chloride absorption by the urinary bladder of the winter flounder. A thiazide-sensitive, electrically neutral transport system. *J Clin Invest*. 1984 Jul;74(1):7–16.
192. de Jong JC, Willems PHGM, Mooren FJM, van den Heuvel LPWJ, Knoers NVAM, Bindels RJM. The structural unit of the thiazide-sensitive NaCl cotransporter is a homodimer. *J Biol Chem*. 2003 Jul 4;278(27):24302–7.
193. Tran JM, Farrell MA, Fanestil DD. Effect of ions on binding of the thiazide-type diuretic metolazone to kidney membrane. *Am J Physiol - Ren Physiol*. 1990 Jan 4;258(4):F908–15.
194. Moreno E, Tovar-Palacio C, Heros P de los, Guzmán B, Bobadilla NA, Vázquez N, et al. A Single Nucleotide Polymorphism Alters the Activity of the Renal Na⁺:Cl⁻ Cotransporter and Reveals a Role for Transmembrane Segment 4 in Chloride and Thiazide Affinity. *J Biol Chem*. 2004 Apr 16;279(16):16553–60.
195. Vormfelde SV, Sehrt D, Toliat MR, Schirmer M, Meineke I, Tzvetkov M, et al. Genetic Variation in the Renal Sodium Transporters NKCC2, NCC, and ENaC in Relation to the Effects of Loop Diuretic Drugs. *Clin Pharmacol Ther*. 2007 Apr 25;82(3):300–9.
196. Kahle KT, MacGregor GG, Wilson FH, Van Hoek AN, Brown D, Ardito T, et al. Paracellular Cl⁻ permeability is regulated by WNK4 kinase: Insight into normal physiology and hypertension. *Proc Natl Acad Sci U S A*. 2004 Oct 12;101(41):14877–82.
197. Náráy-Fejes-Tóth A, Snyder PM, Fejes-Tóth G. The kidney-specific WNK1 isoform is induced by aldosterone and stimulates epithelial sodium channel-mediated Na⁺ transport. *Proc Natl Acad Sci U S A*. 2004 Dec 14;101(50):17434–9.
198. Leng Q, Kahle KT, Rinehart J, MacGregor GG, Wilson FH, Canessa CM, et al. WNK3, a kinase related to genes mutated in hereditary hypertension with hyperkalemia, regulates the K⁺ channel ROMK1 (Kir1.1). *J Physiol*. 2006 Mar 1;571(Pt 2):275–86.
199. Choate KA, Kahle KT, Wilson FH, Nelson-Williams C, Lifton RP. WNK1, a kinase mutated in inherited hypertension with hyperkalemia, localizes to diverse Cl⁻-transporting epithelia. *Proc Natl Acad Sci*. 2003 Jan 21;100(2):663–8.
200. Rinehart J, Kahle KT, de Los Heros P, Vazquez N, Meade P, Wilson FH, et al. WNK3 kinase is a positive regulator of NKCC2 and NCC, renal cation-Cl⁻ cotransporters required for normal blood pressure homeostasis. *Proc Natl Acad Sci U S A*. 2005 Nov 15;102(46):16777–82.

201. O'Reilly M, Marshall E, Macgillivray T, Mittal M, Xue W, Kenyon CJ, et al. Dietary electrolyte-driven responses in the renal WNK kinase pathway in vivo. *J Am Soc Nephrol JASN*. 2006 Sep;17(9):2402–13.
202. He G, Wang H-R, Huang S-K, Huang C-L. Intersectin links WNK kinases to endocytosis of ROMK1. *J Clin Invest*. 2007 Apr 2;117(4):1078–87.
203. Xu B, Min X, Stippec S, Lee B-H, Goldsmith EJ, Cobb MH. Regulation of WNK1 by an Autoinhibitory Domain and Autophosphorylation. *J Biol Chem*. 2002 Dec 13;277(50):48456–62.
204. Min X, Lee B-H, Cobb MH, Goldsmith EJ. Crystal Structure of the Kinase Domain of WNK1, a Kinase that Causes a Hereditary Form of Hypertension. *Structure*. 2004 Jul;12(7):1303–11.
205. Wang Z, Yang C-L, Ellison DH. Comparison of WNK4 and WNK1 kinase and inhibiting activities. *Biochem Biophys Res Commun*. 2004 May 7;317(3):939–44.
206. Lenertz LY, Lee B-H, Min X, Xu B, Wedin K, Earnest S, et al. Properties of WNK1 and Implications for Other Family Members. *J Biol Chem*. 2005 Jul 22;280(29):26653–8.
207. Yang C-L, Zhu X, Ellison DH. The thiazide-sensitive Na-Cl cotransporter is regulated by a WNK kinase signaling complex. *J Clin Invest*. 2007 Nov 1;117(11):3403–11.
208. O'Reilly M, Marshall E, Speirs HJL, Brown RW. WNK1, a gene within a novel blood pressure control pathway, tissue-specifically generates radically different isoforms with and without a kinase domain. *J Am Soc Nephrol JASN*. 2003 Oct;14(10):2447–56.
209. Delaloy C, Lu J, Houot A-M, Disse-Nicodeme S, Gasc J-M, Corvol P, et al. Multiple Promoters in the WNK1 Gene: One Controls Expression of a Kidney-Specific Kinase-Defective Isoform. *Mol Cell Biol*. 2003 Dec;23(24):9208–21.
210. Naito S, Ohta A, Sohara E, Ohta E, Rai T, Sasaki S, et al. Regulation of WNK1 kinase by extracellular potassium. *Clin Exp Nephrol*. 2011 Apr;15(2):195–202.
211. Wade JB, Fang L, Liu J, Li D, Yang C-L, Subramanya AR, et al. WNK1 kinase isoform switch regulates renal potassium excretion. *Proc Natl Acad Sci U S A*. 2006 May 30;103(22):8558–63.
212. Piala AT, Moon TM, Akella R, He H, Cobb MH, Goldsmith EJ. Chloride sensing by WNK1 involves inhibition of autophosphorylation. *Sci Signal*. 2014 May 6;7(324):ra41.

213. Yang C-L, Zhu X, Wang Z, Subramanya AR, Ellison DH. Mechanisms of WNK1 and WNK4 interaction in the regulation of thiazide-sensitive NaCl cotransport. *J Clin Invest*. 2005 May;115(5):1379–87.
214. Yang C-L, Angell J, Mitchell R, Ellison DH. WNK kinases regulate thiazide-sensitive Na-Cl cotransport. *J Clin Invest*. 2003 Apr 1;111(7):1039–45.
215. Subramanya AR, Yang C-L, Zhu X, Ellison DH. Dominant-negative regulation of WNK1 by its kidney-specific kinase-defective isoform. *Am J Physiol Renal Physiol*. 2006 Mar;290(3):F619-624.
216. Xu B, Stippec S, Chu P-Y, Lazrak A, Li X-J, Lee B-H, et al. WNK1 activates SGK1 to regulate the epithelial sodium channel. *Proc Natl Acad Sci U S A*. 2005 Jul 19;102(29):10315–20.
217. Cheng C-J, Huang C-L. Activation of PI3-kinase stimulates endocytosis of ROMK via Akt1/SGK1-dependent phosphorylation of WNK1. *J Am Soc Nephrol JASN*. 2011 Mar;22(3):460–71.
218. Delaloy C, Emilie Elvira-Matelot, Zhou X, Imbert-Teboul M, Houot A-M, Jeunemaitre X, et al. Deletion of WNK1 first intron results in misregulation of both isoforms in renal and extrarenal tissues. *Hypertension*. 2008 Dec;52(6):1149–54.
219. Elvira-Matelot E, Clemessy M, Zhou X, Imbert-Teboul M, Houot A-M, Jeunemaitre X, et al. Deletion of WNK1 first intron results in misregulation of both isoforms in renal and extrarenal tissues. *Hypertension*. 2008 Dec;52(6):1149–54.
220. San-Cristobal P, de los Heros P, Ponce-Coria J, Moreno E, Gamba G. WNK kinases, renal ion transport and hypertension. *Am J Nephrol*. 2008;28(5):860–70.
221. Holden S, Cox J, Raymond FL. Cloning, genomic organization, alternative splicing and expression analysis of the human gene WNK3 (PRKWKN3). *Gene*. 2004 Jun 23;335:109–19.
222. Heros P de los, Kahle KT, Rinehart J, Bobadilla NA, Vázquez N, Cristobal PS, et al. WNK3 bypasses the tonicity requirement for K-Cl cotransporter activation via a phosphatase-dependent pathway. *Proc Natl Acad Sci U S A*. 2006 Jul 2;103(6):1976–81.
223. Kahle KT, Rinehart J, de Los Heros P, Louvi A, Meade P, Vazquez N, et al. WNK3 modulates transport of Cl⁻ in and out of cells: implications for control of cell volume and neuronal excitability. *Proc Natl Acad Sci U S A*. 2005 Nov 15;102(46):16783–8.
224. Mercado A, Vázquez N, Song L, Cortés R, Enck AH, Welch R, et al. NH₂-terminal heterogeneity in the KCC3 K⁺-Cl⁻ cotransporter. *Am J Physiol - Ren Physiol*. 2005 Dec 1;289(6):F1246–61.

225. Lytle C, McManus T. Coordinate modulation of Na-K-2Cl cotransport and K-Cl cotransport by cell volume and chloride. *Am J Physiol - Cell Physiol*. 2002 Nov 1;283(5):C1422–31.
226. Glover M, Zuber AM, O'Shaughnessy KM. Renal and Brain Isoforms of WNK3 Have Opposite Effects on NCCT Expression. *J Am Soc Nephrol*. 2009 Jan 6;20(6):1314–22.
227. Verissimo F, Jordan P. WNK kinases, a novel protein kinase subfamily in multi-cellular organisms. *Oncogene*. 2001 Sep 6;20(39):5562–9.
228. Kahle KT, Gimenez I, Hassan H, Wilson FH, Wong RD, Forbush B, et al. WNK4 regulates apical and basolateral Cl⁻ flux in extrarenal epithelia. *Proc Natl Acad Sci U S A*. 2004 Feb 17;101(7):2064–9.
229. Terker AS, Zhang C, McCormick JA, Lazelle RA, Zhang C, Meermeier NP, et al. Potassium modulates electrolyte balance and blood pressure through effects on distal cell voltage and chloride. *Cell Metab*. 2015 Jan 6;21(1):39–50.
230. Li C, Li Y, Li Y, Liu H, Sun Z, Lu J, et al. Glucocorticoid repression of human with-no-lysine (K) kinase-4 gene expression is mediated by the negative response elements in the promoter. *J Mol Endocrinol*. 2008 Jan;40(1):3–12.
231. Nguyen Dinh Cat A, Ouvrard-Pascaud A, Tronche F, Clemessy M, Gonzalez-Nunez D, Farman N, et al. Conditional transgenic mice for studying the role of the glucocorticoid receptor in the renal collecting duct. *Endocrinology*. 2009 May;150(5):2202–10.
232. Chávez-Canales M, Zhang C, Soukaseum C, Moreno E, Pacheco-Alvarez D, Vidal-Petiot E, et al. WNK-SPAK-NCC cascade revisited: WNK1 stimulates the activity of the Na-Cl cotransporter via SPAK, an effect antagonized by WNK4. *Hypertension*. 2014 Nov;64(5):1047–53.
233. Wilson FH, Kahle KT, Sabath E, Lalioti MD, Rapson AK, Hoover RS, et al. Molecular pathogenesis of inherited hypertension with hyperkalemia: the Na-Cl cotransporter is inhibited by wild-type but not mutant WNK4. *Proc Natl Acad Sci U S A*. 2003 Jan 21;100(2):680–4.
234. Yang S-S, Morimoto T, Rai T, Chiga M, Sohara E, Ohno M, et al. Molecular pathogenesis of pseudohypoaldosteronism type II: generation and analysis of a Wnk4(D561A/+) knockin mouse model. *Cell Metab*. 2007 May;5(5):331–44.
235. Ohta A, Rai T, Yui N, Chiga M, Yang S-S, Lin S-H, et al. Targeted disruption of the Wnk4 gene decreases phosphorylation of Na-Cl cotransporter, increases Na excretion and lowers blood pressure. *Hum Mol Genet*. 2009 Oct 15;18(20):3978–86.

236. Cai H, Cebotaru V, Wang Y-H, Zhang X-M, Cebotaru L, Guggino SE, et al. WNK4 kinase regulates surface expression of the human sodium chloride cotransporter in mammalian cells. *Kidney Int.* 2006 Jun;69(12):2162–70.
237. Kahle KT, Wilson FH, Leng Q, Lalioti MD, O'Connell AD, Dong K, et al. WNK4 regulates the balance between renal NaCl reabsorption and K⁺ secretion. *Nat Genet.* 2003 Dec;35(4):372–6.
238. Ring AM, Cheng SX, Leng Q, Kahle KT, Rinehart J, Lalioti MD, et al. WNK4 regulates activity of the epithelial Na⁺ channel in vitro and in vivo. *Proc Natl Acad Sci U S A.* 2007 Mar 6;104(10):4020–4.
239. Yamauchi K, Rai T, Kobayashi K, Sohara E, Suzuki T, Itoh T, et al. Disease-causing mutant WNK4 increases paracellular chloride permeability and phosphorylates claudins. *Proc Natl Acad Sci U S A.* 2004 Mar 30;101(13):4690–4.
240. Diakov A, Korbmacher C. A novel pathway of epithelial sodium channel activation involves a serum- and glucocorticoid-inducible kinase consensus motif in the C terminus of the channel's alpha-subunit. *J Biol Chem.* 2004 Sep 10;279(37):38134–42.
241. Yoo D, Kim BY, Campo C, Nance L, King A, Maouyo D, et al. Cell Surface Expression of the ROMK (Kir 1.1) Channel Is Regulated by the Aldosterone-induced Kinase, SGK-1, and Protein Kinase A. *J Biol Chem.* 2003 Jun 20;278(25):23066–75.
242. van der Lubbe N, Lim CH, Fenton RA, Meima ME, Jan Danser AH, Zietse R, et al. Angiotensin II induces phosphorylation of the thiazide-sensitive sodium chloride cotransporter independent of aldosterone. *Kidney Int.* 2011 Jan;79(1):66–76.
243. Mamenko M, Zaika O, Ilatovskaya DV, Staruschenko A, Pochynyuk O. Angiotensin II increases activity of the epithelial Na⁺ channel (ENaC) in distal nephron additively to aldosterone. *J Biol Chem.* 2012 Jan 2;287(1):660–71.
244. Castañeda-Bueno M, Arroyo JP, Zhang J, Puthumana J, Yarborough O, Shibata S, et al. Phosphorylation by PKC and PKA regulate the kinase activity and downstream signaling of WNK4. *Proc Natl Acad Sci.* 2017 Jan 31;114(5):E879–86.
245. Gagnon KBE, England R, Delpire E. Volume sensitivity of cation-Cl⁻ cotransporters is modulated by the interaction of two kinases: Ste20-related proline-alanine-rich kinase and WNK4. *Am J Physiol - Cell Physiol.* 2006 Jan 1;290(1):C134–42.
246. Vitari AC, Thastrup J, Rafiqi FH, Deak M, Morrice NA, Karlsson HKR, et al. Functional interactions of the SPAK/OSR1 kinases with their upstream activator WNK1 and downstream substrate NKCC1. *Biochem J.* 2006 Jul 1;397(1):223–31.

247. Dowd BFX, Forbush B. PASK (Proline-Alanine-rich STE20-related Kinase), a Regulatory Kinase of the Na-K-Cl Cotransporter (NKCC1). *J Biol Chem.* 2003 Jul 25;278(30):27347–53.
248. Piechotta K, Garbarini N, England R, Delpire E. Characterization of the interaction of the stress kinase SPAK with the Na⁺-K⁺-2Cl⁻ cotransporter in the nervous system: evidence for a scaffolding role of the kinase. *J Biol Chem.* 2003 Dec 26;278(52):52848–56.
249. Ponce-Coria J, San-Cristobal P, Kahle KT, Vazquez N, Pacheco-Alvarez D, Heros P de los, et al. Regulation of NKCC2 by a chloride-sensing mechanism involving the WNK3 and SPAK kinases. *Proc Natl Acad Sci.* 2008 Jun 17;105(24):8458–63.
250. Tamari M, Daigo Y, Nakamura Y. Isolation and characterization of a novel serine threonine kinase gene on chromosome 3p22-21.3. *J Hum Genet.* 1999;44(2):116–20.
251. Baas AF, Boudeau J, Sapkota GP, Smit L, Medema R, Morrice NA, et al. Activation of the tumour suppressor kinase LKB1 by the STE20-like pseudokinase STRAD. *EMBO J.* 2003 Jun 16;22(12):3062–72.
252. Boudeau J, Baas AF, Deak M, Morrice NA, Kieloch A, Schutkowski M, et al. MO25 α/β interact with STRAD α/β enhancing their ability to bind, activate and localize LKB1 in the cytoplasm. *EMBO J.* 2003 Oct 1;22(19):5102–14.
253. Hawley SA, Boudeau J, Reid JL, Mustard KJ, Udd L, Mäkelä TP, et al. Complexes between the LKB1 tumor suppressor, STRAD α/β and MO25 α/β are upstream kinases in the AMP-activated protein kinase cascade. *J Biol.* 2003;2(4):28.
254. Hawley SA, Davison M, Woods A, Davies SP, Beri RK, Carling D, et al. Characterization of the AMP-activated protein kinase kinase from rat liver and identification of threonine 172 as the major site at which it phosphorylates AMP-activated protein kinase. *J Biol Chem.* 1996 Nov 1;271(44):27879–87.
255. Zhang BB, Zhou G, Li C. AMPK: an emerging drug target for diabetes and the metabolic syndrome. *Cell Metab.* 2009 May;9(5):407–16.
256. Filippi BM, de los Heros P, Mehellou Y, Navratilova I, Gourlay R, Deak M, et al. MO25 is a master regulator of SPAK/OSR1 and MST3/MST4/YSK1 protein kinases. *EMBO J.* 2011 May 4;30(9):1730–41.
257. Stogios PJ, Privé GG. The BACK domain in BTB-kelch proteins. *Trends Biochem Sci.* 2004 Dec;29(12):634–7.
258. Adams J, Kelso R, Cooley L. The kelch repeat superfamily of proteins: propellers of cell function. *Trends Cell Biol.* 2000 Jan;10(1):17–24.

259. Peng J-B, Wu G. Kelch-like 3 (KLHL3) controls WNK4 ubiquitination and degradation. *FASEB J.* 2013 Jan 4;27(1 Supplement):911.14-911.14.
260. Shibata S, Zhang J, Puthumana J, Stone KL, Lifton RP. Kelch-like 3 and Cullin 3 regulate electrolyte homeostasis via ubiquitination and degradation of WNK4. *Proc Natl Acad Sci.* 2013 Jul 5;110(19):7838–43.
261. Shibata S, Arroyo JP, Castañeda-Bueno M, Puthumana J, Zhang J, Uchida S, et al. Angiotensin II signaling via protein kinase C phosphorylates Kelch-like 3, preventing WNK4 degradation. *Proc Natl Acad Sci U S A.* 2014 Oct 28;111(43):15556–61.
262. Yoshizaki Y, Mori Y, Tsuzaki Y, Mori T, Nomura N, Wakabayashi M, et al. Impaired degradation of WNK by Akt and PKA phosphorylation of KLHL3. *Biochem Biophys Res Commun.* 2015 Nov 13;467(2):229–34.
263. Glover M, Ware JS, Henry A, Wolley M, Walsh R, Wain LV, et al. Detection of mutations in KLHL3 and CUL3 in families with FHHt (familial hyperkalaemic hypertension or Gordon's syndrome). *Clin Sci Lond Engl* 1979. 2014 May 1;126(Pt 10):721–6.
264. Ohta A, Schumacher F-R, Mehellou Y, Johnson C, Knebel A, Macartney TJ, et al. The CUL3-KLHL3 E3 ligase complex mutated in Gordon's hypertension syndrome interacts with and ubiquitylates WNK isoforms: disease-causing mutations in KLHL3 and WNK4 disrupt interaction. *Biochem J.* 2013 Apr 1;451(1):111–22.
265. Susa K, Sohara E, Rai T, Zeniya M, Mori Y, Mori T, et al. Impaired degradation of WNK1 and WNK4 kinases causes PHAII in mutant KLHL3 knock-in mice. *Hum Mol Genet.* 2014 Oct 1;23(19):5052–60.
266. Wakabayashi M, Mori T, Isobe K, Sohara E, Susa K, Araki Y, et al. Impaired KLHL3-Mediated Ubiquitination of WNK4 Causes Human Hypertension. *Cell Rep.* 2013 Mar 28;3(3):858–68.
267. Schumacher F-R, Siew K, Zhang J, Johnson C, Wood N, Cleary SE, et al. Characterisation of the Cullin-3 mutation that causes a severe form of familial hypertension and hyperkalaemia. *EMBO Mol Med.* 2015 Oct;7(10):1285–306.
268. Ingebritsen TS, Stewart AA, Cohen P. The protein phosphatases involved in cellular regulation. 6. Measurement of type-1 and type-2 protein phosphatases in extracts of mammalian tissues; an assessment of their physiological roles. *Eur J Biochem FEBS.* 1983 May 2;132(2):297–307.
269. Tumlin JA, Someren JT, Swanson CE, Lea JP. Expression of calcineurin activity and alpha-subunit isoforms in specific segments of the rat nephron. *Am J Physiol - Ren Physiol.* 1995 Jan 10;269(4):F558–63.

270. Gagliardino JJ, Krinks MH, Gagliardino EE. Identification of the calmodulin-regulated protein phosphatase, calcineurin, in rat pancreatic islets. *Biochim Biophys Acta*. 1991 Feb 19;1091(3):370–3.
271. Mukai H, Chang C-D, Tanaka H, Ito A, Kuno T, Tanaka C. cDNA cloning of a novel testis-specific calcineurin B-like protein. *Biochem Biophys Res Commun*. 1991 Sep 30;179(3):1325–30.
272. Tash JS, Krinks M, Patel J, Means RL, Klee CB, Means AR. Identification, characterization, and functional correlation of calmodulin-dependent protein phosphatase in sperm. *J Cell Biol*. 1988 Jan 5;106(5):1625–33.
273. Muramatsu T, Giri PR, Higuchi S, Kincaid RL. Molecular cloning of a calmodulin-dependent phosphatase from murine testis: identification of a developmentally expressed nonneural isoenzyme. *Proc Natl Acad Sci*. 1992 Jan 15;89(2):529–33.
274. Kuno T, Mukai H, Ito A, Chang CD, Kishima K, Saito N, et al. Distinct cellular expression of calcineurin A alpha and A beta in rat brain. *J Neurochem*. 1992 May;58(5):1643–51.
275. Guerini D, Montell C, Klee CB. Molecular cloning and characterization of the genes encoding the two subunits of *Drosophila melanogaster* calcineurin. *J Biol Chem*. 1992 May 11;267(31):22542–9.
276. Liu L, Zhang J, Yuan J, Dang Y, Yang C, Chen X, et al. Characterization of a human regulatory subunit of protein phosphatase 3 gene (PPP3RL) expressed specifically in testis. *Mol Biol Rep*. 2005 Mar;32(1):41–5.
277. Aitken A, Klee CB, Cohen P. The structure of the B subunit of calcineurin. *Eur J Biochem*. 1984;139(3):663–671.
278. Kakalis LT, Kennedy M, Sikkink R, Rusnak F, Armitage IM. Characterization of the calcium-binding sites of calcineurin B. *FEBS Lett*. 1995 Mar 27;362(1):55–8.
279. Linse S, Helmersson A, Forsén S. Calcium binding to calmodulin and its globular domains. *J Biol Chem*. 1991 May 5;266(13):8050–4.
280. VanScyoc WS, Sorensen BR, Rusinova E, Laws WR, Ross JBA, Shea MA. Calcium binding to calmodulin mutants monitored by domain-specific intrinsic phenylalanine and tyrosine fluorescence. *Biophys J*. 2002 Nov;83(5):2767–80.
281. Kissinger CR, Parge HE, Knighton DR, Lewis CT, Pelletier LA, Tempczyk A, et al. Crystal structures of human calcineurin and the human FKBP12–FK506–calcineurin complex. *Nature*. 1995 Dec 7;378(6557):641–4.
282. Crivici A, Ikura M. Molecular and Structural Basis of Target Recognition by Calmodulin. *Annu Rev Biophys Biomol Struct*. 1995;24(1):85–116.

283. Yang S-A, Klee CB. Low Affinity Ca²⁺-Binding Sites of Calcineurin B Mediate Conformational Changes in Calcineurin A. *Biochemistry (Mosc)*. 2000 Dec 1;39(51):16147–54.
284. Sabatini DM, Erdjument-Bromage H, Lui M, Tempst P, Snyder SH. RAFT1: A mammalian protein that binds to FKBP12 in a rapamycin-dependent fashion and is homologous to yeast TORs. *Cell*. 1994 Jul 15;78(1):35–43.
285. Briones AM, Cat AND, Callera GE, Yogi A, Burger D, He Y, et al. Adipocytes Produce Aldosterone Through Calcineurin-Dependent Signaling Pathways Implications in Diabetes Mellitus–Associated Obesity and Vascular Dysfunction. *Hypertension*. 2012 Jan 5;59(5):1069–78.
286. Yamashiro T, Kuge H, Zhang J, Honke K. Calcineurin mediates the angiotensin II-induced aldosterone synthesis in the adrenal glands by up-regulation of transcription of the CYP11B2 gene. *J Biochem (Tokyo)*. 2010 Jan 7;148(1):115–23.
287. Suzuki E, Nishimatsu H, Satonaka H, Walsh K, Goto A, Omata M, et al. Angiotensin II Induces Myocyte Enhancer Factor 2- and Calcineurin/Nuclear Factor of Activated T Cell-Dependent Transcriptional Activation in Vascular Myocytes. *Circ Res*. 2002 May 17;90(9):1004–11.
288. Lea JP, Jin SG, Roberts BR, Shuler MS, Marrero MB, Tumlin JA. Angiotensin II Stimulates Calcineurin Activity in Proximal Tubule Epithelia through AT-1 Receptor-Mediated Tyrosine Phosphorylation of the PLC- γ 1 Isoform. *J Am Soc Nephrol*. 2002 Jan 7;13(7):1750–6.
289. Siekierka JJ, Hung SH, Poe M, Lin CS, Sigal NH. A cytosolic binding protein for the immunosuppressant FK506 has peptidyl-prolyl isomerase activity but is distinct from cyclophilin. *Nature*. 1989 Oct 26;341(6244):755–7.
290. Marks AR. Cellular functions of immunophilins. *Physiol Rev*. 1996 Jul;76(3):631–49.
291. Stepkowski SM. Molecular targets for existing and novel immunosuppressive drugs. *Expert Rev Mol Med*. 2000 Jun 21;2(4):1–23.
292. Brown EJ, Albers MW, Bum Shin T, Ichikawa K, Keith CT, Lane WS, et al. A mammalian protein targeted by G1-arresting rapamycin–receptor complex. *Nature*. 1994 Jun 30;369(6483):756–8.
293. Garzón-Muvdi T, Pacheco-Alvarez D, Gagnon KBE, Vázquez N, Ponce-Coria J, Moreno E, et al. WNK4 kinase is a negative regulator of K⁺-Cl⁻ cotransporters. *Am J Physiol Renal Physiol*. 2007 Apr;292(4):F1197-1207.
294. Palmer BF. Managing hyperkalemia caused by inhibitors of the renin-angiotensin-aldosterone system. *N Engl J Med*. 2004 Aug 5;351(6):585–92.

295. Coe F. Treatment of Hypercalciuria. *N Engl J Med*. 1984 Jul 12;311(2):116–8.
296. Bartosh SM, Alonso EM, Whittington PF. Renal outcomes in pediatric liver transplantation. *Clin Transplant*. 1997 Oct;11(5 Pt 1):354–60.
297. Garty H, Benos DJ. Characteristics and regulatory mechanisms of the amiloride-blockable Na⁺ channel. *Physiol Rev*. 1988 Apr;68(2):309–73.
298. Grinstein S, Elij D. Intracellular Calcium and the Regulation of Sodium Transport in the Frog Skin. *Proc R Soc Lond B Biol Sci*. 1978;202(1148):353–60.
299. Kiuchi-Saishin Y, Gotoh S, Furuse M, Takasuga A, Tano Y, Tsukita S. Differential Expression Patterns of Claudins, Tight Junction Membrane Proteins, in Mouse Nephron Segments. *J Am Soc Nephrol*. 2002 Jan 4;13(4):875–86.
300. Muto S, Hata M, Taniguchi J, Tsuruoka S, Moriwaki K, Saitou M, et al. Claudin-2-deficient mice are defective in the leaky and cation-selective paracellular permeability properties of renal proximal tubules. *Proc Natl Acad Sci*. 2010 Apr 27;107(17):8011–6.
301. Rouse D, Ng RC, Suki WN. Calcium transport in the pars recta and thin descending limb of Henle of the rabbit, perfused in vitro. *J Clin Invest*. 1980 Jan;65(1):37–42.
302. Hebert SC. Molecular mechanisms. *Semin Nephrol*. 1999 Nov;19(6):504–23.
303. Hebert SC, Brown EM, Harris HW. Role of the Ca(2⁺)-sensing receptor in divalent mineral ion homeostasis. *J Exp Biol*. 1997 Jan 1;200(2):295–302.
304. Bourdeau JE, Langman CB, Bouillon R. Parathyroid hormone-stimulated calcium absorption in cTAL from vitamin D-deficient rabbits. *Kidney Int*. 1987 Apr;31(4):913–7.
305. Bourdeau JE, Burg MB. Effect of PTH on calcium transport across the cortical thick ascending limb of Henle's loop. *Am J Physiol*. 1980 Aug;239(2):F121-126.
306. Goodman WG, Quarles LD. Development and progression of secondary hyperparathyroidism in chronic kidney disease: lessons from molecular genetics. *Kidney Int*. 2008 Aug;74(3):276–88.
307. Jayakumar A, Cheng L, Liang CT, Sacktor B. Sodium gradient-dependent calcium uptake in renal basolateral membrane vesicles. Effect of parathyroid hormone. *J Biol Chem*. 1984 Sep 10;259(17):10827–33.
308. van Abel M, Hoenderop JGJ, van der Kemp AWCM, Friedlaender MM, van Leeuwen JPTM, Bindels RJM. Coordinated control of renal Ca(2⁺)

- transport proteins by parathyroid hormone. *Kidney Int.* 2005 Oct;68(4):1708–21.
309. Hwang EF, Williams I, Kovacs G, Peti-Peterdi J, Siroky B, Rice WC, et al. Impaired ability of the Na⁺/Ca²⁺ exchanger from the Dahl/Rapp salt-sensitive rat to regulate cytosolic calcium. *Am J Physiol - Ren Physiol.* 2003 May 1;284(5):F1023–31.
310. Ruknudin A, He S, Lederer WJ, Schulze DH. Functional differences between cardiac and renal isoforms of the rat Na⁺-Ca²⁺ exchanger NCX1 expressed in *Xenopus* oocytes. *J Physiol.* 2000 Dec 1;529(3):599–610.
311. Ruknudin AM, Wei S-K, Haigney MC, Lederer WJ, Schulze DH. Phosphorylation and other conundrums of Na/Ca exchanger, NCX1. *Ann N Y Acad Sci.* 2007 Mar;1099:103–18.
312. Hagen EAE van der, Loon EPM van, Verkaart S, Latta F, Bindels RJM, Hoenderop JGJ. The Na⁺/Ca²⁺ Exchanger 1 (NCX1) Variant 3 as the Major Extrusion System in Renal Distal Tubular Transcellular Ca²⁺-Transport. *Nephron.* 2015;131(2):145–52.
313. Hoenderop JG, De Pont JJ, Bindels RJ, Willems PH. Hormone-stimulated Ca²⁺ reabsorption in rabbit kidney cortical collecting system is cAMP-independent and involves a phorbol ester-insensitive PKC isotype. *Kidney Int.* 1999 Jan;55(1):225–33.
314. Groot T de, Lee K, Langeslag M, Xi Q, Jalink K, Bindels RJM, et al. Parathyroid Hormone Activates TRPV5 via PKA-Dependent Phosphorylation. *J Am Soc Nephrol.* 2009 Jan 8;20(8):1693–704.
315. Cha S-K, Wu T, Huang C-L. Protein kinase C inhibits caveolae-mediated endocytosis of TRPV5. *Am J Physiol - Ren Physiol.* 2008 May 1;294(5):F1212–21.
316. Dusso AS, Brown AJ, Slatopolsky E. Vitamin D. *Am J Physiol - Ren Physiol.* 2005 Jul 1;289(1):F8–28.
317. Murayama A, Takeyama K, Kitanaka S, Kodera Y, Kawaguchi Y, Hosoya T, et al. Positive and negative regulations of the renal 25-hydroxyvitamin D3 1 α -hydroxylase gene by parathyroid hormone, calcitonin, and 1 α ,25(OH)₂D₃ in intact animals. *Endocrinology.* 1999 May;140(5):2224–31.
318. Shimada T, Mizutani S, Muto T, Yoneya T, Hino R, Takeda S, et al. Cloning and characterization of FGF23 as a causative factor of tumor-induced osteomalacia. *Proc Natl Acad Sci.* 2001 May 22;98(11):6500–5.
319. Imai M, Ishikawa K, Matsukawa N, Kida I, Ohta J, Ikushima M, et al. Klotho protein activates the PKC pathway in the kidney and testis and suppresses 25-hydroxyvitamin D3 1 α -hydroxylase gene expression. *Endocrine.* 2004 Dec;25(3):229–34.

320. Hoenderop JGJ, Müller D, Kemp AWCMVD, Hartog A, Suzuki M, Ishibashi K, et al. Calcitriol Controls the Epithelial Calcium Channel in Kidney. *J Am Soc Nephrol*. 2001 Jan 7;12(7):1342–9.
321. Krajisnik T, Olauson H, Mirza MAI, Hellman P, Akerström G, Westin G, et al. Parathyroid Klotho and FGF-receptor 1 expression decline with renal function in hyperparathyroid patients with chronic kidney disease and kidney transplant recipients. *Kidney Int*. 2010 Nov;78(10):1024–32.
322. Lim K, Lu T-S, Molostvov G, Lee C, Lam FT, Zehnder D, et al. Vascular Klotho deficiency potentiates the development of human artery calcification and mediates resistance to fibroblast growth factor 23. *Circulation*. 2012 May 8;125(18):2243–55.
323. Lim K, Groen A, Molostvov G, Lu T, Lilley KS, Snead D, et al. α -Klotho Expression in Human Tissues. *J Clin Endocrinol Metab*. 2015 Oct;100(10):E1308–18.
324. Imura A, Tsuji Y, Murata M, Maeda R, Kubota K, Iwano A, et al. alpha-Klotho as a regulator of calcium homeostasis. *Science*. 2007 Jun 15;316(5831):1615–8.
325. Matsumura Y, Aizawa H, Shiraki-Iida T, Nagai R, Kuro-o M, Nabeshima Y. Identification of the human klotho gene and its two transcripts encoding membrane and secreted klotho protein. *Biochem Biophys Res Commun*. 1998 Jan 26;242(3):626–30.
326. Urakawa I, Yamazaki Y, Shimada T, Iijima K, Hasegawa H, Okawa K, et al. Klotho converts canonical FGF receptor into a specific receptor for FGF23. *Nature*. 2006 Dec 7;444(7120):770–4.
327. Shimada T, Kakitani M, Yamazaki Y, Hasegawa H, Takeuchi Y, Fujita T, et al. Targeted ablation of Fgf23 demonstrates an essential physiological role of FGF23 in phosphate and vitamin D metabolism. *J Clin Invest*. 2004 Feb;113(4):561–8.
328. Akey JM, Swanson WJ, Madeoy J, Eberle M, Shriver MD. TRPV6 exhibits unusual patterns of polymorphism and divergence in worldwide populations. *Hum Mol Genet*. 2006 Jul 1;15(13):2106–13.
329. Vennekens R, Hoenderop JG, Prenen J, Stuiver M, Willems PH, Droogmans G, et al. Permeation and gating properties of the novel epithelial Ca(2+) channel. *J Biol Chem*. 2000 Feb 11;275(6):3963–9.
330. Wissenbach U, Niemeyer BA, Fixemer T, Schneidewind A, Trost C, Cavalié A, et al. Expression of CaT-like, a Novel Calcium-selective Channel, Correlates with the Malignancy of Prostate Cancer. *J Biol Chem*. 2001 Jan 6;276(22):19461–8.

331. Hoenderop JGJ, Voets T, Hoefs S, Weidema F, Prenen J, Nilius B, et al. Homo- and heterotetrameric architecture of the epithelial Ca²⁺ channels TRPV5 and TRPV6. *EMBO J*. 2003 Feb 17;22(4):776–85.
332. Erler I, Hirnet D, Wissenbach U, Flockerzi V, Niemeyer BA. Ca²⁺-selective Transient Receptor Potential V Channel Architecture and Function Require a Specific Ankyrin Repeat. *J Biol Chem*. 2004 Aug 13;279(33):34456–63.
333. Lambers TT, Weidema AF, Nilius B, Hoenderop JGJ, Bindels RJM. Regulation of the Mouse Epithelial Ca²⁺ Channel TRPV6 by the Ca²⁺-sensor Calmodulin. *J Biol Chem*. 2004 Sep 7;279(28):28855–61.
334. de Groot T, Kovalevskaya NV, Verkaart S, Schilderink N, Felici M, van der Hagen EAE, et al. Molecular mechanisms of calmodulin action on TRPV5 and modulation by parathyroid hormone. *Mol Cell Biol*. 2011 Jul;31(14):2845–53.
335. Voets T, Janssens A, Droogmans G, Nilius B. Outer Pore Architecture of a Ca²⁺-selective TRP Channel. *J Biol Chem*. 2004 Sep 4;279(15):15223–30.
336. Yeh B-I, Sun T-J, Lee JZ, Chen H-H, Huang C-L. Mechanism and Molecular Determinant for Regulation of Rabbit Transient Receptor Potential Type 5 (TRPV5) Channel by Extracellular pH. *J Biol Chem*. 2003 Dec 19;278(51):51044–52.
337. Cha S-K, Huang C-L. WNK4 Kinase Stimulates Caveola-mediated Endocytosis of TRPV5 Amplifying the Dynamic Range of Regulation of the Channel by Protein Kinase C. *J Biol Chem*. 2010 Feb 26;285(9):6604–11.
338. Jiang Y, Ferguson WB, Peng J-B. WNK4 enhances TRPV5-mediated calcium transport: potential role in hypercalciuria of familial hyperkalemic hypertension caused by gene mutation of WNK4. *Am J Physiol Renal Physiol*. 2007 Feb;292(2):F545-554.
339. Embark HM, Setiawan I, Poppendieck S, van de Graaf SFJ, Boehmer C, Palmada M, et al. Regulation of the epithelial Ca²⁺ channel TRPV5 by the NHE regulating factor NHERF2 and the serum and glucocorticoid inducible kinase isoforms SGK1 and SGK3 expressed in *Xenopus* oocytes. *Cell Physiol Biochem Int J Exp Cell Physiol Biochem Pharmacol*. 2004;14(4–6):203–12.
340. Sandulache D, Grahammer F, Artunc F, Henke G, Hussain A, Nasir O, et al. Renal Ca²⁺ handling in *sgk1* knockout mice. *Pflugers Arch*. 2006 Jul;452(4):444–52.
341. Ramachandran C, Brunette MG. The renal Na⁺/Ca²⁺ exchange system is located exclusively in the distal tubule. *Biochem J*. 1989 Jan 1;257(1):259–64.
342. McDaniel LD, Lederer WJ, Kofuji P, Schulze DH, Kieval R, Schultz RA. Mapping of the human cardiac Na⁺/Ca²⁺ exchanger gene (*NCX1*) by

fluorescent in situ hybridization to chromosome region 2p22-->p23. *Cytogenet Cell Genet.* 1993;63(3):192–3.

343. Nicholas SB, Philipson KD. Cardiac expression of the Na⁺/Ca²⁺ exchanger NCX1 is GATA factor dependent. *Am J Physiol - Heart Circ Physiol.* 1999 Jul 1;277(1):H324–30.
344. Dyck C, Omelchenko A, Elias CL, Quednau BD, Philipson KD, Hnatowich M, et al. Ionic Regulatory Properties of Brain and Kidney Splice Variants of the Ncx1 Na⁺–Ca²⁺ Exchanger. *J Gen Physiol.* 1999 Nov 1;114(5):701–11.
345. Quednau BD, Nicoll DA, Philipson KD. Tissue specificity and alternative splicing of the Na⁺/Ca²⁺ exchanger isoforms NCX1, NCX2, and NCX3 in rat. *Am J Physiol.* 1997 Apr;272(4 Pt 1):C1250-1261.
346. Kofuji P, Lederer WJ, Schulze DH. Mutually exclusive and cassette exons underlie alternatively spliced isoforms of the Na/Ca exchanger. *J Biol Chem.* 1994 Feb 18;269(7):5145–9.
347. Schulze DH, Polumuri SK, Gille T, Ruknudin A. Functional Regulation of Alternatively Spliced Na⁺/Ca²⁺ Exchanger (NCX1) Isoforms. *Ann N Y Acad Sci.* 2002 Nov 1;976(1):187–96.
348. Nicoll DA, Ottolia M, Philipson KD. Toward a topological model of the NCX1 exchanger. *Ann N Y Acad Sci.* 2002 Nov;976:11–8.
349. Besserer GM, Ottolia M, Nicoll DA, Chaptal V, Cascio D, Philipson KD, et al. The second Ca²⁺-binding domain of the Na⁺ Ca²⁺ exchanger is essential for regulation: crystal structures and mutational analysis. *Proc Natl Acad Sci U S A.* 2007 Nov 20;104(47):18467–72.
350. Formisano L, Saggese M, Secondo A, Sirabella R, Vito P, Valsecchi V, et al. The two isoforms of the Na⁺/Ca²⁺ exchanger, NCX1 and NCX3, constitute novel additional targets for the prosurvival action of Akt/protein kinase B pathway. *Mol Pharmacol.* 2008 Mar;73(3):727–37.
351. Shigekawa M, Katanosaka Y, Wakabayashi S. Regulation of the Cardiac Na⁺/Ca²⁺ Exchanger by Calcineurin and Protein Kinase C. *Ann N Y Acad Sci.* 2007 Mar 1;1099(1):53–63.
352. Iwamoto T, Shigekawa M. Differential inhibition of Na⁺/Ca²⁺ exchanger isoforms by divalent cations and isothiourea derivative. *Am J Physiol.* 1998 Aug;275(2 Pt 1):C423-430.
353. Yu SP, Choi DW. Na(+)-Ca²⁺ exchange currents in cortical neurons: concomitant forward and reverse operation and effect of glutamate. *Eur J Neurosci.* 1997 Jun;9(6):1273–81.

354. Bindokas VP, Miller RJ. Excitotoxic degeneration is initiated at non-random sites in cultured rat cerebellar neurons. *J Neurosci Off J Soc Neurosci*. 1995 Nov;15(11):6999–7011.
355. Wolf JA, Stys PK, Lusardi T, Meaney D, Smith DH. Traumatic axonal injury induces calcium influx modulated by tetrodotoxin-sensitive sodium channels. *J Neurosci Off J Soc Neurosci*. 2001 Mar 15;21(6):1923–30.
356. Morad M, Cleemann L, Menick DR. NCX1 phosphorylation dilemma: a little closer to resolution. Focus on “Full-length cardiac Na⁺/Ca²⁺ exchanger 1 protein is not phosphorylated by protein kinase A”. *Am J Physiol - Cell Physiol*. 2011 May 1;300(5):C970–3.
357. El-Yazbi AF, Cho WJ, Schulz R, Daniel EE. Calcium extrusion by plasma membrane calcium pump is impaired in caveolin-1 knockout mouse small intestine. *Eur J Pharmacol*. 2008 Sep 4;591(1–3):80–7.
358. Jensen TP, Buckby LE, Empson RM. Expression of plasma membrane Ca²⁺ ATPase family members and associated synaptic proteins in acute and cultured organotypic hippocampal slices from rat. *Dev Brain Res*. 2004 Sep 17;152(2):129–36.
359. Oceandy D, Cartwright EJ, Emerson M, Prehar S, Baudoin FM, Zi M, et al. Neuronal nitric oxide synthase signaling in the heart is regulated by the sarcolemmal calcium pump 4b. *Circulation*. 2007 Jan 30;115(4):483–92.
360. Strehler EE, Zacharias DA. Role of Alternative Splicing in Generating Isoform Diversity Among Plasma Membrane Calcium Pumps. *Physiol Rev*. 2001 Jan 1;81(1):21–50.
361. Liu L, Ishida Y, Okunade G, Pyne-Geithman GJ, Shull GE, Paul RJ. Distinct roles of PMCA isoforms in Ca²⁺ homeostasis of bladder smooth muscle: evidence from PMCA gene-ablated mice. *Am J Physiol - Cell Physiol*. 2007 Jan 1;292(1):C423–31.
362. Olson S, Wang MG, Carafoli E, Strehler EE, McBride OW. Localization of two genes encoding plasma membrane Ca²⁺-transporting ATPases to human chromosomes 1q25-32 and 12q21-23. *Genomics*. 1991 Apr;9(4):629–41.
363. Wang MG, Yi H, Hilfiker H, Carafoli E, Strehler EE, McBride OW. Localization of two genes encoding plasma membrane Ca²⁺ ATPases isoforms 2 (ATP2B2) and 3 (ATP2B3) to human chromosomes 3p26-->p25 and Xq28, respectively. *Cytogenet Cell Genet*. 1994;67(1):41–5.
364. Stauffer TP, Guerini D, Carafoli E. Tissue distribution of the four gene products of the plasma membrane Ca²⁺ pump. A study using specific antibodies. *J Biol Chem*. 1995 May 19;270(20):12184–90.

365. Stauffer TP, Hilfiker H, Carafoli E, Strehler EE. Quantitative analysis of alternative splicing options of human plasma membrane calcium pump genes. *J Biol Chem*. 1993 Dec 5;268(34):25993–6003.
366. Caride AJ, Chini EN, Penniston JT, Dousa TP. Selective decrease of mRNAs encoding plasma membrane calcium pump isoforms 2 and 3 in rat kidney. *Kidney Int*. 1999 Nov;56(5):1818–25.
367. Kip SN, Strehler EE. Characterization of PMCA isoforms and their contribution to transcellular Ca^{2+} flux in MDCK cells. *Am J Physiol - Ren Physiol*. 2003 Jan 1;284(1):F122–32.
368. Hagen EAE van der, Lavrijsen M, Zeeland F van, Praetorius J, Bonny O, Bindels RJM, et al. Coordinated regulation of TRPV5-mediated Ca^{2+} transport in primary distal convolution cultures. *Pflüg Arch - Eur J Physiol*. 2014 Nov 1;466(11):2077–87.
369. Hoenderop JGJ, van Leeuwen JPTM, van der Eerden BCJ, Kersten FFJ, van der Kemp AWCM, Méryllat A-M, et al. Renal Ca^{2+} wasting, hyperabsorption, and reduced bone thickness in mice lacking TRPV5. *J Clin Invest*. 2003 Dec;112(12):1906–14.
370. Rimessi A, Coletto L, Pinton P, Rizzuto R, Brini M, Carafoli E. Inhibitory interaction of the 14-3-3{epsilon} protein with isoform 4 of the plasma membrane Ca^{2+} -ATPase pump. *J Biol Chem*. 2005 Nov 4;280(44):37195–203.
371. Enyedi A, Verma AK, Heim R, Adamo HP, Filoteo AG, Strehler EE, et al. The Ca^{2+} affinity of the plasma membrane Ca^{2+} pump is controlled by alternative splicing. *J Biol Chem*. 1994 Jan 7;269(1):41–3.
372. Chicka MC, Strehler EE. Alternative splicing of the first intracellular loop of plasma membrane Ca^{2+} -ATPase isoform 2 alters its membrane targeting. *J Biol Chem*. 2003 May 16;278(20):18464–70.
373. Vorherr T, Kessler T, Hofmann F, Carafoli E. The calmodulin-binding domain mediates the self-association of the plasma membrane Ca^{2+} pump. *J Biol Chem*. 1991 Jan 5;266(1):22–7.
374. Kosk-Kosicka D, Bzdega T. Activation of the erythrocyte Ca^{2+} -ATPase by either self-association or interaction with calmodulin. *J Biol Chem*. 1988 Dec 5;263(34):18184–9.
375. Zacharias DA, Strehler EE. Change in plasma membrane Ca^{2+} -ATPase splice-variant expression in response to a rise in intracellular Ca^{2+} . *Curr Biol CB*. 1996 Dec 1;6(12):1642–52.
376. Guerini D, Wang X, Li L, Genazzani A, Carafoli E. Calcineurin controls the expression of isoform 4CII of the plasma membrane Ca^{2+} pump in neurons. *J Biol Chem*. 2000 Feb 4;275(5):3706–12.

377. Buch MH, Pickard A, Rodriguez A, Gillies S, Maass AH, Emerson M, et al. The sarcolemmal calcium pump inhibits the calcineurin/nuclear factor of activated T-cell pathway via interaction with the calcineurin A catalytic subunit. *J Biol Chem*. 2005 Aug 19;280(33):29479–87.
378. Holton M, Yang D, Wang W, Mohamed TMA, Neyses L, Armesilla AL. The interaction between endogenous calcineurin and the plasma membrane calcium-dependent ATPase is isoform specific in breast cancer cells. *FEBS Lett*. 2007 Aug 21;581(21):4115–9.
379. Mangialavori I, Ferreira-Gomes M, Pignataro MF, Strehler EE, Rossi JPFC. Determination of the Dissociation Constants for Ca²⁺ and Calmodulin from the Plasma Membrane Ca²⁺ Pump by a Lipid Probe That Senses Membrane Domain Changes. *J Biol Chem*. 2010 Jan 1;285(1):123–30.
380. James PH, Pruschy M, Vorherr TE, Penniston JT, Carafoli E. Primary structure of the cAMP-dependent phosphorylation site of the plasma membrane calcium pump. *Biochemistry (Mosc)*. 1989 May 16;28(10):4253–8.
381. Enyedi A, Verma AK, Filoteo AG, Penniston JT. Protein Kinase C Activates the Plasma Membrane Ca²⁺ Pump Isoform 4b by Phosphorylation of an Inhibitory Region Downstream of the Calmodulin-binding Domain. *J Biol Chem*. 1996 Dec 13;271(50):32461–7.
382. Smallwood JI, Gügi B, Rasmussen H. Regulation of erythrocyte Ca²⁺ pump activity by protein kinase C. *J Biol Chem*. 1988 Feb 15;263(5):2195–202.
383. Lambers TT, Mahieu F, Oancea E, Hoofd L, de Lange F, Mensenkamp AR, et al. Calbindin-D28K dynamically controls TRPV5-mediated Ca²⁺ transport. *EMBO J*. 2006 Jul 12;25(13):2978–88.
384. Lee C-T, Chen H-C, Lai L-W, Yong K-C, Lien Y-HH. Effects of furosemide on renal calcium handling. *Am J Physiol Renal Physiol*. 2007 Oct;293(4):F1231-1237.
385. Duarte CG, Winnacker JL, Becker KL, Pace A. Thiazide-Induced Hypercalcemia. *N Engl J Med*. 1971 Apr 15;284(15):828–30.
386. Nijenhuis T, Hoenderop JGJ, Loffing J, van der Kemp AWCM, van Os CH, Bindels RJM. Thiazide-induced hypocalciuria is accompanied by a decreased expression of Ca²⁺ transport proteins in kidney. *Kidney Int*. 2003 Aug;64(2):555–64.
387. Loffing J, Loffing-Cueni D, Hegyi I, Kaplan MR, Hebert SC, Le Hir M, et al. Thiazide treatment of rats provokes apoptosis in distal tubule cells. *Kidney Int*. 1996 Oct;50(4):1180–90.

388. Lee C-T, Shang S, Lai L-W, Yong K-C, Lien Y-HH. Effect of thiazide on renal gene expression of apical calcium channels and calbindins. *Am J Physiol - Ren Physiol*. 2004 Dec 1;287(6):F1164–70.
389. Yang S-S, Lo Y-F, Yu I-S, Lin S-W, Chang T-H, Hsu Y-J, et al. Generation and analysis of the thiazide-sensitive Na⁺-Cl⁻ cotransporter (Ncc/Slc12a3) Ser707X knockin mouse as a model of Gitelman syndrome. *Hum Mutat*. 2010 Dec;31(12):1304–15.
390. Mayan H, Munter G, Shaharabany M, Mouallem M, Pauzner R, Holtzman EJ, et al. Hypercalciuria in familial hyperkalemia and hypertension accompanies hyperkalemia and precedes hypertension: description of a large family with the Q565E WNK4 mutation. *J Clin Endocrinol Metab*. 2004 Aug;89(8):4025–30.
391. Achard J-M, Warnock DG, Disse-Nicodème S, Fiquet-Kempf B éatrice, Corvol P, Fournier A, et al. Familial hyperkalemic hypertension: phenotypic analysis in a large family with the WNK1 deletion mutation. *Am J Med*. 2003 Apr 15;114(6):495–8.
392. Mayan H, Carmon V, Oleinikov K, London S, Halevy R, Holtzman EJ, et al. Hypercalciuria in Familial Hyperkalemia and Hypertension with KLHL3 Mutations. *Nephron*. 2015;130(1):59–65.
393. McCarron DA, Pingree PA, Rubin RJ, Gaucher SM, Molitch M, Krutzik S. Enhanced parathyroid function in essential hypertension: a homeostatic response to a urinary calcium leak. *Hypertension*. 1980 Apr;2(2):162–8.
394. Strazzullo P, Nunziata V, Cirillo M, Giannattasio R, Ferrara LA, Mattioli PL, et al. Abnormalities of calcium metabolism in essential hypertension. *Clin Sci Lond Engl* 1979. 1983 Aug;65(2):137–41.
395. McCarron DA, Rankin LI, Bennett WM, Krutzik S, McClung MR, Luft FC. Urinary calcium excretion at extremes of sodium intake in normal man. *Am J Nephrol*. 1981;1(2):84–90.
396. Kleeman CR, Bohannon J, Bernstein D, Ling S, Maxwell MH. Effect of variations in sodium intake on calcium excretion in normal humans. *Proc Soc Exp Biol Med Soc Exp Biol Med N Y N*. 1964 Jan;115:29–32.
397. Silver J, Rubinger D, Friedlaender MM, Popovtzer MM. Sodium-dependent idiopathic hypercalciuria in renal-stone formers. *Lancet Lond Engl*. 1983 Aug 27;2(8348):484–6.
398. Lemann J, Pleuss JA, Hornick L, Hoffman RG. Dietary NaCl-restriction prevents the calciuria of KCl-deprivation and blunts the calciuria of KHCO₃-deprivation in healthy adults. *Kidney Int*. 1995 Mar;47(3):899–906.
399. MacGregor GA, Markandu ND, Sagnella GA, Singer DR, Cappuccio FP. Double-blind study of three sodium intakes and long-term effects of sodium

- restriction in essential hypertension. *Lancet Lond Engl.* 1989 Nov 25;2(8674):1244–7.
400. Cappuccio FP, Markandu ND, Carney C, Sagnella GA, MacGregor GA. Double-blind randomised trial of modest salt restriction in older people. *Lancet Lond Engl.* 1997 Sep 20;350(9081):850–4.
401. Nouvenne A, Meschi T, Prati B, Guerra A, Allegri F, Vezzoli G, et al. Effects of a low-salt diet on idiopathic hypercalciuria in calcium-oxalate stone formers: a 3-mo randomized controlled trial. *Am J Clin Nutr.* 2010 Mar;91(3):565–70.
402. Galletti F, Ferrara I, Stinga F, Sacchi A, Barba G, Iacone R, et al. Effect of intravenous sodium chloride on renal sodium and calcium handling in hypertensive patients with different sensitivities to sodium chloride. *J Hypertens Suppl Off J Int Soc Hypertens.* 1993 Dec;11(5):S194-195.
403. Cappuccio FP, Siani A, Barba G, Mellone MC, Russo L, Farinaro E, et al. A prospective study of hypertension and the incidence of kidney stones in men. *J Hypertens.* 1999 Jul;17(7):1017–22.
404. Morgagni GB. *De sedibus et causis Morborum, per Anatomen indagatis: libri quinque.* Venice: Typographia Remondiniana; 1761. 452 p.
405. Taylor EN, Fung TT, Curhan GC. DASH-style diet associates with reduced risk for kidney stones. *J Am Soc Nephrol JASN.* 2009 Oct;20(10):2253–9.
406. Omasits U, Ahrens CH, Müller S, Wollscheid B. Protter: interactive protein feature visualization and integration with experimental proteomic data. *Bioinformatics.* 2014 Mar 15;30(6):884–6.
407. Käll L, Krogh A, Sonnhammer ELL. Advantages of combined transmembrane topology and signal peptide prediction--the Phobius web server. *Nucleic Acids Res.* 2007 Jul;35(Web Server issue):W429-432.
408. Chauhan JS, Rao A, Raghava GPS. In silico Platform for Prediction of N-, O- and C-Glycosites in Eukaryotic Protein Sequences. *PLOS ONE.* 2013 Jun 28;8(6):e67008.
409. Lorenz C, Pusch M, Jentsch TJ. Heteromultimeric CLC chloride channels with novel properties. *Proc Natl Acad Sci U S A.* 1996 Nov 12;93(23):13362–6.
410. Gonzales MF, Brooks T, Pukatzki SU, Provenzano D. Rapid protocol for preparation of electrocompetent *Escherichia coli* and *Vibrio cholerae*. *J Vis Exp JoVE.* 2013 Oct 8;(80).
411. Zerangue N, Schwappach B, Jan YN, Jan LY. A New ER Trafficking Signal Regulates the Subunit Stoichiometry of Plasma Membrane KATP Channels. *Neuron.* 1999 Mar;22(3):537–48.

412. Consortium TU. UniProt: a hub for protein information. *Nucleic Acids Res.* 2015 Jan 28;43(D1):D204–12.
413. Fezai M, Ahmed M, Hosseinzadeh Z, Elvira B, Lang F. SPAK and OSR1 Sensitive Kir2.1 K⁺ Channels. *Neurosignals.* 2015 Dec 17;23(1):20–33.
414. Field J, Nikawa J, Broek D, MacDonald B, Rodgers L, Wilson IA, et al. Purification of a RAS-responsive adenylyl cyclase complex from *Saccharomyces cerevisiae* by use of an epitope addition method. *Mol Cell Biol.* 1988 May;8(5):2159–65.
415. Brizzard B. Epitope Tagging. *BioTechniques.* 2008 Apr;44:693–5.
416. Schwappach B, Zerangue N, Jan YN, Jan LY. Molecular Basis for KATP Assembly: Transmembrane Interactions Mediate Association of a K⁺ Channel with an ABC Transporter. *Neuron.* 2000 Apr;26(1):155–67.
417. Chan KW, Zhang H, Logothetis DE. N-terminal transmembrane domain of the SUR controls trafficking and gating of Kir6 channel subunits. *EMBO J.* 2003 Aug 1;22(15):3833–43.
418. Balduzzi R, Cupello A, Diaspro A, Ramoino P, Robello M. Confocal microscopic study of GABAA receptors in *Xenopus* oocytes after rat brain mRNA injection: modulation by tyrosine kinase activity. *Biochim Biophys Acta BBA - Mol Cell Res.* 2001 May 28;1539(1):93–100.
419. Yang Y, Cui Y, Wang W, Zhang L, Bufford L, Sasaki S, et al. Molecular and functional characterization of a vasotocin-sensitive aquaporin water channel in quail kidney. *Am J Physiol - Regul Integr Comp Physiol.* 2004 Oct 1;287(4):R915–24.
420. Ghim C-M, Lee SK, Takayama S, Mitchell RJ. The art of reporter proteins in science: past, present and future applications. *BMB Rep.* 2010 Jul;43(7):451–60.
421. Devonald MAJ, Smith AN, Poon JP, Ihrke G, Karet FE. Non-polarized targeting of AE1 causes autosomal dominant distal renal tubular acidosis. *Nat Genet.* 2003 Feb;33(2):125–7.
422. Ihrke G, Bruns JR, Luzio JP, Weisz OA. Competing sorting signals guide endolyn along a novel route to lysosomes in MDCK cells. *EMBO J.* 2001 Nov 15;20(22):6256–64.
423. Singer JD, Gurian-West M, Clurman B, Roberts JM. Cullin-3 targets cyclin E for ubiquitination and controls S phase in mammalian cells. *Genes Dev.* 1999 Sep 15;13(18):2375–87.
424. Lin X-C, Sui W-G, Qi S-W, Tang D-E, Cong S, Zou G-M, et al. Quantitative proteomic profiling of renal tissue in human chronic rejection biopsy samples after renal transplantation. *Transplant Proc.* 2015 Mar;47(2):323–31.

425. Rinschen MM, Yu M-J, Wang G, Boja ES, Hoffert JD, Pisitkun T, et al. Quantitative phosphoproteomic analysis reveals vasopressin V2-receptor-dependent signaling pathways in renal collecting duct cells. *Proc Natl Acad Sci*. 2010 Feb 23;107(8):3882–7.
426. Gonzales PA, Pisitkun T, Hoffert JD, Tchapyjnikov D, Star RA, Kleta R, et al. Large-scale proteomics and phosphoproteomics of urinary exosomes. *J Am Soc Nephrol JASN*. 2009 Feb;20(2):363–79.
427. Gunaratne R, Braucht DWW, Rinschen MM, Chou C-L, Hoffert JD, Pisitkun T, et al. Quantitative phosphoproteomic analysis reveals cAMP/vasopressin-dependent signaling pathways in native renal thick ascending limb cells. *Proc Natl Acad Sci U S A*. 2010 Aug 31;107(35):15653–8.
428. Hoffert JD, Pisitkun T, Wang G, Shen R-F, Knepper MA. Quantitative phosphoproteomics of vasopressin-sensitive renal cells: Regulation of aquaporin-2 phosphorylation at two sites. *Proc Natl Acad Sci*. 2006 Feb 5;103(18):7159–64.
429. Megger DA, Pott LL, Ahrens M, Padden J, Bracht T, Kuhlmann K, et al. Comparison of label-free and label-based strategies for proteome analysis of hepatoma cell lines. *Biochim Biophys Acta BBA - Proteins Proteomics*. 2014 May;1844(5):967–76.
430. Fila J, Honys D. Enrichment techniques employed in phosphoproteomics. *Amino Acids*. 2012 Sep;43(3):1025–47.
431. Yue X, Schunter A, Hummon AB. Comparing Multi-Step IMAC and Multi-Step TiO₂ Methods for Phosphopeptide Enrichment. *Anal Chem*. 2015 Sep 1;87(17):8837–44.
432. Beltran L, Cutillas PR. Advances in phosphopeptide enrichment techniques for phosphoproteomics. *Amino Acids*. 2012 Sep 1;43(3):1009–24.
433. Szklarczyk D, Morris JH, Cook H, Kuhn M, Wyder S, Simonovic M, et al. The STRING database in 2017: quality-controlled protein-protein association networks, made broadly accessible. *Nucleic Acids Res*. 2017 Jan 4;45(D1):D362–8.
434. Shannon P, Markiel A, Ozier O, Baliga NS, Wang JT, Ramage D, et al. Cytoscape: A Software Environment for Integrated Models of Biomolecular Interaction Networks. *Genome Res*. 2003 Jan 11;13(11):2498–504.
435. Nepusz T, Yu H, Paccanaro A. Detecting overlapping protein complexes in protein-protein interaction networks. *Nat Methods*. 2012 May;9(5):471–2.
436. Schwartz D, Gygi SP. An iterative statistical approach to the identification of protein phosphorylation motifs from large-scale data sets. *Nat Biotechnol*. 2005 Nov;23(11):1391–8.

437. Chou MF, Schwartz D. Biological sequence motif discovery using motif-x. *Curr Protoc Bioinforma*. 2011 Sep;Chapter 13:Unit 13.15-24.
438. Thomas PD, Campbell MJ, Kejariwal A, Mi H, Karlak B, Daverman R, et al. PANTHER: A Library of Protein Families and Subfamilies Indexed by Function. *Genome Res*. 2003 Jan 9;13(9):2129–41.
439. Hornbeck PV, Zhang B, Murray B, Kornhauser JM, Latham V, Skrzypek E. PhosphoSitePlus, 2014: mutations, PTMs and recalibrations. *Nucleic Acids Res*. 2015 Jan;43(Database issue):D512-520.
440. Sievers F, Wilm A, Dineen D, Gibson TJ, Karplus K, Li W, et al. Fast, scalable generation of high-quality protein multiple sequence alignments using Clustal Omega. *Mol Syst Biol*. 2011 Jan 1;7(1):539.
441. Franceschini A, Lin J, von Mering C, Jensen LJ. SVD-phy: improved prediction of protein functional associations through singular value decomposition of phylogenetic profiles. *Bioinforma Oxf Engl*. 2016 Apr 1;32(7):1085–7.
442. Yoon J, Blumer A, Lee K. An algorithm for modularity analysis of directed and weighted biological networks based on edge-betweenness centrality. *Bioinforma Oxf Engl*. 2006 Dec 15;22(24):3106–8.
443. Gonzalez E, McGraw TE. Insulin-modulated Akt subcellular localization determines Akt isoform-specific signaling. *Proc Natl Acad Sci U S A*. 2009 Apr 28;106(17):7004–9.
444. Mackenzie RW, Elliott BT. Akt/PKB activation and insulin signaling: a novel insulin signaling pathway in the treatment of type 2 diabetes. *Diabetes Metab Syndr Obes Targets Ther*. 2014 Feb 13;7:55–64.
445. Amanchy R, Periaswamy B, Mathivanan S, Reddy R, Tattikota SG, Pandey A. A curated compendium of phosphorylation motifs. *Nat Biotechnol*. 2007 Mar;25(3):285–6.
446. Garai Á, Zeke A, Gógl G, Törö I, Ferenc F, Blankenburg H, et al. Specificity of Linear Motifs That Bind to a Common Mitogen-Activated Protein Kinase Docking Groove. *Sci Signal*. 2012 Oct 9;5(245):ra74.
447. Roux PP, Blenis J. ERK and p38 MAPK-Activated Protein Kinases: a Family of Protein Kinases with Diverse Biological Functions. *Microbiol Mol Biol Rev*. 2004 Jun;68(2):320–44.
448. Pelech SL. Networking with proline-directed protein kinases implicated in tau phosphorylation. *Neurobiol Aging*. 1995 Jun;16(3):247-256; discussion 257-261.
449. Obata T, Yaffe MB, Leparc GG, Piro ET, Maegawa H, Kashiwagi A, et al. Peptide and Protein Library Screening Defines Optimal Substrate Motifs for AKT/PKB. *J Biol Chem*. 2000 Nov 17;275(46):36108–15.

450. Manning BD, Cantley LC. AKT/PKB Signaling: Navigating Downstream. *Cell*. 2007 Jun 29;129(7):1261–74.
451. Rust HL, Thompson PR. Kinase Consensus Sequences – A Breeding Ground for Crosstalk. *ACS Chem Biol*. 2011 Sep 16;6(9):881–92.
452. Marin O, Meggio F, Draetta G, Pinna LA. The consensus sequences for cdc2 kinase and for casein kinase-2 are mutually incompatible. A study with peptides derived from the beta-subunit of casein kinase-2. *FEBS Lett*. 1992 Apr 13;301(1):111–4.
453. Villén J, Beausoleil SA, Gerber SA, Gygi SP. Large-scale phosphorylation analysis of mouse liver. *Proc Natl Acad Sci U S A*. 2007 Jan 30;104(5):1488–93.
454. van Wijk KJ, Friso G, Walther D, Schulze WX. Meta-Analysis of Arabidopsis thaliana Phospho-Proteomics Data Reveals Compartmentalization of Phosphorylation Motifs[C][W]. *Plant Cell*. 2014 Jun;26(6):2367–89.
455. Kohlstedt K, Shoghi F, Müller-Esterl W, Busse R, Fleming I. CK2 Phosphorylates the Angiotensin-Converting Enzyme and Regulates Its Retention in the Endothelial Cell Plasma Membrane. *Circ Res*. 2002 Oct 18;91(8):749–56.
456. Weinman EJ, Cunningham R, Wade JB, Shenolikar S. The role of NHERF-1 in the regulation of renal proximal tubule sodium–hydrogen exchanger 3 and sodium-dependent phosphate cotransporter 2a. *J Physiol*. 2005 Aug 1;567(1):27–32.
457. Mohebbi N, Mihailova M, Wagner CA. The calcineurin inhibitor FK506 (tacrolimus) is associated with transient metabolic acidosis and altered expression of renal acid-base transport proteins. *Am J Physiol - Ren Physiol*. 2009 Jan 8;297(2):F499–509.
458. He P, Zhao L, No YR, Karvar S, Yun CC. NHERF1 PDZ1 domain and IRBIT interact and mediate the activation of Na⁺/H⁺ exchanger NHE3 by angiotensin II. *Am J Physiol - Ren Physiol*. 2016 Jun 8;F343–51.
459. Grimsrud PA, Carson JJ, Hebert AS, Hubler SL, Niemi NM, Bailey DJ, et al. A quantitative map of the liver mitochondrial phosphoproteome reveals posttranslational control of ketogenesis. *Cell Metab*. 2012 Nov 7;16(5):672–83.
460. Hsu PP, Kang SA, Rameseder J, Zhang Y, Ottina KA, Lim D, et al. The mTOR-regulated phosphoproteome reveals a mechanism of mTORC1-mediated inhibition of growth factor signaling. *Science*. 2011 Jun 10;332(6035):1317–22.
461. Demirkan G, Yu K, Boylan JM, Salomon AR, Gruppuso PA. Phosphoproteomic profiling of in vivo signaling in liver by the mammalian target of rapamycin complex 1 (mTORC1). *PLoS One*. 2011;6(6):e21729.

462. Deng W-J, Nie S, Dai J, Wu J-R, Zeng R. Proteome, phosphoproteome, and hydroxyproteome of liver mitochondria in diabetic rats at early pathogenic stages. *Mol Cell Proteomics MCP*. 2010 Jan;9(1):100–16.
463. Mostovenko E, Hassan C, Rattke J, Deelder AM, van Veelen PA, Palmblad M. Comparison of peptide and protein fractionation methods in proteomics. *EuPA Open Proteomics*. 2013;1:30–7.
464. Spät P, Maček B, Forchhammer K. Phosphoproteome of the cyanobacterium *Synechocystis* sp. PCC 6803 and its dynamics during nitrogen starvation. *Front Microbiol*. 2015;6:248.
465. Rosenberg A, Soufi B, Ravikumar V, Soares NC, Krug K, Smith Y, et al. Phosphoproteome dynamics mediate revival of bacterial spores. *BMC Biol*. 2015;13:76.
466. Dammer EB, Lee AK, Duong DM, Gearing M, Lah JJ, Levey AI, et al. Quantitative Phosphoproteomics of Alzheimer's Disease Reveals Crosstalk between Kinases and Small Heat Shock Proteins. *Proteomics*. 2015 Jan;15(0):508–19.
467. Cho H, Mu J, Kim JK, Thorvaldsen JL, Chu Q, Crenshaw EB, et al. Insulin resistance and a diabetes mellitus-like syndrome in mice lacking the protein kinase Akt2 (PKB beta). *Science*. 2001 Jun 1;292(5522):1728–31.
468. George S, Rochford JJ, Wolfrum C, Gray SL, Schinner S, Wilson JC, et al. A family with severe insulin resistance and diabetes due to a mutation in AKT2. *Science*. 2004 May 28;304(5675):1325–8.
469. Feliers D, Duraisamy S, Faulkner JL, Duch J, Lee AV, Abboud HE, et al. Activation of renal signaling pathways in db/db mice with type 2 diabetes. *Kidney Int*. 2001 Aug;60(2):495–504.
470. Catena C, Cavarape A, Novello M, Giacchetti G, Sechi LA. Insulin receptors and renal sodium handling in hypertensive fructose-fed rats. *Kidney Int*. 2003 Dec;64(6):2163–71.
471. Nishida H, Sohara E, Nomura N, Chiga M, Alessi DR, Rai T, et al. PI3K/Akt Signaling Pathway Activates the WNK-OSR1/SPAK-NCC Phosphorylation Cascade in Hyperinsulinemic db/db Mice. *Hypertension*. 2012 Oct;60(4):981–90.
472. Shao J, Yamashita H, Qiao L, Friedman JE. Decreased Akt kinase activity and insulin resistance in C57BL/KsJ-Lepr^{db/db} mice. *J Endocrinol*. 2000 Oct;167(1):107–15.
473. Wang R-H, Kim H-S, Xiao C, Xu X, Gavrilova O, Deng C-X. Hepatic Sirt1 deficiency in mice impairs mTORc2/Akt signaling and results in hyperglycemia, oxidative damage, and insulin resistance. *J Clin Invest*. 2011 Nov;121(11):4477–90.

474. Alessi DR, Andjelkovic M, Caudwell B, Cron P, Morrice N, Cohen P, et al. Mechanism of activation of protein kinase B by insulin and IGF-1. *EMBO J*. 1996 Dec 2;15(23):6541–51.
475. Park CH, Kim YS, Kim YH, Choi MY, Yoo JM, Kang SS, et al. Calcineurin mediates AKT dephosphorylation in the ischemic rat retina. *Brain Res*. 2008 Oct 9;1234:148–57.
476. Ni YG, Wang N, Cao DJ, Sachan N, Morris DJ, Gerard RD, et al. FoxO transcription factors activate Akt and attenuate insulin signaling in heart by inhibiting protein phosphatases. *Proc Natl Acad Sci U S A*. 2007 Dec 18;104(51):20517–22.
477. Vitari AC, Deak M, Collins BJ, Morrice N, Prescott AR, Phelan A, et al. WNK1, the kinase mutated in an inherited high-blood-pressure syndrome, is a novel PKB (protein kinase B)/Akt substrate. *Biochem J*. 2004 Feb 15;378(Pt 1):257–68.
478. Odunewu-Aderibigbe A, Fliegel L. Protein mediated regulation of the NHE1 isoform of the Na⁺/H⁺ exchanger in renal cells. A regulatory role of Hsp90 and AKT kinase. *Cell Signal*. 2017 Aug 1;36:145–53.
479. Takahashi S, Mendelsohn ME. Synergistic activation of endothelial nitric-oxide synthase (eNOS) by HSP90 and Akt: calcium-independent eNOS activation involves formation of an HSP90-Akt-CaM-bound eNOS complex. *J Biol Chem*. 2003 Aug 15;278(33):30821–7.
480. Johnson JL, Toft DO. A novel chaperone complex for steroid receptors involving heat shock proteins, immunophilins, and p23. *J Biol Chem*. 1994 Oct 7;269(40):24989–93.
481. Galigniana MD, Radanyi C, Renoir JM, Housley PR, Pratt WB. Evidence that the peptidylprolyl isomerase domain of the hsp90-binding immunophilin FKBP52 is involved in both dynein interaction and glucocorticoid receptor movement to the nucleus. *J Biol Chem*. 2001 May 4;276(18):14884–9.
482. Galigniana MD, Erlejman AG, Monte M, Gomez-Sanchez C, Piwien-Pilipuk G. The hsp90-FKBP52 complex links the mineralocorticoid receptor to motor proteins and persists bound to the receptor in early nuclear events. *Mol Cell Biol*. 2010 Mar;30(5):1285–98.
483. Syed AA, Halpin CG, Irving JAE, Unwin NC, White M, Bhopal RS, et al. A common intron 2 polymorphism of the glucocorticoid receptor gene is associated with insulin resistance in men. *Clin Endocrinol (Oxf)*. 2008 Jun 1;68(6):879–84.
484. Zhou B, Wang D, Feng X, Zhang Y, Wang Y, Zhuang J, et al. WNK4 inhibits NCC protein expression through MAPK ERK1/2 signaling pathway. *Am J Physiol - Ren Physiol*. 2012 Mar 1;302(5):F533–9.

485. Rosenbaek LL, Assentoft M, Pedersen NB, MacAulay N, Fenton RA. Characterization of a novel phosphorylation site in the sodium-chloride cotransporter, NCC. *J Physiol*. 2012 Dec 1;590(23):6121–39.
486. Procino G, Carmosino M, Marin O, Brunati AM, Contri A, Pinna LA, et al. Ser-256 phosphorylation dynamics of Aquaporin 2 during maturation from the ER to the vesicular compartment in renal cells. *FASEB J Off Publ Fed Am Soc Exp Biol*. 2003 Oct;17(13):1886–8.
487. Knepper MA. Molecular physiology of urinary concentrating mechanism: regulation of aquaporin water channels by vasopressin. *Am J Physiol - Ren Physiol*. 1997 Jan 1;272(1):F3–12.
488. Roche JV, Survery S, Kreida S, Nesverova V, Ampah-Korsah H, Gourdon M, et al. Phosphorylation of human aquaporin 2 (AQP2) allosterically controls its interaction with the lysosomal trafficking protein LIP5. *J Biol Chem*. 2017 Jul 14;M117.788364.
489. Moeller HB, Praetorius J, Rützler MR, Fenton RA. Phosphorylation of aquaporin-2 regulates its endocytosis and protein–protein interactions. *Proc Natl Acad Sci U S A*. 2010 Jan 5;107(1):424–9.
490. Lu HJ, Matsuzaki T, Bouley R, Hasler U, Qin Q-H, Brown D. The phosphorylation state of serine 256 is dominant over that of serine 261 in the regulation of AQP2 trafficking in renal epithelial cells. *Am J Physiol Renal Physiol*. 2008 Jul;295(1):F290-294.
491. Rinschen MM, Klokkers J, Pavenstädt H, Neugebauer U, Schlatter E, Edemir B. Different effects of CsA and FK506 on aquaporin-2 abundance in rat primary cultured collecting duct cells. *Pflugers Arch*. 2011 Oct;462(4):611–22.
492. Esteva-Font C, Ars E, Guillen-Gomez E, Campistol JM, Sanz L, Jiménez W, et al. Cyclosporin-induced hypertension is associated with increased sodium transporter of the loop of Henle (NKCC2). *Nephrol Dial Transplant Off Publ Eur Dial Transpl Assoc - Eur Ren Assoc*. 2007 Oct;22(10):2810–6.
493. Aker S, Heering P, Kinne-Saffran E, Deppe C, Grabensee B, Kinne RK. Different effects of cyclosporine a and FK506 on potassium transport systems in MDCK cells. *Exp Nephrol*. 2001;9(5):332–40.
494. Weinman EJ, Steplock D, Shenolikar S. NHERF-1 uniquely transduces the cAMP signals that inhibit sodium–hydrogen exchange in mouse renal apical membranes. *FEBS Lett*. 2003 Feb 11;536(1–3):141–4.
495. Kobayashi K, Monkawa T, Hayashi M, Saruta T. Expression of the Na⁺/H⁺ exchanger regulatory protein family in genetically hypertensive rats. *J Hypertens*. 2004 Sep;22(9):1723–30.

496. Heering P, Ivens K, Aker S, Grabensee B. Distal tubular acidosis induced by FK506. *Clin Transplant*. 1998 Oct;12(5):465–71.
497. Dinour D, Chang M-H, Satoh J, Smith BL, Angle N, Knecht A, et al. A Novel Missense Mutation in the Sodium Bicarbonate Cotransporter (NBCe1/SLC4A4) Causes Proximal Tubular Acidosis and Glaucoma through Ion Transport Defects. *J Biol Chem*. 2004 Oct 12;279(50):52238–46.
498. Laing CM, Toye AM, Capasso G, Unwin RJ. Renal tubular acidosis: developments in our understanding of the molecular basis. *Int J Biochem Cell Biol*. 2005 Jun;37(6):1151–61.
499. Curthoys NP, Moe OW. Proximal Tubule Function and Response to Acidosis. *Clin J Am Soc Nephrol CJASN*. 2014 Sep 5;9(9):1627–38.
500. Osis G, Handlogten ME, Lee H-W, Hering-Smith KS, Huang W, Romero MF, et al. Effect of NBCe1 deletion on renal citrate and 2-oxoglutarate handling. *Physiol Rep*. 2016 Apr;4(8).
501. Vallon V. The proximal tubule in the pathophysiology of the diabetic kidney. *Am J Physiol - Regul Integr Comp Physiol*. 2011 May;300(5):R1009–22.
502. Sharif A, Cohn S. Post-transplantation diabetes—state of the art. *Lancet Diabetes Endocrinol*. 2016 Apr;4(4):337–49.
503. Furth S, Neu A, Colombani P, Plotnick L, Turner ME, Fivush B. Diabetes as a complication of tacrolimus (FK506) in pediatric renal transplant patients. *Pediatr Nephrol Berl Ger*. 1996 Feb;10(1):64–6.
504. Ruderman N, Prentki M. AMP kinase and malonyl-CoA: targets for therapy of the metabolic syndrome. *Nat Rev Drug Discov*. 2004 Apr;3(4):340–51.
505. Paulais M, Bloch-Faure M, Picard N, Jacques T, Ramakrishnan SK, Keck M, et al. Renal phenotype in mice lacking the Kir5.1 (Kcnj16) K⁺ channel subunit contrasts with that observed in SeSAME/EAST syndrome. *Proc Natl Acad Sci U S A*. 2011 Jun 21;108(25):10361–6.
506. Lea JP, Sands JM, McMahon SJ, Tumlin JA. Evidence that the inhibition of Na⁺/K⁺-ATPase activity by FK506 involves calcineurin. *Kidney Int*. 1994 Sep;46(3):647–52.
507. Sha Q, Pearson W, Burcea LC, Wigfall DA, Schlesinger PH, Nichols CG, et al. Human FXD2 G41R mutation responsible for renal hypomagnesemia behaves as an inward-rectifying cation channel. *Am J Physiol Renal Physiol*. 2008 Jul;295(1):F91–99.
508. Hauwaert CV der, Savary G, Gnemmi V, Glowacki F, Pottier N, Bouillez A, et al. Isolation and Characterization of a Primary Proximal Tubular Epithelial Cell Model from Human Kidney by CD10/CD13 Double Labeling. *PLOS ONE*. 2013 Jun 14;8(6):e66750.

509. Helbert MJ, Dauwe SE, De Broe ME. Flow cytometric immunodissection of the human distal tubule and cortical collecting duct system. *Kidney Int.* 2001 Feb;59(2):554–64.
510. Wright PA, Burg MB, Knepper MA. [12] Microdissection of kidney tubule segments. *Methods Enzymol.* 1990 Jan 1;191:226–31.
511. Emmert-Buck MR, Bonner RF, Smith PD, Chuaqui RF, Zhuang Z, Goldstein SR, et al. Laser capture microdissection. *Science.* 1996 Nov 8;274(5289):998–1001.
512. Woroniecki RP, Bottinger EP. Laser capture microdissection of kidney tissue. *Methods Mol Biol Clifton NJ.* 2009;466:73–82.
513. Craven RA, Totty N, Harnden P, Selby PJ, Banks RE. Laser capture microdissection and two-dimensional polyacrylamide gel electrophoresis: evaluation of tissue preparation and sample limitations. *Am J Pathol.* 2002 Mar;160(3):815–22.
514. Raynaud FI, Eccles SA, Patel S, Alix S, Box G, Chuckowree I, et al. Biological properties of potent inhibitors of class I phosphatidylinositide 3-kinases: from PI-103 through PI-540, PI-620 to the oral agent GDC-0941. *Mol Cancer Ther.* 2009 Jul;8(7):1725–38.
515. Hirai H, Sootome H, Nakatsuru Y, Miyama K, Taguchi S, Tsujioka K, et al. MK-2206, an allosteric Akt inhibitor, enhances antitumor efficacy by standard chemotherapeutic agents or molecular targeted drugs in vitro and in vivo. *Mol Cancer Ther.* 2010 Jul;9(7):1956–67.
516. Musante L, Tataruch DE, Holthofer H. Use and Isolation of Urinary Exosomes as Biomarkers for Diabetic Nephropathy. *Front Endocrinol.* 2014;5:149.
517. Ko B, Cooke LL, Hoover RS. Parathyroid hormone (PTH) regulates the sodium chloride cotransporter via Ras guanyl releasing protein 1 (Ras-GRP1) and extracellular signal-regulated kinase (ERK)1/2 mitogen-activated protein kinase (MAPK) pathway. *Transl Res J Lab Clin Med.* 2011 Nov;158(5):282–9.
518. Ferreira MC de J, Héliès-Toussaint C, Imbert-Teboul M, Bailly C, Verbavatz J-M, Bellanger A-C, et al. Co-expression of a Ca²⁺-inhibitable adenylyl cyclase and of a Ca²⁺-sensing receptor in the cortical thick ascending limb cell of the rat kidney. Inhibition of hormone-dependent cAMP accumulation by extracellular Ca²⁺. *J Biol Chem.* 1998 Dec 6;273(24):15192–202.
519. Matsuda Y, Saegusa H, Zong S, Noda T, Tanabe T. Mice lacking Ca_v2.3 (alpha1E) calcium channel exhibit hyperglycemia. *Biochem Biophys Res Commun.* 2001 Dec 14;289(4):791–5.
520. Schuh K, Uldrijan S, Gambaryan S, Roethlein N, Neyses L. Interaction of the Plasma Membrane Ca²⁺ Pump 4b/Cl with the Ca²⁺/Calmodulin-

- dependent Membrane-associated Kinase CASK. *J Biol Chem*. 2003 Mar 14;278(11):9778–83.
521. Hryciw DH, Jenkin KA, Simcocks AC, Grinfeld E, McAinch AJ, Poronnik P. The interaction between megalin and CIC-5 is scaffolded by the Na⁺-H⁺ exchanger regulatory factor 2 (NHERF2) in proximal tubule cells. *Int J Biochem Cell Biol*. 2012 May;44(5):815–23.
522. Lloyd SE, Pearce SH, Fisher SE, Steinmeyer K, Schwappach B, Scheinman SJ, et al. A common molecular basis for three inherited kidney stone diseases. *Nature*. 1996 Feb 1;379(6564):445–9.
523. Wrong OM, Norden AG, Feest TG. Dent's disease; a familial proximal renal tubular syndrome with low-molecular-weight proteinuria, hypercalciuria, nephrocalcinosis, metabolic bone disease, progressive renal failure and a marked male predominance. *QJM Mon J Assoc Physicians*. 1994 Aug;87(8):473–93.
524. Mochizuki T, Wu G, Hayashi T, Xenophontos SL, Veldhuisen B, Saris JJ, et al. PKD2, a gene for polycystic kidney disease that encodes an integral membrane protein. *Science*. 1996 May 31;272(5266):1339–42.
525. Rosado JA. *Calcium Entry Pathways in Non-excitabile Cells*. Springer; 2016. 469 p.
526. de Cavanagh EMV, Ferder LF, Ferder MD, Stella IY, Toblli JE, Inserra F. Vascular structure and oxidative stress in salt-loaded spontaneously hypertensive rats: effects of losartan and atenolol. *Am J Hypertens*. 2010 Dec;23(12):1318–25.
527. Ziemiański S, Panczenko-Kresowska B, Okolska G, Wielgus-Serafińska E, Zelakiewicz K. Effect of dietary fats on experimental hypertension. *Ann Nutr Metab*. 1985;29(4):223–31.
528. Tucker RG, Ball CO, Darby WJ, Early WR, Kory RC, Youmans JB, et al. Chronic sodium chloride toxicity in the albino rat. III. Maturity characteristics, survivorship, and organ weights. *J Gerontol*. 1957 Apr;12(2):182–9.
529. Ball CO, Meneely GR. Observations on dietary sodium chloride. *J Am Diet Assoc*. 1957 Apr;33(4):366–70.
530. Chen J, Delaney KH, Kwiecien JM, Lee RM. The effects of dietary sodium on hypertension and stroke development in female stroke-prone spontaneously hypertensive rats. *Exp Mol Pathol*. 1997;64(3):173–83.
531. Wyss JM, Roysommuti S, King K, Kadisha I, Regan CP, Berecek KH. Salt-induced hypertension in normotensive spontaneously hypertensive rats. *Hypertension*. 1994 Jun;23(6 Pt 1):791–6.

532. Goor MK van, Verkaart S, Dam TJ van, Huynen MA, Wijst J van der. Interspecies differences in PTH-mediated PKA phosphorylation of the epithelial calcium channel TRPV5. *Pflüg Arch - Eur J Physiol*. 2017 May 22;1–11.
533. Mellor H, Parker PJ. The extended protein kinase C superfamily. *Biochem J*. 1998 Jun 1;332(2):281–92.
534. Redling S, Pfaff IL, Leitges M, Vallon V. Immunolocalization of protein kinase C isoenzymes α , β I, β II, δ , and ϵ in mouse kidney. *Am J Physiol - Ren Physiol*. 2004 Aug 1;287(2):F289–98.
535. Chabardès D, Firsov D, Aarab L, Clabecq A, Bellanger A-C, Siaume-Perez S, et al. Localization of mRNAs encoding Ca^{2+} -inhibitable adenylyl cyclases along the renal tubule. Functional consequences for regulation of the cAMP content. *J Biol Chem*. 1996 Sep 8;271(32):19264–71.
536. Gao MH, Tang T, Guo T, Miyanochara A, Yajima T, Pestonjamas K, et al. Adenylyl cyclase type VI increases Akt activity and phospholamban phosphorylation in cardiac myocytes. *J Biol Chem*. 2008 Nov 28;283(48):33527–35.
537. Parajuli LK, Nakajima C, Kulik A, Matsui K, Schneider T, Shigemoto R, et al. Quantitative regional and ultrastructural localization of the $\text{Ca}_v2.3$ subunit of R-type calcium channel in mouse brain. *J Neurosci Off J Soc Neurosci*. 2012 Sep 26;32(39):13555–67.
538. Holmkvist J, Tojjar D, Almgren P, Lyssenko V, Lindgren CM, Isomaa B, et al. Polymorphisms in the gene encoding the voltage-dependent Ca^{2+} channel $\text{Ca}_v2.3$ (CACNA1E) are associated with type 2 diabetes and impaired insulin secretion. *Diabetologia*. 2007 Dec;50(12):2467–75.
539. Natrajan R, Little SE, Reis-Filho JS, Hing L, Messahel B, Grundy PE, et al. Amplification and Overexpression of CACNA1E Correlates with Relapse in Favorable Histology Wilms' Tumors. *Clin Cancer Res*. 2006 Dec 15;12(24):7284–93.
540. Sakata Y, Saegusa H, Zong S, Osanai M, Murakoshi T, Shimizu Y, et al. $\text{Ca}_v2.3$ (α 1E) Ca^{2+} channel participates in the control of sperm function. *FEBS Lett*. 2002 Apr 10;516(1–3):229–33.
541. Saegusa H, Matsuda Y, Tanabe T. Effects of ablation of N- and R-type Ca^{2+} channels on pain transmission. *Neurosci Res*. 2002 May;43(1):1–7.
542. Lu Z-J, Pereverzev A, Liu H-L, Weiergräber M, Henry M, Krieger A, et al. Arrhythmia in isolated prenatal hearts after ablation of the $\text{Ca}_v2.3$ (α 1E) subunit of voltage-gated Ca^{2+} channels. *Cell Physiol Biochem Int J Exp Cell Physiol Biochem Pharmacol*. 2004;14(1–2):11–22.

543. Muller YL, Hanson RL, Zimmerman C, Harper I, Sutherland J, Kobes S, et al. Variants in the Cav2.3 ($\alpha 1E$) Subunit of Voltage-Activated Ca^{2+} Channels Are Associated With Insulin Resistance and Type 2 Diabetes in Pima Indians. *Diabetes*. 2007 Jan 12;56(12):3089–94.
544. Jing X, Li D-Q, Olofsson CS, Salehi A, Surve VV, Caballero J, et al. $CaV2.3$ calcium channels control second-phase insulin release. *J Clin Invest*. 2005 Jan 3;115(1):146–54.
545. Osowski CM, Urano F. Measuring ER stress and the unfolded protein response using mammalian tissue culture system. *Methods Enzymol*. 2011;490:71–92.
546. Sun Y, Zhang T, Li L, Wang J. Induction of apoptosis by hypertension via endoplasmic reticulum stress. *Kidney Blood Press Res*. 2015;40(1):41–51.
547. Özcan U, Cao Q, Yilmaz E, Lee A-H, Iwakoshi NN, Özdelen E, et al. Endoplasmic Reticulum Stress Links Obesity, Insulin Action, and Type 2 Diabetes. *Science*. 2004 Oct 15;306(5695):457–61.
548. Bollo M, Paredes RM, Holstein D, Zheleznova N, Camacho P, Lechleiter JD. Calcineurin interacts with PERK and dephosphorylates calnexin to relieve ER stress in mammals and frogs. *PLoS One*. 2010 Aug 5;5(8):e11925.
549. Roderick HL, Lechleiter JD, Camacho P. Cytosolic Phosphorylation of Calnexin Controls Intracellular Ca^{2+} Oscillations via an Interaction with *Serca2b*. *J Cell Biol*. 2000 Jun 12;149(6):1235–48.
550. Peppiatt-Wildman CM, Crawford C, Hall AM. Fluorescence imaging of intracellular calcium signals in intact kidney tissue. *Nephron Exp Nephrol*. 2012;121(1–2):e49-58.
551. Labarca M, Nizar JM, Walczak EM, Dong W, Pao AC, Bhalla V. Harvest and primary culture of the murine aldosterone-sensitive distal nephron. *Am J Physiol - Ren Physiol*. 2015 Jun 1;308(11):F1306–15.
552. Brands MW, Manhiani MM. Sodium-retaining effect of insulin in diabetes. *Am J Physiol Regul Integr Comp Physiol*. 2012 Dec;303(11):R1101-1109.
553. Blazer-Yost BL, Esterman MA, Vlahos CJ. Insulin-stimulated trafficking of ENaC in renal cells requires PI 3-kinase activity. *Am J Physiol Cell Physiol*. 2003 Jun;284(6):C1645-1653.
554. Lang F, Klingel K, Wagner CA, Stegen C, Warntges S, Friedrich B, et al. Deranged transcriptional regulation of cell-volume-sensitive kinase hSGK in diabetic nephropathy. *Proc Natl Acad Sci U S A*. 2000 Jul 5;97(14):8157–62.
555. Mima A, Ohshiro Y, Kitada M, Matsumoto M, Gerald P, Li C, et al. Glomerular-specific protein kinase C- β -induced insulin receptor substrate-

- 1 dysfunction and insulin resistance in rat models of diabetes and obesity. *Kidney Int.* 2011 Apr;79(8):883–96.
556. Oyadomari S, Takeda K, Takiguchi M, Gotoh T, Matsumoto M, Wada I, et al. Nitric oxide-induced apoptosis in pancreatic β cells is mediated by the endoplasmic reticulum stress pathway. *Proc Natl Acad Sci.* 2001 Nov 9;98(19):10845–50.
557. Schwaller B. Cytosolic Ca²⁺ buffers. *Cold Spring Harb Perspect Biol.* 2010 Nov;2(11):a004051.
558. Faas GC, Raghavachari S, Lisman JE, Mody I. Calmodulin as a Direct Detector of Ca²⁺ Signals. *Nat Neurosci.* 2011 Mar;14(3):301–4.
559. Yuan W, Pan W, Kong J, Zheng W, Szeto FL, Wong KE, et al. 1,25-dihydroxyvitamin D₃ suppresses renin gene transcription by blocking the activity of the cyclic AMP response element in the renin gene promoter. *J Biol Chem.* 2007 Oct 12;282(41):29821–30.
560. Cherniack EP, Levis S, Troen BR. Hypovitaminosis D: a widespread epidemic. *Geriatrics.* 2008 Apr;63(4):24–30.
561. Holick MF. Vitamin D: importance in the prevention of cancers, type 1 diabetes, heart disease, and osteoporosis. *Am J Clin Nutr.* 2004 Mar;79(3):362–71.
562. Littlejohns TJ, Henley WE, Lang IA, Annweiler C, Beauchet O, Chaves PHM, et al. Vitamin D and the risk of dementia and Alzheimer disease. *Neurology.* 2014 Sep 2;83(10):920–8.
563. Arunabh S, Pollack S, Yeh J, Aloia JF. Body fat content and 25-hydroxyvitamin D levels in healthy women. *J Clin Endocrinol Metab.* 2003 Jan;88(1):157–61.
564. Bhandari SK, Pashayan S, Liu ILA, Rasgon SA, Kujubu DA, Tom TY, et al. 25-hydroxyvitamin D levels and hypertension rates. *J Clin Hypertens Greenwich Conn.* 2011 Mar;13(3):170–7.
565. Chiu KC, Chu A, Go VLW, Saad MF. Hypovitaminosis D is associated with insulin resistance and beta cell dysfunction. *Am J Clin Nutr.* 2004 May;79(5):820–5.
566. Filipov JJ, Zlatkov BK, Dimitrov EP, Svinarov D. Relationship between vitamin D status and immunosuppressive therapy in kidney transplant recipients. *Biotechnol Biotechnol Equip.* 2015 Mar 4;29(2):331–5.
567. Aggarwal M, Sahoo SP, Bhandari HS, Kriplani J, Mithal A. Prevalence of vitamin D deficiency in post renal transplant patients. *Indian J Endocrinol Metab.* 2012 Mar;16(2):274–6.

568. Stein EM, Cohen A, Freeby M, Rogers H, Kokolus S, Scott V, et al. Severe vitamin D deficiency among heart and liver transplant recipients. *Clin Transplant*. 2009;23(6):861–5.
569. Lee C-T, Ng H-Y, Lien Y-H, Lai L-W, Wu M-S, Lin C-R, et al. Effects of cyclosporine, tacrolimus and rapamycin on renal calcium transport and vitamin D metabolism. *Am J Nephrol*. 2011;34(1):87–94.
570. Li YC, Kong J, Wei M, Chen Z-F, Liu SQ, Cao L-P. 1,25-Dihydroxyvitamin D(3) is a negative endocrine regulator of the renin-angiotensin system. *J Clin Invest*. 2002 Jul;110(2):229–38.
571. Tomaschitz A, Pilz S, Ritz E, Grammer T, Drechsler C, Boehm BO, et al. Independent association between 1,25-dihydroxyvitamin D, 25-hydroxyvitamin D and the renin-angiotensin system: The Ludwigshafen Risk and Cardiovascular Health (LURIC) study. *Clin Chim Acta Int J Clin Chem*. 2010 Sep 6;411(17–18):1354–60.
572. Vaidya A, Forman JP, Hopkins PN, Seely EW, Williams JS. 25-Hydroxyvitamin D is associated with plasma renin activity and the pressor response to dietary sodium intake in Caucasians. *J Renin-Angiotensin-Aldosterone Syst JRAAS*. 2011 Sep;12(3):311–9.
573. Gedik O, Akalin S. Effects of vitamin D deficiency and repletion on insulin and glucagon secretion in man. *Diabetologia*. 1986 Mar;29(3):142–5.
574. Inomata S, Kadowaki S, Yamatani T, Fukase M, Fujita T. Effect of 1 alpha (OH)-vitamin D3 on insulin secretion in diabetes mellitus. *Bone Miner*. 1986 Jun;1(3):187–92.
575. Christakos S, Liu Y. Biological actions and mechanism of action of calbindin in the process of apoptosis. *J Steroid Biochem Mol Biol*. 2004 May;89–90(1–5):401–4.
576. Zhuang H, Lin Y, Yang G. Effects of 1,25-dihydroxyvitamin D3 on proliferation and differentiation of porcine preadipocyte in vitro. *Chem Biol Interact*. 2007 Nov 20;170(2):114–23.
577. Bellows CG, Wang YH, Heersche JN, Aubin JE. 1,25-dihydroxyvitamin D3 stimulates adipocyte differentiation in cultures of fetal rat calvaria cells: comparison with the effects of dexamethasone. *Endocrinology*. 1994 May;134(5):2221–9.
578. Emanuela F, Grazia M, Marco DR, Maria Paola L, Giorgio F, Marco B. Inflammation as a Link between Obesity and Metabolic Syndrome [Internet]. *Journal of Nutrition and Metabolism*. 2012 [cited 2017 Jul 1]. Available from: <https://www.hindawi.com/journals/jnme/2012/476380/>
579. Patel S, Farragher T, Berry J, Bunn D, Silman A, Symmons D. Association between serum vitamin D metabolite levels and disease activity in patients

- with early inflammatory polyarthritis. *Arthritis Rheum.* 2007 Jul;56(7):2143–9.
580. van Etten E, Mathieu C. Immunoregulation by 1,25-dihydroxyvitamin D3: basic concepts. *J Steroid Biochem Mol Biol.* 2005 Oct;97(1–2):93–101.
581. Bhalla AK, Amento EP, Serog B, Glimcher LH. 1,25-Dihydroxyvitamin D3 inhibits antigen-induced T cell activation. *J Immunol Baltim Md 1950.* 1984 Oct;133(4):1748–54.
582. Xiao H, Lu Y, Li C, Cheng X, Li N, Liu M, et al. Correlation of serum 25-hydroxyvitamin D and parathyroid hormone levels with metabolic syndrome in aged males. *Zhonghua Yi Xue Za Zhi.* 2014 Sep 30;94(36):2828–32.
583. Ford ES, Zhao G, Li C, Pearson WS. Serum concentrations of vitamin D and parathyroid hormone and prevalent metabolic syndrome among adults in the United States. *J Diabetes.* 2009 Dec;1(4):296–303.
584. Saab G, Whaley-Connell A, Bombeck A, Kurella Tamura M, Li S, Chen S-C, et al. The Association between Parathyroid Hormone Levels and the Cardiorenal Metabolic Syndrome in Non-Diabetic Chronic Kidney Disease. *Cardiorenal Med.* 2011 May;1(2):123–30.
585. Kim J. Association between serum vitamin D, parathyroid hormone and metabolic syndrome in middle-aged and older Korean adults. *Eur J Clin Nutr.* 2015 Apr;69(4):425–30.
586. Kamycheva E, Sundsfjord J, Jorde R. Serum parathyroid hormone level is associated with body mass index. The 5th Tromsø study. *Eur J Endocrinol.* 2004 Aug;151(2):167–72.
587. Ljunghall S, Jakobsson S, Joborn C, Palmér M, Rastad J, Akerström G. Longitudinal studies of mild primary hyperparathyroidism. *J Bone Miner Res Off J Am Soc Bone Miner Res.* 1991 Oct;6 Suppl 2:S111-116; discussion S121-124.
588. Silverberg SJ, Lewiecki EM, Mosekilde L, Peacock M, Rubin MR. Presentation of asymptomatic primary hyperparathyroidism: proceedings of the third international workshop. *J Clin Endocrinol Metab.* 2009 Feb;94(2):351–65.
589. Grant FD, Mandel SJ, Brown EM, Williams GH, Seely EW. Interrelationships between the renin-angiotensin-aldosterone and calcium homeostatic systems. *J Clin Endocrinol Metab.* 1992 Oct;75(4):988–92.
590. Hulter HN, Melby JC, Peterson JC, Cooke CR. Chronic continuous PTH infusion results in hypertension in normal subjects. *J Clin Hypertens.* 1986 Dec;2(4):360–70.
591. Brown J, de Boer IH, Robinson-Cohen C, Siscovick DS, Kestenbaum B, Allison M, et al. Aldosterone, Parathyroid Hormone, and the Use of Renin-

- Angiotensin-Aldosterone System Inhibitors: The Multi-Ethnic Study of Atherosclerosis. *J Clin Endocrinol Metab.* 2015 Feb;100(2):490–9.
592. Pilz S, Tomaschitz A, März W, Cavalier E, Ritz E. Aldosterone and parathyroid hormone: a complex and clinically relevant relationship. *Calcif Tissue Int.* 2010 Oct;87(4):373–4.
593. Saussine C, Judes C, Massfelder T, Musso MJ, Simeoni U, Hannedouche T, et al. Stimulatory action of parathyroid hormone on renin secretion in vitro: a study using isolated rat kidney, isolated rabbit glomeruli and superfused dispersed rat juxtaglomerular cells. *Clin Sci Lond Engl* 1979. 1993 Jan;84(1):11–9.
594. Barkan A, Marilus R, Winkelsberg G, Yeshurun D, Blum I. Primary hyperparathyroidism: possible cause of primary hyperaldosteronism in a 60-year-old woman. *J Clin Endocrinol Metab.* 1980 Jul;51(1):144–7.
595. Bernini G, Moretti A, Lonzi S, Bendinelli C, Miccoli P, Salvetti A. Renin-angiotensin-aldosterone system in primary hyperparathyroidism before and after surgery. *Metabolism.* 1999 Mar;48(3):298–300.
596. Burnstein MI, Kottamasu SR, Pettifor JM, Sochett E, Ellis BI, Frame B. Metabolic bone disease in pseudohypoparathyroidism: radiologic features. *Radiology.* 1985 May;155(2):351–6.
597. Brickman AS, Stern N, Sowers JR. Hypertension in pseudohypoparathyroidism type I. *Am J Med.* 1988 Dec 1;85(6):785–92.
598. Atchison DK, Ortiz-Capisano MC, Beierwaltes WH. Acute activation of the calcium-sensing receptor inhibits plasma renin activity in vivo. *Am J Physiol Regul Integr Comp Physiol.* 2010 Oct;299(4):R1020-1026.
599. Ortiz-Capisano MC, Reddy M, Mendez M, Garvin JL, Beierwaltes WH. Juxtaglomerular cell CaSR stimulation decreases renin release via activation of the PLC/IP(3) pathway and the ryanodine receptor. *Am J Physiol Renal Physiol.* 2013 Feb 1;304(3):F248-256.
600. Kisch ES, Dluhy RG, Williams GH. Regulation of renin release by calcium and ammonium ions in normal man. *J Clin Endocrinol Metab.* 1976 Dec;43(6):1343–50.
601. Watkins BE, Davis JO, Lohmeier TE, Freeman RH. Intrarenal site of action of calcium on renin secretion in dogs. *Circ Res.* 1976 Dec;39(6):847–53.
602. Isaac R, Raymond JP, Rainfray M, Ardaillou R. Effects of an acute calcium load on plasma ACTH, cortisol, aldosterone and renin activity in man. *Acta Endocrinol (Copenh).* 1984 Feb;105(2):251–7.
603. Atchison DK, Harding P, Beierwaltes WH. Hypercalcemia reduces plasma renin via parathyroid hormone, renal interstitial calcium, and the calcium-sensing receptor. *Hypertension.* 2011 Oct;58(4):604–10.

604. Richards AM, Espiner EA, Nicholls MG, Ikram H, Hamilton EJ, Maslowski AH. Hormone, calcium and blood pressure relationships in primary hyperparathyroidism. *J Hypertens*. 1988 Sep;6(9):747–52.
605. Valvo E, Bedogna V, Gammara L, Casagrande P, Ortalda V, Maschio G. Systemic hemodynamic pattern in primary hyperparathyroidism and its changes after parathyroidectomy. *Miner Electrolyte Metab*. 1991;17(3):147–52.
606. Heit JJ, Apelqvist ÅA, Gu X, Winslow MM, Neilson JR, Crabtree GR, et al. Calcineurin/NFAT signalling regulates pancreatic β -cell growth and function. *Nature*. 2006 Sep 21;443(7109):345–9.
607. Neal JW, Clipstone NA. Calcineurin Mediates the Calcium-dependent Inhibition of Adipocyte Differentiation in 3T3-L1 Cells. *J Biol Chem*. 2002 Dec 20;277(51):49776–81.